



International Committee for Future Accelerators

Sponsored by the Particles and Fields Commission of IUPAP

Beam Dynamics Newsletter

No. 35

**Issue Editor:
C. Biscari**

**Editor in Chief:
W. Chou**

December 2004

Contents

1	FOREWORD.....	7
1.1	FROM THE CHAIRMAN.....	7
1.2	FROM THE EDITOR.....	7
1.3	SPECIAL REPORT - L. C. TENG'S AUTOBIOGRAPHY: ACCELERATORS AND I.....	8
1.3.1	Chicago Cyclotron.....	8
1.3.2	Minnesota Linac.....	9
1.3.3	Argonne: ZGS and MURA.....	10
1.3.4	Fermilab.....	12
1.3.5	Taiwan Light Source.....	16
1.3.6	Loma Linda Proton Therapy Facility.....	17
1.3.7	Argonne: APS.....	17
1.3.8	Postscript – Random Confessions.....	18
1.4	ANNOUNCEMENT - LEE C. TENG'S RETIREMENT CELEBRATION.....	19
2	COHERENT SYNCHROTRON RADIATION IN STORAGE RINGS	20
2.1	AN INTRODUCTION TO COHERENT SYNCHROTRON RADIATION IN STORAGE RINGS	20
2.1.1	Introduction.....	20
2.1.2	CSR: Past, Present & Future.....	22
2.1.3	Acknowledgements.....	23
2.1.4	References.....	23
2.2	STABLE CSR IN STORAGE RINGS: A MODEL.....	27
2.2.1	Introduction.....	27
2.2.2	Coherent Synchrotron Radiation Basics.....	28
2.2.3	CSR Form Factor for Non-Gaussian Longitudinal Distributions.....	29
2.2.4	Generating Non-Gaussian Bunches.....	30
2.2.4.1	Nonlinear Dynamics Effects.....	30
2.2.4.2	Collective Effects.....	30
2.2.5	The Free Space SR Wake Regime.....	33
2.2.6	The Microbunching Instability.....	34
2.2.7	On Optimized Stable CSR Source Based on a Storage Ring.....	34
2.2.8	Conclusions.....	38
2.2.9	Acknowledgements.....	38
2.2.10	References.....	38
2.3	MICROBUNCH INSTABILITY THEORY AND SIMULATIONS.....	39
2.3.1	Introduction.....	39
2.3.2	Properties of CSR.....	40
2.3.3	Radiation Reaction Force—CSR wake field.....	41
2.3.4	CSR Instability.....	42

2.3.5	Rings with Wigglers.....	43
2.3.6	Discrete modes near shielding threshold.....	44
2.3.7	Simulation of Multiparticle Dynamics in the Presence of CSR.....	45
	2.3.7.1 Field Computation	45
	2.3.7.2 Numerical Modeling of Phase Space Dynamics.....	49
	2.3.7.3 Possible Improvements in the Vlasov Solution	54
2.3.8	Acknowledgments.....	55
2.3.9	References	55
2.4	INITIAL SCIENTIFIC USES OF COHERENT SYNCHROTRON RADIATION IN ELECTRON STORAGE RINGS.....	57
2.4.1	Introduction.....	57
2.4.2	Sub-terahertz response of stressed and unstressed Ge:Ga photoconductive detectors.....	59
2.4.3	Observation of the Josephson plasma resonance in optimally doped $\text{Bi}_2\text{Sr}_2\text{CaCu}_2\text{O}_{8-\delta}$	61
2.4.4	THz scanning near-field microspectroscopy on biological samples.....	64
2.4.5	Summary	69
2.4.6	References	69
2.5	OPTIMIZING RING-BASED CSR SOURCES.....	70
2.5.1	Introduction.....	70
2.5.2	General Considerations	72
2.5.3	Circe Ring Design & Beamline Extraction.....	73
2.5.4	CIRCE Performance.....	76
2.5.5	Broadband Bursting mode.....	77
2.5.6	Laser slicing of beams.....	77
2.5.7	Conclusion.....	80
2.5.8	Acknowledgments.....	81
2.5.9	References	81
2.6	THE BESSY LOW ALPHA OPTICS AND THE GENERATION OF COHERENT SYNCHROTRON RADIATION	82
2.6.1	Introduction.....	82
2.6.2	The BESSY II Low Alpha Optics.....	83
2.6.3	Limits of Short Bunches.....	85
2.6.4	Coherent Synchrotron Radiation.....	87
2.6.5	Current Dependent Bunch Length	90
2.6.6	Scaling of the Threshold Current	92
2.6.7	Summary	93
2.6.8	Acknowledgements	93
2.6.9	References	93
2.7	SOLEIL AS CSR SOURCE (PROSPECTS AND PRELIMINARY ESTIMATIONS).....	95
2.7.1	Introduction.....	95
2.7.2	Operation with Low Momentum Compaction Factor.....	95
2.7.3	CSR Produced in the Electron Beam Femtosecond Slicing Experiment...97	97
2.7.4	Transverse Deflection of the Electron Bunches in RF Cavities.....	98
2.7.5	Acknowledgements	99

2.7.6	References	99
2.8	OBSERVATION OF INTENSE TERAHERTZ BURSTS AT UVSOR-II	100
2.8.1	Introduction	100
2.8.2	Experiments.....	100
2.8.2.1	Storage ring	100
2.8.2.2	Infrared Beam-line and Detector.....	100
2.8.2.3	Results	101
2.8.3	Summary	103
2.8.4	References	104
2.9	OBSERVATION OF CSR AT NEWSUBARU.....	104
2.9.1	Introduction	104
2.9.2	NewSUBARU in Quasi-Isochronous Mode.....	104
2.9.3	Measurement of Radiation Power	105
2.9.4	Acknowledgement.....	106
2.9.5	References	107
2.10	TERAHERTZ COHERENT SYNCHROTRON RADIATION AT DAΦNE.....	107
2.10.1	Introduction	107
2.10.2	The microbunching instability in DAΦNE	108
2.10.3	DAΦNE as an ultra-stable source of CSR	110
2.10.3.1	DAΦNE as a CSR source with the existing 368 MHz RF system	110
2.10.3.2	DAΦNE as a CSR source with the 1.3 GHz SC RF system	112
2.10.3.3	Two low alpha lattices for DAΦNE as a CSR Source.....	114
2.10.4	Conclusions	117
2.10.5	References	117
2.11	FAR-INFRARED DETECTORS FOR COHERENT SYNCHROTRON RADIATION.....	117
2.11.1	Introduction	117
2.11.2	Detectors.....	118
2.11.2.1	Silicon bolometer	119
2.11.2.2	InSb hot electron bolometer	120
2.11.2.3	Superconducting hot electron bolometer	120
2.11.2.4	Photoconductive detectors	121
2.11.3	Results obtained at BESSY	121
2.11.4	Conclusion.....	123
2.11.5	References	124
3	INTERNATIONAL LINEAR COLLIDER (ILC).....	125
3.1	REPORT ON THE ILC WORKSHOP KEK (JAPAN) NOVEMBER 2004.....	125
3.1.1	Introduction	125
3.1.2	Opening Plenary	125
3.1.3	WG1 - Overall Design.....	126
3.1.4	WG2 - Main Linacs	127
3.1.5	WG3 – Injector	128
3.1.6	WG4 - Beam Delivery.....	129

3.1.7	WG5 - High Gradient Cavities.....	130
3.1.8	Discussion on GDI Organization.....	131
3.1.9	Conclusion.....	132
3.1.10	References.....	132
4	ACTIVITY REPORTS.....	133
4.1	BEAM PHYSICS AT THE UNIVERSITY OF MARYLAND ELECTRON RING (UMER)...	133
4.1.1	UMER Layout and Beam Parameters.....	134
4.1.2	Beam Transport Optimization.....	135
4.1.3	Beam Dynamics.....	137
4.1.4	Future Work.....	138
4.1.5	Acknowledgements.....	138
4.1.6	References.....	138
4.2	SESAME.....	139
4.2.1	Introduction.....	139
4.2.2	Transverse Beam Dynamics.....	139
4.2.3	Longitudinal Beam Dynamics and Instabilities.....	140
4.2.4	The Vacuum Chamber Impedance.....	140
4.2.5	Longitudinal Coupled Bunch Instability.....	141
5	RECENT DOCTORAL THESES.....	143
6	FORTHCOMING BEAM DYNAMICS EVENTS.....	144
6.1	32 ND ADVANCED ICFA BEAM DYNAMICS WORKSHOP ON ENERGY RECOVERING LINACS, "ERL2005".....	144
7	ANNOUNCEMENTS OF THE BEAM DYNAMICS PANEL.....	146
7.1	ICFA BEAM DYNAMICS NEWSLETTER.....	146
7.1.1	Aim of the Newsletter.....	146
7.1.2	Categories of Articles.....	146
7.1.3	How to Prepare a Manuscript.....	147
7.1.4	Distribution.....	147
7.1.5	Regular Correspondents.....	148
7.2	ICFA BEAM DYNAMICS PANEL MEMBERS.....	149

1 Foreword

1.1 From the Chairman

Weiren Chou, [Fermilab
chou@fnal.gov](mailto:chou@fnal.gov)

We have seen veterans in the high-energy physics field for 30, 35 or even 40 years before they retire. But very rarely, would we find someone who has been in this field for more than a half-century! Dr. Lee C. Teng, who started his career in HEP in 1947, officially retired from Argonne National Laboratory on September 30, 2004. During those 57 years, Lee has made tremendous contributions to particle accelerators. We invited him to write a brief autobiography, which is included in this issue and will serve as a valuable historic record.

The International Linear Collider (ILC) has been picking up momentum since the technology decision last August. The first international workshop was held last month at KEK, Japan. The second one will be in August 2005 at Snowmass, U.S.A. A number of meetings and topical workshops are also planned. Starting with this issue, we will have a special ILC section in each Newsletter issue. Your contributions to this section are greatly encouraged.

The *World Accelerator Catalog* project is progressing well. More than 20 laboratories and institutions from around the world have responded to a request from the panel chair and assigned official contact person(s) for each accelerator in their lab. These people will be responsible for providing the machine parameters for the catalog. A relational database based on PHP and MySQL is under construction and should be ready soon.

The 32nd ICFA Advanced Beam Dynamics Workshop (ABDW), *ERL2005*, has been rescheduled to March 19-23, 2005 at Jefferson Laboratory, U.S.A.

The Beam Dynamics Panel will meet during PAC05 to discuss plans for the following two years. Suggestions or comments from the readers concerning the panel's activities are welcome.

1.2 From the Editor

Caterina Biscari, [LNF-INFN
caterina.biscari@lnf.infn.it](mailto:caterina.biscari@lnf.infn.it)

The phenomenon of the coherent synchrotron radiation (CSR) emitted by ultra relativistic electrons, known since the past forties, has become of great actuality with the development of high peak current facilities, both in single pass mode and in storage rings.

The interest for the utilization of high power radiation in the terahertz and far infrared region in the field of chemical, physical and biological processes has lead several synchrotron radiation facilities to test the possibility of producing CSR in a controlled way. The first successful experiments and utilization of the radiation are part of the recent history. The ALS group has proposed the construction of a facility wholly

dedicated to the CSR production, and many of the existing synchrotron radiation facilities have included the CSR production among their future plans.

We have dedicated the special theme of this issue to the CSR in storage rings. Theory, simulations, experimental results, diagnostics and proposals for new facilities are presented, together with an interesting overview on the utilization of the CSR produced in BESSY.

I have received with great pleasure Prof. Teng's autobiography and his historical overview of half a century of the accelerator physics in which he has always played the leading role.

Two young scientists participating to the SESAME synchrotron light source project have written a general report on their beam dynamics activities. SESAME is a wide scientific collaboration in the Asian Middle East area, born under UNESCO aegis, and led by Gaetano Vignola. It is now in the construction phase.

Interesting is also the description of the small electron ring at Maryland University. This is an example of how this Newsletter can be used as communication means by the small and medium size facilities, where often new ideas and concepts can be easily produced and tested.

I repeat here Weiren's invitation to contribute to the newly founded Newsletter ILC section, and I present the first contribution related to the first official meeting of the entire Linear Collider community, held in November 2004 at KEK.

Finally I want to thank Pina Possanza, secretary of the Divisione Acceleratori of LNF, for her professional editing of the whole issue.

1.3 Special report - L. C. Teng's autobiography: Accelerators and I

Lee C. Teng, [ANL
teng@aps.anl.gov](mailto:teng@aps.anl.gov)

1.3.1 Chicago Cyclotron

It all started in 1947 when I came to the United States to pursue graduate studies in physics at the University of Chicago (U of C). To keep my body and soul fed I worked in the physics department. The jobs I remembered best were first as a teaching assistant for Prof. Enrico Fermi's one-year course on quantum mechanics and then as a cyclotron assistant for the 450-MeV proton synchrocyclotron then under construction at the Institute for Nuclear Studies (INS), later renamed the Enrico Fermi Institute. With hardly any knowledge of accelerators and beam dynamics, I was told to think of some way to extract the beam after it had been accelerated because there was no good way of doing that. The only way at the time was to insert a scatterer at the final orbit to elastically scatter some beam out. The efficiency was, of course, miserable. I was told to work with Dr. James Tuck, who had just arrived from England and was on his way to a job at Los Alamos. While waiting for Dr. Tuck's security clearance, the director of the cyclotron project, Prof. Herbert Anderson, agreed to keep him on as a temporary research associate. He was aware that in a betatron a reduction of the magnetic field in a narrow azimuthal sector beyond the extraction radius produced by an iron shim (called the "peeler") will cause the beam to step radially outward just in front of the peeler. The beam can then be extracted by a high-voltage electric septum. I plotted the

orbits for our synchrocyclotron with a peeler. It didn't work. The beam always blew up vertically. However, the orbit plot suggested that if another sector of increased field were added some 90° downstream, the beam might step out. We called the second field bump the "regenerator" and called the whole scheme "regenerative extraction." To this day, this is still the best and only beam extraction system for cyclotrons and an extraction efficiency of nearly 50% has been obtained.

In those days, to do orbit tracing we had only mechanical "computers" with gears and levers, such as "Marchant" and "Freden" calculators. These could carry out the four arithmetical operations (later Freden came out with a machine that could also find square roots). These calculators, together with slide rules and graduated straight edges, graduated protractors and compasses were the only orbit-tracking devices available. Maintaining adequate precision was a major problem. I had to invent all kinds of rather tricky procedures and algorithms. At one time I had as many as three of my fellow graduate students helping me do the orbit tracking. This regenerative extraction system is now known as resonant extraction in modern terminology. The integer resonance $\nu_x = 1$ is excited by a $\sin 2\theta$ quadrupole term. A betatron generally has $\nu_x > 1/2$ and a synchrocyclotron has $\nu_x < 1/2$ (actually $\nu_x \cong 0$ at the final energy), which accounts for the difference.

The shims were sized and shaped by the cut-and-measure method. I had to crawl in between the magnet poles to manually traverse the test coil to measure the field bumps. Without an appreciation of the required accuracy, my first peeler-regenerator set simply did not work at all. The beam vanished at the extraction radius and my shims were immediately yanked out. The regenerative extraction system was finally made to work in 1953 by Albert Crewe on the Liverpool cyclotron. He was then invited to come to the U of C to extract the beam from the synchrocyclotron.

The discovery of the 3-3 resonance in pp scattering (the Δ particles) was made by the Fermi group using an internal target.

In addition to the synchrocyclotron, the U of C-INS also operated a 100-MeV betatron purchased from the General Electric Co. and an old 30-inch Lawrence cyclotron used by chemists. I learned to operate all these machines to keep my paychecks coming during summer of 1951 after my assistantship ended. In 1951 I got my Ph.D. under Prof. Gregor Wentzel with a particle theory thesis on the polarization of a vector meson at production in pp collisions, and joined the faculty of the University of Minnesota.

1.3.2 Minnesota Linac

At the University of Minnesota (U of M) I taught courses on nuclear physics, and quantum field theory, but another piece of accelerator work knocked on my door. In 1951 the Physics Department of the U of M was in the midst of building a 50-MeV proton linear accelerator. Like all Alvarez linacs in those days this one had copper rf liners inside a steel vacuum tank. To obtain radial focusing for the beam, copper grids were brazed to the upstream ends of the drift tubes. This made the electric field in the gaps convergent but the grids intercepted a good fraction of the beam and kept the beam intensity low. In 1952 alternating gradient (AG) focusing and quadrupole magnets were invented by Courant, Livingston, Snyder, and Blewett. Their application to the linac seemed natural and straightforward, so I designed a quadrupole focusing system for the linac using the matrix formulation that I learned from doing the regenerative extraction

system. I believe this was the first application of matrix formulation to AG focusing systems. The actual replacement of the grids by quadrupoles was not done until after I left Minnesota because this entailed the construction of a completely new set of drift tubes.

One day while we were discussing the AG effect, I mentioned to Prof. Johnny Williams, an accomplished experimentalist and director of the linac project, that if he really wanted to be convinced of and to confirm quantitatively the combined focusing action of a focusing-defocusing array, why not just get some optical lenses, shine a beam of light through them, and measure the beam width. He was so amused by the suggestion that he went out the next day and bought a bunch of classroom demonstration lenses and had a ball with them. From then on, he kept telling everybody "It took a theorist to tell an experimenter to go ahead and measure it!" Prof. Williams recommended me to Jack Livingood at Argonne National Laboratory for the Argonne accelerator project. When the term of my appointment at the University of Minnesota was up, I accepted an undergraduate teaching position at Wichita State University to wait for my Argonne appointment. Because I was to be the first non-U.S. citizen hired by Argonne, the appointment took a long time and finally came in 1955.

1.3.3 Argonne: ZGS and MURA

In 1953 two weak-focusing synchrotrons were in operation on both coasts: the 6-GeV Bevatron in Berkeley and the 3-GeV Cosmotron in Brookhaven where the construction of the 30-GeV strong-focusing synchrotron AGS was also about to begin. Everybody was in agreement that the next high-energy accelerator should be built in the Midwest. The most logical site for the synchrotron was clearly Argonne National Laboratory, but for some reason the high-energy physicists in midwestern universities felt strongly against having the facility situated in and administered by Argonne. They formed an independent organization named the Midwestern Universities Research Association expecting to eventually establish an independent laboratory to design, build, and operate the facility. The staff of MURA were all high-caliber physicists from university faculties. They quickly invented the Fixed Field Alternating Gradient (FFAG) ring accelerator and in due time advanced the understanding and the analysis of particle beam dynamics in accelerators to a new height. MURA felt strongly committed to its own invention, the FFAG. Over a two-year period MURA submitted three different accelerator proposals to the Atomic Energy Commission (AEC), all based on the FFAG principle. The trouble was that the FFAG, with its fixed field, was good for high intensity but not high energy. None of their proposals gave energies higher than the 30-GeV AGS already under construction. The proposals were all turned down.

The animosity between MURA and Argonne luckily stayed only at the top administration level. Argonne accelerator physicists, including myself, regularly attended MURA technical meetings in Madison, WI. I was fascinated by the FFAG technology and did my share to contribute to it. At my suggestion, the first Argonne proposal was also FFAG based. To reach high energy I had to tandem two FFAGs together (first 2 GeV, then 25 GeV). I used my regenerative extraction scheme and its inverse—"regenerative injection"—together to form an essentially c.w. beam transfer. This proposal, submitted in 1955, was also turned down. Then, a resolution to "resolve" the MURA-Argonne impasse was invented by the General Advisory Committee of the AEC. One day in January 1956, the edict filtered down to us that

Argonne should design and build an accelerator based on time-tested technology (which evidently excluded everything based on the AG principle), it should have an energy of 10 to 15 GeV, and it should be built fast to beat the 10-GeV Synchrophasotron which was nearing completion in Dubna, USSR. MURA should continue to do R&D for the construction of a future high-tech machine. This was a terrible blow (in fact, a near-death blow) to the small group of accelerator physicists gathered at Argonne. We went away in solitude to lick our wounds and to search our souls. But once the initial shock and agony subsided and we understood and accepted our fate, we decided to make the best of it.

The 12-page proposal for such a machine was submitted in February 1956 and was approved on the spot. The machine would be called the Zero Gradient Synchrotron (ZGS). In April the Particle Accelerator Division (PAD) was formed at Argonne to manage the project. Jack Livingood was appointed the division director and I was made the Accelerator Theory group leader. Later in 1956 Jack took us to Berkeley to pay homage to his early mentor, the grand patriarch of accelerators and big-time research, Ernest Lawrence. I think Jack wanted to get a word of approval from him for the machine. But, of course, Lawrence knew better than to express any strong feeling either one way or the other. Later, I had several occasions to meet and talk with Lawrence one-on-one. He was easy to talk to and did not seem to deserve the reputation of being a holy terror. But then, I never worked for him.

In 1958 after the R&D and prototype work were completed, Livingood resigned and Albert Crewe from U of C took over the directorship. In 1961 I succeeded Crewe as director of the Particle Accelerator Division. Notwithstanding the name, in addition to the ZGS my division was responsible for the operation of a 30-inch hydrogen bubble chamber built by MURA and a 40-inch propane/freon bubble chamber built by the University of Michigan. We also designed, built, and operated all the primary and secondary beamlines, and a pion focusing “horn” for a neutrino beamline. When I agreed to accept the PAD directorship I knew I was making a drastic departure from a fancy-free theorist to an administrator. I took this new job seriously and devoted full time to running the many projects in the division and to liaison with Washington and with the high-energy physics community. I learned a lot, but did not do any physics throughout my tenure as director.

With the ZGS we contributed many innovations:

- We employed edge focusing at the ends of the dipoles. This enabled us to use flat field, hence the most efficient window-frame design for the dipole bending magnets and the name Zero Gradient Synchrotron. We could then reach 12.5 GeV at 21.5 T with reasonable magnet size and power consumption.
- We used a double vacuum chamber with rough vacuum in between to make the chamber thickness manageable.
- We created a separation between the low- and high-energy orbits for beam extraction using the then popular Piccioni system. Eventually this was replaced by a resonant (regenerative) extraction system.
- We upgraded the intensity by converting to charge exchange injection of H⁻ ions. The highest intensity obtained was 0.73×10^{13} p/pulse, which was not too shabby even by the standards of the strong focusing machines.
- The ZGS was the first high-energy machine to accelerate a polarized proton beam.

On the frontier of new technologies I can recall the following achievements:

- We attained a record voltage of 200 kV over 2 cm in a DC particle separator with hot glass electrodes.
- We developed the copper-matrix stabilized NbTi filament superconducting wire and used it in a magnet for a small He bubble chamber.

The ZGS was very prolific in doing high-energy physics experiments, a tribute to the high-energy experimentalists in the Midwest. Also, the ZGS is likely to be the last and the highest energy weak-focusing synchrotron ever built.

When the ZGS started operation, the high-energy experimentalists in the Midwest were happy to have a nearby facility at which to do their experiments regardless of the type of accelerator. But the old animosity toward Argonne and its operator, the University of Chicago, persisted, so the MURA universities demanded of AEC that MURA should have control of the ZGS facility at Argonne. However, MURA did not want to be encumbered by the problems of the other parts of Argonne, so a tripartite contract was invented. The Argonne Universities Association (AUA) was formed in 1968 to control the operation of the ZGS facilities, and the University of Chicago was to continue operating the rest of Argonne. A triangular logo was designed with the top vertex labelled ANL and the two base vertices labelled AUA and U of C.

Actually this ad hoc contractual excursion to tripartitism was quite unnecessary. All of us working at the ZGS had always understood that the *raison d'être* of a high-energy facility is to do high-energy research, and that the majority of high-energy experimentalists are from universities. On the other hand, I believe that the AUA also understood the way we felt at ZGS because they never made any excessive demands or imposed any unreasonable restrictions upon us.

With the ZGS in full operation, the MURA movement lost a major part of its momentum and zeal. In 1965 President Johnson dissolved MURA. Later when a 400-GeV accelerator started operation 20 miles away in Fermilab, a 12-GeV accelerator became superfluous. The ZGS was decommissioned in 1979 after 16 years of operation. Having lost its charge, the AUA was dissolved in 1982. The Argonne logo was retained, however, with the AUA vertex relabelled DOE (the AEC morphed into ERDA in 1975, and then into the DOE in 1977).

1.3.4 Fermilab

Informal discussions about accelerators for several-hundred-GeV energies had been carried on among the accelerator community as early as 1960. I participated in these discussions from the beginning. We realized that for such a synchrotron the proper injection energy of 5-10 GeV was too costly for a linac. Thus, a booster synchrotron was needed to boost the energy of the beam from that of the linac to the injection energy of the main synchrotron.

A national effort for the design of a 200-GeV machine was organized at Berkeley in 1963. I headed the design effort for the booster. The output of the Berkeley study was submitted to the AEC as a proposal in 1965. By early 1967 a site at Weston, Illinois, was chosen, and Robert Wilson of Cornell University had accepted the appointment as director. The official authorization was signed in November 1967. It may have been the first time ever that the authorization was not for the full \$400M budget as estimated in the proposal, but for an arbitrarily reduced amount of \$250M, together with a directive "Do whatever you can with it!"

By 1967 the Argonne PAD was operating fairly smoothly, so I showed up at Fermilab on Day One—June 1, 1967. Fermilab was then called the National Accelerator Laboratory (NAL) and housed on the rented 10th floor of an office building near the Oak Brook shopping mall. I took leave from Argonne and worked full time at NAL for three months for free. In September 1967, after we had enough time to “feel each other out,” Wilson made me a job offer, and I accepted it on the spot. This is why I have a Fermilab badge number of 22 instead of 2 or 3. After I left Argonne, the PAD, which was too large and unwieldy with ~500 people, was split into the Accelerator Division and the High Energy Facilities Division.

Wilson believed in a dynamic organization that was flexible and fast moving. Although my title was the head of Accelerator Theory, I could nose into all parts and phases of the system and was able to influence all their designs. Because at this time the NAL project was the “only game in town,” there was no shortage of able and eager accelerator people knocking at the door. There were even volunteers willing to commute from Europe. From this large pool of talented people Wilson was able to pick those who agreed with his own “rough and tumble” style. This, in addition to his own fast-moving leadership, led to an incredibly fast schedule with milestones: Day One: June 1, 1967; Proposal submitted: January 1968; Groundbreaking: December 1, 1968; and First 200-GeV beam: March 1, 1972.

Many of the design features of the Fermilab 400-GeV synchrotron were premier departures from the conventions of the time; some were even considered reckless. They have nonetheless been adopted in the design of all subsequent high-energy machines around the world and are now considered the norm. These include:

- Separated function lattice,
- Housing accelerators and beamlines in underground tunnels for shielding,
- Long magnets with integral vacuum chamber and prestressed to be self supporting,
- Electrostatic wire-plane septum for high efficiency slow extraction,
- Shell-type winding of superconducting coils and dynamic liquid-He cooling system, and numerous other small advances.

The Accelerator Theory group at that time was incredibly strong with people like Ernest Courant, Lloyd Smith, Sho Ohnuma, etc., but Wilson’s flexible mode of operation would get me to do all kinds of odd jobs both technical and nontechnical. I will mention only a few to show the dynamic atmosphere of Fermilab in those days. Soon after the construction started I was assigned the job of coordinating the designs of collider projects. We designed a 100 GeV-100 GeV pp collider using conventional magnets and a 200 GeV-200 GeV collider using superconducting magnets. Both fell by the wayside. Later, in collaboration with Argonne, a 400 GeV-400 GeV collider (POP AE) was studied; this was also laid aside. This may just have been Wilson’s way to keep us busy.

Bob Wilson also doubled as the head of the Accelerator Division; however, his other duties frequently prevented him from tending to the accelerator. Often, I had to run the Accelerator Division in his stead, sometimes for as long as several weeks at a stretch.

For a year I was chairman of the Computer Committee. I told Bob once that if it was for only one year, I would be willing to do anything, and he took me up on it.

It happened that during that year we were selecting, configuring, purchasing, and eventually taking delivery of a new mainframe system. So I was able to make a substantial contribution. At the end of the year I had learned a lot about hardware units and systems.

Together with the R&D of superconducting magnets there was a small band of highly technical people doing superconducting magnet measurements. Wilson didn't know what to do with them organizationally, so he inserted them in the Accelerator Theory group. Then, I had to quickly learn all about screw compressors, cold boxes, Thompson valves, etc.

In 1976 Wilson launched a major R&D effort to develop superconducting accelerator magnets. Naturally I participated eagerly in this effort. To study different designs, one-meter-long prototypes were built and tested. The operation was so well streamlined that the turnaround time for checking out a specific design from concept to building prototype to test results was shortened to only one week. This way a large number of design concepts were tested. By 1978 sufficiently good and reliable magnet designs were available for use in whole accelerators, but the DOE was reluctant to fund the project and even tried to quell the effort to design the "Energy Doubler" (later named the Tevatron). Some of us accelerator physicists had to go underground and do the design work in secret. Wilson resigned in 1978 in protest at lack of funding and Leon Lederman was appointed as the second director of Fermilab. The DOE eventually approved the project, and the world's first 800-GeV beam was accelerated in the world's first superconducting accelerator in February 1984.

During this time CERN was designing and constructing an antiproton source using stochastic cooling invented by Simon Van der Meer. Operating the SPS as a storage ring at the lower energy of 270 GeV, they obtained 540 GeV in the center-of-mass and were able to discover the W and Z bosons of the weak interaction. Thus, Fermilab missed out on this major discovery.

Superconducting magnets are best for DC operation. Furthermore, at 800 GeV fixed target operation is already far into the diminished return for increasing center-of-mass energy. An upgraded and improved CERN-style antiproton source was constructed to use with the Tevatron running DC to yield $\bar{p}p$ collisions at 900 GeV on 900 GeV. This Tevatron Collider system with many modifications and improved luminosity is now in a many year long "Run II." Along the way during "Run I" I lost a bottle of wine in a wager with Leon Lederman when the Tevatron luminosity jumped higher than I expected.

There were also many projects in other laboratories on which I collaborated. Some that come to mind include:

- Sextupole lattice accelerator a la Orlov, smoke-ring accelerator a la Sarantsev, and heavy ion fusion at LBNL
- 600- to 1000-GeV accelerators at BNL
- Kaon factories at TRIUMF and at LANL
- Study of collider designs at CERN

Some of the activities also involved review or advisory committee participation. I should also tell about my more demanding endeavors!

Bob Wilson was unhappy with the Fermilab cafeteria, so he appointed a cafeteria committee to implement improvements and appointed me the chairman. I had no idea what a cafeteria committee should do. So I attacked it like a physics project. I persuaded the CERN Italian gourmet cafeteria to be our sister cafeteria and invited their chef to come visit us. He acted as critique, tutor, and mentor to our chef for two weeks and on departure gave me an extensive report and suggestions. The cafeteria committee remained active for several years. Whether it did any good I cannot tell, but Bob seemed pleased.

Here is another one. Shortly after the Gang of Four was smashed, Wilson invited ten accelerator physicists from the Peoples Republic of China to visit Fermilab. China had planned on building a 50-GeV proton synchrotron and was happy to send people over to observe and learn. And I was put in charge. I put them up in the Fermilab Village dormitories and furnished them office space in Wilson Hall. But living on site without being able to drive a car is not easy. I mobilized my wife to take them shopping for food and everything else. I myself gave them lectures on accelerator hardware, technology, and philosophy (they were fairly well versed in accelerator theory). I also led them on tours around the lab to visit staff and their equipment. After three months they had had enough of the monastic life, but they did carry home a lot of information and knowledge, and memories of their visit.

All during this period I did general accelerator physics work whenever I had time. The work on crossing the transition energy is perhaps worth mentioning. When the AG lattice was first proposed, people in the Soviet Union were leery about the proposed method of crossing transition by jumping the accelerating rf phase. They suggested that by introducing reverse bending they could move the transition energy to infinity or even make it imaginary (negative momentum compaction). The trouble was that with the reverse bending, the ring circumference (hence the cost) was substantially higher for a given energy. (The Serpukhov AG synchrotron was first designed for 50 GeV with reverse bending. Later when transition was crossed successfully at CERN and at AGS, they took out the reversing and modified the design to go to 70 GeV.) I studied the problem. I first tried to understand in detail the effects of bending, focusing, and straight sections on dispersion. It then became clear that by judiciously arranging and adjusting the bending, focusing, and straight sections one can make the momentum compaction go to zero or even negative without reverse bends. This work was published in the now discontinued journal *Particle Accelerators* by invitation of the then editor-in-chief, John Blewett. As usual, my papers were written to clarify the concept and/or the principle, with the details left for the readers to work out for their specific applications. I am happy to say that most of my papers led to specific applications and some of the details of applications were also published. The transition crossing by rf phase jumping worked fine at low beam intensity. At high intensities the longitudinal space-charge force, which, of course, cannot be jumped like the rf force, caused a mismatch before and after the crossing. This got worse at higher and higher intensities. The best solution was to always use no-transition lattices. For existing machines, an ingenious triple rf phase-jump scheme was proposed at CERN to rematch the beam. I later introduced some improvements in the scheme and found that there was always unavoidable beam blow-up by microwave instability at the crossing.

In the early 1980s when the Tevatron construction was proceeding smoothly, various demands from outside Fermilab began to occupy my time. I was looking for projects that were shorter term both in construction time and in pay-off time compared

to high-energy machines such as the SSC, which was authorized to begin construction in 1989. This led to my collaboration with the Taiwan Light Source project, the Loma Linda Proton Therapy project, and the Argonne Advanced Photon Source project.

1.3.5 Taiwan Light Source

My association with Taiwan began on my first trip there in 1956 by invitation of the Taiwan Ministry of Education to give a lecture tour and to see my parents for the first time since I left China in 1947. I have always considered Taiwan my “root in exile” after my parents moved there following the take-over of Mainland China by Mao Tse-Tung. I did what I could to help Taiwan. I helped Professor Mei I-Chi to re-establish an exile Tsinghua University in Hsinchu and gave the first graduate courses on electrodynamics, classical and quantum mechanics and quantum field theory. I also arranged to have some surplus equipment from Argonne sent to Tsinghua University and to my alma mater, Fu-Jen University that was also re-established in Taiwan.

My specific association with the Taiwan Light Source began in 1982 when two academicians of Academia Sinica (Chinese National Academy in Taiwan Drs. C.L. Yuan and C.S. Wu, proposed to the academy president to construct a synchrotron radiation source in Taiwan. The Taiwan government in 1983 accepted their proposal, and a Board of Directors was established the same year. Since I was the only academician and board member with accelerator experience, I was asked to serve as the first director to get the “Synchrotron Radiation Research Center” started. For nearly two years, I took a part-time leave from Fermilab. With the help of my friends in the U.S., a design for a 1.5-GeV third-generation storage ring with injection from a 100-MeV linac was completed. An initial group of ~20 key personnel was recruited from universities and laboratories in Taiwan. I gave them regular introductory lectures in accelerator technology and on the specific 1.5-GeV design. I also constituted a Review Committee composed mostly of people from Europe and the U.S. and had a first meeting in BNL. The initial office/laboratory space was established in a rental high-rise office building in Taipei and the laboratory site was selected to be in a science-industrial park in Hsinchu, some 40 miles south of Taipei. Eventually the commuting between Fermilab and Taiwan proved to be too weary. I resigned as director and stayed on only as a member of the Board of Directors. This design, modified by the addition of a 1.5-GeV booster synchrotron for full-energy injection, was constructed in 1993. It now operates ~7000 hr/year with >95% reliability. The facility has some 20 beamlines and a user body of ~1500 scientists and students.

An effort has recently been started to construct a second facility—a 3-GeV synchrotron radiation source. After a recent realignment, the Center now has the status of a private organization operated by a Board of Trustees and funded by the government through a foundation. I continue my association as a trustee.

My association with mainland China started later. After Mr. Deng Xiaoping returned to power in 1977, I re-established contact with several universities and the Academy of Sciences laboratories in China. Now I travel to China at least once a year on average to serve on review or advisory committees or to give talks at workshops or conferences.

1.3.6 Loma Linda Proton Therapy Facility

A neutron therapy facility was built at Fermilab in 1976 using neutrons generated by a 66-MeV proton beam from the injector linac. At Fermilab there was also interest in proton therapy especially since proton therapy was first proposed by Bob Wilson. This interest led to a series of workshops at Fermilab and the formation of the Proton Therapy Coordination Group. Several PTCOG meetings were held at Fermilab and attended by physicists and radiation therapists from laboratories and hospitals nationwide. At one of the meetings in 1986 the head of the radiology department of Loma Linda Hospital in California, Dr. Jim Slater, asked Fermilab to carry out the design and construction of a proton accelerator together with the beam transports required by a clinical therapy facility. The hospital was to provide funding. Phil Livdahl, associate director of Fermilab, took a personal interest in leading the project and asked me to join the group.

The accelerator had to be able to provide rapidly variable energy up to 250 MeV with uniform long-spill extracted beam for raster-scan irradiation over a tumor. The intensity requirement was, however, not very stringent. I decided that these requirements were most easily and most economically fulfilled by a weak focusing synchrotron (a ZGS!) with a repetition rate of 2 Hz and slow resonant extraction. Several choices of injector were available. We chose a compact 2-MeV RFQ. When the project first began in 1987, the only full-time people involved were Livdahl, a mechanical engineer, and myself but we had all of Fermilab from which we could get temporary help and all kinds of information. The synchrotron was built in about a year, assembled and commissioned at Fermilab, then disassembled and shipped to Loma Linda. Although Fermilab was not responsible for the treatment rooms, the gantries, the beam delivery nozzles, etc., we did participate heavily in the discussion and design of these components as well. During my participation in this project I learned a great deal about radiation-biology effects, dosimetry, etc., and grew to understand and appreciate the mentality of radiation therapists.

For many years the Loma Linda proton facility has been operating reliably and smoothly with precision and flexibility. It established Loma Linda as the first hospital with clinical proton therapy capability.

1.3.7 Argonne: APS

After the ZGS was decommissioned the accelerator staff at Argonne began looking for the next accelerator project. A small successful one was the 500-MeV rapid cycling proton synchrotron used for the Intense Pulsed Neutron Source for doing neutron scattering experiments. Several other proposals they made to DOE, however, did not receive approval.

Since 1984 Argonne had been working on the design of a 6-GeV (later upgraded to 7-GeV) synchrotron radiation source with the intention of making a proposal to DOE for construction. I was offered a prestigious part-time "Argonne Fellowship" in 1985 and 1986 to review and to help with the design. The upgraded 7-GeV Advanced Photon Source Conceptual Design Report was published in 1987. The project was approved by the DOE in May 1988 and Dave Moncton was appointed as the overall director.

I was asked to head the Accelerator Physics efforts in 1989. The magnitude of the project and the nature of the job were just what I wanted, so I happily accepted and made the move back to Argonne.

The design of APS was fairly conservative. During construction and commissioning we did have to make some last-minute corrections and patchworks, but nothing more than the expected and tolerable amount. With radiation damping the electron beam is much more forgiving of field errors and inaccuracies. However, one unique demanding feature was that while for colliders the precise characteristics of the circulating beams are crucial only at the collision points, in a synchrotron radiation source the beam is used as radiation source all around the ring, hence the beam characteristics are important everywhere. Thus, the detailed features of the magnet lattice must be carefully considered in the design and precisely controlled during operation. Another demanding feature was that because of radiation outgassing from the vacuum chamber wall, better wall conditioning and more pumping capacity were needed. Insufficient appreciation of this feature led to commissioning difficulties for the early synchrotron radiation storage rings.

The useful lifetime of a synchrotron radiation facility tends to be much longer than that of a high-energy collider. Although discoveries produced by high-energy experiments are intellectually exciting, the synchrotron radiation research and experiments are “useful” for human lives and sometimes even lead to “production runs.” After a discovery, a high-energy experiment can always run on to measure the next decimal place, but unless it proves to have conceptual importance, the interest in the next decimal place will wane.

1.3.8 Postscript – Random Confessions

I was trained at the U of C as a quantum field theorist. My association with accelerators began also at the U of C with the Fermi cyclotron because of the necessity to survive. From that time on, accelerator projects that beckoned my attention just came along one after another. Looking back, I never had time to ponder the wisdom and the implications of making the transition from particle to accelerator physics, but I did occasionally wonder what I could have accomplished if I had stayed in particle physics.

Writing has never come easy for me. I have kept stacks of notebooks containing hand-scribbled records of things I thought of or worked out but never had the will or the time to write up for publication. The trouble is that even with sincere desire and efforts my indexing system for these tomes is not very good. It happens too often that when I go to look for something I know is in a notebook, I cannot find it.

I have always enjoyed teaching. It is a delight to see lights of “Eureka” flicker into the students’ eyes. It is also absolutely true that teaching is the best way to really understand the subject yourself. At my age now I feel that the most useful and noble thing I can do is to pass my knowledge onto the younger generation. So I give lectures and classes at every opportunity.

When I was young I used to think the only science worth pursuing was that dealing with the “ultimates” such as the “elementary particles” and the “cosmos,” and questions of how bulk matters form and behave (even of how, out of inanimate bulk matters, life and intelligence sprang) were “details.” As I grow older, I gradually have come to admit the importance and relevance of the world of materials and of humankind. So I started to work on “useful” things like synchrotron radiation sources and radiation

therapies. But I still think the “cosmic” problems of the 21st Century, such as the unification of all forces and what are dark matter and dark energy, are extremely fascinating.

I retired on September 30, 2004.

1.4 Announcement - Lee C. Teng's Retirement Celebration

<http://www.aps.anl.gov/asd/teng/symposium.htm>

After a long and distinguished career, our colleague and friend, Lee C. Teng, has retired. His contributions to accelerator physics over his entire 57 years of service in the field are both significant and numerous. We are planning to honor his achievements with a commemoration to be held on February 24, 2005 at Argonne National Laboratory. The ceremony will begin around 3:00 pm with a symposium celebrating Lee's scientific contributions, followed by a banquet at the Argonne Guest House. The final program will be announced shortly. Please hold the date and share this information with your colleagues. For information or to R.S.V.P., please contact Kathy Harkay at RSVP-Teng@aps.anl.gov. Your best wishes or kind thoughts may be sent to messages-Teng@aps.anl.gov.

Sincerely,

The Organizing Committee

W. Chou, FNAL
C. Eyberger, ANL
R. Gerig, ANL
K. Harkay, ANL
S. Holmes, FNAL
K. Jaje, ANL
M.K. Jakovich, ANL
R Lanham, ANL
S. Milton, ANL
A. Nassiri, ANL

2 Coherent Synchrotron Radiation in Storage Rings

2.1 An Introduction to Coherent Synchrotron Radiation in Storage Rings

J.B. Murphy, [NLSL-BNL](#)
jbm@bnl.gov

2.1.1 Introduction

The author will assume the reader has a basic familiarity with the properties of “incoherent” synchrotron radiation (ISR), which can be found in many excellent articles and books [1-3]. To give definition to the term “coherent synchrotron radiation (CSR)” we excerpt a few passages from the pioneering papers in the early days of the synchrotron. McMillan in 1945 gives the following description of CSR [4]:

“A single electron of total energy E (rest energy = E_r) moving in a circle of radius R , radiates energy at the rate L (electron volts per turn), given by:

$$L = 400\pi \frac{e}{R} \left(\frac{E}{E_r} \right)^4, \quad (1)$$

where e is the electronic charge in e.s.u., and $E \gg E_r$. In the synchrotron one has the case of a rather concentrated group of electrons moving in the orbit, and the total amount of radiation depends on the coherence between the waves emitted by the individual electrons. For example, if there were complete coherence, the radiation per electron would be N times that given by (1), where N is the number of electrons in the group”.

McMillan goes on to cite work by Schwinger and lists the following *conclusions* [4]:

- a) “Most of the energy in (1) lies in very high harmonics,
- b) The coherence between the high harmonics from different electrons tends to become very small if the group has an appreciable angular spread,
- c) The low harmonics are partially coherent, and give an energy loss per electron per turn (L') depending on N , but not on E if $E \gg E_r$,
- d) Because of fluctuations from a uniform distribution, each electron also radiates the same amount L that it would if alone in the orbit. The radiation per electron is thus $L+L'$.”

Schwinger himself, in his abstract for an invited paper at the 1946 APS Meeting, elucidates a bit further on the nature of CSR and a means to suppress it [5]:

“In addition to the individual or incoherent radiation effects of the electrons, there exists, in the synchrotron, a coherent radiation arising from the electron bunching along

the circular trajectory. This type of radiative energy loss is independent of E , for the coherent spectrum is limited by the length of the electron bunch. Since the latter is not a small fraction of the orbit circumference, the coherent radiation is emitted at long wavelengths, and may be effectively suppressed by metallic shielding.”

Schiff [6], also citing Schwinger, gives a quantitative description of CSR in the frequency domain. He begins by defining the energy in the n^{th} frequency harmonic of the radiation emitted by a single particle on a circular orbit as [6, 9],

$$W_n = \frac{\omega e^2 n}{R} \left[2\beta^2 J'_{2n}(2n\beta) - (1 - \beta^2) \int_0^{2n\beta} J_{2n}(x) dx \right] \quad (2)$$

The total energy radiated by N particles, moving in the same orbit, with the same speed and having instantaneous angular positions ϕ_s , is then given by a weighted sum,

$$W_{tot} = \sum_n \left| \sum_{s=1}^N \exp(in\phi_s) \right|^2 W_n. \quad (3)$$

Schiff's expression clearly indicates the potential for interference between the various electrons depending on their relative phases. For example, if N particles are bunched at the same azimuthal position the total radiated power is then,

$$W_{tot} = N^2 \sum_n W_n, \quad (4)$$

which is a factor of N^2 , not simply N , times that for a single electron. If the positions of the individual electrons are random and uncorrelated but characterized by a normalized distribution function $f(\phi)$ the total power is given by,

$$W_{tot} = \sum_n \left[N + (N^2 - N) \left| \int f(\phi) e^{in\phi} d\phi \right|^2 \right] W_n \quad (5)$$

The first term in the square bracket is the ISR which is independent of the electron distribution and the second term is the CSR which is proportional to the Fourier transform of the longitudinal electron distribution.

From the qualitative descriptions of McMillan and Schwinger one can understand CSR as the *coherent* radiation that arises from an interference of the *electric fields* of azimuthally “bunched” electrons as they're bent in a magnetic field. Recall that the ISR is a sum of the *intensities* emitted by the individual electrons and is independent of the relative phases of the electrons. Schiff's quantitative description shows that the frequency spectrum of the longitudinal electron distribution is a central idea in the theory of CSR, the overall electron bunch length and its detailed shape play a role. As such CSR is intimately linked to many aspects of accelerator physics such as radiation, impedance and wakefields, potential well distortion and instabilities.

In the following section we'll “zoom out to gaze at the big picture” and briefly survey the entire field of CSR in the last century.

2.1.2 CSR: Past, Present & Future

A quick glance at the extensive chronological reference list here within, suggests that the field of CSR can loosely be catalogued into seven distinct eras spanning more than a century:

- Electromagnetic Radiation in the Early Twentieth Century (~1900) [7-9]
- The Dawn of Particle Accelerators (~1944) [4-6, 10-14]
- Electron Ring Accelerators & Synchrotron Radiation Impedance (~1968) [20-28]
- Experimental Evidence of CSR in Linac Transport Lines (~1989) [36, 48-50]
- CSR Theory Revival: Impedances & Wakefields (~1990) [38-42, 51-63]
- Experimental Evidence of CSR in Storage Rings (~1997) [64, 67-80]
- CSR as a Useful Source of THz and Infrared Radiation (~2004) [87, 92].

The reader will be well served by a careful examination of Schott's [9] astounding seminal monograph as it contains all the basics of incoherent synchrotron radiation, multiparticle coherence and even the earliest hints of a longitudinal wakefield analysis of synchrotron radiation [55, 60]. While Schott's work appears to be of a purely academic nature, it begins to find practical applications in the mid 1940s with the birth of particle accelerators. Both Schiff [6] and Schwinger [11, 13] reference Schott in their analysis of the limitations that synchrotron radiation, both incoherent and coherent, might impose on the energy reach of the fledgling particle accelerators (betatrons, synchrotrons, etc.). Schwinger [5, 11], and later Nodvick and Saxon [14], discuss the use of metallic parallel plates to suppress CSR and eliminate it as a barrier to the development of the early accelerators. It is perhaps for this reason that CSR seems to fade from the literature for nearly a quarter of century. Blewett, gives an informative personal perspective on the early years of synchrotron radiation [2].

CSR resurfaces in the late 1960s when electron ring accelerators (ERA) are in vogue. While the work in the 1940s emphasized only the "radiation" associated with CSR, the ERA researchers put forth the notion of a "synchrotron radiation impedance", containing both a real part as well as an imaginary part [24, 27, 28]. For $1 \ll n \ll \gamma^3$, the region of interest to CSR, the impedance in the absence of any bounding surfaces can be written as [27, 28],

$$Z_n[\Omega] \approx Z_0 \cdot \frac{\Gamma(2/3)}{3^{1/3}} \cdot \left(\frac{\sqrt{3}}{2} - i \frac{1}{2} \right) \cdot n^{1/3} \quad (6)$$

The ERA researchers also derived expressions for the impedance including metallic shielding plates and the effects of toroidal walls surrounding the electron beam [28]. The latter introduce resonances with slow phase velocity whispering gallery modes [28, see also 40-42]. With the impedance concept firmly in hand researchers began to examine the possibility of longitudinal instabilities being driven by the CSR impedance [21-25, 27]. Once again CSR is a threat to the development of particle accelerators!

As is usually the case, the time domain or wakefield approach can yield complementary information. The early work on CSR wakefields can be found in references [15-17, 20, 26] where it was used to consider the effects of CSR on the equilibrium electron bunch distribution or so called "longitudinal potential well distortion" (see also [59, 88]). The wakefield for CSR is "peculiar" in that essentially all the wakefield is in front of the exciting charge due to the relativistic "angular

compression” of the fields, this is in marked contrast to the usual notion of “trailing” wakefields associated with cavities, etc [55-63].

The pursuit of ERAs fizzled out in the mid seventies and CSR undergoes a brief hiatus only to be resurrected in the early 1980s as a hero rather than as a villain [30, 32, 34]. CSR was now being proposed as a way to greatly enhance the emission of “low frequency” synchrotron radiation from electron storage rings for use by infrared researchers. However it was going to take until 1989 for solid experimental evidence of CSR to be published, and to many people’s surprise it was in a transport line of a linac driven system not in an electron storage ring [36, 48-50]! Solid experimental evidence for CSR in rings would take nearly a decade to come to fruition.

By the late 1980s numerous electron storage rings had been built and operated as dedicated synchrotron light sources. Accelerator scientists were actively pursuing free electron lasers driven by high brightness photoinjectors, coupled to linacs and magnetic bunch compression systems, as the next big thing. The desire to understand CSR in both rings and linear machines sparked a new wave of interest in the underlying theory and a wealth of papers can be found in literature in the decade of the 1990s [38-46, 51-66].

In the late 1990s the first definitive experimental evidence of CSR in electron storage rings appears in the literature. Work on the rings at NIST, NSLS VUV, BESSY II, MAX and ALS can be found in the references [64, 67-80]. Both bursting and steady state CSR was observed and theories were developed to explain these exciting results, some based on a CSR driven instability and others due to a static longitudinal potential well distortion [81-84, 86, 88]. As noted earlier short electron bunches are key to CSR and a lot of interesting work on low momentum compaction lattices has been performed [68, 72, 76, 89]. The BESSY group has recently reported generating sub picosecond (~ 780 fs) electron bunches by this method [89].

Finally, in 2004 we have the publication in Physical Review B of the first experimental results having used CSR as a dedicated source of probing radiation to explore Josephson plasma resonances in $\text{Bi}_2\text{Sr}_2\text{CaCu}_2\text{O}_8$ [87]. Perhaps CSR in rings has reached its pinnacle as the construction of new dedicated rings for the production of CSR is now being considered [54, 75, 92].

Many of the topics mentioned in this introductory note will be expanded upon in detail in the succeeding articles.

2.1.3 Acknowledgements

The author would like to thank his colleagues at the NSLS, Albert Hofmann of CERN, Karl Bane & Bob Warnock of SLAC and the staffs of ALS & BESSY for many useful discussions. While the author has strived to include an extensive bibliography, it is inevitable that many papers will have been missed and apologies are extended to those authors. The references are chronological by year, but in no particular order for a given year.

2.1.4 References

- [1] J.D. Jackson, *Classical Electrodynamics*, Wiley, New York (1975).
- [2] J.P. Blewett, “Synchrotron Radiation – 1873 to 1947”, *NIM A* 266, p. 1 (1988).
- [3] A. Hofmann, “*The Physics of Synchrotron Radiation*”, Cambridge (2004).
- [4] E.M. McMillan, “Radiation from a Group of Electrons Moving in a Circular Orbit”, *Phys. Rev.* 68, p. 144 (1945).

- [5] J. Schwinger, "Electron Radiation in High Energy Accelerators", *Phy. Rev.* **70**, p. 798 (1946).
- [6] L.I. Schiff, "Production of Particle Energies beyond 200 MeV", *Rev. Sci. Instr.* **17**, p. 6 (1946).
- [7] A. Lienard, "Electric & Magnetic Field Produced by an Electric Charge Concentrated at a Point and Traveling on an Arbitrary Path (translation from French)", *L'Eclairage Electrique* **16**, p. 5 (1898).
- [8] J.E. Weichert, *Archives Neerlandaises*, p. 549 (1900).
- [9] G.A. Schott, *Electromagnetic Radiation*, Cambridge (1912).
- [10] D. Iwanenko and I. Pomeranchuk, "On the Maximal Energy Attainable in a Betatron", *Phys. Rev.* **65**, p. 343 (1944).
- [11] J. Schwinger, "On Radiation by Electrons in a Betatron" (1945), reprinted as LBNL-39088 (1966).
- [12] J.P. Blewett, "Radiation Losses in the Induction Electron Accelerator", *Phys. Rev.* **69**, p. 87 (1946).
- [13] J. Schwinger, "On the Classical Radiation of Accelerated Electrons", *Phys. Rev.* **75**, p. 1912 (1949).
- [14] J.S. Nodvick and D.S. Saxon, "Suppression of Coherent Radiation by Electrons in a Synchrotron", *Phys. Rev.* **96**, p. 180 (1954).
- [15] L.V. Iogansen & M.S. Rabinovich, "Coherent Electron Radiation in the Synchrotron I", *Sov. Phys. JETP* **35** (8), p. 708 (1959).
- [16] L.V. Iogansen & M.S. Rabinovich, "Coherent Electron Radiation in the Synchrotron II", *Sov. Phys. JETP* **37** (10), p. 83 (1960).
- [17] L.V. Iogansen & M.S. Rabinovich, "Coherent Electron Radiation in the Synchrotron III", *Sov. Phys. JETP* **38**, p. 1183 (1960).
- [18] J. Vaclavik, *Czech. J. Phys.* **12**, p. 432 (1962).
- [19] K.W. Robinson, "Storage Ring for Obtaining Synchrotron Radiation with Line Spectra", CEAL-1032 (1966).
- [20] E. Ferlenghi, "Effect of the Coherent Radiation on the Phase Distribution of a Relativistic Bunch", *Nuovo Cimento* **48B** (1967) 73.
- [21] R.J. Briggs, "Coherent Radiative Instabilities of the Compressed Electron Ring", UCRL-18103, p. 434 (1968).
- [22] C. Pellegrini and A.M. Sessler, "Effect of Coherent Radiation during Ring Compression", UCRL-18103, p. 434 (1968).
- [23] C. Pellegrini and A.M. Sessler, "Curvature Effects and the Shape of Bunches in Electron Storage Rings", *Nuovo Cimento* **53B**, p. 198 (1968).
- [24] A.G. Bonch-Osmolovski and E.A. Perelshtein, "Longitudinal Instabilities in Annular Charged Beams", *Radiofizika* **13**, p. 1080 and 1089 (1970).
- [25] C. Pellegrini and A.M. Sessler, "The Equilibrium Length of High Current Bunches in Electron Storage Rings", *Nuovo Cimento*, Vol 3A, No. 1, p. 116 (1971).
- [26] P. Goldreich and D.A. Keeley, "Coherent Synchrotron Radiation", *Astrophysical Journal* **170** (1971) 463.
- [27] B.G. Schinov, A.G. Bonch-Osmolovski, V.G. Makhankov and V.N. Tsytovitch, "The Development of Radiation Instability", *Plasma Physics* **15** (1973) 211.
- [28] A. Faltens and L.J. Laslett, "Longitudinal Coupling Impedance of a Stationary Electron Ring in a Cylindrical Geometry", *Part. Accel.* **4** (1973) 151; and in 1975 Isabelle Summer Study, BNL-20550 (1975).
- [29] N.A. Korkhmazyan, L.A. Gevorgyan and M.L. Petrosyan, "Effect of Electron Distribution on the Coherent Radiation from an Electron Bunch", *Sov. Phys. Tech. Phys.* **22** (8) (1977) 917.
- [30] F.C. Michel, "Intense Coherent Sub millimeter Radiation in Electron Storage Rings", *Phys. Rev. Lett.*, **48** (9) p. 580 (1982).

- [31] M. Bassetti and D. Brandt, "Some Properties of the Azimuthal Component of the Electric Field of a Particle on a Circular Trajectory", CERN/LEP-TH/83-1 (1983).
- [32] J. Yarwood, T. Shuttleworth, J.B. Hasted and T. Nanba, "A New Radiation Source for the Infrared Region", *Nature* 312 (1984) 742.
- [33] E. Keil, "Notes on the First Workshop on Radiation Impedance", CERN LEP-TH/85-40 (1985).
- [34] D.J. Wingham, "Electron Synchrotron Radiation in the Far Field", *Phys. Rev. D*, 35 (8) (1987) 2584.
- [35] G. Decker, "The Attainment of Large Accelerating Gradients Using Near Field Synchrotron Radiation", AIP Conf. Proc. 193, p. 61 (1989).
- [36] T. Nakazato et al., "Observation of Coherent Synchrotron Radiation", *Phys. Rev. Lett.*, 63 (1989) 1245.
- [37] G. Williams et al., "Coherence Effects in Long Wavelength Infrared Synchrotron Radiation Emission", *PRL*, Vol. 62, No. 3, p. 261 (1989).
- [38] K.Y. Ng and R.L. Warnock, "Reactive Impedance of A Smooth Toroidal Chamber below the Resonance Region", *Phys. Rev. D*, 40, 231 (1989).
- [39] K.Y. Ng and R.L. Warnock, "Longitudinal Impedance of a Smooth Toroidal Chamber at Low and Intermediate Frequencies", *SLAC-PUB-4932* (1989).
- [40] K.Y. Ng, "Resonant Impedance in a Toroidal Beam Pipe", *Part. Accel.*, **25**, p. 153 (1990).
- [41] R.L. Warnock, "Shielded Coherent Synchrotron Radiation and Its Effect on Very Short Bunches", *SLAC-PUB-5375* (1990).
- [42] R.L. Warnock and P. Morton, "Field Excited by a Beam in a Smooth Torodial Chamber", *Part. Accel.* **25**, p. 113 (1990).
- [43] N.P. Klepikov and I.M. Ternov, "Coherent Synchrotron Radiation of a Bunch of Particles", *NIM A* 308, p. 113 (1991).
- [44] S. Heifets and A. Michailichenko, "On the Impedance Due to Synchrotron Radiation", *Proc. 1991 Part. Acc. Conf.*, p. 458 (1991).
- [45] S.G. Artunian and M.R. Mailian, "Geometrical Approach in Accelerator Physics", Proc. 1991 PAC, p. 198 (1991).
- [46] L.A. Wainstein et al., "Radiation from the Relativistic Electron Interacting with the Whispering Gallery Mode", *NIM A* 308, p. 94 (1991).
- [47] C. Hirschmugl et al., "Multiparticle Coherence Calculations for Synchrotron Radiation Emission", *Phys. Rev. A*, Vol. 44, No. 2, p. 1316 (1991).
- [48] E. Blum, U. Happek and A.J. Sievers, "Observation of Coherent Synchrotron Radiation at the Cornell Linac", *NIM A*, 307, p. 568 (1991).
- [49] K. Ishi et al., "Spectrum of Coherent Synchrotron Radiation in the Far Infrared Region", *Phys. Rev. A*, 43 (10), p. 5597 (1991).
- [50] Y. Shibata et al., "Observation of Interference between Coherent Synchrotron Radiation from Periodic Bunches", *Phys. Rev. A*, 44 (6), p. R3445 (1991).
- [51] A.V. Burov & E.A. Perevedentsev, "Coherent Synchrotron Radiation And Its Effect On The Bunch Lengthening", Proc. High Energy Acc. Conf., p. 1112-1114 (1992).
- [52] M.M. Karliner et al., "The Impedance of a Toroidal Chamber with Walls of Finite Conductivity", BINP Report 93-90 (1993).
- [53] J.L. Delhez et al., "An Analytical Treatment of Self Fields in a Relativistic Bunch of Charged Particles in a Circular Orbit", Proc. 1993 PAC, p. 3423 (1993).
- [54] J.B. Murphy and S. Krinsky, "Millimeter Wave Coherent Synchrotron Radiation in the SXLS Phase I Electron Storage Ring", *NIM A* 346, p. 571 (1994).
- [55] J.B. Murphy, S. Krinsky and R.L. Gluckstern, "Longitudinal Wakefield for Synchrotron Radiation", *Proc. 1995 Part. Acc. Conf.*, p. 2980 (1995).
- [56] Y. S. Derbenev et al., "Microbunch Radiative Tail-Head Interaction", DESY FEL Report TESLA-FEL 95-05, September 1995.
- [57] S.A. Kheifets and B. Zotter, "Coherent Synchrotron Radiation Wakefield & Impedance", *CERN 95-43* (1995).

- [58] R. Warnock and K. Bane, "Coherent Synchrotron Radiation and Stability of A Short Bunch in A Compact Storage Ring", SLAC-PUB-95-6837 (1995).
- [59] K. Bane, S. Krinsky & J.B. Murphy, "Longitudinal Potential Well Distortion Due to the Synchrotron Radiation Wakefield", *Proc. Micro Bunches Workshop*, AIP Conf. Proc. 367, p. 191 (1996).
- [60] J.B. Murphy, S. Krinsky & R.L. Gluckstern, "Longitudinal Wakefield for an Electron Moving in a Circular Orbit", *Particle Accelerators*, Vol. 57, p. 9 (1997).
- [61] E.L. Saldin et al., "On the Coherent Radiation of an Electron Bunch Moving in an Arc of a Circle", *NIM A 398*, p. 373 (1997).
- [62] R. Li, C.L. Bohn and J.J. Bisognano, "Analysis On The Steady-State Coherent Synchrotron Radiation with Strong Shielding", *Proc. 1997 PAC*, p. 1644 (1997).
- [63] R. Li, C.L. Bohn and J.J. Bisognano, "Shielded Transient Self-Interaction Of A Bunch Entering A Circle From A Straight Path", *Proc. 1997 PAC*, p. 1641 (1997).
- [64] A.R. Hight-Walker et al., *Proc. SPIE Int. Soc. Opt. Eng.* **3153**, 42 (1997).
- [65] R. Kato et al., "Suppression and Enhancement of Coherent Synchrotron Radiation in the Presence of Two Parallel Conducting Plates", *Phys.Rev. E*, Vol. 57, No. 3, p.3454 (1998).
- [66] E.L. Saldin et al., "Analytical Treatment of the Radiative Interaction of Electrons in a Bunch Passing a Bending Magnet", *NIM A 407*, p. 112 (1998).
- [67] M. Bergher, "Measurements of Spontaneous Synchrotron Oscillation in the Super ACO Storage Ring", *NIM A 395*, 259 (1997).
- [68] G.L. Carr et al., "Investigation of Coherent Emission from the NSLS VUV Ring", *Proc. 1999 Particle Accelerator Conference*, p. 134 (1999).
- [69] A. Anderson et al., "Observation of Coherent Synchrotron Radiation from a 1 mm Electron Bunch at the MAX-I Storage Ring", *Opt. Eng.* **39**, 3099 (2000).
- [70] M. Abo-Bakr et al., "Coherent mm-Radiation Experiments at the BESSY II Storage Ring", *Proc. of 7th EPAC*, p. 720 (2000).
- [71] U. Arp et al., "Spontaneous Coherent Microwave Emission and the Sawtooth Instability in a Compact Storage Ring", *Phys. Rev. ST Accel. Beams*, **4**, 054401 (2001).
- [72] G.L. Carr et al., "Observation of Coherent Synchrotron Radiation from the NSLS VUV Ring", *NIM A 463*, p. 387 (2001).
- [73] B. Podobedov et al., "Longitudinal Density Modulation Of Unstable Bunches Emitting Coherent IR", *Proc. 2001 IEEE PAC*, p. 1921 (2001).
- [74] S. Kramer and B. Podobedov, "Coherent Microwave Synchrotron Radiation in the VUV Ring", *Proc. 2002 EPAC*, p. 1523 (2002).
- [75] W.C. Barry et al., *Proc. of the 8th EPAC*, p. 656 (2002).
- [76] M. Abo-Bakr, J. Feikes, K. Holldack, and G. Wüstefeld, H.-W. Hübers, "Steady-State Far-Infrared Coherent Synchrotron Radiation detected at BESSY II", *PRL*, Vol. 88, No. 25, p. 254801-1 (2002).
- [77] J.M. Byrd, W.P. Leemans, A. Loftsdottir, B. Marcelis, M.C. Martin, W.R. McKinney, F. Sannibale, T. Scarvie and C. Steier, "Observation of Broadband Self-Amplified Spontaneous Coherent Terahertz Synchrotron Radiation in a Storage Ring", *PRL*, Vol. 89, No. 22, p. 224801-1 (2002).
- [78] M. Abo-Bakr, J. Feikes, K. Holldack, P. Kuske, W.B. Peatman, U. Schade and G. Wustefeld, H.-W. Hubers, "Brilliant, Coherent Far-Infrared (THz) Synchrotron Radiation", *PRL*, Vol. 90, No. 9, p. 094801-1 (2003).
- [79] M. Abo-Bakr et al., "Coherent Emission of Synchrotron Radiation and Longitudinal Instabilities", *Proc. 2003 IEEE PAC*, p. 3023 (2003).
- [80] M. Abo-Bakr et al., "Bunch Length Measurements At BESSY", *Proc. of the 2003 IEEE PAC*, p. 3020 (2003).
- [81] G. Stupakov and S. Heifets, "Beam Instability and Microbunching Due to Coherent Synchrotron Radiation", *Phys. Rev. ST Accel. Beams*, Vol. 5, 054402 (2002).
- [82] M. Venturini and R. Warnock, "Bursts of Coherent Synchrotron Radiation in Electron Storage Rings: A Dynamical Model", *Phys. Rev. Lett.*, **89**, 224802 (2002).

- [83] G. V. Stupakov and I. A. Kotelnikov, "Shielding and Synchrotron Radiation in Toroidal Waveguide", *Phys. Rev. ST Accel. Beams*, 6, 034401 (2003).
- [84] S. Heifets and G. Stupakov, "Nonlinear Regime of a Single Mode CSR Instability", *Proc. 2003 IEEE PAC*, p. 3135 (2003).
- [85] J. Wu et al., "Calculation of the Coherent Synchrotron Radiation Impedance from A Wiggler", *Proc. 2003 IEEE PAC*, p. 1038 (2003).
- [86] G. Stupakov, "Theory and Observations of Microbunching Instability in Electron Machines", *Proc. 2003 IEEE PAC*, p. 102 (2003).
- [87] J. Singley et al., "Measuring the Josephson Plasma Resonance in $\text{Bi}_2\text{Sr}_2\text{CaCu}_2\text{O}_8$ Using Intense Coherent THz Synchrotron Radiation", *Phys. Rev. B*, **69**, 092512 (2004).
- [88] F. Sannibale et al., "A Model Describing Stable Coherent Synchrotron Radiation in Storage Rings", *Phys. Rev. Lett.* 93, 094801 (2004).
- [89] J. Feikes, K. Holldack, P. Kuske & G. Wustefeld, "Sub-Picosecond Electron Bunches in the BESSY Storage Ring", *Proc. of EPAC 2004*, p. 1951 (2004).
- [90] J. Feikes, K. Holldack, P. Kuske & G. Wustefeld, "Compressed Electron Bunches For THz Generation Operating BESSY II In A Dedicated Low Alpha Mode", *Proc. of EPAC 2004*, p. 2287 (2004).
- [91] J.M. Byrd et al., "Coherent Infrared Radiation from the ALS Generated Via Femtosecond Laser Modulation of the Electron Beam", *Proc. of EPAC 2004*, p. 2445 (2004).
- [92] J.M. Byrd et al., "CIRCE, the Coherent Infrared Center at the ALS", *Proc. of EPAC 2004*, p. 2433 (2004).

2.2 Stable CSR in storage rings: a model

F. Sannibale, J. M. Byrd, Á. Loftsdóttir, M. Venturini, [LBNL](#)
 M. Abo-Bakr, J. Feikes, K. Holldack, P. Kuske, G. Wüstefeld, [BESSY](#)
 H.-W. Hübers, [DLR](#) - R. Warnock, [SLAC](#)
fsannibale@lbl.gov

2.2.1 Introduction

A comprehensive historical view of the work done on coherent synchrotron radiation (CSR) in storage rings is given in reference [1]. Here we want just to point out that even if the issue of CSR in storage rings was already discussed over 50 years ago, it is only recently that a considerable number of observations have been reported. In fact, intense bursts of coherent synchrotron radiation with a stochastic character were measured in the terahertz frequency range, at several synchrotron light source storage rings [2-8]. It has been shown [8-11], that this bursting emission of CSR is associated with a single bunch instability, usually referred as microbunching instability (MBI), driven by the fields of the synchrotron radiation emitted by the bunch itself.

Of remarkably different characteristics was the CSR emission observed at BESSY II in Berlin, when the storage ring was tuned into a special low momentum compaction mode [12, 13]. In fact, the emitted radiation was not the quasi-random bursting observed in the other machines, but a powerful and stable flux of broadband CSR in the terahertz range. This was an important result, because it experimentally demonstrated the concrete possibility of constructing a stable broadband source with extremely high power in the terahertz region. Since the publication of the first successful experiment using the ring as a CSR source [14], BESSY II has regular scheduled user's shifts dedicated to CSR experiments. At the present time, several other laboratories are investigating the possibility of a CSR mode of operation [15-17] and a design for a new ring optimized for CSR is at an advanced stage [18].

In what follows, we describe a model that first accounts for the BESSY II observations and then indicates that the special case of BESSY II is actually quite general and typical when relativistic electron storage rings are tuned for short bunches. The model provides a scheme for predicting and optimizing the performance of ring-based CSR sources with a stable broadband photon flux in the terahertz region of up to ~ 9 orders of magnitude larger than in existing “conventional” storage rings. Such a scheme is of interest not only for the design of new sources but also for the evaluation and optimization of the CSR performance in existing electron storage rings. The presented results are mainly based on reference [19].

2.2.2 Coherent Synchrotron Radiation Basics

Coherent synchrotron radiation occurs when the electrons in a bunch emit synchrotron radiation (SR) in phase. In an intuitive picture, in a bunched beam this happens when the bunch length is comparable to the wavelength of the radiation under observation. Because of coherence, CSR intensity is proportional to the square of the number of particles per bunch in contrast to the linear dependence of the usual incoherent radiation. Since in storage rings, the number of particles per bunch is typically big (greater than $\sim 10^6$), the potential intensity gain for a CSR source is very large. In a more quantitative description, we have for the radiated power spectrum [20, 21]:

$$\frac{dP}{d\lambda} = \frac{dp}{d\lambda} \left[N(1 - g(\lambda)) + N^2 g(\lambda) \right] \quad (1)$$

where λ is the wavelength of the radiation, p is the single particle emitted power, N is the number of particles per bunch and g is the so-called CSR form factor given by:

$$g(\lambda) = \left| \int_{-\infty}^{+\infty} n(z) e^{2\pi i \cos(\theta) z/\lambda} dz \right|^2 \quad (2)$$

where $n(z)$ is the normalized longitudinal distribution of the bunch and θ is the angle between the longitudinal direction z and the observation point. For θ equal to zero the CSR form factor is just the square of the Fourier transform of the bunch distribution. Note that, because $n(z)$ is normalized, $0 \leq g \leq 1$. Here $dp/d\lambda$ is defined to account for shielding due to the conductive vacuum chamber. The shielding effect has been studied by several authors over many years [22-27]. A salient feature is that $dp/d\lambda$ drops off abruptly for λ greater than the shielding cutoff wavelength λ_0 , which is estimated to be about $2h(h/\rho)^{1/2}$, where h is the chamber total height and ρ is the radius of curvature of the particle trajectory. The first term in Eq.(1) linear in N , is the incoherent component of the power. The second term, proportional to N^2 , represents the potentially much larger coherent component. Thus, to have significant CSR at the wavelength of interest we must have simultaneously $g(\lambda) > 1/(N-1) \sim 1/N$ and $\lambda < \lambda_0$. As an example, for the case of a Gaussian distribution, equation (2) can be analytically evaluated and the following criterion for the CSR emission for Gaussian bunches can be derived for $\theta = 0$:

$$\frac{2\pi\sigma_z}{\sqrt{\ln(N)}} < \lambda < \lambda_0 = 2h \left(\frac{h}{\rho} \right)^{1/2} \quad (3)$$

with σ_z the rms bunch length. Equation (3) presents a weak dependence on N variations and shows that in order to have CSR emission, we need short bunches and large cutoff

wavelengths. By evaluating (3) for the case of real machines, one realizes that CSR can be practically observed in the terahertz frequency range (at 1 THz, $\lambda \sim 300 \mu\text{m}$). Additionally, for most of the existing storage rings in their standard operation configuration, the bunches are usually too long and/or the vacuum chamber shielding is too strong, so that essentially no CSR can be observed. This is the reason that at BESSY II they were using a low momentum compaction lattice for shortening their bunches. But before analyzing the BESSY results, we want to do some additional consideration on the CSR form factor g .

2.2.3 CSR Form Factor for Non-Gaussian Longitudinal Distributions

We are interested in investigating the CSR form factor $g(\lambda)$ for non-Gaussian bunch distributions. Figure 1, shows g calculated for a Gaussian distribution and for the interesting cases of two more extreme distributions: rectangular and saw-tooth like. In the example, all distributions have the same rms length.

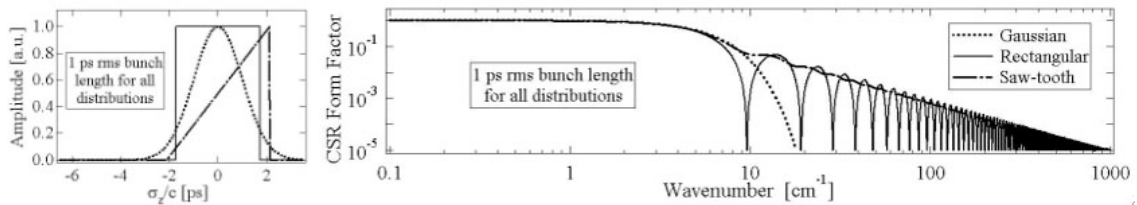


Figure 1: Gaussian, rectangular and saw-tooth like distributions and relative CSR form factors for the case of 1 ps rms bunch length. The CSR factor is expressed as a function of the wavenumber $1/\lambda$.

Figure 1 clearly shows that the two sharper edged distributions remarkably extend the CSR factor, and consequently the CSR emission, towards shorter wavelengths with respect to the Gaussian case. The saw-tooth like distribution in particular, seems to represent the “optimal” shape from the CSR point of view. The possibility of having equilibrium distributions in storage rings approaching a saw-tooth like shape is not unrealistic. As will be better discussed in the next paragraph, several factors can generate asymmetric longitudinal distributions. For example, it is well known that any beam impedance with non-zero real part (resistive component) produces asymmetric bunches with a sharper edge.

The bunch distribution in the BESSY II low momentum compaction configuration used for the CSR production, was significantly asymmetric, as proved by streak camera measurements [28] and by the fact that the extension of the high frequency part of the measured CSR spectra in [13] cannot be explained by assuming Gaussian bunches.

2.2.4 Generating Non-Gaussian Bunches

Low current equilibrium longitudinal distributions in electron storage rings are usually Gaussian. Anyway, several factors can contribute to “distort” the bunch distribution. In order to understand the BESSY II results and to eventually find a way to generate saw-tooth like distributions in a storage ring, we need to consider all such factors and evaluate their relative importance. We can classify them into two main categories: nonlinear dynamics and collective effects. Radio frequency (RF) and lattice nonlinearities belong to the first group, while SR and conductive vacuum chamber wakefields fall into the second one.

2.2.4.1 *Nonlinear Dynamics Effects*

For most storage rings RF nonlinearities are very small and can be neglected. The situation can be different when the storage ring includes a higher harmonic RF system. Such systems are specifically designed to modify the bunch distribution and their effect must be accounted for. At BESSY II, there is a higher harmonic system but it is passive and at the very low currents of the CSR mode of operation (few tens of $\mu\text{A}/\text{bunch}$) its effect is negligible.

We want now to investigate the case of strong lattice nonlinearities. As explained earlier, short bunches are preferred for producing CSR and a typical way to shorten the bunch is by lowering the storage ring momentum compaction. Anyway, for very small momentum compaction values (smaller than $\sim 10^{-5}$), as the ones used in the BESSY II CSR lattice, the energy dependent terms of the momentum compaction can become important and generate strong distortions of the orbits in the longitudinal phase space. Such a situation can potentially lead to non-Gaussian equilibrium distributions. We have done extensive simulations using the BESSY II parameters and also investigating the case of extremely distorted longitudinal phase space topologies. The clear result was that lattice nonlinearities can generate significant distortions in the energy distribution of the bunch but very small distortions of the spatial distribution.

2.2.4.2 *Collective Effects*

In the analysis of the collective effects we start first with the wakes due to the SR in a bending magnet, and later consider the ones associated with the vacuum chamber. A large number of storage rings have insertion devices (ID) but in our analysis we will not consider their SR wakes. In a ring with IDs, this is the equivalent of assuming that the ID gaps are open (as they were during the BESSY II CSR measurements). Analytical expressions for the SR radiation wake in a wiggler have been derived [29] and could be used for further investigation.

For the SR wake in the bends, we use the analytical expressions where the vacuum chamber shielding is represented by the parallel plates model [22-27]. In “standard” wakes, the fields excited in the vacuum chamber by the particles in the head of the bunch can only affect the particles in the tail. In the SR radiation wake case, it is exactly the opposite, the particles in the tail modify the energy of the ones in the head. This happens when a relativistic electron in a bunch is traveling on a curved trajectory radiating SR. Contrarily to the electron, the emitted photons proceed on a straight line and because of this, the electron velocity component parallel to the photon trajectory is smaller than the photon speed. This allows for a photon emitted in the tail of the bunch to reach the electrons in the head and to interact with them.

To find the equilibrium longitudinal bunch distribution in the presence of wakes we use the well-known Haïssinski equation [30]:

$$I(\tau) = K \exp \left[-\frac{(c\tau)^2}{2\sigma_{z0}^2} - \frac{c^2}{\sigma_{z0}^2 \dot{V}_{RF}} \int_{-\infty}^{\infty} I(\tau-t)S(t)dt \right] \quad (4)$$

where $I(\tau)$ is the longitudinal current distribution, τ is position of the particle in the bunch in time units, c is the speed of light, σ_{z0} is the natural bunch length, \dot{V}_{RF} is the

time derivative of the radio frequency voltage at the synchronous phase, K is a normalization constant and $S(t)$ is the wake in the step response form:

$$S(t) = \frac{2\pi\rho}{e} \int_{-\infty}^t E_w(t') dt' \quad (5)$$

with e the electron charge and E_w the electric field associated to the wake under consideration. The integration limits in Eq. (4) and Eq. (5) are for the general case of wakes with nonzero values in front and behind the generating particle (combination of vacuum chamber and SR wakes).

Figure 2 shows the numerical solutions of equation (4) for the case of BESSY II for different currents per bunch and using the shielded SR wake. The results show several interesting features: with growing current per bunch, the distribution leans forward with an increasingly sharp leading edge, the bunch rear becomes less steep, the bunch centroid shifts to earlier times (synchronous phase shift) and the rms length of the distribution increases but only slightly. It is worth noticing that the calculated distributions clearly lean towards the CSR ideal saw-tooth like shape. The ‘‘hump’’ on the highest current curve is due to the shielding effect of the vacuum chamber.

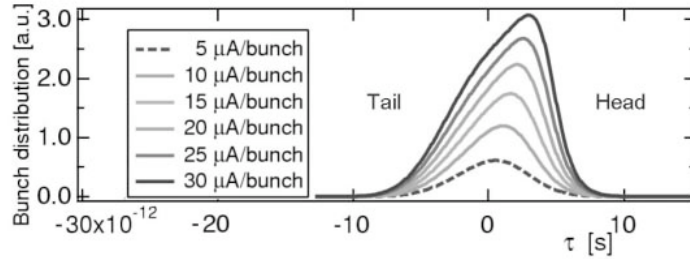


Figure 2: Calculated equilibrium distributions using the shielded SR wake. Case of the BESSY II in the configuration for CSR production.

For a quantitative comparison with the BESSY results, we define for a given current and wavenumber ($1/\lambda$), the CSR gain as the ratio between the radiation intensities when CSR is present and when the emission is completely incoherent. This new quantity has the big advantage with respect to the absolute flux, that it is independent of the calibration of the measurement system. Its value approaches 1 when the CSR emission is very small ($g \sim 0$) and N when it is large ($g \sim 1$). Figure 3 shows the CSR gain measured at BESSY II [13] and the calculated distributions as a function of the radiation wavenumber for two different currents per bunch. Also shown is the calculated CSR gain for the undistorted Gaussian distribution. The shaded areas represent the shielded SR calculations obtained by varying the natural bunch length over a 10% range. This choice can be explained as follows. The natural bunch length used as input parameter for the simulations was derived from measurements of the synchrotron frequency, of the RF voltage and of other machine quantities. The experimental error for this evaluation is consistent with a 10% uncertainty.

The comparison in Fig. 3 shows the general good agreement between calculations and data and also the strong power enhancement at the higher wavenumbers that the distorted case presents with respect to the Gaussian one. In Ref. [13] a 40 μA curve is also shown, but the data are unusable for comparison because of the presence of CSR bursting, this current being above MBI threshold [8-11].

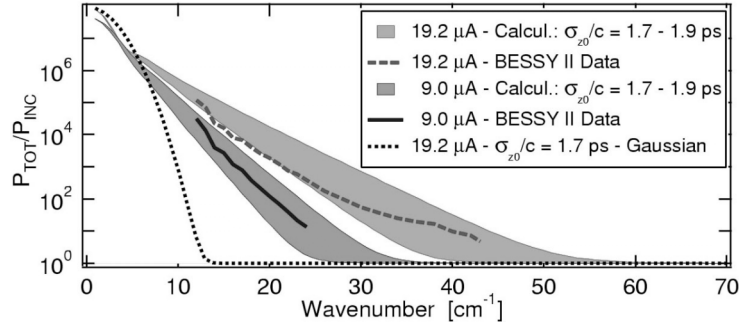


Figure 3: CSR gain as a function of the wavenumber. The BESSY II data for two different currents per bunch are compared with the shielded SR calculation and with the curve for a Gaussian distribution of the same length.

We will now introduce in our analysis the vacuum chamber wakes starting with the resistive wall (RW) one [31, 32]. The nonzero resistivity of the storage ring vacuum chamber is responsible for this wake that, when strong enough, can produce equilibrium bunch distributions with the saw-tooth like shape similar to the SR wake case. In our calculations, the long-range approximation for the RW wake was used, being appropriate for the BESSY II case. Figure 4 shows, for a particular case of BESSY II, the comparison between the CSR gain curves calculated using the shielded SR wake with (dotted line) and without (dashed line) the inclusion of the RW wake. The effect of the RW wake is clearly very small and slightly decreases the CSR gain.

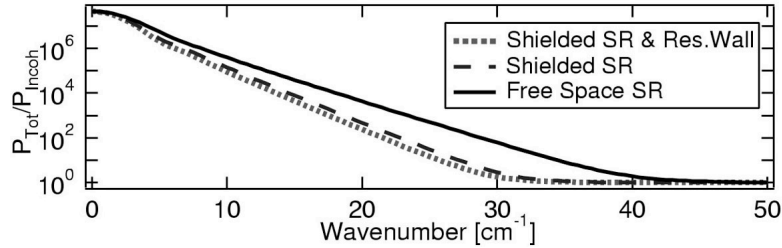


Figure 4: CSR gain vs. radiation wavenumber calculated using the shielded SR wake with (dotted line) and without (dashed line) the resistive wall wake. The solid line shows the gain calculated with the free space SR wake. Case of BESSY II with 9.0 μA per bunch and 1.7 ps natural bunch length.

It is somehow surprising that the RW wake decreases the CSR gain. In fact, by producing the same kind of distortion of the SR wake, one would expect an increase in the CSR gain. The explanation is that the RW generates at the same time a significant bunch lengthening, which reduces the CSR emission at shorter wavelengths. This second effect is stronger than the distortion enhancement and the net result is a decrease of the CSR gain. Additional calculations using different models for the BESSY II vacuum chamber broadband impedance showed a negligible contribution from this kind of wake at these low current-short bunches conditions.

2.2.5 The Free Space SR Wake Regime

The solid line in Fig. 4 shows the CSR gain calculated using the free space (FS) SR wake [25, 26] for the interesting case where the vacuum chamber shielding is negligible. Compared to the FS case, the vacuum chamber shielding reduces the gain significantly,

pointing out the important result that for maximizing the CSR gain in an optimized source the shielding effect must be kept negligible.

For the case of the parallel plates model and Gaussian bunches, a simple criterion for the shielding importance is given by [25]:

$$\Sigma = \frac{\sigma_z}{h} \left(\frac{2\rho}{h} \right)^{1/2} \leq 0.2 \quad (6)$$

If Eq. (6) is fulfilled, then the shielding effect is negligible and the FS SR wake can be used (note that $\Sigma \propto \sigma_z/\lambda_0$). Two examples: in the case of BESSY II with $\sigma_z \sim 1$ mm, $\rho = 4.35$ m and $h = 3.5$ cm, $\Sigma \sim 0.45$ and the shielding effect is relevant, while in a hypothetical but realistic CSR source with $\sigma_z = 300$ μm , $h = 4$ cm and $\rho = 1.33$ m, $\Sigma \sim 0.06$ and the shielding is negligible. Summarizing, we have seen that it is possible to design a realistic storage ring where the shielding effects are negligible. Additionally, by using for the vacuum chamber a low resistivity material, aluminum for example, we will be able to control the effects of the RW wake down to negligible levels as well. We also showed that in this situation, the FS SR wake becomes dominant and the CSR emission is maximized. We need now to understand how to exploit this situation for the optimization of a CSR source quantitatively. The FS SR wake, in the step response shape, can be expressed with very good approximation as [25-27]:

$$S(\tau) \equiv \begin{cases} -Z_0 \left(\frac{\rho}{3c} \right)^{1/3} \tau^{-1/3} & \tau > 0 \\ 0 & \tau \leq 0 \end{cases} \quad (7)$$

with $Z_0 = \mu_0 c = 376.7 \Omega$.

Figure 5 shows an example of equilibrium bunch distributions obtained by solving the Haïssinski equation using the wake (7) for positive momentum compaction. Again, as in the shielded case of Fig. 2, the asymmetry increases with current but now, at the higher currents, the hump is disappeared and the curves are really close to the ideal saw-tooth like shape.

Based on this result, one could think that for maximizing the CSR emission, it is sufficient to keep increasing the current per bunch. Unfortunately, there is a limit and this is set by the MBI, the same instability responsible for the CSR burst mentioned in the introduction.

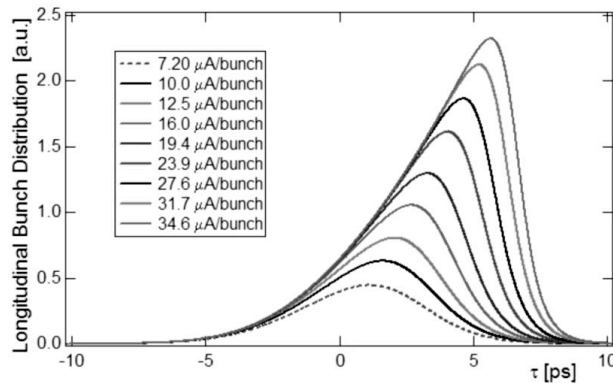


Figure 5: Example of calculated bunch distributions for the case of the free space SR wake and positive momentum compaction.

2.2.6 The Microbunching Instability

We discuss now the case of the MBI that can be excited by the SR radiation wake in the bends of electron storage rings [8-11]. Fluctuations in the longitudinal bunch distribution, with characteristic length shorter than the bunch length, can radiate coherently. Above a current per bunch threshold, the SR emission becomes strong enough to enhance these longitudinal fluctuations, triggering a chain effect leading to microbunching and instability. The appearance of such microstructures is associated with the emission of burst of CSR in the terahertz frequency range. Indicating with N_{MBI} the threshold, a stability criterion for the MBI can be expressed as [8-10]:

$$N \leq N_{MBI} = A \left(\frac{B}{E} \right)^{1/3} f_{RF} V_{RF} \frac{\sigma_{z0}^3}{\lambda^{2/3}} \quad (8)$$

with $A = \left(\frac{1}{2} \pi^{7/6} e^{4/3} / r_0 m_0 c^{8/3} \right) = 4.528 \times 10^{-3}$ [SI units], r_0 the electron classical radius, m_0 its rest mass, B the magnetic field in the bend magnet, f_{RF} and V_{RF} the frequency and the peak voltage of the RF system respectively and E the beam energy.

For the large majority of the experiments using terahertz radiation, stability of the photon flux is a fundamental requirement. In a storage ring, the MBI with its terahertz bursts can seriously jeopardize the performance as a CSR source if not controlled.

In the next paragraph, we describe a scheme that allows to adjust the parameters of a ring such that the CSR power and bandwidth are maximized while remaining below the threshold for the MBI.

2.2.7 On Optimized Stable CSR Source Based on a Storage Ring

Assuming that criterion (6) is fulfilled and that all the other wakes are negligible, we can use the FS SR wake and following the approach used in ref. [33] we express the bunch population N as:

$$N = \frac{1}{ec^2 Z_0} \left(\frac{3}{\rho} \right)^{1/3} \dot{V}_{RF} \sigma_{z0}^{7/3} F(\kappa) \quad (9)$$

The numerical factor $F(\kappa) = \int_{-\infty}^{\infty} y_{\kappa}(x) dx$ is the integral of the solution of the equilibrium equation:

$$y_{\kappa}(x) = \kappa \exp \left[-\frac{x^2}{2} + \text{sgn}(\alpha) \int_0^{\infty} y_{\kappa}(x-z) z^{-1/3} dz \right] \quad (10)$$

which is a dimensionless form of the Haïssinski equation (4) for the special case of the FS SR wake (7), with $x = c\tau/\sigma_{z0}$ and $y_{\kappa} = (Z_0 c / \dot{V}_{RF}) \left(\rho / 3\sigma_{z0}^4 \right)^{1/3} I$. The factor $\text{sgn}(\alpha)$ is the sign of the momentum compaction α . The quantity F depends only on the dimensionless normalization parameter κ . As κ increases, F , N , and the bunch distortion all increase. F can be thought as a quantitative indication of the bunch distortion: the

larger F the larger the distortion and, for what we have shown in the previous paragraphs, the more extended is the CSR spectrum.

For a linear RF system at the synchronous phase, $\dot{V}_{RF} = 2\pi f_{RF} V_{RF}$ and for a relativistic electron storage ring, $\rho = E/ecB$, which used in (9) give:

$$N = C \left(\frac{B}{E} \right)^{1/3} f_{RF} V_{RF} \sigma_{z0}^{7/3} F(\kappa) \quad (11)$$

with $C = (2\pi/Z_0) \left(\frac{3}{e^2 c^5} \right)^{1/3} = 6.068 \times 10^{-4}$ [SI units].

The expression for $dp/d\lambda$ when the wavelength is shorter than λ_0 but much larger than the SR critical wavelength, is given by [31]:

$$\frac{dp}{d\lambda} = \left(\frac{2^{10} \pi^7 c^8}{3e} \right)^{1/3} \frac{r_0 m_0}{\Gamma(1/3) L} \left(\frac{E}{B} \right)^{1/3} \frac{1}{\lambda^{7/3}} \quad (12)$$

with L the ring length and with the gamma function $\Gamma(1/3) \sim 2.679$, By using Eq. (11), Eq. (12) in Eq. (1) for $Ng(\lambda) \gg 1$, we can write the power spectrum for a ring with N_b bunches as:

$$\frac{dP}{d\lambda} = D \frac{N_b}{L} (f_{RF} V_{RF})^2 \left(\frac{B}{E} \right)^{1/3} \left(\frac{\sigma_{z0}^2}{\lambda} \right)^{7/3} F(\kappa)^2 g(\lambda) \quad (13)$$

with $D = \left(\frac{2^{16} 3 \pi^{13}}{e^5 c^2} \right)^{1/3} \left(r_0 m_0 / Z_0^2 \Gamma(1/3) \right) = 2.642 \times 10^{-21}$ [SI units].

To optimize the intensity and spectral bandwidth given by (13) we must first be sure that our distribution is stable. Or in other words, that the bunch population is maintained below the threshold for the MBI. By combining Eq. (8) and Eq. (11), the following stability criterion is obtained:

$$F \leq F_{\max} = G \left(\sigma_{z0} / \lambda \right)^{2/3} \quad (14)$$

where $G = \left(\frac{2^{3/2} \pi^{7/6}}{3^{1/3}} \right) \approx 7.456$ is a dimensionless constant. It must be remarked that the MBI theory was derived for the case of a coasting beam. Anyway, simulations and experimental results at the Advanced Light Source (ALS) in Berkeley and at BESSY II [10, 11] showed that the model works also for bunched beams and that the theory is able to predict the instability threshold when in Eq. (8) $\lambda \sim \sigma_{z0}$. By (14) the corresponding threshold for F becomes:

$$F \leq F_{\max} \approx G \quad (15)$$

The value of κ for maximum F is obtained by solving (10), increasing κ to a value κ_{\max} (~ 0.292 , for the positive momentum compaction case) such that $F(\kappa_{\max}) = G$.

Now let us examine the terms of Eq. (13) with more attention. Expressing the CSR form factor g (Eq. (2)) in terms of y_κ , we find for $\theta = 0$:

$$g(\lambda) = \frac{1}{F(\kappa)^2} \left| \int_{-\infty}^{\infty} y_\kappa(x) e^{i2\pi \frac{\sigma_{z0}}{\lambda} x} dx \right|^2 \quad (16)$$

Eq. (16) shows that, in the case of the FS SR wake, $g(\lambda)$ is a function only of the ratio σ_{z0}/λ and of κ . It is interesting to notice that for large λ values, the integral in Eq. (16) tends to F so that g tends to 1. Figure 6 shows $y_{\kappa_{max}}(x)$ and Eq. (16) for positive momentum compaction and for the CSR optimized case when $\kappa = \kappa_{max}$.

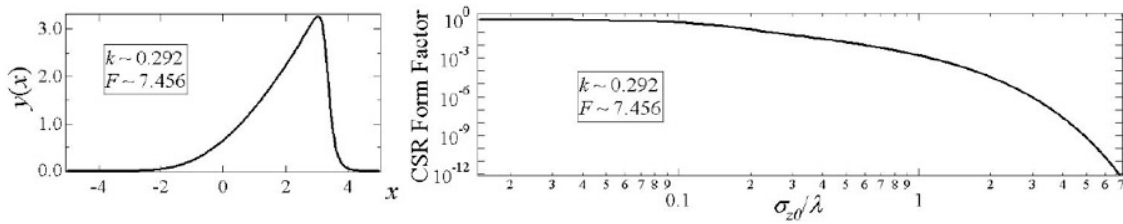


Figure 6. The “universal” distribution $y_{\kappa_{max}}$ and CSR form factor for the case of the FS SR wake, calculated for $\kappa = \kappa_{max}$ and positive momentum compaction.

The curve in the right part of Fig.6 allows calculating the CSR form factor of the optimized source, by knowing only the natural bunch length σ_{z0} , while the curve on the left defines the bunch distribution when σ_{z0} and N are known. N is simply given by (11) with F replaced by G . The CSR spectrum for our stable optimized source is now completely defined and can be evaluated by using Eq. (1).

We want now to choose our parameters in order to maximize the CSR bandwidth and power. Eq. (16) shows that, for a fixed κ (κ_{max} in our case), the spectrum extends to larger wave numbers as σ_{z0} is decreased. On the other hand, the factor $\sigma_{z0}^{14/3}$ in Eq. (13) sharply degrades the overall intensity if σ_{z0} is too small. By an appropriate compromise in the choice of σ_{z0} we get a suitable spectral bandwidth.

Once that choice is made and we have set $F = G$ in Eq. (13), we can still vary the other factors in this equation to maximize radiation intensity while respecting technical constraints. Explicitly, Eq. (13) asks for i) a large peak RF voltage V_{RF} , this can be obtained by superconductive systems but of course with increased costs; ii) a high bending magnet magnetic field B , but the same arguments used for V_{RF} apply also here; iii) a high f_{RF} , but for example, availability of high frequency systems, coupled bunches instabilities and cavities aperture could become an issue; iv) a lower beam energy E , but the decreased stiffness and the weaker damping could represent a problem from the accelerator physics point of view; v) a small L , which will make the ring more compact and less expensive, but on the other hand a longer ring serves more users and the presence of reasonably long straight sections can allow for insertion devices and for several possible interesting applications and upgrades [18].

It must be remarked that the momentum compaction, which does not appear explicitly in Eq. (13), is used in this scheme for keeping constant σ_{z0} when the other quantities are varied.

Figure 7 shows an example of the impressive performance that a source designed with the presented criteria can achieve. In this particular combination of the Eq. (13) parameters, three modes of operation, trading between power and bandwidth, are plotted and can be selected with continuity by simply tuning the lattice momentum compaction from 4.3×10^{-4} to 3.9×10^{-3} . Also shown for comparison are the curves for a “conventional” SR source (the ALS) and for BESSY II in the special CSR mode.

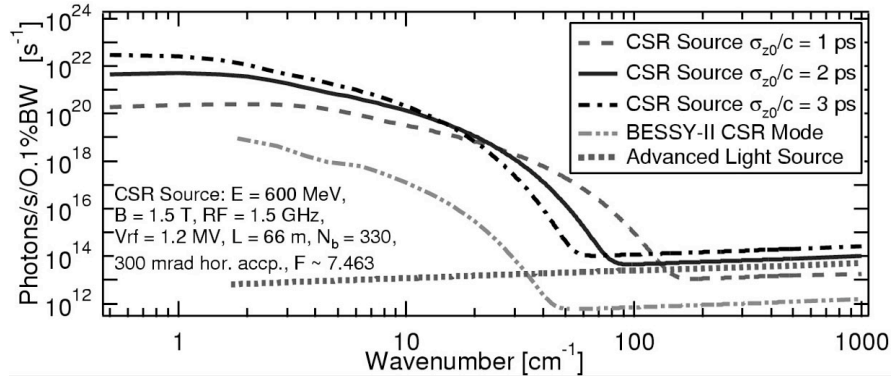


Figure 7. Example of source optimized for the CSR production using the criteria described in this paper. The photon flux is compared with the cases of a conventional SR source (ALS) and of BESSY II CSR mode with 400 bunches, $19.2 \mu\text{A}/\text{bunch}$, $\sigma_{z0}/c = 1.8 \text{ ps}$ and 60 mrad horizontal acceptance.

Criterion (15), when used in Eq. (11) with a given σ_{z0} , sets the threshold for the single bunch current that can be stored without experiencing the MBI. The strong dependence of this threshold on σ_{z0} explains why the SR wake becomes dominant in the short bunch regime, making the longitudinal dynamics practically independent from the vacuum chamber wakes. This result has the quite general implication that very short and stable bunches can be obtained only at the cost of very small currents per bunch. For example, in our hypothetical CSR source of Fig. 7, in order to go from σ_{z0} equal to 3 ps to 1 ps , the current per bunch must drop from $\sim 1.2 \text{ mA}$ to $\sim 90 \mu\text{A}$ to preserve stability.

We have analyzed only the case for positive momentum compaction. For negative values of this parameter, the situation is similar but not completely identical. For example, as shown in [33], a comparable saw-tooth distortion of the distribution is obtained but also some simultaneous bunch lengthening. This does not seem to be promising from the CSR point of view but for an accurate answer a complete analysis is necessary.

Equation (9) shows that N is proportional to the time derivative of the RF voltage. For simplicity, in our analysis we have assumed a single RF system with frequency f_{RF} . In the more general case, we could have the simultaneous presence of different systems with different frequencies. In particular, as suggested in [35], it could be interesting to study the case where an additional higher harmonic RF system is used for increasing the absolute value of the RF voltage derivative at the synchronous phase.

2.2.8 Conclusions

We have presented a model that describes CSR in electron storage rings. We used it for explaining the observations at BESSY II and for developing ring based sources optimized for the CSR generation in the terahertz frequency range, with photon flux up to 9 orders of magnitude larger than in existing conventional storage rings. In particular, it has been shown that the CSR performance is maximized when the vacuum chamber shielding is negligible and the synchrotron radiation wake dominates over the vacuum chamber ones. Stability criteria for controlling the synchrotron radiation induced microbunching instability were included as well, in order to generate a stable flux of CSR as required from most terahertz applications. The model can be also used for predicting the CSR possibilities for existing storage rings.

A quite general result of our analysis is that for storage rings in the short bunches regime (~ 1 ps), the synchrotron radiation wake becomes dominant determining alone the longitudinal dynamics of the bunch. In this situation, the intensity of the wake becomes so intense that the induced microbunching instability severely limits the maximum stable current per bunch to very low values.

Finally, we want to remark that the CSR enhancement at shorter wavelengths due to SR induced bunch distortions was first mentioned in Ref. [33].

2.2.9 Acknowledgements

We acknowledge contributions of M. C. Martin, D. Robin, E. Forest, J. Murphy, and U. Schade. This work was supported by the Director, Office of Science, U.S. Department of Energy under Contracts No. DE-AC03-76SF00098 and No. DE-AC03-76SF00515.

2.2.10 References

- [1] J.B. Murphy, this newsletter.
- [2] A.R. High-Walker, *et al.*, Proc. SPIE Int. Soc. Opt. Eng. **3153**, 42 (1997).
- [3] M. Berger, Nucl. Instrum. Methods Phys. Res. Sect. A **395**, 259 (1997).
- [4] G.L. Carr, *et al.*, Proceeding of the 1999 IEEE Particle Accelerator Conference, New York, NY, March 1999, p. 134, and Nucl. Instrum. Methods Phys. Res. Sect. A **463**, 387 (2001).
- [5] Å. Anderson, *et al.*, Opt. Eng. (Bellingham, Wash.) **39**, 3099 (2000).
- [6] M. Abo-Bakr, *et al.*, Proceedings of the 7th European Particle Accelerator Conference, Vienna, 2000, p. 720.
- [7] U. Arp, *et al.*, Phys. Rev. ST Accel. Beams **4**, 054401 (2001).
- [8] J. M. Byrd, *et al.*, Phys. Rev. Lett. **89**, 224801 (2002).
- [9] S. Heifets and G. Stupakov, Phys. Rev. ST Accel. Beams **5**, 054402 (2002).
- [10] M. Venturini and R. Warnock, Phys. Rev. Lett. **89**, 224802 (2002).
- [11] M. Abo-Bakr, *et al.*, Proceeding of the 2003 IEEE Particle Accelerator Conference, Portland, OR, 2003, p. 3023.
- [12] M. Abo-Bakr, *et al.*, Phys. Rev. Lett. **88**, 254801 (2002).
- [13] M. Abo-Bakr, *et al.*, Phys. Rev. Lett. **90**, 094801 (2003).
- [14] J. Singley, *et al.*, Phys. Rev. B. **69**, 092512 (2004).
- [15] C. Biscari, *et al.*, DAΦNE Technical Note G-61, July 28, 2004.
- [16] The Metrology Light Source of the Physikalisch-Technische Bundesanstalt under construction in Berlin-Adlershof (Germany).

- [17] ESRF, Grenoble, France, this newsletter.
- [18] J.M. Byrd, *et al.*, Proceedings of the 9th European Particle Accelerator Conference, Lucerne, 2004, p. 2433.
- [19] F. Sannibale, *et al.*, Phys. Rev. Lett. **93**, 094801 (2004).
- [20] L.I. Shift, Rev. Sci. Instr. **17**, 6 (1946).
- [21] G. Williams, *et al.*, Phys. Rev. Lett. **62**, 261 (1989).
- [22] J. Schwinger, Phys. Rev. **70**, 798 (1946) and LBNL-39088 (1966).
- [23] J. S. Nodvick and D. S. Saxon, Phys. Rev. **96**, 180 (1954)
- [24] R. Warnock and P. Morton, Part. Accel. **25**, 113 (1990).
- [25] J.B. Murphy, S. Krinsky and R. L. Gluckstern, Proceeding of the 1995 IEEE Particle Accelerator Conference, Dallas, TX, May 1995, p. 2980 and Part. Accel. **57**, 9 (1997).
- [26] Y. S. Derbenev, *et al.*, DESY Report No. TESLA-FEL 95-05, 1995.
- [27] G. Stupakov and I. Kotelnikov, Phys. Rev. ST Accel. Beams **6**, 034401 (2003).
- [28] M. Abo-Bakr, *et al.*, Proceeding of the 2003 IEEE Particle Accelerator Conference, Portland, OR, 2003, p. 3020.
- [29] J. Wu, *et al.*, Phys. Rev. ST Accel. Beams **6**, 040701 (2003).
- [30] J. Haïssinski, Il Nuovo Cimento **18B**, 72 (1973).
- [31] A. W. Chao, *Physics of Collective Beam Instabilities in High Energy Accelerators* (Wiley, New York, 1993).
- [32] K. Bane and M. Sands, in *Micro-Bunches Workshop, Upton, NY, 1995*, edited by E. B. Blum *et al.*, AIP Conf. Proc. No. 367 (AIP, New York, 1996), p. 131.
- [33] K. Bane, S. Krinsky, and J. B. Murphy, in *Micro-Bunches Workshop, Upton, NY, 1995*, edited by E. B. Blum *et al.*, AIP Conf. Proc. No. 367 (AIP, New York, 1996), p.191.
- [34] A. Hofmann, in “*Synchrotron Radiation and Free Electron Lasers*”, CERN Report No. CAS-CERN-98-04, 1998, p. 1.
- [35] J. Feikes, *et al.*, Proceedings of the 9th European Particle Accelerator Conference, Lucerne, 2004, p. 1951.

2.3 Microbunch Instability Theory and Simulations

G. Stupakov and R. Warnock, [SLAC
stupakov@slac.stanford.edu](http://www.slac.stanford.edu/~stupakov)

2.3.1 Introduction

Over the last years there have been several reports of quasiperiodic bursts of coherent synchrotron radiation (CSR) in electron rings in the microwave and far-infrared range. The observations were made on synchrotron radiation light sources, which include the Synchrotron Ultraviolet Radiation Facility SURF II [1], the VUV ring at the National Synchrotron Light Source at BNL [2,3], second-generation light sources MAX-I [4], BESSY II [5], and ALS [6]. General features of those observations can be summarized as follows. Above a threshold current, there is a strongly increased radiation of the beam in the range of wavelengths shorter than the bunch length. At large currents, this radiation is observed as a sequence of random bursts. In the bursting regime, intensity of the radiation scales approximately as square of the number of particles in the bunch, indicating a coherent nature of the phenomenon.

It is generally accepted that the source of this radiation is related to the microbunching of the beam arising from development of a microwave instability caused

by the coherent synchrotron radiation of the beam. A relativistic electron beam moving in a circular orbit in free space can radiate coherently if the wavelength of the synchrotron radiation exceeds the length of the bunch. In accelerators coherent radiation of the bunch is usually suppressed by the shielding effect of the conducting walls of the vacuum chamber [7,8,9], which gives an exponential cutoff of wavelengths greater than a certain threshold. However, an initial density fluctuation with a characteristic length much shorter than the shielding threshold would radiate coherently. If the radiation reaction force is such that it results in the growth of the initial fluctuation one can expect an instability that leads to micro-bunching of the beam and an increased coherent radiation at short wavelengths. A possibility of CSR instability was pointed out in Refs. [10,11].

2.3.2 Properties of CSR

In application to the CSR instability, we are interested in the synchrotron radiation at wavelengths of the order of a size of microbunches, with a frequency ω typically well below the critical frequency for the synchrotron radiation. For an ultrarelativistic particle with the Lorentz factor $\gamma \gg 1$, in this range of frequencies, the spectrum of the radiation $dP/d\omega$ (per unit length of path) can be written as

$$\frac{dP}{d\omega} = \frac{3^{1/6}}{\pi} \Gamma\left(\frac{2}{3}\right) \left(\frac{\omega}{\omega_H}\right)^{1/3} \frac{e^2 \omega_H}{c^2}, \quad (1)$$

where $\omega_H = eB/(\gamma mc)$, with B the magnetic field, e the electron charge, m the electron mass, c the speed of light, and Γ the gamma-function. The characteristic angular spread θ of the radiation with reduced wavelength $\tilde{\lambda}$ (where $\tilde{\lambda} = c/\omega = 1/k$) is of order of $\theta \sim (\tilde{\lambda}/R)^{1/3}$, where R is the bending radius, $R = c/\omega_H$. Another important characteristic of the radiation is the formation length l_f : $l_f \sim \tilde{\lambda}/\theta^2 \sim (\tilde{\lambda}R^2)^{1/3}$ —this is the length after which the electromagnetic field of the particle moving in a circular orbit “disconnects” from the source and freely propagates away. In a vacuum chamber with perfectly conducting walls, whether this “disconnection” actually occurs depends on another parameter, often called the “transverse coherence size”, l_\perp . An estimate for l_\perp is: $l_\perp \sim l_f \theta \sim \tilde{\lambda}/\theta \sim (\tilde{\lambda}^2 R)^{1/3}$. One of the physical meanings of l_\perp is that it is equal to the minimal spot size to which the radiation can be focused. Another meaning of this parameter is that it defines a scale for radiation coherence in the transverse direction. Electrons in a transverse cross section of a bunch of size σ_\perp would radiate coherently only if $\sigma_\perp \leq l_\perp$. We emphasize here that both parameters, l_\perp and l_f , are functions of frequency, with the scalings $l_\perp \propto \omega^{-3/2}$ and $l_f \propto \omega^{-1/2}$.

Closely related to the transverse coherence size is the shielding of the radiation by conducting walls: if the walls are closer than l_\perp to the beam, the field lines during circular motion close onto the conducting walls, rather than disconnect from the charge. This means that the radiation at the wavelengths where $l_\perp \geq a$, where a is the pipe radius, is suppressed, or shielded.

For a bunch with N electrons, the radiation of each electron interferes with others. Assuming full transverse coherence (a one dimensional model of the beam), the total radiation of the bunch is [12]:

$$\left. \frac{dP}{d\omega} \right|_{\text{bunch}} = \frac{dP}{d\omega} N \left(1 + N |\hat{f}(\omega)|^2 \right), \quad (2)$$

where $\hat{f}(\omega) = \int_{-\infty}^{\infty} dz f(z) e^{i\omega z/c}$ is the Fourier transform of the longitudinal distribution function of the beam $f(z)$ (normalized by $\int_{-\infty}^{\infty} f(z) dz = 1$). The first term on the right hand side of Eq. (2) is due to incoherent, and the second one – to coherent radiation. For a smooth distribution function (e.g., Gaussian, with rms bunch length σ_z), the Fourier image $\hat{f}(\omega)$ vanishes for $\lambda \leq \sigma_z$, and the radiation is incoherent. However, beam density modulation with $\lambda \leq \sigma_z$ would contribute to $\hat{f}(c/\lambda)$ and result in coherent radiation, if the amplitude of the perturbation is such that $|\hat{f}(c/\lambda)| \geq N^{-1/2}$.

2.3.3 Radiation Reaction Force—CSR wake field

The collective force acting on the beam due to its coherent synchrotron radiation is described in terms of the so called CSR longitudinal wake [13,14,15]. For an ultrarelativistic particle, in one-dimensional approximation, this wake (per unit length of path) is given by the following formula:

$$w(z) = -\frac{2}{3^{4/3} R^{2/3} z^{4/3}}. \quad (3)$$

The wake is valid for distances z such that $R \gg z \gg R/\gamma^3$ —a general behavior of the wake function including also distances $z \sim R/\gamma^3$ is shown in Fig. 1.

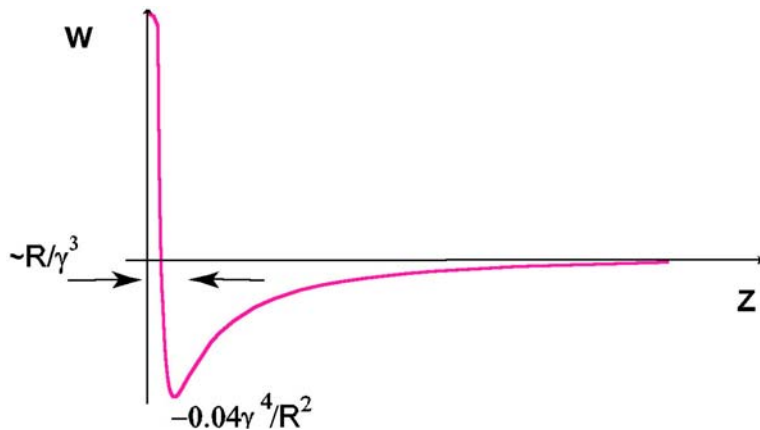


Figure 1: CSR wake as a function of distance. A simple formula (3) is applicable for not very short distances, to the right of the minimum of the wake. The wake reaches minimum at $z \sim R/\gamma^3$, with the minimum value of $-0.04\gamma^4/R^2$.

The wake is localized in front of the particle in contrast to “traditional” wakes in accelerator physics which trail the source charge [16]. This is explained by the fact that the charge follows a circular orbit and the radiation propagates along chords getting ahead of the source. The wake given by Eq. (3) has a strong singularity at $z \rightarrow 0$. In calculations, this singularity is eliminated by integration by parts and using the fact that the area under the curve $w(z)$ is equal to zero.

A simple wake Eq. (3) assumes a small transverse beam size [15], $\sigma_{\perp} \leq l_{\perp} \sim (\hat{\lambda}^2 R)^{1/3}$, and neglects the shielding effect of the conducting walls. It is valid only for long enough magnets, $l_{magnet} \gg l_f$, when transient effects at the entrance to and exit from the magnet can be neglected. A detailed study of transient effects in a short magnet can be found in Refs. [17,18].

Using the wake field Eq. (3) one can calculate the CSR longitudinal impedance Z :

$$Z(k) = \frac{1}{c} \int_0^{\infty} dz w(z) e^{-ikz} = \frac{2}{3^{1/3}} \Gamma\left(\frac{2}{3}\right) e^{i\pi/6} \frac{k^{1/3}}{cR^{2/3}} . \quad (4)$$

The real part of this impedance is related to the spectrum of the energy loss of a charge due to radiation: $dP/d\omega = (e^2/\pi) \text{Re} Z$, see Eq. (1). Plots of a CSR wake for a Gaussian bunch can be found in Refs. [14,15].

2.3.4 CSR Instability

Due to the CSR wake, an initial small density perturbation δn induces energy modulation in the beam δE . A finite momentum compaction factor of the ring converts δE into a density modulation. At the same time, the energy spread of the beam tends to smear out the initial density perturbation. Under certain conditions, which depend on the beam current, energy spread, and the wavelength of the modulation, the process can lead to an exponential growth of the perturbation.

A quantitative description of the instability can be obtained if we assume that the wavelength of the perturbation is much shorter than the bunch length, $\hat{\lambda} \ll \sigma_z$, and use a coasting beam approximation. In this case, the dispersion relation for the frequency ω is given by the Keil-Schnell formula [19]:

$$\frac{inr_0 c^2 Z(k)}{\gamma} \int_{-\infty}^{\infty} \frac{d\delta (df/d\delta)}{\omega + ck\eta\delta} = 1, \quad (5)$$

where n is the number of particles per unit length, η is the momentum compaction factor of the ring, $r_0 = e^2/mc^2$, $Z(k)$ is the CSR impedance given by Eq. (4), $f(\delta)$ is the energy distribution function normalized so that $\int f(\delta) d\delta = 1$. To take into account straight sections in the ring, where $R = \infty$ and there is no CSR wake, Z is replaced with a weighted impedance: $Z \rightarrow ZR/\langle R \rangle$, where $\langle R \rangle = C/2\pi$.

The plot of $\text{Re } \omega$ and $\text{Im } \omega$ calculated from Eq. (5) for a Gaussian energy distribution with an rms relative energy spread δ_0 , and $\eta > 0$ is shown in Fig. 2.

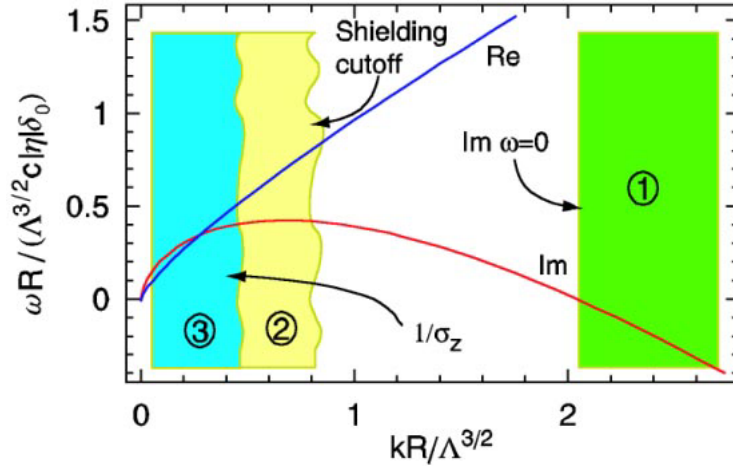


Figure 2: Plot of real (blue) and imaginary (red) parts of frequency ω as functions of k for positive η . Normalization of the frequency ω and the wavenumber k on the axes involves the parameter Λ defined by Eq. (6).

It is convenient to introduce the dimensionless parameter Λ :

$$\Lambda = \frac{1}{|\eta| \gamma \delta_0^2} \frac{I}{I_A} \frac{R}{\langle R \rangle}, \quad (6)$$

where $I_A = mc^3/e = 17.5$ kA is the Alfvén current. The maximum growth rate is reached at $kR = 0.68\Lambda^{3/2}$ and is equal to $(\text{Im } \omega)_{\max} = 0.43\Lambda^{3/2}c\eta\delta_0/R$.

Three colored areas in this plot refer to stability regions in the parameter space. In the green area 1, the beam is stable because $\text{Im } \omega < 0$ due to Landau damping. This region corresponds to high frequencies, $kR > 2.0\Lambda^{3/2}$. In the yellow region 2, where $kR^{1/2}/a^{3/2}$ (a is the transverse size of the vacuum chamber), the instability is suppressed by shielding of the radiation. Finally, at even lower frequencies, in the blue area 3, the wavelength of the instability exceeds the bunch length and the coasting beam theory breaks down. The wavy lines between stability regions indicate fuzziness of the transition boundaries in our model.

There are several effects that are neglected in the simple theory described above. First, a zero transverse emittance of the beam was assumed. Second, the synchrotron damping γ_d due to incoherent radiation was neglected which makes the growth rate of the instability somewhat smaller, $\text{Im } \omega \rightarrow \text{Im } \omega - \gamma_d$ [20]. Finally, the retardation effects were neglected which is valid if the formation time for the radiation is smaller than the instability growth time, $t_f \sim l_f/c \ll 1/\text{Im } \omega$. In most cases characteristic for modern rings, those effects are relatively minor.

2.3.5 Rings with Wigglers

In the damping ring of the Next Linear Collider [21], there are long magnetic wigglers, which introduce an additional contribution to the radiation impedance. The analysis of the CSR instability in such a ring requires knowledge of the impedance of the synchrotron radiation in the wiggler. Based on the earlier study of the coherent

radiation from a wiggler [22], in Ref. [23], a steady-state wake averaged over the wiggler period has been derived for the case $K^2/2 \gg 1$ (where K is the wiggler parameter) and $\gamma \gg 1$. The most interesting from the point of view of instability is a low-frequency part of the impedance, given by the following formula (per unit length of path):

$$Z_{\text{wiggler}}(\omega) \approx \frac{Z_0 \omega}{4c} \left[1 - \frac{2i}{\pi} \log \frac{\omega}{\omega_*} \right], \quad (7)$$

where $\omega_* = 4\gamma^2 c k_w / K^2$ and $Z_0 = 377 \text{ Ohm}$. Eq. (1) is valid for $\omega \ll \omega_*$.

Results of the analysis of CSR instability in the NLC ring, taking into account the wiggler CSR impedance can be found in Ref. [24].

2.3.6 Discrete modes near shielding threshold

There are several reasons why the simple theory of CSR microbunching instability developed in Ref. [25] is not applicable near the shielding threshold, $\lambda \sim a^{3/2}/R^{1/2}$. The most important one is that CSR does not have a continuous spectrum here, and the modes that can interact with the beam are discrete. The discreteness of the spectrum has been demonstrated in early papers [9,26] for toroids of rectangular cross section. A more recent analysis of the shielded CSR impedance [27] extends the previous treatment of the problem and deals with arbitrary shapes of the toroid cross section.

Each synchronous mode in the toroid is characterized by frequency ω_n , a loss factor κ_n (per unit length), and a group velocity $v_{g,n}$. The wake associated with the n -th mode is

$$w_n(z) = 2\kappa_n \cos\left(\frac{\omega_n}{c} z\right).$$

This wake, for lowest modes, propagates behind the particle. Calculation of ω_n , κ_n , and $v_{g,n}$, in the general case of arbitrary cross section requires numerical solution of two coupled partial differential equations [27]. For a toroid of round cross section of radius a , the lowest mode has been found to have the frequency $\omega_1 = 2.12cR^{1/2}a^{-3/2}$, the loss factor $\kappa_1 = 2.11a^{-2}$ and the group velocity $1 - v_{g,1}/c = 1.1a/R$.

Near the shielding threshold, the CSR instability should be treated as an interaction of the beam with single modes, [28]. When the wavelength of the mode is smaller than the bunch length, one can still use the coasting beam approximation, but one cannot neglect retardation effects. Assuming an ideal toroidal chamber with a constant cross section (no straight sections in the ring), it turns out that the theory of single-mode instability [28] parallels that of SASE FEL (see, e.g., [29]). It gives the maximum growth rate of the instability for n th mode equal to $\sqrt{3}\rho_n\omega_n/2$ where

$$\rho_n = \left[\frac{I}{I_A} \frac{c^2 \eta \kappa}{\omega_n^2 \gamma} \left(1 - \frac{v_{g,n}}{c} \right) \right]^{1/3} \quad (8)$$

is an analog of the Pierce parameter in FELs.

The nonlinear regime of the instability in this approximation has been studied in Refs. [28,30].

2.3.7 Simulation of Multiparticle Dynamics in the Presence of CSR

We consider the dynamics of a bunched electron beam subject to the fields generated by itself, both through synchrotron radiation and through effects that are present even without trajectory curvature: space charge and influence of the vacuum chamber. Numerical simulation of such a system has two aspects: (1) the algorithm for computing the fields given the charge/current density; (2) the algorithm to follow particle motion given the fields.

2.3.7.1 Field Computation

In free space the field generated by the bunch is unambiguous in principle, being given in terms of scalar and vector potentials of the form

$$\psi(\mathbf{r}, t) = \frac{1}{4\pi} \int d\mathbf{r}' \frac{S(\mathbf{r}', t - |\mathbf{r} - \mathbf{r}'|/c)}{|\mathbf{r} - \mathbf{r}'|}, \quad (9)$$

where the source S is the charge density for the scalar potential or the current density for the vector potential. Evaluation of this formula can be nontrivial, but it has been noticed recently that evaluation is much easier if one takes the second argument of the source (retarded time) as one of the integration variables [31].

Study of models (dating back to the 1940's) indicates that field components of sufficiently long wavelength are exponentially suppressed by the vacuum chamber, the suppression setting in at the so-called "shielding cutoff" which is roughly $\lambda_0 = 2h(h/R)^{1/2}$, where h is the vertical aperture of the chamber and R is the bending radius. If and only if the bunch form has significant Fourier components with wavelength λ somewhat smaller than λ_0 , those components will radiate a field that is close to the free-space field of wavelength λ , and in turn be influenced by that field. Thus, if bunch instability is due to CSR itself, a knowledge of the free-space field may be sufficient to find the current threshold of instability, since the cutoff is fairly abrupt. To some approximation, a mode can be considered as either completely shielded or free.

Nevertheless, for a full picture of beam dynamics it usually seems better to include a shielding model in detail. This was judged important for the bursting mode of CSR production [32], where in the course of time the bunch sometimes has substantial components satisfying $\lambda \leq \lambda_0$ and sometimes not, with periodic continuous transitions between the two situations during which partial shielding occurs.

Unfortunately, our present ability to calculate effects of shielding is rather limited. One usually relies on a model in which the vacuum chamber is represented by infinite parallel plates with separation h , perfectly conducting, with particles circulating between the plates in planes parallel to the plates. If the orbits are circular one gets the cutoff mentioned above. For general planar orbits, including for instance race track trajectories, the method of images suffices to satisfy the field boundary conditions on the plates. Then Eq.(1) still applies if it is augmented to include an infinite sequence of image bunches [31] in the source S . Only a few images in the sequence are needed in practice. The field from non-circular orbits with image charges can be computed from

existing codes [33,34], but those codes have usually been applied to single-pass systems such as bunch compressors, rather than to storage rings. It is not clear that they would be tractable for a dynamical simulation of a storage ring.

For circular orbits the parallel plate model was solved long ago, in the sense that an impedance or wake potential was determined which gives the voltage induced by a *rigid* bunch in the form

$$\begin{aligned} V(\theta, t) &= -2\pi RE(\theta, t) \\ &= \omega_0 Q \sum_n e^{in(\theta - \omega_0 t)} Z(n) \lambda_n = -Q \int W\left(\frac{R}{\sigma_z}(\theta - \omega_0 t - \theta')\right) \lambda(\theta') d\theta', \end{aligned} \quad (10)$$

where E is the longitudinal electric field (averaged over the transverse charge distribution), Z is the impedance, W is the corresponding wake potential, and Q is the total charge. The azimuthal location in the lab frame is θ , the orbit radius is R , and the angular revolution frequency $\omega_0 = \beta_0 c/R$. In (2) we use the notation $Z(n)$ that is common when periodicity of fields is emphasized; in the previous notation of (4) this would be written as $Z(n/R)$. The charge density in the beam frame, normalized to unit integral, is $\lambda(\theta)$. The Fourier transform of the charge density is

$$\lambda_n = \frac{1}{2\pi} \int_0^{2\pi} e^{-in\theta} \lambda(\theta) dq. \quad (11)$$

Following earlier papers, we make the argument of W dimensionless, using the nominal bunch length σ_z as a scale factor. The formula for Z in terms of Bessel functions is derived in [35], and the equivalent W (modulo certain approximations) is found in [36].

To apply (10) to the realistic case of a deforming bunch and non-circular orbits we make two reasonable assumptions. First we replace the rigid charge density $\rho(q)$ by the density $\rho(q, t)$ at the current time, obtaining

$$\begin{aligned} V(\theta, t) &\approx \omega_0 Q \sum_n e^{in(\theta - \omega_0 t)} Z(n) \lambda_n(t) \\ &= -Q \int W\left(\frac{R}{\sigma_z}(\theta - \omega_0 t - \theta')\right) \lambda(\theta', t) d\theta'. \end{aligned} \quad (12)$$

Second, we identify R with the bending radius (or average bending radius) of the ring, rather than with $C/(2\pi)$ for a ring with circumference C . This identification is made *only* for the computation of the CSR force; otherwise the real ring parameters are used in the equations of motion. Effectively we are neglecting the CSR force in transitions between bends and straight sections, hoping that the neglected force, averaged over a turn, will have a small effect.

The formula (12) is not exact even in the case of circular orbits. Since it depends only on the present value of the charge density it does not account fully for retardation if the density is evolving in time. A light signal emitted from the bunch can catch up with the bunch at a later time when the charge density is altered. This effect is of course

embodied in the “retarded potential” (9), and one could go back to (9) in the hope of deriving a tractable formula for the force that could be used in a dynamical simulation.

$$V(\theta, t) \approx 2\omega_o Q \operatorname{Re} \sum_{n=1}^{\infty} e^{in(\theta - \omega_o t)} \left[Z(n, n\omega_o) \lambda_n(t) + \frac{\partial \tilde{Z}}{\partial \omega}(n, n\omega_o) i \lambda_n'(t) - i \frac{Z_o \pi R}{2\beta_o h} \sum_p \Lambda_p \int_0^t dt' \lambda_n'(t') (e^{iA(p,n)(t'-t)} + e^{iB(p,n)(t'-t)}) \right] \quad (13)$$

where $\tilde{Z}(n, \omega)$ is $Z(n, \omega)$ minus its pole terms, $Z_o = 120\pi \Omega$ is the impedance of free space, Λ_p is a factor characterizing the vertical charge distribution [35], and

$$\begin{aligned} A(p, n) &= \alpha_p c - n\omega_o, \\ B(p, n) &= -\alpha_p c - n\omega_o. \end{aligned} \quad (14)$$

The integrals over past values of $\lambda_n' = \partial \lambda_n / \partial t$ are associated with wave guide cutoffs. The formula (13) is not difficult to apply, since the integrals can be stored and incremented by a small amount at each time step. To date we do not have a similarly efficient method to account for retardation in a space-time approach.

To go beyond the parallel plate model we can consider a toroidal model of the vacuum chamber, again taking only circular orbits of radius R . The case of a circular torus with rectangular cross section and perfectly conducting walls can be solved in terms of Bessel functions [9,37]. It gives a complete impedance $Z(n, \omega)$ which shares some properties with that for the parallel plates; it gives a shielding cutoff that is roughly the same, and it again has poles in ω at wave guide cutoffs. The physical picture is different, however, since the structure is closed. Energy cannot be radiated to infinity, and there are eigenmodes of the whole structure that are often described as “whispering gallery” modes. These show up as additional poles on the real ω axis. To see the connection with whispering gallery architecture, let the inner torus radius go to zero, so that we have a cylindrical gallery with height h and radius $b > R$, but with $b - R$ small, of order h . The beam excites modes that are concentrated near the cylindrical surface, very similar to corresponding modes of the torus [9]. These modes are well above the wave guide cutoff in frequency, so that they are associated with waves that propagate around the periphery of the gallery.

The question arises as to whether a real vacuum chamber, with corrugations from cavities, bellows, etc., and wall resistance, could support some vestige of these “full structure” modes of the smooth toroidal or cylindrical chamber. If the structure has perfect mechanical stability, it seems likely that vestigial whispering gallery modes do exist. They would of course have less spatial homogeneity than in the ideal case, and would involve coupling of various mode numbers n . Even if they exist in principle, could they be excited and be persistent enough to affect the beam in an observable way? This is an intriguing question that needs further study. On the theoretical side it seems quite possible to study perturbations of the smooth chamber for convenient simple forms of the perturbation, say by a mode matching or integral equation technique. One should also think about possible experimental observation of whispering modes.

It is noteworthy that the induced voltage for the toroidal or cylindrical model has quite a different form in comparison to (12). For those models $Z(n, \omega)$ is analytic in the ω -plane except for poles at waveguide cutoffs and resonance frequencies, and tends to a constant as $\omega \rightarrow \infty$ in complex directions. Consequently, one can evaluate the ω -integral in the definition of V by the method of residues. For the cylindrical model the resulting exact formula for the voltage is

$$\begin{aligned}
V(\theta, t) = & \pi \omega_o Q Z_o \frac{R}{h} \sum_p \Lambda_p \left[\left(\frac{R}{b} \right)^{1/2} \lambda(\theta - \omega_o t, t) + 2 \operatorname{Re} \sum_{n=1}^{\infty} e^{in(\theta - \omega_o t)} \int_0^t dt' \lambda_n(t') \right. \\
& + \left[\sum_s r^E(n, s) (e^{iA^E(p, n, s)(t'-t)} + e^{iB^E(p, n, s)(t'-t)}) + \sum_s \frac{r^M(n, s)}{\omega_*(p, n, s)} (e^{iA^M(p, n, s)(t'-t)} - e^{iB^M(p, n, s)(t'-t)}) \right. \\
& \left. \left. + r(n) (A(p, n) e^{iA(p, n)(t'-t)} + B(p, n) e^{iB(p, n)(t'-t)}) \right] \right]. \quad (15)
\end{aligned}$$

The second line of the right hand side arises from transverse electric (TE) and transverse magnetic (TM) modes (transverse to the cylinder axis, not the beam direction), which have frequencies determined by zeros of Bessel functions and their derivatives; namely,

$$\begin{aligned}
TE: \quad \omega'_*(p, n, s) &= \frac{c}{b} [(\alpha_p b)^2 + j_{ns}'^2]^{1/2}, \quad J'_n(j'_{ns}) = 0, \\
TM: \quad \omega_*(p, n, s) &= \frac{c}{b} [(\alpha_p b)^2 + j_{ns}^2]^{1/2}, \quad J_n(j_{ns}) = 0. \quad (16)
\end{aligned}$$

The factors $r^{E, M}$ come from residues of the resonance poles and have the forms

$$\begin{aligned}
r^E(n, s) &= \frac{\pi^2 c R}{2b^2} \frac{[j'_{ns} J'_n(j'_{ns} R/b) Y'_n(j'_{ns})]^2}{(n/j'_{ns})^2 - 1} \\
r^M(n, s) &= -\frac{\pi^2 n}{2\beta_0} [\alpha_p c J_n(j_{ns} R/b) Y_n(j_{ns})]^2, \quad (17)
\end{aligned}$$

whereas $r(n)$, from residues of waveguide cutoff poles, is

$$r(n) = \frac{1}{2\beta_0} \left(1 - \left(\frac{R}{b} \right)^{2n} \right). \quad (18)$$

The exponents involve A, B as in (14) and also

$$\begin{aligned}
A^E(p, n, s) &= \omega'_*(p, n, s) - n\omega_o, & B^E(p, n, s) &= -\omega'_*(p, n, s) - n\omega_o, \\
A^M(p, n, s) &= \omega_*(p, n, s) - n\omega_o, & B^M(p, n, s) &= -\omega_*(p, n, s) - n\omega_o. \quad (19)
\end{aligned}$$

For the toroidal model the result is similar to (15), except that one is dealing with poles from zeros of cross products of Bessel functions [9].

The first term in (15), which arises from the constant term in the impedance, is merely proportional to the present value of the charge density in the beam frame. If the total induced voltage were just a multiple of the charge density, which would be the idealized case that is usually called a “purely resistive wake”. Besides this resistive term in (15) we have *only* retardation terms, integrals over prior values of the charge distribution. Some of these, especially those corresponding to the lowest TE resonance with $\omega'_*(p, n, s) \approx n\omega_0$, $p = s = 1$, are expected to be dynamically important. If so, we see that a wake potential description of the induced voltage as in (12) is strictly invalid. We are dealing with an unfamiliar situation that needs further exploration.

Oide claims, without a full proof, that a purely resistive wake gives an unstable beam for arbitrarily small current [38]. If that is true, then the first term in (15) has a destabilizing effect that may or may not be compensated by the other terms. In fact, it is hard to see how this model with a closed chamber and no wall resistance could give a stable beam since energy must just build up without bound in resonant modes. Correspondingly, a linearized Vlasov analysis of a coasting beam indicates a zero current threshold for instability, if we retain just a single resonance pole term in $Z(n, \omega)$.

As was shown in [9], one can give a reasonable approximate account of wall resistance in the cylindrical and toroidal models, but then the residue method that led to (15) does not work, since one gets a branch point from the square root frequency dependence of the skin depth. An interesting open question is then to find a good approximate expression for V including wall resistance.

If we account for resistivity in the above mentioned coasting beam analysis, merely by displacing the resonance pole to the lower half-plane by an amount given in the results of [9], then we get a non-zero current threshold of instability, but one (for the resistivity of aluminum) that is much smaller than that of the parallel plate model. Unfortunately, this leaves us in the dark about the quantitative dynamical role of shielding for CSR in rings. Perhaps both wall resistance and corrugations will be necessary in an acceptable model of a closed chamber.

2.3.7.2 Numerical Modeling of Phase Space Dynamics

Undoubtedly, the most popular method to simulate multiparticle dynamics is the macroparticle method, sometimes called the particle-in-cell method [39]. For electron rings the macroparticle method must usually be augmented to account for incoherent synchrotron radiation. That is done by adding a damping term and pseudo-random momentum kicks to the single-particle equations of motion, the latter to model random emission of single photons. Another approach, which has aesthetic appeal, is to do a numerical solution of the Vlasov-Fokker-Planck (VFP) equation. This accomplishes the same thing, in principle, as the macroparticle method, but with much less numerical noise. It has been quite successful in the case of a two-dimensional phase space, and efforts are underway to extend this success to higher dimensions. The VFP equation is a nonlinear integro - partial differential equation with at least three independent variables, and one might think that a numerical code to solve it would be very complicated. Fortunately, that is not the case; the coding is no harder than for the macroparticle method, maybe even simpler.

For longitudinal motion in a storage ring above transition with linear RF the VFP equation for the phase space density $f(q, p, \tau)$ has the form [32,40]

$$\begin{aligned}\frac{\partial f}{\partial \tau} &= A_V(f) + A_{FP}(f), \\ A_V(f) &= -p \frac{\partial f}{\partial q} + [q + I_c F(q, f, \tau)] \frac{\partial f}{\partial p}, \\ A_{FP}(f) &= \frac{2}{\omega_s t_d} \frac{\partial}{\partial p} \left(pf + \frac{\partial f}{\partial p} \right),\end{aligned}\tag{20}$$

where the dimensionless phase space variables are $q = z/\sigma_z$ and $p = -(E - E_0)/\sigma_E$, with z being the distance from the reference particle (positive in front), and $E - E_0$ the displacement from the nominal energy; we normalize by the low-current r.m.s. bunch length and energy spread, σ_z and σ_E . The dimensionless time is $\tau = \omega_s t$, where ω_s is the synchrotron frequency, and t_d is the longitudinal damping time. The collective force is $F = -V/Q$, with V the induced voltage as discussed above, and $I_c = e^2 N / (2\pi \nu_s \sigma_E)$ is the normalized current, with ν_s the synchrotron tune. In most work to date the parallel plate model of shielding has been used, with V in the approximation (12).

The Vlasov equation without account of damping and fluctuations from incoherent synchrotron radiation is $\partial f / \partial \tau = A_V(f)$. The Fokker-Planck term A_{FP} , to represent damping and fluctuations, is in some sense small owing to slow damping (the large value of $\omega_s t_d$). We integrate (20) as an initial value problem, proceeding in small time steps $d\tau$. Since the Vlasov and Fokker-Planck operators require entirely different numerical techniques, we use *operator splitting*: for a time step $d\tau$, first advance f by $\partial f / \partial \tau = A_V(f)$, and then by $\partial f / \partial \tau = A_{FP}(f)$. The Vlasov step is unstable if done by a simple finite difference approximation of A_V and any sort of time stepping, but stable if done by the *method of local characteristics*, equivalent to approximating the Perron-Frobenius operator by discretization. On the other hand, the Fokker-Planck step is easily done by a finite difference formula for A_{FP} , with the elementary Euler method for the time step.

In the method of local characteristics we suppose that the coherent force is nearly independent of time over a sufficiently small time interval $\Delta\tau$, so that we have a single-particle map defined locally in time. This volume-preserving map is denoted by $M_{\tau \rightarrow \tau + \Delta\tau}(z)$, $z = (q, p)$. Then the Perron-Frobenius (PF) operator \mathfrak{M} associated with M gives the time evolution of the distribution function:

$$f(z, \tau + \Delta\tau) = \mathfrak{M}f(z, \tau) = f(M^{-1}(z), \tau).\tag{21}$$

This is just another way of stating that the probability of finding a particle in a phase space volume element dz is preserved:

$$f(M(z), \tau + \Delta\tau) d(M(z)) = f(z, \tau) dz.\tag{22}$$

A discretization of \mathfrak{M} simply consists of choosing a finite-dimensional approximation of f . For instance, f might be described by its values on a grid $\{z_i\}$, with polynomial interpolation to off-grid points. In that case, evaluation of $\mathfrak{M}f(z_i, \tau)$ would be done by interpolation, since $M^{-1}(z_i)$ is an off-grid point in general. In the literature the discretized PF method is often called the *semi-Lagrangian method* [41]. In plasma physics it dates back at least to the work of Cheng and Knorr [42] in 1976.

There are myriad possibilities for discretizing \mathfrak{M} . In a study of longitudinal motion in the SLC damping rings, without CSR, a simple locally quadratic representation of f was used successfully [43]. For recent work on CSR [40,32] a method of Yabe *et al.* [44] was applied. That method, which was able to deal with the small wavelength bunch perturbations from CSR, was reviewed in an appendix of [40].

There are myriad possibilities for discretizing \mathfrak{M} . In a study of longitudinal motion in the SLC damping rings, without CSR, a simple locally quadratic representation of f was used successfully [43]. For recent work on CSR [40,32] a method of Yabe *et al.* [44] was applied. That method, which was able to deal with the small wavelength bunch perturbations from CSR, was reviewed in an appendix of [40].

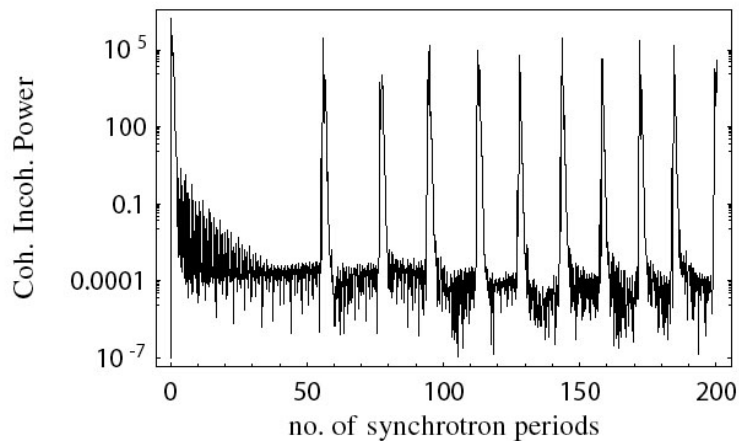


Figure 3: Coherent over incoherent power

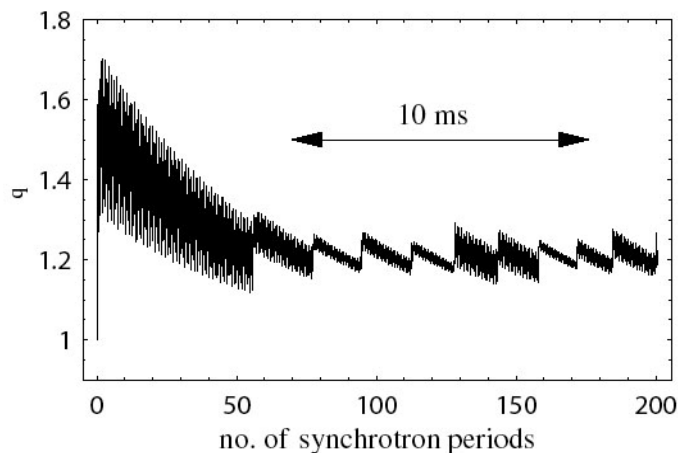


Figure 4: Bunch length vs. time

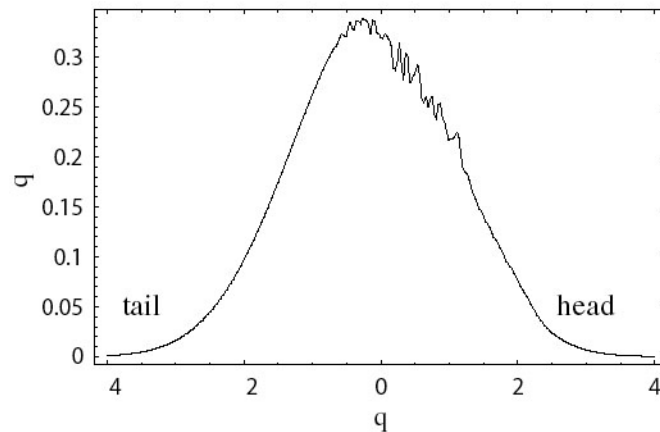


Figure 5: Bunch density with “microbunching”

One can also study microbunching without radiation damping, and there was a motivation for doing so in the design of a compact low energy storage ring [40,45] having a damping time that is effectively infinite, being large compared to the storage time. Such a study was carried out in [40] using just the Vlasov equation without Fokker-Planck terms, again with the parallel plate impedance giving the only collective force. This impedance gives the full field of the model and therefore includes a significant space charge component, owing to the low energy (25 MeV) of the example. Figure 6 shows a grey scale plot of the phase space density, and a graph of the charge density, at three successive times: $\tau = 1.2, 3.2, 9.6$ or $0.19, 0.51, 1.5$ in units of the synchrotron period. Here we see very clearly the evolution described above: initial small ripples quickly amplified in a linear regime, and then a dramatic smoothing and broadening of the distribution through nonlinearity, all within a time comparable to the synchrotron period.

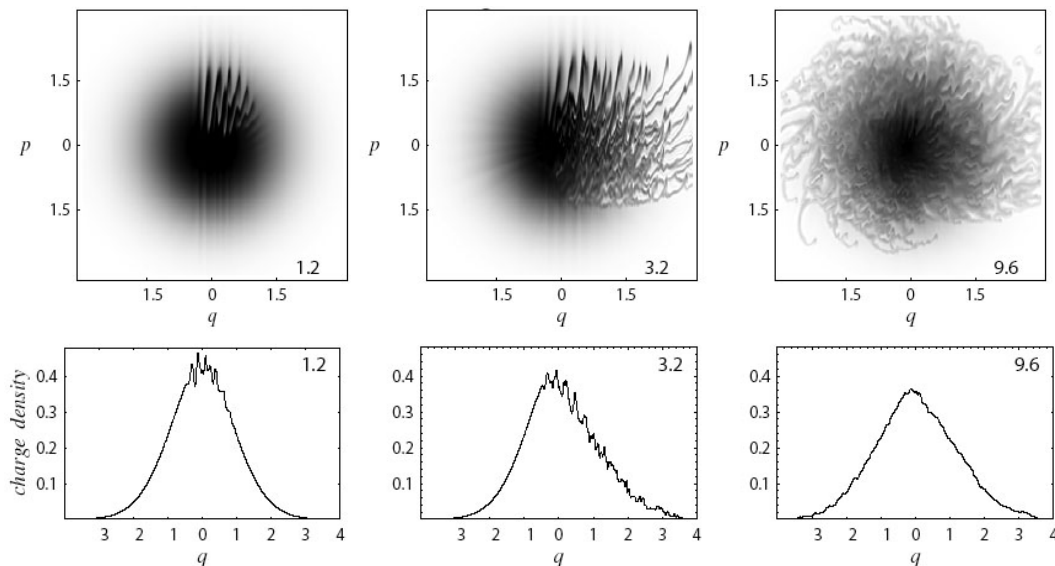


Figure 6: Time evolution of bunch under effect of CSR in a compact storage ring. Density plots in phase space (top row) and charge density (second row). Pictures are taken at (normalized) time $\tau = 1.2, 3.2,$ and 9.6 . Instability initiated by a small perturbation with mode number $n = 702$ (wavelength $\lambda = 2.2$ mm). A unit of q corresponds to 1 cm.

In [40] the time domain simulation was also used to check the validity of the threshold for instability as determined by the linearized Vlasov equation for a coasting beam with current equal to the peak current of the bunch. The agreement between the two determinations was satisfactory, showing that the Boussard criterion works in this case.

In [46] some preliminary work was done to assess the importance of corrections to (12) as stated in (13). Figure 7 shows an evaluation of the three terms in (13), again for the example of the compact storage ring [40]. The calculation was done with a smooth switching on of the current, in accord with the theory of [35]. After initial transients die out the effect of the corrections is fairly small. Further work needs to be done in extending the computation to a longer time interval.

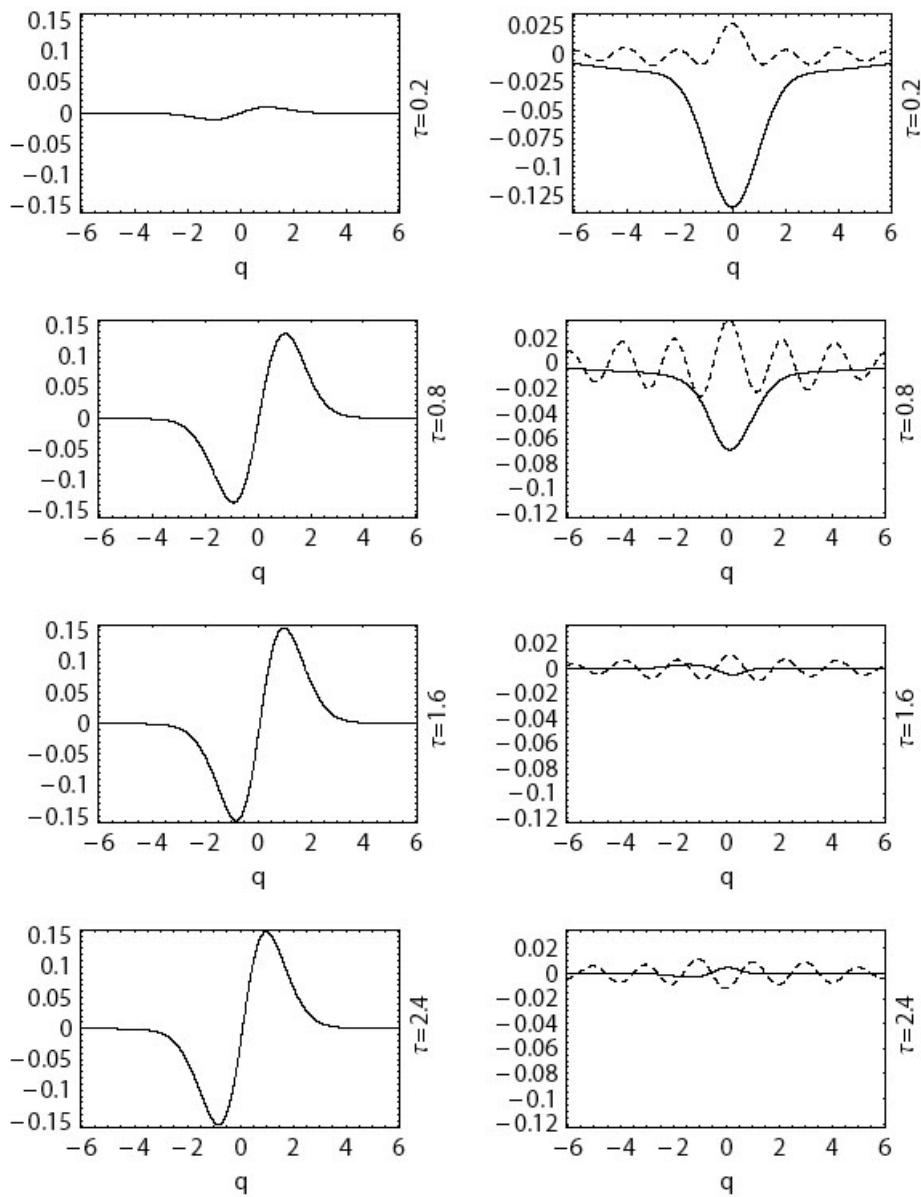


Figure 7: Collective force $I_c F(q)$ at successive times. First term of Eq.(13) on left graph, second (solid) and third (dashed) on right.

2.3.7.3 Possible Improvements in the Vlasov Solution

It would be interesting to explore the effects of the horizontal transverse charge distribution, as has been done for CSR in single-pass systems. If that problem is to be treated by solving the VFP equation, now in 4-dimensional phase space, then more attention should be paid to efficiency of the numerical algorithm to avoid excessively long computations. In principle the Perron-Frobenius operator \mathfrak{M} preserves positivity of f and the value of the total probability $\int f(q, p, \tau) dq dp = 1$. After discretization these properties do not hold unless one adopts some special technique. To date in 2-D phase space we have used positivity and probability conservation as criteria for choice of the mesh cell size, requiring that f be positive unless its magnitude is less than some small amount and that its integral be 1 within a small error. In higher dimensions this is not so feasible, since one tries to economize by using a coarse mesh that allows significant negative values of f .

An algorithm that automatically preserves both positivity and total probability may have a better chance of giving satisfactory results with a relatively coarse mesh. One such scheme was suggested in [31]. The idea is to represent the distribution function as a sum of tensor products of B-splines, with the coefficients given by Schönberg's Variation Diminishing Approximation [47]. In this approximation the coefficients are values of the function at averages of spline knot positions, and since B-splines are non-negative this means that positivity is preserved. To ensure probability conservation one can simply divide by the integral of the new function after each time step. That was found not to be a good idea in non-positive schemes, but it may work better in this case.

The B-splines have "small support", meaning that only a few members of a B-spline basis are non-zero at a single point. This means that evaluation of the distribution to compute the collective force will be fast. On the other hand, the tensor product basis has its limitations, as does Schönberg's method that provides only an approximation with error of second order in the cell size (in each dimension).

To overcome the limitations of tensor product bases, and to provide approximations of higher order, it seems interesting to consider *radial basis functions* [48]. Each basis function is associated with a point in phase space (a "site"), and is a function only of the Euclidean distance from the site. The sites can have arbitrary positions. A function is represented as a linear superposition of basis functions with coefficients determined so as to interpolate values of the function at sites. Applied to our case this would not ensure positivity, but one may hope that the good approximation properties of the basis in high dimensions provide an advantage. Because a large number of sites will be required, and because the interpolant must be redetermined at each time step, it seems necessary to use basis functions with small support ([48], Chap.6). Then one has small systems of linear equations to determine the coefficients.

Shepard's method is another idea for interpolation in high dimensions with arbitrary interpolation points, again using functions of the distance from sites [48,49,50]. It is very simple to implement, requires no solution of linear equations, and would provide a positive interpolation. Its approximation properties leave something to be desired, one peculiarity being that the interpolant has a flat spot (local extremum) at interpolation points. Nevertheless, it might be an interesting candidate in the quest for a Vlasov solver that could compete in speed with the macroparticle method in high dimensions.

Within a particular choice of interpolation method for discretizing the PF operator there are further ideas for improving efficiency. Preliminary work indicated that it might be useful to taper the mesh cell size in such a way as to give roughly equal probabilities of finding a particle in all cells. If the distribution is roughly Gaussian that is easy to do using the inverse error function. Sonnendrücker and collaborators are exploring the possibility of adaptive meshes [41], which change in time to follow the region in which the distribution is appreciable in magnitude. A “one shot” adaptation was proposed in [31], where coordinates were chosen so as to put the Vlasov equation in the interaction picture; namely, the initial conditions of the motion as it would be in the absence of collective effects. When collective effects are turned on these variables have relatively little variation with time. Consequently, an interpolation scheme chosen for good efficiency at time zero should also be good at later times. In this approach the projection to get the charge/current density from the distribution is more costly than usual, because the integrations are not along coordinate axes of the new variables.

Finally, we mention the *finite volume method*, which offers a positive and conserving algorithm that is different in technique from the PF operator discretization, although similar in spirit since it is derived directly from probability conservation [51,52].

2.3.8 Acknowledgments

Sam Heifets, Marco Venturini and James Ellison played a large role in much of the work discussed here. Our research was supported in part by U. S. Department of Energy contract DE-AC02-76SF00515.

2.3.9 References

- [1] U.Arps, G.T. Fraser, A.R.H. Walker, T.B. Lucatorto, K.K. Lehmann, K. Harkay, N. Sereno, and K.-J. Kim, *Phys. Rev. ST Accel. Beams* **4**, 054401 (2001).
- [2] G.L. Carr, S. L. Kramer, J. B. Murphy, R. P. S. M. Lobo, and D. B. Tanner, *Nuclear Instruments and Methods, Sec. A* **463**, 387 (2001).
M. Abo-Bakr et al., “Brilliant, Coherent Far-Infrared (THz) Synchrotron Radiation”, *Phys. Rev. Lett.* **90**, 094801 (2003).
- [3] B. Podobodov, G. Carr, S. Kramer, and J. Murphy, in *Proceedings of the 2001 Particle Accelerator Conference* (IEEE, Piscataway, NJ, 2001).
- [4] Å. Andersson, M. S. Johnson, and B. Nelander, *Opt. Eng.* **39**(12), 3099 (2000).
- [5] M. Abo-Bakr, J. Feikes, K. Holldack, G. Wüstefeld, and H.-W. Hübers, *Phys. Rev. Lett.* **88**, 254801 (2002).
- [6] J. Byrd, W. P. Leemans, Á. Loftsdóttir, B. Marcellis, M. C. Martin, W. R. McKinney, F. Sannibale, T. Scarvie, and C. Steier, *Phys. Rev. Lett.* **89**, 224801 (2002).
- [7] J. Schwinger, *On radiation by electrons in a betatron* (1945), unpublished, transcribed in Lawrence Berkeley Laboratory report LBL-39088, ed. M. Furman (1996).
- [8] L. Schiff, *Rev. Sci. Instr.* **17**, 6 (1946).
- [9] R.L. Warnock and P. Morton, *Part. Accel.* **25**, 113 (1990).
- [10] R.L. Warnock and K. Bane, in *Proc. IEEE Particle Accelerator Conference and International Conference on High-Energy Accelerators, Dallas, 1995* (IEEE, Piscataway, NJ, 1996).
- [11] J.-M. Wang, *Phys. Rev.* **E58**, 984 (1998).
- [12] A. W. Chao and M. Tigner, *Handbook of Accelerator Physics and Engineering* (World Scientific, Singapore, 2002), 2nd ed.

- [13] L. V. Iogansen and M. S. Rabinovich, *Sov. Phys. JETP* **37**, 83 (1960).
- [14] J.B. Murphy, S. Krinsky, and R. L. Gluckstern, in *Proc. IEEE Particle Accelerator Conference and International Conference on High-Energy Accelerators, Dallas, 1995* (IEEE, Piscataway, NJ, 1996), (IEEE Conference Record 95CH35843).
- [15] Y.S. Derbenev, J. Rossbach, E.L. Saldin, and V.D. Shiltsev, *Microbunch Radiative Tail-Head Interaction*, DESY FEL Report TESLA-FEL 95-05, Deutsches Elektronen-Synchrotron, Hamburg, Germany (1995).
- [16] A.W. Chao, *Physics of Collective Beam Instabilities in High Energy Accelerators* (Wiley, New York, 1993).
- [17] E.L. Saldin, E.A. Schneidmiller, and M.V. Yurkov, *Nuclear Instruments and Methods, Sec. A* **398**, 373 (1997).
- [18] G. Stupakov and P. Emma, in *Proceedings of 8th European Particle Accelerator Conference* (Paris, France, 2002), p. 1479.
- [19] J.-L. Laclare, in *Proc. CERN Accelerator School, Gif-sur-Yvette, 1984*, edited by P. Bryant and S. Turner (European Lab. for Particle Physics, Geneva, Switzerland, 1985), no. 85-19 in CERN Yellow Report, pp. 377–414.
- [20] S. Heifets and G. V. Stupakov, *Derivation of microwave instability dispersion relation with account of synchrotron damping and quantum fluctuations*, Preprint SLAC-PUB-8803, SLAC (2001).
- [21] A. Wolski, *NLC damping rings: Lattice parameters, information and resources*, URL: <http://awolski.lbl.gov/nlcdrlattice/default.htm>.
- [22] E.L. Saldin, E. A. Schneidmiller, and M.V. Yurkov, *Nuclear Instruments and Methods, Sec. A* **417**, 158 (1998).
- [23] J. Wu, T. Raubenheimer, and G. Stupakov, *Phys. Rev. ST Accel. Beams* **6**, 040701 (2003).
- [24] J. Wu, T. O. Raubenheimer, G.V. Stupakov, and Z. Huang, *Phys. Rev. ST Accel. Beams* **6**, 104404 (2003).
- [25] S. Heifets and Stupakov G. V., *Phys. Rev. ST Accel. Beams* **5**, 054402 (2002).
- [26] K.-Y. Ng, *Part. Accel* **25**, 153 (1990).
- [26] H. Lihn et al., “Measurement of subpico second electron pulses”, *Phys. Rev. E* **53**, 6413, (1996).
- [27] G. V. Stupakov and I. A. Kotelnikov, *Phys. Rev. ST Accel. Beams* **6**, 034401 (2003).
- [28] S. Heifets and G. Stupakov, *Phys. Rev. ST Accel. Beams* **6**, 064401 (2003).
- [29] R. Gluckstern, S. Krinsky, and H. Okamoto, *Phys. Rev.* **E47**, 4412 (1993).
- [30] S. Heifets, *The single-mode CSR instability for a bunched beam*, Report SLAC-PUB-9626, SLAC (2003)..
- [31] R. Warnock, G. Bassi, and J. A. Ellison, “Vlasov Treatment of Coherent Synchrotron Radiation from Arbitrary Planar Orbits”, *Proc. 2004 Internat. Comp. Accel. Phys. Conf.*, St. Petersburg, Russia (to be published in *Nucl. Instr. Meth. Sci. Res.*), available as SLAC preprint SLAC-PUB-10760 (2004).
- [32] M. Venturini and R. Warnock, *Phys. Rev. Lett.* **89**, 224802 (2002).
- [33] R. Li, *Nuc. Instrum. Methods Phys. Res., Sect.A* **429**, 310 (1998).
- [34] A. Kabel, M. Dohlus, and T. Limberg, *Nuc. Instrum. Methods Phys. Res., Sect.A* **455**,185 (2000); M. Dohlus, A. Kabel, and T. Limberg, *ibid.* **445**, 338 (2000).
- [35] R. Warnock, R. D. Ruth, M. Venturini, and J. Ellison, “Impedance Description of Coherent Synchrotron Radiation with Account of Bunch Deformation”, to be published in *Phys. Rev. ST Accel. Beams*.
- [36] J. B. Murphy, S. Krinsky, and R. L. Gluckstern, *Part. Accel.* **57**, 9 (1997).
- [37] K.-Y. Ng, *Part Accel.* **25**, 153 (1990).
- [38] K. Oide, KEK preprint 94-138 (1994).
- [39] R. W. Hockney and J. W. Eastwood, *Computer Simulation Using Particles* (Inst. Phys. Pub., Bristol, 1988).

- [40] M. Venturini, R. Warnock, R. Ruth, and J. A. Ellison, "Coherent Synchrotron Radiation and Bunch Stability in a Compact Storage Ring", to be published in *Phys. Rev. ST Accel. Beams*.
- [41] F. Filbet and E. Sonnendrücker, *Comp. Phys. Commun.* **150**, 247 (2003).
- [42] C. Z. Cheng and G. Knorr, *J. Comput. Phys.* **22**, 330 (1976).
- [43] R. Warnock and J. Ellison, in *Proc. 2nd ICFA Advanced Workshop on Physics of High Brightness Beams*, UCLA, Los Angeles, November 9-12, 1999 (World Scientific, Singapore, 2000) and SLAC-PUB-8404 (2000).
- [44] T. Nakamura and T. Yabe, *Comp. Phys. Commun.* **120**, 122 (1999), and earlier work cited therein.
- [45] R. J. Loewen, *A Compact Light Source: Design and Technical Feasibility Study of a Laser-Electron Storage Ring X-Ray Source*, Ph.D. Thesis, Stanford University, 2003, issued as Stanford Linear Accelerator Center report SLAC-R-632.
- [46] R. Warnock and M. Venturini, *Proc. 2003 Part. Accel. Conf., Portland, OR*, paper RPPB061.
- [47] C. de Boor, *A Practical Guide to Splines*, (Springer, New York, 2002).
- [48] M. D. Buhmann, *Radial Basis Functions*, (Cambridge Univ. Press, 2003).
- [49] D. Shepard, *Proc. 23rd Nat. Conf. ACM*, 517-523 (1968).
- [50] R.E. Barnhill, R.P. Dube, and F.F. Little, *Rocky Mountain J. Math.* **13**, 365 (1983).
- [51] For an introduction see lectures of P. Frolkovič,
<http://www.iwr.uni-heidelberg.de/Peter.Frolkovic/lecture.pdf>
- [52] R. J. LeVeque, *Finite Volume Methods for Hyperbolic Problems*, (Cambridge U. Press, 2002).

2.4 Initial scientific uses of coherent synchrotron radiation in electron storage rings

D.N. Basov⁴, J. Feikes¹, D. Fried⁵, K. Holldack¹, H.W. Hübers², P. Kuske¹,
 M.C. Martin³, S.G. Pavlov², U. Schade¹, E.J. Singley³, G. Wüstefeld¹,
¹BESSY, ²DLR, ³ALS-LBL, ⁴UCSD-Physics,
⁵[UCSF-Biomaterials&Bioengineering Div, Preventive&Restorative Dental Sc. Dept](http://www.ucsf.edu/biomaterials/bioengineering)
schade@bessy.de

2.4.1 Introduction

The terahertz (THz) and sub-THz region of the electromagnetic spectrum bridges the infrared and the microwave. This boundary region is beyond the normal reach of optical and electronic measurement techniques normally associated with these better-known neighbors. Only over the past decade has this THz region become scientifically accessible with broadband sources of moderate intensity being produced by ultra-fast laser pulses incident on biased semiconductors or non-linear crystals [1, 2]. Very recently, a much higher power source of THz radiation was demonstrated: coherent synchrotron radiation (CSR) from short, relativistic electron bunches [3-5]. Coherent synchrotron radiation will open up new territory in the THz frequency range with intensities many orders of magnitude higher than previous sources. The energy range between microwave and the far infrared, $3 - 33 \text{ cm}^{-1}$ (0.1 - 1 THz), has proven to be challenging to access and is therefore referred to as the "THz gap". However, with the new CSR source at BESSY [3, 5] we have been able to extend traditional infrared measurements down into this sub-terahertz frequency range. This source is broadband

and is made up of longitudinally coherent single-cycle sub-picosecond pulses with a high repetition rate (100's of MHz). With the combination of high intensity and short pulse duration new opportunities for scientific research and applications are enabled across a diverse array of disciplines from condensed matter physics, to medical, technological, manufacturing, space and defense industries. Imaging, spectroscopy, femtosecond dynamics, and driving novel non-linear processes are all among the potential applications. The high average power of the CSR source allows one to extend experimental conditions to lower frequencies than have been possible with thermal and conventional synchrotron sources (Figure 1). In this paper, we make use of the stable CSR THz source at BESSY for three initial scientific demonstration experiments.

The coherent synchrotron radiation at BESSY was used to precisely measure transitions of singly ionized shallow acceptors in semiconductors by means of photoconductive spectroscopy. As a prototype material for these experiments germanium doped by gallium (Ge:Ga) was used. Ge:Ga is a widely used detector material for applications at terahertz frequencies. Detectors of this system have for instance been used onboard of ISO [6], ESA's Infrared Space Observatory, and are currently in use in NASA's Spitzer space telescope. A thorough understanding of the detector response is of prime importance for the interpretation of the data measured with these expensive instruments. THz CSR provides a powerful tool to characterize the response of these detectors as well as to investigate the physical mechanisms involved in the detection process. The results obtained at BESSY allow to identify the origin of a long wavelength ($> 300 \mu\text{m}$) response. It can be attributed to transitions from excited Ga states into the valence band. The results indicate that a cascade type of relaxation exists in Ge:Ga at 4.5 K.

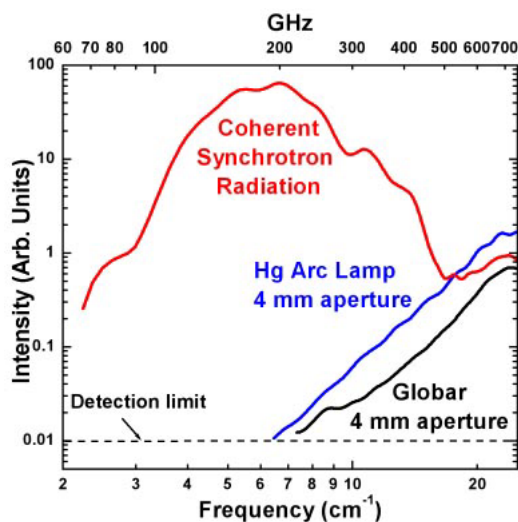


Figure 1: Measured far-IR intensity for the BESSY CSR source, compared to mercury arc and tungsten conventional thermal sources. While the turn-on of the CSR source below 2 cm^{-1} is a real effect of the CSR emission process, the drop off at the low frequency end is due to a combination of diffraction losses in the optical path of the beamline and the cutoffs of the optical components, such as the mylar beamsplitter, in the interferometer.

In another experiment at BESSY we used the high brilliance of the CSR for optical reflectivity measurements of the c-axis Josephson plasma resonance (JPR) in the highly anisotropic, optimally doped high-temperature superconductor $\text{Bi}_2\text{Sr}_2\text{CaCu}_2\text{O}_8$ at low

frequencies [7], which is not reachable by conventional sources for optical measurement on high-temperature superconductors. Despite being perhaps the most frequently studied high- T_c compound, the JPR, which is a direct probe of the superfluid density, has until now not been observed due to its frequency being lower than can be reached by traditional optical spectroscopy systems. In the particular experiment we obtain the magnitude and temperature dependence of the Josephson plasma frequency in zero magnetic field.

The high brilliance of this new accelerator-based coherent source at BESSY is also employed for scanning near-field microscopy in the THz and sub-THz range where spatial resolution below the diffraction limit is achieved [8]. Together with a Martin-Puplett spectrometer this technique enables spectroscopic mapping of samples under investigation. The potential of the technique is exemplified by images of biological samples. Strongly absorbing living leaves have been imaged in transmittance with a spatial resolution of 130 μm at about 12 wavenumbers (0.36 THz). The THz near-field images reveal distinct structural differences of leaves from different plants investigated. The CSR source can also be used for spectral imaging of bulky organic tissues. Human teeth samples of various thicknesses have been imaged between 2 and 20 wavenumbers (between 0.06 and 0.6 THz). Regions of enamel and dentin within tooth samples are spatially and spectrally resolved, and buried caries lesions are imaged through both the outer enamel and into the underlying dentin.

2.4.2 Sub-terahertz response of stressed and unstressed Ge:Ga photoconductive detectors

Germanium doped with gallium (Ge:Ga) is widely used for sensitive detectors of far-infrared (FIR) or terahertz (THz) radiation [9]. The detection mechanism is based on a transition from the Ga ground state to the valence band. The long-wavelength cutoff of such detectors is determined by the energy of the ground state, for Ge:Ga $\sim 120 \mu\text{m}$ [10]. This cutoff can be extended to longer wavelengths ($\sim 240 \mu\text{m}$) by applying a compressive force to the crystal [11]. A compressive force along the $\langle 100 \rangle$ crystal axis removes the degeneracy at the top of the valence band and decreases the acceptor binding energy [12]. Detectors of this type are utilized in many space or airborne observatories for far-infrared astronomy. Examples are ISO, ESA's Infrared Space Observatory [6], the Spitzer Space Telescope [13], which is currently in operation, and SOFIA, the Stratospheric Observatory for Infrared Astronomy, a DLR-NASA observatory [14]. Despite the wide use of this type of detector there remain some fundamental questions: A long wavelength response at $1\text{-}10 \text{ cm}^{-1}$ which increases with applied stress was observed by several groups in unstressed Ge:Ga [15, 16]. However the origin of the response remained unclear. Another peculiarity of Ge:Ga, which is controversially discussed is, whether the cascade capture model is the appropriate explanation for hole capture by attractive hydrogen centers such as Ga in p-type germanium [17]. It has been proposed that direct capture into the ground state exceeds cascade capture for $T > 3 \text{ K}$ for singly ionized acceptors [18, 19].

The experiments have been performed at the THz port of the IRIS beamline [20] at BESSY using a polarizing step scan Fourier transform spectrometer (FTS) [21]. Single sided interferograms have been measured. The unapodized resolution was 0.15 cm^{-1} . BESSY was operated in a dedicated low α mode ($\alpha = 4 \times 10^{-5}$) with a current of about 40 mA. In this way powerful and coherent THz synchrotron (CSR) radiation below

50 cm^{-1} was generated [3, 5]. The unstressed Ge:Ga is a cube of 4 mm side length with a doping concentration of $6 \times 10^{15} \text{ cm}^{-3}$ and a compensation of about 1%. The stressed Ge:Ga is a cube of $1 \times 1 \times 1 \text{ mm}^{-3}$ with a Ga doping concentration of $2 \times 10^{14} \text{ cm}^{-3}$ and a compensation of less than 1%. Stress was applied by a screw and a piston. A ball bearing decoupled the torque from the screw from the detector. By this means a compressive force of $\sim 6 \times 10^8 \text{ Pa}$ was applied along the $\langle 100 \rangle$ crystal axis. The samples were mounted in a liquid Helium cryostat. The temperature of the samples was 4.5 K. A cold black polyethylene filter was mounted in front of the samples to reduce background radiation. The THz CSR radiation from BESSY passed through the FTS and was concentrated onto the samples by a parabolic mirror and a cone. The photocurrent induced by the CSR in the samples was detected by a lock-in amplifier with reference to the 1.25 MHz revolution frequency of BESSY.

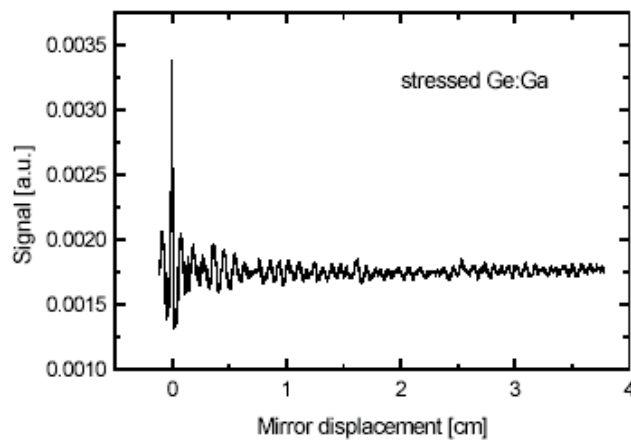


Figure 2: Interferogram obtained from the stressed Ge:Ga crystal

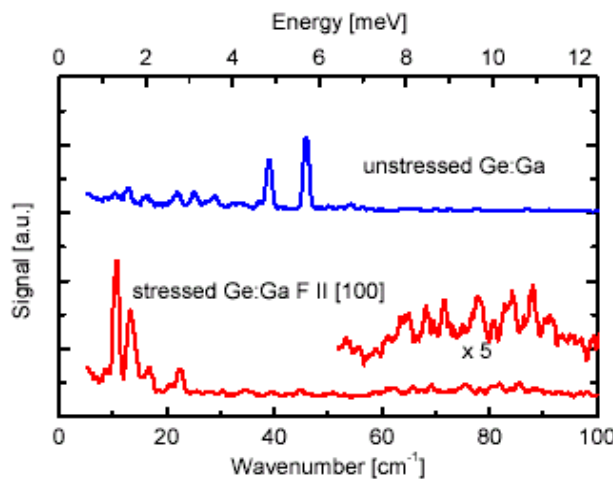


Figure 3: Photoconductivity spectra of unstressed and stressed Ge:Ga.

A typical interferogram is shown in Fig. 2 while Fig. 3 displays the photoconductivity spectra for stressed and unstressed Ge:Ga. The upper trace in Fig. 3 is the spectrum of unstressed Ge:Ga. The two peaks between 4 meV and 6 meV are due to the Sb donors, which are the compensating dopants in Ge:Ga. The larger peak at 5.72 meV

corresponds to the transition from the $1s(A_1)$ ground state to the $2p_0$ state (5.71 meV [22, 23]) and the smaller peak at 4.82 meV to the transition from the $2p_0$ state to the conduction band (4.74 meV [22, 23]). The small peaks below 3 meV are due to transitions from bound excited states of Ga to the valence band.

The results show a significant response of Ge:Ga detectors at long wavelengths outside the bands for which they are originally designed. For any detector application care should be taken to block the long wavelength response by appropriate filters. In addition, the results indicate that a cascade type of relaxation exists in Ge:Ga at 4.5 K. In case of direct capture to the ground state none of the excited states would be observable.

2.4.3 Observation of the Josephson plasma resonance in optimally doped $\text{Bi}_2\text{Sr}_2\text{CaCu}_2\text{O}_{8-\delta}$

One of the most outstanding problems in the field of high temperature superconductivity is determining how the normal state quasi-2D metal is related to the 3D superconducting state. For all cuprate superconductors the gross electronic properties within the CuO_2 planes are similar, exhibiting a “bad metal” behavior. The carrier concentration is low and the damping is strong. In contrast, the electronic properties perpendicular to the CuO_2 planes cover a broad spectrum, from marginally conducting overdoped $\text{YBa}_2\text{Cu}_3\text{O}_7$, to the essentially insulating character of $\text{Bi}_2\text{Sr}_2\text{CaCu}_2\text{O}_8$. The role of this varying degree of anisotropy in the CuO_2 intralayer and interlayer electronic properties in producing high temperature superconductivity is still unresolved [24].

The energy scale of the Josephson plasma edge is directly related to the degree of anisotropy of the material. In nearly all families of high temperature superconductors the plasma edge has been observed in the far infrared frequency range [25]. The one exception is in the extremely anisotropic $\text{Bi}_2\text{Sr}_2\text{CaCu}_2\text{O}_8$ (Fig. 4, left) where at optimal doping the plasma edge has not been seen. By doping this compound with Pb, and hence lowering the anisotropy (and T_c), the plasma edge is observed near 40 cm^{-1} [26]. Additionally, when reducing the carrier doping a resonance is observed in magnetoabsorption experiments in the microwave region, usually attributed to the Josephson plasma effect [27]. Our reflectivity measurements on optimally doped $\text{Bi}_2\text{Sr}_2\text{CaCu}_2\text{O}_8$ down to 4 cm^{-1} using the coherent synchrotron radiation at BESSY show the Josephson plasma resonance, clearly.

In order to make specular reflectance measurements at wavelengths in excess of 1 mm, it is necessary to have a sample larger than the wavelength of the probing radiation. Since single crystal of high temperature superconductors with c-axis dimension $\gg 1$ mm are difficult to prepare, a mosaic of several pieces of a crystal was assembled with a net c-axis length of ~ 5 mm (Fig. 4, right). While this circumvents problems of diffraction effects, additional complications arise due to reflection from the conducting epoxy that binds the individual crystals together. Absolute values of the reflectivity were obtained by coating the sample in situ with a thin layer of gold, and using the gold-coated sample as a reference.

The top panel of Fig. 5 shows the experimental reflectance in the sub-terahertz region on a logarithmic frequency scale. It is useful to examine the normal state spectrum at 90 K (black curve) to discuss the signal to noise ratio in different frequency regions. On the high energy side of the spectrum the signal to noise is $\pm 5\%$. This is due

to the relatively low intensity of the source at these energies (Fig. 1). The largest noise contribution is in a small band near 20cm^{-1} , where the uncertainty is now $\pm 10\%$. This is 50 Hz electrical noise in the synchrotron electron beam and/or the beamline. The Fourier transform interferometer modulates this to the frequency range near 20cm^{-1} . Most significant is the relatively small error of $\pm 2\%$ in the very low frequency range. Hence, the best response of the CSR measurement system is at the most inaccessible region for traditional infrared sources.

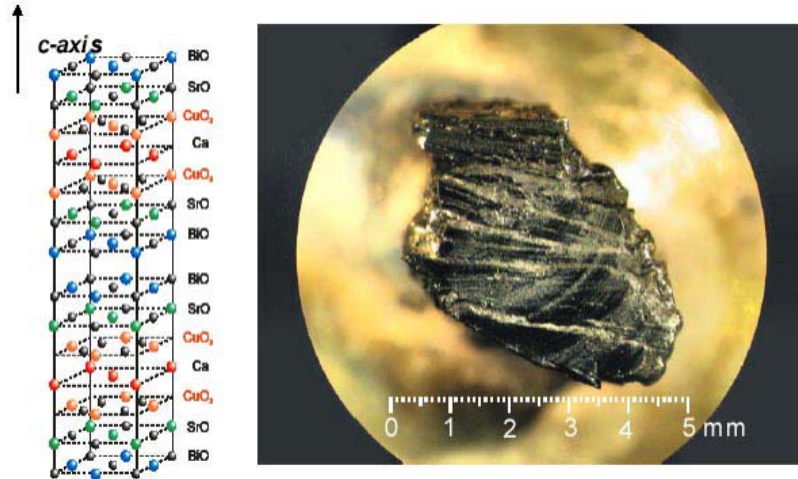


Figure 4: Structure of $\text{Bi}_2\text{Sr}_2\text{CaCu}_2\text{O}_8$ (left) and the mosaic of the single crystals used in this investigation (right). To account the contribution to the measured reflectance the area of epoxy showing was estimated and the experimental reflectance was corrected accordingly.

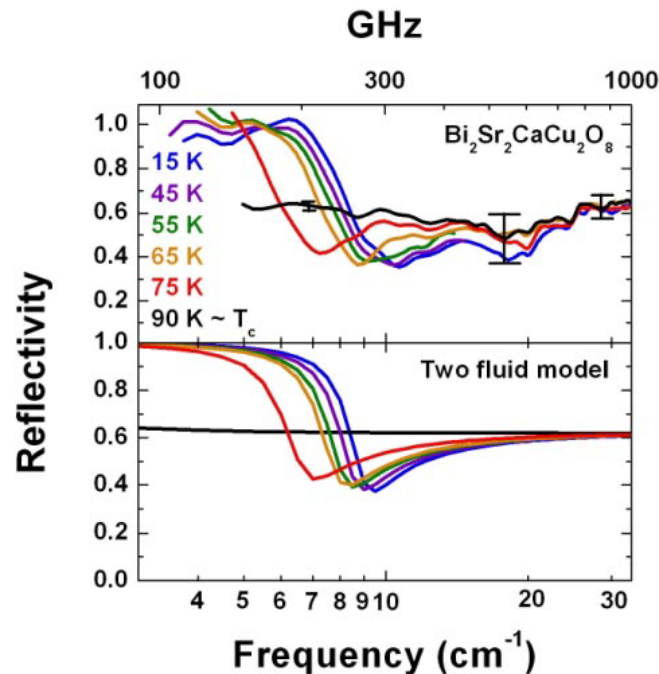


Figure 5: Measured c-axis polarized near-normal reflectivity of $\text{Bi}_2\text{Sr}_2\text{CaCu}_2\text{O}_8$ (upper panel) for various temperatures at or below the superconducting transition temperature, T_c . A resonance that shifts with temperature and disappears above T_c is clearly observed. The lower panel shows the calculated reflectivity of a superconductor with a shifting Josephson Plasma Resonance.

In contrast to the nearly flat and featureless spectrum at $T = T_c$, the $R(\omega)$ spectra at $T < T_c$ show a strong ω dependence. Below T_c the spectrum has a shallow minimum followed by a strong rise in the reflectivity. At the lowest frequency the spectra saturate to a constant value near unity. As the temperature decreases while the sample is in the superconducting state, both the minimum and reflectance edge increase in frequency, although this shift nearly saturates by 15 K. The reflectance edge in the superconducting state signals the flow of supercurrents along the c-axis. Since the density of superfluid increases as the temperature is lowered, the reflectance edge shifts to higher frequencies.

In order to extract quantitative information from the spectrum we model the reflectance with a two fluid model. One component consists of the dissipationless supercurrents, while the other is an over-damped plasmon [28]. The second term is necessary to account for finite reflectivity at the plasma minimum, and the rounding at the top of the reflectance edge. The bottom panel of Fig. 5 shows the results of this modeling. The magnitude, the frequency and the temperature dependence of the data in the top panel are well accounted for.

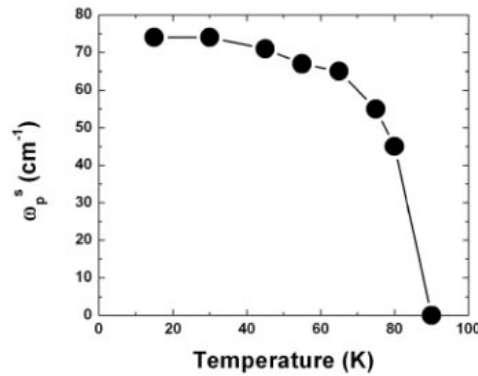


Figure 6: Superfluid plasma frequency as a function of temperature. Plasma frequency was determined from fitting the reflectance spectra with the two fluid model shown in the bottom panel of Figure 5.

Using the above modeling we are also able to extract the value of the unscreened Josephson plasma frequency. At 15 K we obtain a value of $\omega_{ps} = 74 \text{ cm}^{-1}$. This value corresponds to a c-axis penetration depth value of $\lambda_c = 21 \text{ }\mu\text{m}$. The complete temperature dependence of the Josephson plasma frequency is summarized in Fig. 6. The plasma frequency rises quickly below T_c , and is nearly saturated at the low temperature limit by $T_c/2$.

Another dip in our experimental data near 20 cm^{-1} might be a transverse Josephson plasma mode [29] in $\text{Bi}_2\text{Sr}_2\text{CaCu}_2\text{O}_8$ caused by the two different distances between CuO layers in the crystal structure. This feature in the data is, however, located right where the signal to noise ratio is the worst due to interference from 50 Hz pickups. This will be investigated further.

We report here the directly measured the Josephson plasma resonance in optimally doped $\text{Bi}_2\text{Sr}_2\text{CaCu}_2\text{O}_8$ for the first time by applying the powerful coherent synchrotron radiation source at BESSY. The results presented provide a connection between the magnetoabsorption experiments performed on underdoped $\text{Bi}_2\text{Sr}_2\text{CaCu}_2\text{O}_8$ and the infrared experiments in other families of high temperature superconductors.

2.4.4 THz scanning near-field microspectroscopy on biological samples

The spatial resolution of conventional THz imaging is diffraction limited and thus only features with a dimension from hundred micrometers to millimeters are resolvable. This limit can be overcome by utilizing near-field imaging techniques [30] achieving spatial resolutions of up to $\lambda/1000$ [31]. However, extremely brilliant sources are necessary to compensate for intensity losses to confine the THz radiation at the cost of total power.

A THz scanning near-field imaging (SNIM) technique benefiting from the broadband and highly brilliant coherent synchrotron radiation (CSR) from an electron storage ring [3, 5] is established at BESSY utilizing a detection method based on locking onto the intrinsic time structure of the synchrotron radiation. The CSR source at BESSY is a pulsed source with a frequency of 1.25 MHz determined by the time the relativistic electron bunch needs to travel one orbit with a circumference of 240 m. The emitted CSR power varies with the square of the decaying electron ring current stored which has to be taken into account for data normalization.

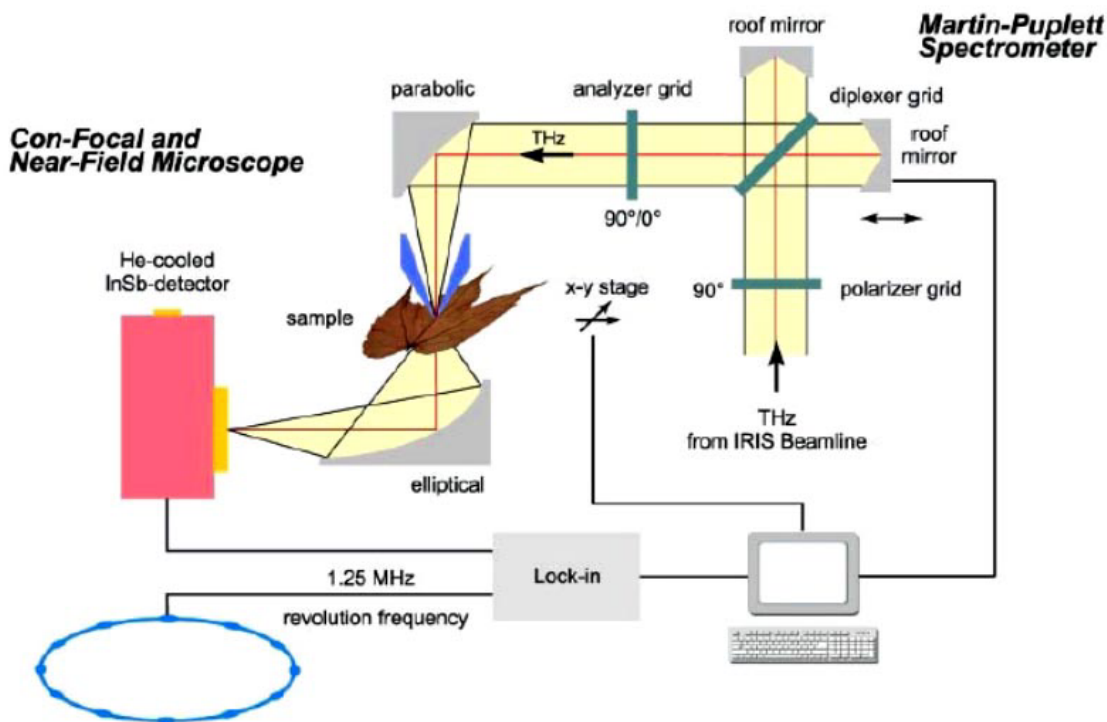


Figure 7: Schematic diagram of the THz scanning near-field infrared microscopy (SNIM) setup.

The THz SNIM is attached to the infrared beamline IRIS [20] at BESSY and the setup is shown in Fig. 7. The far-infrared port of the beamline provides a collimated CSR THz beam which is about 98% linearly polarized. The THz beam passes through a Martin-Puplett spectrometer before being transferred to the SNIM where it is focused into a conical waveguide with a circular cross-section and an exit aperture of a diameter smaller than the wavelength. The sample is held in front of the exit aperture by a spring ensuring that the sample is in direct contact to the probe. Imaging is performed by moving the sample in front of the exit aperture by means of a computer controlled x-y stage. The evanescent field at the exit aperture penetrates the sample and the scattered

radiation containing the spectral information is collected by an ellipsoidal mirror and is then focused onto a LHe-cooled InSb detector. The revolution frequency of the electron bunches stored is used as a reference for lock-in detection of the SNIM signal by a fast liquid He cooled InSb detector. This detection provides a detection dynamics of nine orders of magnitude, which is essential for near-field imaging in strongly absorbing samples since it discriminates intensity from the source against thermal background radiation emitted by the beamline, the sample itself and the environment. The image is generated by interpretation of the SNIM signal versus sample position relative to the cone axis.

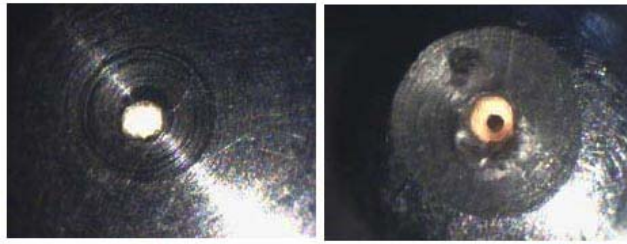


Figure 8: Aperture of 200 μm diameter with a coaxial wire of 80 μm thickness (right) and without a wire (left).

Conical aperture probes with a cone angle of 50° with two different aperture diameters of 100 and 200 μm have been employed for our experiments. Similar near-field probes have been proposed by Keilmann [32]. The conical aperture probe drastically attenuates the free-space THz radiation for wavelengths longer than the cut-off wavelength, $\lambda_c = 1.71 d_c$, where d_c is the relevant cross-section diameter of the cone [33]. The power output of the near-field probe for a specific wavelength then depends on the cone angle and the diameter of the exit aperture [34]. To increase the transmitted power and to shift the transmittance to longer wavelengths we also tested coaxial wire cones as described by Keilmann [33] and which are known to have theoretically no cut-off behavior. Both apertures under investigation, with and without a coaxial wire, are shown in Fig. 8. Fig. 9 shows the single channel spectra of the incident THz beam and the THz beam transmitted through the cones. Since the measurements are performed at ambient atmosphere all single channel spectra presented show distinct water absorption bands that do not interfere with our discussion. As expected from the geometry of the cones the transmitted power is reduced by several orders of magnitude. The transmittance of the cone without the wire has its maximum in the higher frequency range at wavenumbers where the CSR source starts to emit radiation. For the coaxial cone with a wire also a cut-off is observed. However, the maximum transmission shifts to smaller wavenumbers, e.g. to longer wavelengths. In contrast to the cone without the wire the transmission is suppressed for larger wavenumbers, perhaps caused by an insufficient coupling of the plane wave to the cone in this frequency range.

The spatial resolution of the THz SNIM was investigated by scanning the edge of an aluminum film on a Si wafer along the near-field probe. We obtained a spatial resolution that is on the order of the diameter of the aperture. From the 2σ -value of the Gaussian fit of the first derivative of the experimental data, the spatial resolution is estimated to be about 130 μm for the 200 μm aperture probe and can be improved to 70 μm using the 100 μm aperture probe shown in Fig. 10. Taking broadband near-field images the spectral center of gravity at around 12 cm^{-1} is transmitted yielding an

average spatial resolution of $\lambda/6$ for the 200 μm aperture and $\lambda/12$ for the 100 μm aperture, respectively.

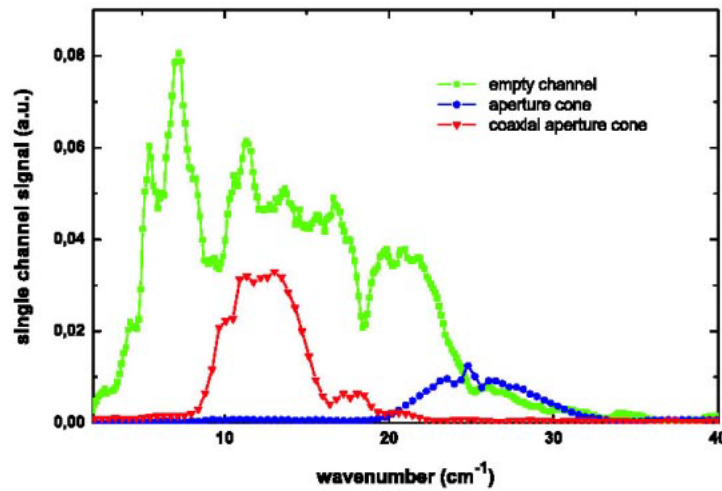


Figure 9: Single channel spectra of the empty spectrometer channel, of the aperture cone and of the coaxial aperture cone. The intensity of the empty channel spectra is attenuated by a factor of 100. Note, that the single channel intensities are shown in a linear scale. Intensities through both cones are for wavenumbers down to 2 cm^{-1} .

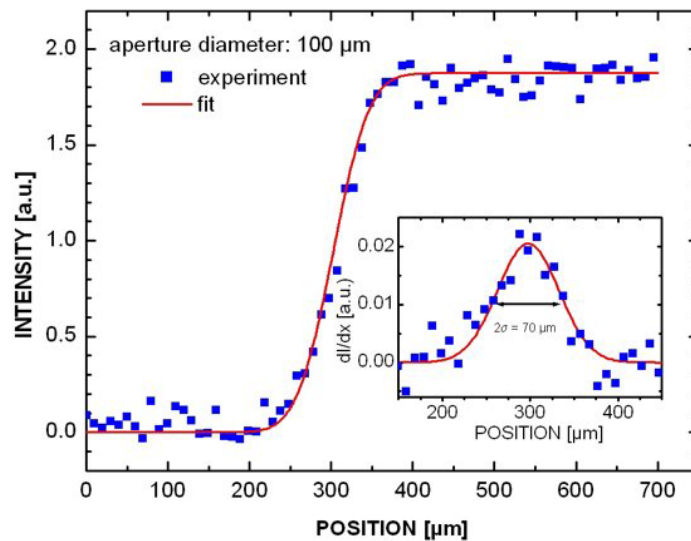


Figure 10: Measured and fitted spatial resolution curves for an exit aperture of 100 μm diameter. The inset shows a Gaussian fit of the first derivative of the measured curve used to determine the spatial resolution.

The THz SNIM concept for applications on biological samples has been tested on leaves [8], where the contrast is mostly formed by the amount of liquid water present. Recently, images of living leaves have also been obtained by other authors [35, 36] from a confocal setup applying THz time-domain spectroscopy (TDS) to investigate the rehydration process of plants after watering. However, the spatial resolution of these investigations is restricted to the order of the wavelength applied. Using the THz SNIM technique presented here, much more detailed images can be obtained.

Figure 11 shows a part of a freshly cut *parthenocissus* leaf imaged in transmission. In its THz near-field image an inner structure of the veins is apparent which is mainly formed by liquid water absorption and possible scattering at the structural boundaries. Both the THz image and the visible light image reveal similar object features but the THz SNIM enables studies of hydration dynamics with a high spatial resolution because it is sensitive to the water concentration in the sample.

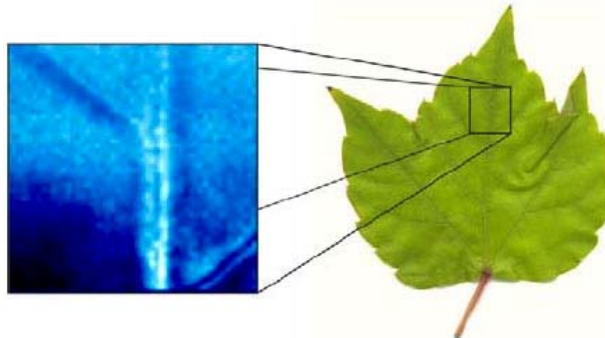


Figure 11: Near-field THz image (left) of a section of a *parthenocissus* leaf. Less absorption is indicated by a darker region in the THz image.

As initial tests of the feasibility of using sub-THz radiation in dentistry for the diagnosis of tooth decay, we have imaged human tooth material using the THz SNIM together with the coherent synchrotron radiation source at BESSY. If caries lesions are detected early enough, they can be arrested without the need for surgical intervention. X-ray imaging is a well-established method to image human teeth. With this method, buried caries lesions can be imaged by a contrast change due to demineralization in the particular tooth region. However, the change in contrast is rather weak and only larger and strongly effected regions become visible in the x-ray image. Additionally, due to the ionizing nature of x-rays this method is not optimal for regular monitoring and many groups are exploring the infrared and THz radiation for medical imaging applications where both early diagnosis and safety issues are important. Recently, a more sensitive imaging method applying near infrared radiation was introduced [37], showing the potential to image early dental decay in the enamel. Tooth decay in the dentin could not be imaged by this method since the dentin is almost opaque in the near infrared. THz pulse imaging in the far infrared wavelength range has been performed for the detection of early stage caries in the enamel layer of thin (100 μm) human tooth cross sections [38] obtaining a higher attenuation of THz radiation in carious enamel as compared with healthy enamel. In contrast to the later confocal imaging investigation we applied the near-field technique and sub-THz radiation to image bulky tooth samples. Simulated buried caries lesions were produced by drilling 1-mm diameter cavity in the proximal region of the tooth and filling the cavity with hydroxyapatite paste [37] as shown in Fig. 12. The integral sub-THz image of the 2.7 mm thick tooth slab is shown in Fig. 13 both for con-focal imaging and near-field imaging. The near-field image was obtained utilizing the 200- μm wire cone while the confocal imaging was performed with the same optical set-up as shown in Fig. 7 except that the near-field cone was now removed. In confocal imaging geometry the tooth can not be spatially resolved and the image is strongly blurred as one would expect from diffraction due to the long wavelengths involved. In contrast the enamel and the dentin regions of the tooth sample as well as the simulated buried caries lesion together with other inner structural diversities are spatially resolved in the near-field image. Spectral near-field images have been obtained

from the same sample. Figure 14 shows a series of images of the area with the simulated lesion for different wavenumbers. In the spectral band between 5 and 7 wavenumbers (2., 3. and 4. frame from left of the upper row in Fig. 14) the lesion is indicated by a lower attenuation of the sub-THz radiation in comparison to the absorption of the surrounding material. Whether this experimentally observed contrast is indicative for buried carious lesions in human teeth is still speculative and further investigations on the optical properties of tooth tissues and on the propagation of sub-THz radiation in inhomogeneous bulky samples have to be conducted.

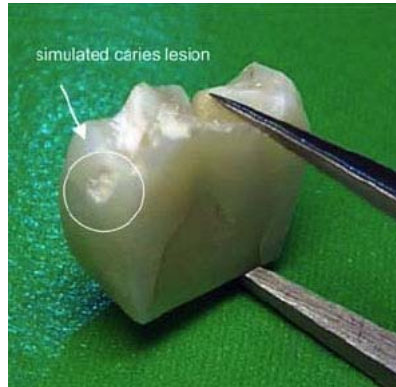


Figure 12: Photograph of a 2.7 m thick human tooth slab. The buried caries lesion is labeled on the left side.

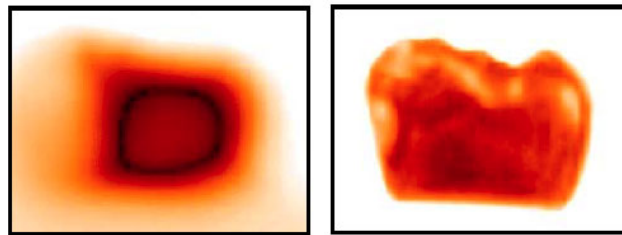


Figure 13: Confocal (left) and near-field (right) integral THz image of the tooth sample of Fig. 12.

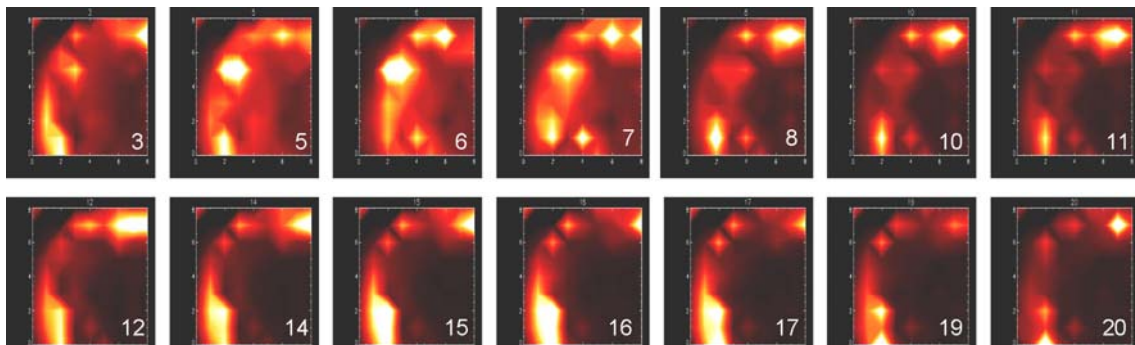


Figure 14: Series of spectral near-field images of the lesion region (upper left corner of the near-field image of Figure 12) between 3 and 20 cm^{-1} (between 0.5 and 3 mm wavelength). The corresponding wavenumber is indicated on top of each spectral frame.

These results on confining sub-THz radiation from an electron storage ring presented may have important implications for extending near-field applications to other imaging or spectroscopic applications in both life and material sciences.

2.4.5 Summary

The production of stable, high power, coherent synchrotron radiation at sub-terahertz frequency at the electron storage ring BESSY opens a new region in the electromagnetic spectrum to explore physical properties of materials. Just as conventional synchrotron radiation has been a boon to x-ray science, coherent synchrotron radiation may lead to many new innovations and discoveries in THz physics. With this new accelerator-based radiation source we have been able to extend traditional infrared measurements down into the experimentally poorly accessible sub-THz frequency range.

The feasibility of using the coherent synchrotron radiation in scientific applications was demonstrated in a series of experiments: We investigated shallow single acceptor transitions in stressed and unstressed Ge:Ga by means of photoconductance measurements below 1 THz. We have directly measured the Josephson plasma resonance in optimally doped $\text{Bi}_2\text{Sr}_2\text{CaCu}_2\text{O}_8$ for the first time and finally we succeeded to confine the sub-THz radiation for spectral near-field imaging on biological samples such as leaves and human teeth.

2.4.6 References

- [1] Auston, D.H. et al., Phys. Rev. Lett **53** (1984), 1555.
- [2] Ferguson, B. and X.C. Zhang, Nature Materials **1** (2002), 26.
- [3] Abo-Bakr, M. et al., Phys. Rev. Lett, **8825** (2002), 254801.
- [4] Carr, G.L. et al., Nature, **420** (2002), 153.
- [5] Abo-Bakr, M. et al., Phys. Rev. Lett. **90** (2003), 094801.
- [6] Wolf, J., Optical Engineering **33** (1994), 1492.
- [7] Singley E.J., et al., , Phys. Rev. B. **69** (2004), 092512.
- [8] Schade, U., et al., Appl. Phys. Lett. **84** (2004), 1422.
- [9] Haller, E. E., Infrared Phys. Technol. **35** (1994), 127.
- [10] Beeman, J. and Haller, E. E., Infrared Phys. Technol. **35** (1994), 827.
- [11] Kazanskii, A. G., et al., Appl. Phys. Lett. **3** (1977), 496.
- [12] Hasegawa, H., Phys. Rev. **129** (1963), 1029.
- [13] Schnurr, R., et al., Proc. of the Conf. on Infrared Astronomical Instrumentation SPIE **3354** (1998), 322.
- [14] Rabanus, D., et al., Proc. of the Conf on Airborne Telescope Systems, SPIE **4014** (2000), 137.
- [15] Kimmitt, M.F., et al., Proc. of the Conf. on Infrared Physics, (1988) 289.
- [16] Meny, C., et al., Proc. of the 15th Int. Conf. on Infrared and Millimeter Waves, (1990), 230.
- [17] Lax, M., Phys. Rev. **119** (1960), 1502.
- [18] Lax, M., Phys. Rev. **119** (1960), 1502.
- [19] Darken, L. S., Phys. Rev. Lett. **69** (1992), 2839.
- [20] Wilke, I., et al., Sol. State Comm. **93** (1995), 409.
- [21] Schade, U., et al., Rev. Sci. Instrum. **73** (2002), 1568.
- [22] Martin, D. H., and Puplett, E., Infrared Phys. **10** (1969), 105.
- [23] Landolt-Börnstein, New Series **II/22b** (1991), 480.
- [24] Anderson, P.W., *The theory of superconductivity in the high-Tc cuprates*. Princeton series in physics. Princeton, N.J., Princeton University Press, 1997.
- [25] Dordevic, S.V., et al., Phys. Rev. B, **65** (2002), 134511.
- [26] Motohashi, T., et al., Phys. Rev. B, **61** (2000), R9269.

- [27] Tsui, O.K.C., et al., Phys. Rev. Lett. **73** (1994), 724.
 [28] The Drude model was used for the over damped plasmon with $\omega_p = 895 \text{ cm}^{-1}$ and $1/\tau = 8,000 \text{ cm}^{-1}$.
 [29] Kakeshita, T., et al., Phys. Rev. Lett. **86** (2001), 4140.
 [30] Knoll, B., and Keilmann, F., Nature **399** (1999), 134.
 [31] Chen, H.-T., et al., Appl. Phys. Lett. **83** (2003), 3009.
 [32] Keilmann, F., U.S. Patent No. 4,994,818 (1991, filed 1989).
 [33] Keilmann, F., Infrared Phys. Technol. **36**, 217 (1995).
 [34] Knoll, B., and Keilmann, F., Opt. Commun. **162**, 177 (1999).
 [35] Mittelman, D., in *Sensing with Terahertz Radiation*, edited by D. Mittelman (Springer, Berlin, 2003), 137.
 [36] Koch, M., in *Sensing with Terahertz Radiation*, edited by D. Mittelman (Springer, Berlin, 2003), 303.
 [37] Jones, R.S., et al., Optics Express **11** (2003), 2259.
 [38] Crawley, D.A., et al., Caries Research **37** (2003), 352.

2.5 Optimizing ring-based CSR sources

J.M. Byrd, S. De Santis, Z. Hao, M. C. Martin, D.V. Munson, D. Li, H. Nishimura,
 D.S. Robin, F. Sannibale, R.D. Schlueter, R. Shoenlein, J.Y. Jung, M. Venturini,
 W. Wan, A. A. Zholents, M. Zolotarev, LBL

JMByrd@lbl.gov

2.5.1 Introduction

Coherent synchrotron radiation (CSR) is a fascinating phenomenon recently observed in electron storage rings and shows tremendous promise as a high power source of radiation at terahertz frequencies. However, because of the properties of the radiation and the electron beams needed to produce it, there are a number of interesting features of the storage ring that can be optimized for CSR. Furthermore, CSR has been observed in three distinct forms: as steady pulses from short bunches, bursts from growth of spontaneous modulations in high current bunches, and from micro modulations imposed on a bunch from laser slicing. These processes have their relative merits as sources and can be improved via the ring design.

The terahertz (THz) and sub-THz region of the electromagnetic spectrum lies between the infrared and the microwave [1]. This boundary region is beyond the normal reach of optical and electronic measurement techniques and sources associated with these better-known neighbors. Recent research has demonstrated a relatively high power source of THz radiation from electron storage rings: coherent synchrotron radiation (CSR) [2]. Besides offering high power, CSR enables broadband optical techniques to be extended to nearly the microwave region [3], and has inherently sub-picosecond pulses. As a result, new opportunities for scientific research and applications are enabled across a diverse array of disciplines: condensed matter physics, medicine, manufacturing, and space and defense industries. CSR will have a strong impact on THz imaging, spectroscopy, femtosecond dynamics, and driving novel non-linear processes.

CSR is emitted by bunches of accelerated charged particles when the bunch length is shorter than the wavelength being emitted. When this criterion is met, all the particles emit in phase, and a single-cycle electromagnetic pulse results with an intensity proportional to the square of the number of particles in the bunch [4, 5]. It is this quadratic dependence that can produce colossal intensities even with fairly low beam currents [2]. Until recently CSR has not typically been observed in electron storage rings because the electron bunch lengths are longer than the waveguide cutoff imposed by the dimensions of the vacuum chamber, so full-bunch coherent emission is suppressed. The first observations of CSR from storage rings were of quasi-chaotic bursts of intensity caused by density modulations in unstable electron bunches [6-9], similar to the self-amplified spontaneous emission (SASE) used in the design of several proposed free electron lasers. While studies of this ‘bursting’ phenomenon have provided glimpses into the powers available with CSR, the unstable nature of the emission makes this a problematic THz source for scientific measurements. We have experimentally verified a model [10] predicting where this unstable bursting regime will occur [9] and have used this experience to design a new source where the bursting instability can be avoided.

Stable CSR has been produced during machine experiments at the BESSY-II storage ring [11, 12] and the first scientific measurements using this CSR source were recently reported [3]. This stable CSR emission is not driven by any instability, yet it extends to higher frequencies than predicted by a simple full-bunch coherence model [12]. This model is described in these proceedings and elsewhere [13]. The combination of the experimentally verified models for stable CSR as well as the threshold of which current levels will produce bursting instabilities allows us to fully design and optimize a new CSR source that will produce copious amounts of stable far-IR, THz and sub-THz, synchrotron radiation.

CSR has also been recently observed in storage rings as a result of laser slicing of the beams [19-21]. In this process, interaction of an electron beam with a femtosecond laser pulse co-propagating through a wiggler modulates the electron energies within a short slice of the electron bunch comparable with the duration of the laser pulse. Propagating around an electron storage ring, this bunch develops a longitudinal density perturbation due to the dispersion of electron trajectories. This perturbation emits short pulses of temporally and spatially coherent terahertz pulses that are inherently synchronized to the modulating laser. Although this technique was originally developed for producing ultrashort x-ray pulses, the CSR emission has interesting possibilities as a source.

In this paper, we present several of the concepts for optimizing a ring for producing both stable CSR and ultrashort terahertz pulses from laser sliced beams in the context of CIRCE (Coherent InfraRed Center), a ring we have proposed which incorporates many of these concepts. Many of these concepts were originally inspired by a compact CSR source described by Murphy et al. [15]. The first section of this paper presents several general considerations for an optimized CSR ring and is followed by details of CIRCE. We present the calculated CIRCE photon flux where a gain of 6 - 9 orders of magnitude is shown compared to existing far-IR sources. Additionally, the particular design of the dipole vacuum chamber has been optimized to allow an excellent transmission of these far-infrared wavelengths. We believe that a small storage ring optimized for CSR such as CIRCE can be constructed for a modest cost.

2.5.2 General Considerations

As discussed in [22], the wavelength range where CSR can be generated lies between the bunch length and the vacuum chamber cutoff and is given by

$$\frac{2\pi\sigma_z}{\sqrt{\ln(N)}} < \lambda < 2h\left(\frac{h}{\rho}\right)^{1/2} \quad (1)$$

where σ_z is the bunch length, N is the number of the electrons in the bunch. The cutoff wavelength of the vacuum chamber $2h\left(\frac{h}{\rho}\right)^{1/2}$ is determined by the chamber full height h ,

and the bending radius ρ . Note that this cutoff wavelength differs from the familiar waveguide cutoff of plane waves. This is due to the opening angle of the radiation. Although shorter wavelengths can be generated from shorter bunches, the threshold of the CSR microbunching instability strongly limits the bunch charge at shorter bunch lengths. From these considerations, we have determined that optimum natural bunch length for maximizing stable CSR emission from the bunch is in the range of a few psec.

The natural bunch length in an electron storage ring shows the following dependence

$$\sigma_z = \frac{\alpha c \sigma_\epsilon}{2\pi f_s} \propto \sqrt{\frac{\alpha E^3}{\rho \omega_{rf} V_{rf}}} \quad (2)$$

where σ_ϵ is the fractional energy spread, f_s is the synchrotron frequency, E is the beam energy, α the momentum compaction, and ω_{rf} and V_{rf} are the RF angular frequency and voltage. The bunch length can be lowered by reducing beam energy and momentum compaction, and increasing the RF frequency and voltage. Our ideas on achieving this within practical limits in a ring are described below.

The criteria for selecting the beam energy are quite different from a typical synchrotron light source. Because of the radiation wavelength is much longer than the critical wavelength (except for impractically low beam energies), the incoherent radiation intensity and spectrum are independent of wavelength. Rather, the energy is chosen from a weaker set constraints. Foremost is the effect on the bunch length via the energy spread (proportional to E) and longitudinal focusing (proportional to $E^{1/2}$). It is critical that the beam energy be chosen such that the energy spread doesn't increase due to instability or from intrabeam scattering. Furthermore, radiation damping decreases sharply with energy (proportional to E^3), increasing the sensitivity to instabilities which increase inversely proportional to energy. However, lower energy favors several aspects of the mechanical design such as magnets. It also significantly reduces the thermal loading on the first mirror in the beamline due to the radiation at the critical wavelength.

The requirements of the machine lattice are significantly different from those of third generation light sources. The transverse emittance does not need to be minimized because the relatively long wavelength radiation. In fact, it may be useful to increase the emittance in order to mitigate intrabeam scattering effects. Furthermore, there are no immediate advantages to small vertical emittance and thus it may be possible to run at an increased coupling. The primary constraint on the optics is the control of the momentum compaction. Because the primary mechanism for shortening the bunch length at a given beam energy is the momentum compaction, this capability must be

included in the optics as well as the ability to control higher order terms in the momentum compaction via additional sextupole and octupole families. We have found that a modified DBA lattice has all of the desired properties [18].

To shorten the bunch length, it is useful to maximize the RF voltage and frequency. This also increases the threshold for the microbunching instability. Following development of superconducting RF cavities for storage rings, we believe the optimum system available is a 1.5 GHz HOM-damped design which may be capable of reaching voltages of 1 MV. Two such systems have recently been designed and installed [16-17]. One interesting feature of this is that the beam loading at lower beam energy and beam current is extremely small, possibly allowing the cavity to operate at high loaded-Q. Furthermore, the total RF power needed to operate such a system could be below a few kW. Higher frequency RF systems are possible but require increasing smaller apertures to reach significant shunt impedances.

Although the ring size places no direct constraints on the physics of CSR emission, the following practical effects should be considered: adequate straight section space for injection and RF system, arc length sufficient for the modified DBA optics described above, and straight section for a wiggler to allowing laser manipulation of the beam.

There are two interesting considerations on the design of the vacuum system. The first is the difficulty in extracting terahertz synchrotron radiation. The vacuum chamber height must be large enough that the radiation over the desired wavelength range is not suppressed due to waveguide cutoff described above. For example, for $\rho=1$ m, $h=1$ cm, very little radiation is emitted for wavelengths longer than $\lambda_{\text{cutoff}}=2$ mm. It is not trivial to extract the CSR because of the relatively large opening angle of the radiation compared with that at the critical wavelength. The opening angle is given by

$$\theta_{\text{rad}} = \left(\frac{\lambda}{2\pi\rho} \right)^{1/3} \quad (3)$$

The beamline typically requires over 100 mrad vertical acceptance to extract most of the radiation at millimeter wavelengths. The second consideration is the geometric impedance of the vacuum chamber. Our studies indicate that the broadband component of this impedance is negligible compared to the radiation impedance. In other words, at bunch lengths short enough to generate CSR, the radiation impedance is dominant and other broadband impedances can be neglected. However, it is important to consider narrowband impedances if the ring is operated in multibunch mode.

2.5.3 Circe Ring Design & Beamline Extraction

We now want to design CIRCE, a ring-based source optimizing the emission and extraction of CSR. In the design of such a source one of the fundamental requirements is the stability of the CSR emission. We have therefore optimized the various machine parameters to maximize the CSR emission while keeping the beam current below the bursting threshold [9,13]. We maximize the CSR bandwidth by designing a vacuum chamber with a very low frequency cutoff to allow for transmission of wavelengths out to ~ 1 cm, and by tuning the ring parameters to increase the static distortion of the electron bunch profile as discussed in [13,22] to extend the CSR emission to shorter wavelengths. A double-bend achromat lattice was chosen to allow significant flexibility in getting to low momentum compaction, a key requirement to produce ~ 1 picosecond

bunch lengths. Lowering the energy of the electron beam to a moderate value of 600 MeV, helps shorten the bunches but is not so low that it becomes difficult to maintain the stability of the electron beam. A higher-frequency RF system (1.5 GHz superconducting) also aids in shortening the electron bunches. Additional families of magnets were added to allow fine control of higher order components of the momentum compaction.

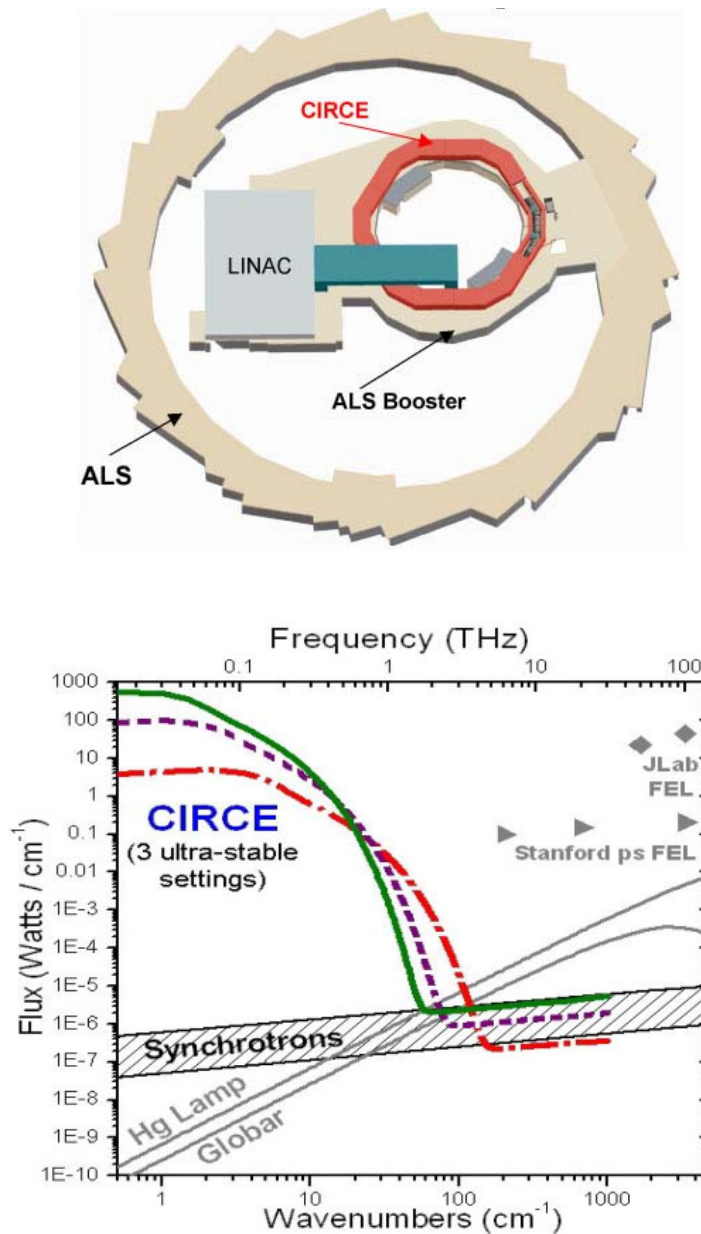


Figure 1. Top) Location of the CIRCE ring on top of the existing ALS booster shielding. The ring design allows for numerous CSR beamlines located directly next to the shield walls and the parasitic use of the ALS injector for full-energy beam injection into CIRCE. Bottom) Flux calculations for CIRCE compared with conventional synchrotron and thermal far-IR sources, as well as two existing free electron lasers. The three CIRCE curves demonstrate how the CIRCE source can be tuned for high power, for extending coherent emission to shorter wavelengths, or somewhere in between.

The optimized size of a ring having all these parameters is almost the same size as the existing Advanced Light Source (ALS) booster ring, which allows an opportune use of available space at the ALS. We propose to build the CIRCE ring on top of the existing booster shielding and make use of the booster for full energy injection, as shown in a 3 dimensional computer aided design (CAD) drawing in Figure 1, top. The booster shielding tunnel is a single, poured in place, 1 meter thick concrete structure. As such it is quite stable with accelerometer measurements showing that the top surface is as stable as the main ALS experimental floor. We plan to build a compact shielding block system very close to the CIRCE ring to allow for the beamlines to fit on the same booster ring shielding surface. This proximity of the beamlines to the source points in the bending magnets gives another advantage for keeping the vibration pickup on the photon beam to a minimum. Initial studies of the ALS infrastructure have found no showstoppers for building the CIRCE ring on this location.

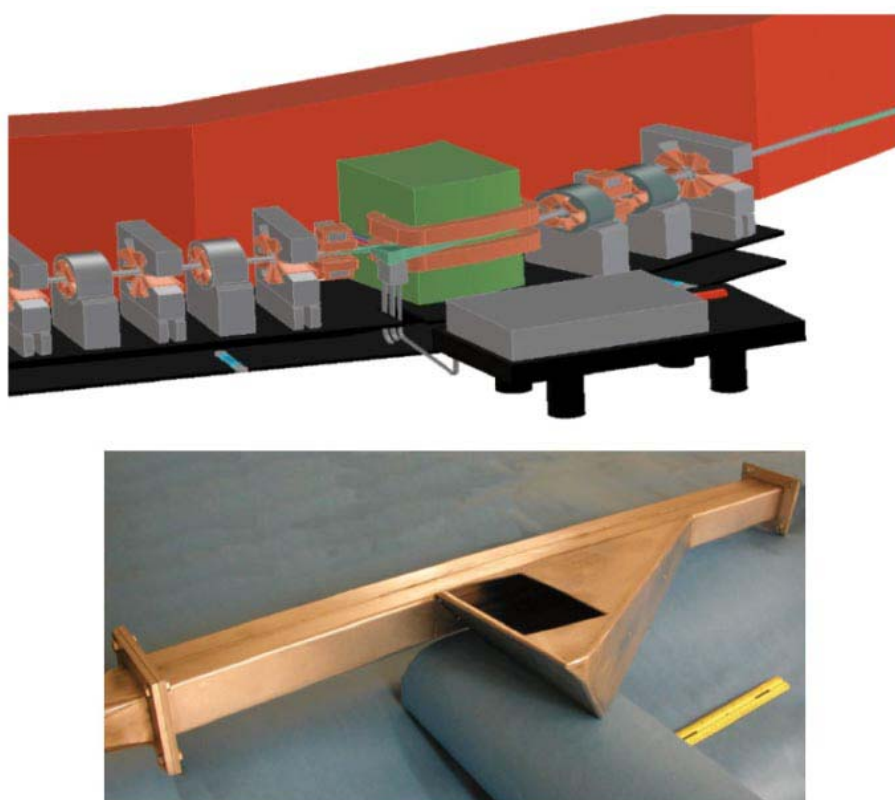


Figure 2. Top) Cutaway view of a dipole source with optical table. The experiment sits less than 1 m from the source of the radiation. Bottom) A photograph of a full-scale prototype chamber fabricated for RF testing. The chamber is designed to collect 300 mrad horizontally and 140 mrad vertically. This very large acceptance means that the first mirror collects 95% of the radiation at 1 mm wavelength, so the CSR extraction is very efficient.

Once the CSR is emitted by the electron bunches, it is important to efficiently collect this powerful THz light. We accomplish this by choosing short radius bending magnets which allow the placement of the first collecting mirror close to the source point, and by a uniquely designed vacuum chamber shown in the left panel of Figure 2. The opening of this vacuum chamber follows the photon beam profile allowing us to collect the light from a full 60% of the electron beam's trajectory within the bending

magnet. The first mirror located at the large end of this chamber will collect 300 mrad horizontally by 140 mrad vertically. This very large vertical collection angle captures 95% of the emitted synchrotron radiation at a 1 mm wavelength, and 100% collection of shorter wavelengths. The right panel of Figure 2 schematically shows how the first mirror will deflect the beam 90 degrees downward, and then will be followed by beamline optics to re-image the light into a spectrometer or other end station equipment located directly outside the shield walls.

The unusual design of the vacuum chamber means that we must concern ourselves with trapped electromagnetic field modes usually referred as high order modes (HOM), which could influence the stability of the electron beam. Accurate simulations of these fields in the chamber have shown only small couplings between these modes and the electron beam. Additionally, the large photon beam aperture after the first mirror allows the HOM to propagate outside the main chamber where they can be easily damped by RF absorbers. Bench measurements on a full-scale mock chamber (shown in the photograph in Figure 2) have completely confirmed the simulations results so that we are confident that HOM will not be an issue for the beam stability [14].

2.5.4 CIRCE Performance

Using the machine parameters for the CIRCE ring in our model for the CSR production from distorted electron bunches, we calculated the THz flux produced by the CIRCE ring. The results are plotted along with conventional synchrotron and thermal far-IR sources in Figure 1. The three different CIRCE curves represent three (of many) possible machine configurations. To maximize the CSR bandwidth toward the short wavelengths, we need to decrease the electron bunch length while keeping the distribution distortion to the maximum allowed by the model stability criterion for the bursting instability [13]. At shorter bunch lengths, the threshold for bursting goes down so the total number of electrons and therefore the total CSR power emitted is limited (red curve in Figure 1). To increase the total power emitted we can lengthen the bunch, while maintaining the maximum distortion. This means the CSR doesn't extend to as short of wavelengths, but it allows for increasing the number of electrons in the bunch (green curve). Since the intensity emitted goes like the number of electrons squared, the flux can be significantly increased in this method.

Table 1. List of performance parameters for the CSR emission of the designed CIRCE ring. Powers and energies are integrated from 1 – 100 cm^{-1} . When two values are presented as a range, they correspond to the red and green curves in Figure 1.

Source Parameter	Value	Ring Parameter	Value
Average Power	13 – 311 Watts	Electron beam energy	600 MeV
Peak Power	3.5 – 28 Kilowatts	Total beam current	20 – 225 mA
Pulse Length	≥ 300 femtoseconds (transform limited)	Momentum compaction	$1-8 \times 10^{-4}$
Repetition Rate	Up to 1.5 GHz	Electron pulse length	1-3 psec
Wavelength range	1 cm-200 micron	RF frequency	1.5 GHz
Energy/pulse	9-210 nJ	RF Voltage	0.6-1.5 MV

Comparing to existing synchrotron and thermal far-IR sources, Figure 1 shows that CIRCE will have between a 6 and 9 order of magnitude increase in average flux. A list of parameters for the CSR light generated by CIRCE is given in Table 1. The emitted

light will come in transform limited pulses with durations of ~ 300 femtoseconds at the shorter wavelengths, and at a repetition rate tunable between 4.5 MHz and 1.5 GHz (varied simply by choosing which electron bunches are filled). Since these pulses are single cycle, they should be coherent with each other, and therefore we are investigating a pulse-stacking resonator. This would allow particular beamlines to amplify the peak power of the pulses at the expense of repetition rate, and allow that user to select the timing of their pulses independent of the other beamlines and users at CIRCE.

2.5.5 Broadband Bursting mode

When the current per bunch exceeds the threshold for the CSR driven instability [3-6], quasi-random bursts of CSR in the terahertz frequency range appear. This instability is associated with the spontaneous generation of temporary microstructures in the bunch longitudinal distribution. These structures last for several turns, radiating CSR with strong fluctuating intensity but at higher frequencies than in the stable mode. This effect can be potentially exploited by experiments that require higher frequency photons but not a stable CSR flux.

Figure 3 shows the result of a simulation of the broadband bursting mode for the CIRCE case. The spectrum for a stable CSR emission below the burst threshold is shown as a dotted line, while the unstable situation above threshold, when bursting is present, is shown as a solid line. The “unstable” spectrum is averaged over several bursts. For wavenumbers from $\sim 70 \text{ cm}^{-1}$ to $\sim 150 \text{ cm}^{-1}$, the unstable case shows about one order of magnitude higher flux. The simulation uses the SET 1 configuration of Table 2 with the current per bunch below and above the instability threshold.

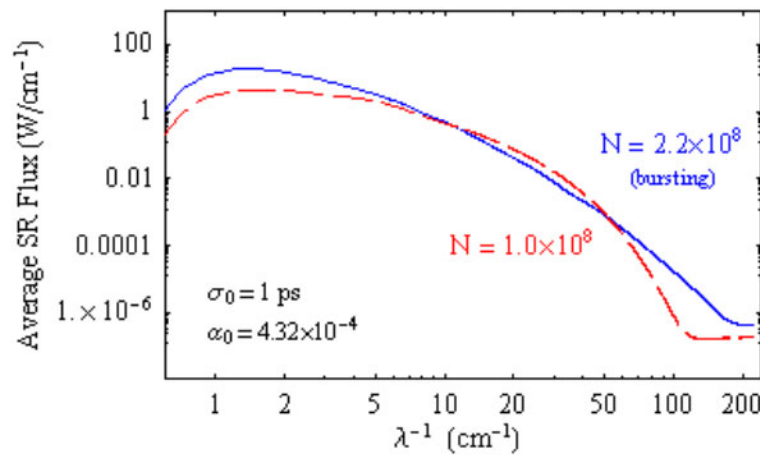


Figure 3: Simulated CSR spectrum for the broadband bursting mode of CIRCE. The roll-off to the left of the curves is due to the vacuum-chamber shielding.

2.5.6 Laser slicing of beams

We are planning to include in one of the CIRCE straight sections a wiggler magnet for allowing femtosecond laser modulation of the electron beam [19]. The first beamline using such a technique, commonly referred also as “slicing”, has been successfully operating at the ALS since 2001 for the production of femtosecond x-ray pulses [20]. In this scheme a short laser pulse is propagated together with the electron beam in a

wiggler for modulating the energy of a short slice (~ 100 fs) of the electron bunch. Due to the nonzero momentum compaction, a density modulation in the bunch longitudinal distribution is induced when the beam propagates along the storage ring. It has been predicted and experimentally confirmed at the ALS [21], that such density modulations radiate intense short pulses of CSR in the terahertz frequency. These CSR pulses are regularly used at the ALS as diagnostics for the fine tuning of the slicing experiment and could be potentially used as a terahertz source as well.

The interaction of a laser with a relativistic electron beam in a wiggler magnet is schematically illustrated in Fig. 4. A 100-fs optical pulse of moderate energy modulates the energy of an ultra-short (~ 30 μm) slice of a stored electron bunch as they co-propagate through a wiggler in a storage ring (Fig. 4a). The energy-modulated electron slice is spatially separated from the main bunch in a dispersive section of the storage ring (Fig. 4b) and is used to radiate fs x-rays at a bend-magnet or insertion-device (Fig. 4c). The energy modulation of electrons creates a small perturbation to the electron bunch longitudinal density consisting of a dip and two side bumps due to the dispersion of the electron trajectories, which causes the high and low energy electrons to move far away from their original positions while the electron bunch moves from the wiggler to the radiation source. This perturbation gives rise to an electron emission of a temporally and spatially coherent infrared light. The intensity of this radiation scales quadratically with the number of misplaced electrons. This scheme is referred to as laser slicing and has been implemented in the ALS as a source of femtosecond x-rays.

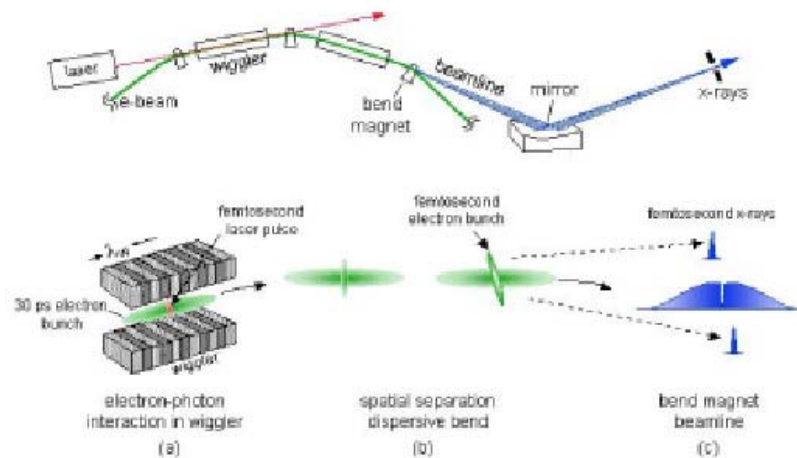


Figure 4 Schematic of laser slicing of an electron beam. The beam energy is modulated via interaction with a laser pulse in a wiggler. The energy modulation leaves a hole in the bunch via time-of-flight dispersion of the modulated beam. The “hole” can then radiate coherently.

Measurements of the infrared radiation at the ALS were performed at two bend magnet sources located one-half sector downstream from the wiggler at the beamline 5.3.1 (BL5.3.1), and 8 sectors downstream from the wiggler at the beamline 1.4 (BL1.4). Figures 5a and c show a calculated electron longitudinal distribution in two source locations and for two lattices assuming energy modulation of six times the natural energy spread and rms pulse length of 45 fsec. In all cases, electrons with $\Delta E < 0$ accumulate toward the head of the bunch while electrons with $\Delta E > 0$ accumulate toward the tail of the bunch, creating a dip in a distribution with two side bumps. The uncorrelated energy spread of electrons causes a smearing of the distributions which is

growing with the increased distance from the wiggler. A corresponding spectrum of the infrared signal for all four cases is shown in Figs. 5b and d.

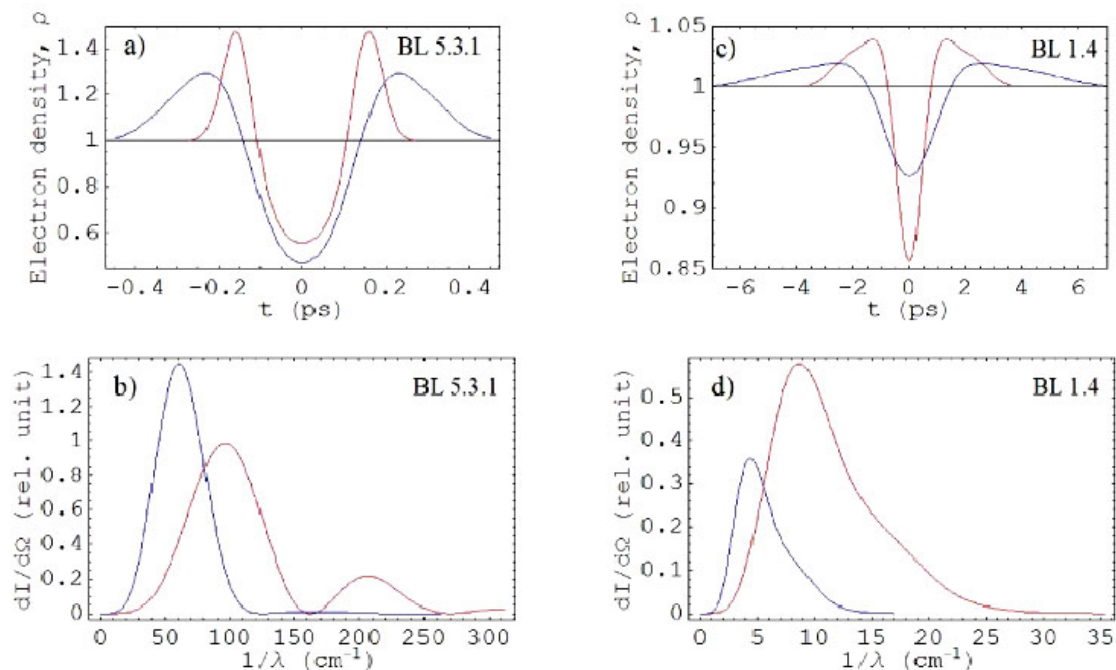


Figure 5: A predicted perturbation in the electron density distribution and a spectrum of the infrared radiation caused by this perturbation shown for BL5.3.1 and BL1.4 for the nominal lattice (red line) and for the experimental lattice with an increased momentum compaction factor (blue line). Plots a) and c) show the distribution and plots b) and d) show the corresponding spectrum.

Figure 6 (left) shows the oscilloscope trace of the infrared signal measured at the BL1.4 for the electron bunch current of about 1 mA, well below a threshold of the bursting instability observed previously. Figure 6 (right) shows the measured spectrum at two points in the ring. Nearer to the slicing (BL5.3.1), the pulse is still narrow and the spectrum peaks at higher frequencies. Farther from the slicing (BL1.4), the pulse has broadened considerable and the spectrum shifts to lower frequencies. The relative amplitude is due to the acceptance of the beamlines. The measured spectra illustrate the difficulties of extracting long wavelength radiation from a conventional light source. For example, the spectrum at BL1.4 appears shifted to higher frequencies than expected because of the low frequency cutoff of the vacuum chamber. The spectrum at 5.3.1 has significant structure due to reflections in the transport of the radiation and due to water vapor absorption.

Figure 7 shows the example of the calculated CSR spectrum for a possible slicing configuration of CIRCE. In this case the beam is modulated inside a wiggler in a straight section and the CSR is collected from a dipole magnet port 2.5 m downstream. The laser pulse, 50 fs FWHM, has the intensity necessary for an energy modulation of the electrons as large as six times the beam energy spread. The current per bunch is 10 mA and the integrated energy of the CSR pulse over 100 mrad horizontal acceptance is $\sim 8.5 \mu\text{J}$. The maximum repetition rate is limited by the requirement on the laser power to 10-100 kHz.

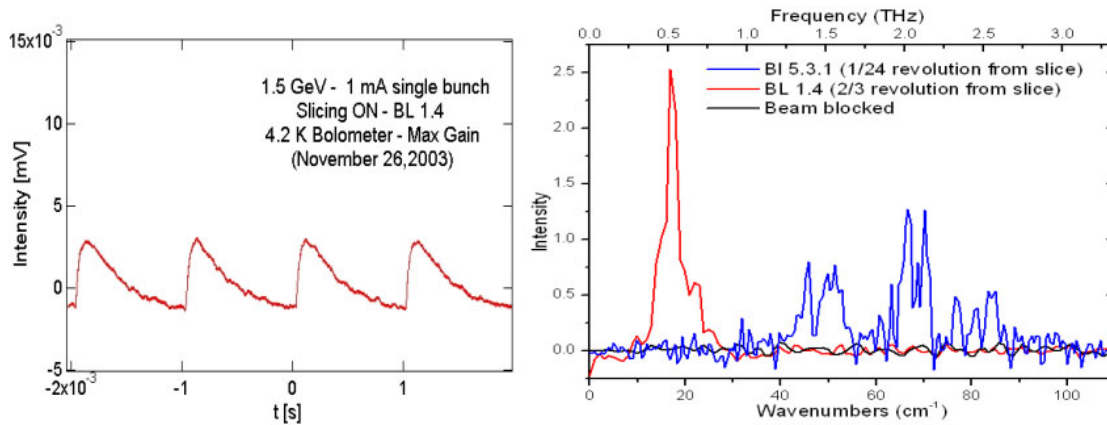


Figure 6: Left) The infrared signal measured with the nominal lattice at the BL1.4 with laser turned on and electron bunch current of ~ 1 mA. Right) Spectra measured at BL 5.3.1. and BL1.4. The structure on the measurement is due to reflections in the beam line and water vapor absorption.

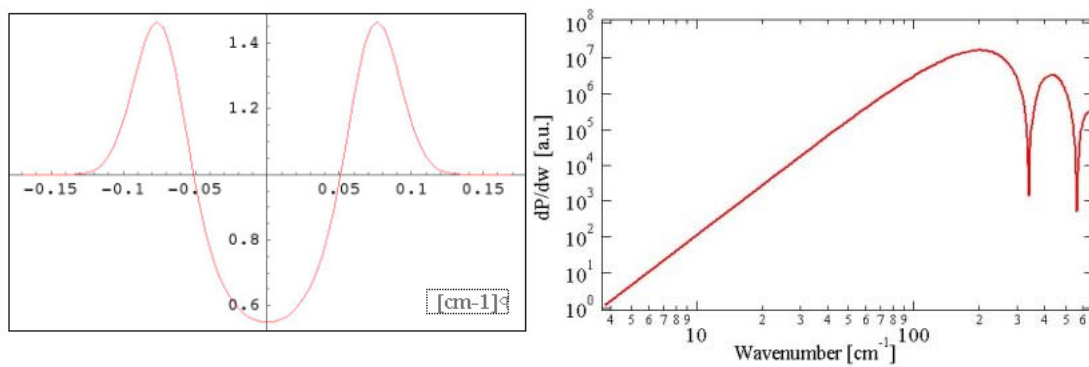


Figure 7: Calculated CSR spectrum for a possible configuration of the laser “slicing” mode in CIRCE.

Comparing the spectra in Figures 1 and 7 one can see how the slicing mode significantly extends the CIRCE capabilities towards higher frequencies. One of the tantalizing possibilities of this technique is the tailoring of the time domain terahertz pulse via appropriate shaping of the laser pulse. This would allow a unique capability in a synchrotron source.

2.5.7 Conclusion

CIRCE will be a *revolutionary* source for a traditionally difficult spectral region at the border between optics and electronics, namely the “THz-gap.” We have explored the virtues of a small ring dedicated to the production of *coherent* far-infrared and THz radiation and have determined conclusively that such a machine will create a true leap forward for the field and is entirely feasible. The total estimated cost for building the ring, including the first several beamlines, is less than \$20 million. Just as conventional synchrotron radiation has been a boon to x-ray science, coherent synchrotron radiation may lead to many new innovations and discoveries in terahertz science.

2.5.8 Acknowledgments

We gratefully acknowledge the work of numerous colleagues at LBNL with many details of the CIRCE design its integration into the ALS facility. We also acknowledge fruitful collaborations with P. Kuske, G. Wüstefeld, and the rest of the CSR team at BESSY. We also are grateful for many discussions with Jim Murphy. This work was supported by the Laboratory Directed Research and Development Program of Lawrence Berkeley National Laboratory under the Department of Energy Contract No. DE-AC03-76SF00098.

2.5.9 References

- [1] Ferguson, B., Zhang, X. C., "Materials for terahertz science and technology", *Nature Materials*, **1** (2002), 26.
- [2] Carr, G.L., M.C. Martin, W.R. McKinney, K. Jordan, G.R. Neil, and G.P. Williams, "High-power terahertz radiation from relativistic electrons", *Nature*, **420** (2002), 153.
- [3] J. Singley *et al.*, "Measuring the Josephson Plasma Resonance in $\text{Bi}_2\text{Sr}_2\text{CaCu}_2\text{O}_8$ Using Intense Coherent THz Synchrotron Radiation", *Phys. Rev. B*, **69**, 092512 (2004).
- [4] Nodvick, J.S., Saxon, D.S., "Suppression of Coherent Radiation by Electrons in a Synchrotron", *Physical Review*, **96** (1954), 180.
- [5] Hirschmugl, C.J., Sagurton, M., Williams, G.P., "Multiparticle coherence calculations for synchrotron-radiation emission", *Physical Review A*, **44** (1991), 1316.
- [6] Andersson, A., Johnson, M. S., Nelander, B., "Coherent synchrotron radiation in the far infrared from a 1-mm electron bunch", *Optical Engineering*, **39** (2000), 3099.
- [7] Arp, U., G.T. Fraser, A.R.H. Walker, T.B. Lucatorto, K.K. Lehmann, K. Harkay, N. Sereno, and K.J. Kim, "Spontaneous coherent microwave emission and the sawtooth instability in a compact storage ring", *Physical Review Special Topics-Accelerators & Beams*, **4** (2001), 054401.
- [8] Carr, G.L., Kramer, S. L., Murphy, J. B., Lobo, R.P.S.M., Tanner, D. B., "Observation of coherent synchrotron radiation from the NSLS VUV ring", *NIMA*, **463** (2001), 387 and G. L. Carr *et al.*, "Investigation of Coherent Emission from the NSLS VUV Ring", *Proc. 1999 Particle Accelerator Conference*, p. 134 (1999).
- [9] Byrd, J.M., W.P. Leemans, A. Loftsdottir, B. Marcelis, M.C. Martin, W.R. McKinney, F. Sannibale, T. Scarvie, and C. Steier, "Observation of broadband self-amplified spontaneous coherent terahertz synchrotron radiation in a storage ring", *Phys. Rev. Lett.*, **89** (2002), 224801.
- [10] Stupakov, G. and S. Heifets, "Beam instability and microbunching due to coherent synchrotron radiation - art. no. 054402", *Physical Review Special Topics-Accelerators & Beams*, **505** (2002), 4402.
- [11] Abo-Bakr, M., Feikes, J., Holldack, K., Wüstefeld, G., Hübers, H. W., "Steady-state far-infrared coherent synchrotron radiation detected at BESSY II", *Physical Review Letters*, **88** (2002), 254801.
- [12] Abo-Bakr, M., Feikes, J., Holldack, K., Kuske, P., Peatman, W.B., Schade, U., Wüstefeld, G., Hübers, H. W., "Brilliant, Coherent Far Infrared (THz) Synchrotron Radiation", *Physical Review Letters*, **90** (2003), 094801.
- [13] Sannibale, F. *et al.*, these proceedings and F. Sannibale *et al.*, "A Model Describing Stable Coherent Synchrotron Radiation in Storage Rings", *Phys. Rev. Lett.* **93**, 094801 (2004).
- [14] Li, D. and S. De Santis, LBL Internal note, CIRCE Note LSCN-IF-1.
- [15] J. Murphy, S. Krinsky, "Millimeter wave coherent synchrotron radiation in an electron storage ring," *NIM A* 346 (1994) 571-577.

- [16] M. Svandrlík et al., "The super-3HC project: An idle superconducting harmonic cavity for bunch length manipulation", ST-M-00-01G, European Particle Accelerator Conference (EPAC 2000), Vienna, Austria, 26-30 Jun 2000.
- [17] M. Pekeler, H. Vogel, P. vom Stein, W. Anders, S. Belomestnykh, J. Knobloch and H. Padamsee, "A Superconducting Landau Accelerator Module for BESSY II," Particle Accelerator Conference (PAC2001), Chicago, Illinois, 18-22 Jun 2001.
- [18] H. Nishimura, D. Robin, F. Sannibale and W. S. Wan, "Lattice studies for CIRCE (Coherent InfraRed Center) at the ALS," LBNL-55647, European Particle Accelerator Conference (EPAC 2004), Lucerne, Switzerland, 5-9 Jul 2004.
- [19] A.A. Zholents, M. Zolotarev, Phys. Rev. Lett. 76, 912, (1996).
- [20] R. W. Schoenlein, et al., Science, Mar 24, (2000) 2237 and R. W. Schoenlein *et al.*, Appl. Phys. B **71**, 1-10, 2000.
- [21] J.M. Byrd, Z. Hao, M.C. Martin, D.S. Robin, F. Sannibale, R.W. Schoenlein, M. Venturini, A.A. Zholents, M.S. Zolotarev, "Coherent Infrared Radiation From The ALS Generated Via Femtosecond Laser Modulation Of The Electron Beam", European Particle Accelerator Conference (EPAC 2004), Lucerne, Switzerland, 5-9 Jul 2004.
- [22] F. Sannibale, et al., these proceedings.

2.6 The BESSY Low Alpha Optics and the Generation of Coherent Synchrotron Radiation

J. Feikes, K. Holldack, P. Kuske, G. Wüstefeld, [BESSY](#)
 H.-W. Hübers, [DLR](#)
wuestefeld@bessy.de

2.6.1 Introduction

The production of short electron bunches in an electron storage ring is of increasing interest. An excellent summary of this subject was presented at the "micro bunches workshop" 1995 [1]. The recent interest in this subject is partly stimulated by the BESSY work on a "low alpha" machine optics, where for the first time stable, powerful coherent synchrotron radiation (CSR) in the THz-range could be produced at moderate bunch currents in an electron storage ring [2]. Additionally, there is interest in the CSR bursting process, which starts above a threshold current [3, 4] and may also lead to a better understanding of the physics and limitations of magnetic bunch compression in FELs. Short bunches are also of increasing demand to generate short X-ray pulses for time resolved measurements. The possibilities and limitations of short electron bunches in storage rings still need further exploration.

The results presented here are summarized contributions from work on CSR at BESSY mostly published in the proceedings of the particle accelerator conferences, PAC and EPAC. Our first paper on this subject was contributed to the PAC 1999 with work on the nonlinear momentum compaction factor, α , of BESSY II [5]. Following this work, a low alpha optics was developed and it could be shown, that the BESSY II ring has the potential for running with a very low alpha value. When this was realized, a far infrared detector was installed at one of the dipole beam ports to search successfully for CSR signals of these short bunches [2]. Both emission modes, stable and bursting CSR, could be detected. Already at currents of the μA level per bunch the emitted CSR is so intense, that it is an excellent tool for beam diagnostics [6] and, at around 100 μA ,

a powerful, broadband sub-THz source. This source is suitable for user applications, as demonstrated in [7, 8]. Presently BESSY is operated once a year for one week in the low alpha mode with bunches of 3 picoseconds (ps) rms length and even shorter as a user facility for THz experiments and short X-ray pulses [9].

In the following chapters results of the work at BESSY on CSR generation are presented. The key to achieve stable or bursting CSR is the low alpha machine optics, which is used for bunch length manipulation. Properties of the optics are presented in chapter 2. Limitations in achieving very short bunches are discussed in chapter 3. The CSR radiation is very sensitive on the bunch shape. By analyzing the radiation, information on the bunch shape is achieved. Autocorrelation methods can be applied and are discussed in chapter 4. The bunch length as a function of the current for different α values are presented in chapter 5. With increasing current the CSR emission process becomes unstable at the bursting instability threshold. This threshold follows a scaling law. This is used to estimate length and current limits for ultra short bunches in the ps range and below, see chapter 6. Recent BESSY results on CSR measurements performed by “femtosecond slicing” are not included; they will be published in a later article [19].

2.6.2 The BESSY II Low Alpha Optics

A special optics, the so called “low alpha” optics was developed for the BESSY II storage ring for bunch length manipulation to generate coherent synchrotron radiation and short X-ray pulses [9]. This optics is a simplified, 16-fold version of the regular BESSY II user optics of 8-fold symmetry, as shown in Fig. 1. In the low alpha mode the “momentum compaction factor”, α , of the machine is reduced, where α is defined as the relative increase of the electron orbit length, dL/L , for electrons with deviating momenta, dp/p :

$$\frac{dL}{L_0} = \alpha \frac{dp}{p_0}$$

By an appropriate detuning of the quadrupoles, α can be varied at fixed transverse working point, starting with $7.3 \cdot 10^{-4}$, of the regular user optics down to 10^{-6} range.

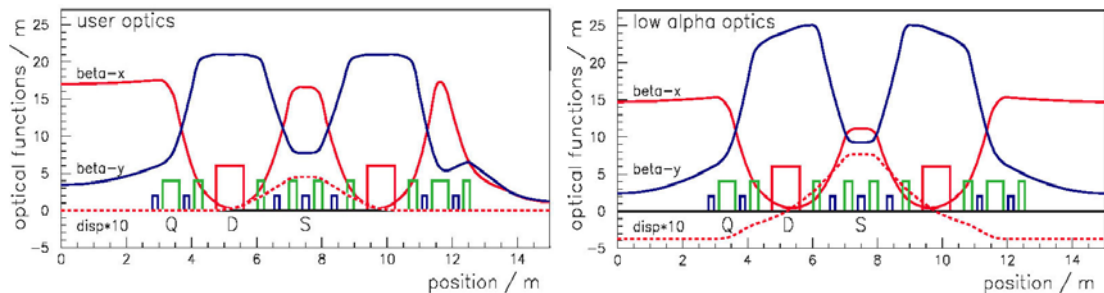


Figure 1: Optical functions of the user (left) and the low alpha optics (right) of one out of 16 ring cells. Dipoles, quadrupoles and sextupoles are indicated by D, Q and S, respectively.

By reducing α , the bunch length becomes shorter in proportion with $\sqrt{\alpha}$ (terms involving $1/\gamma^2$ can be ignored). Quadrupoles control the α_0 term of alpha, expanded

with respect to momentum deviation, $\alpha = \alpha_0 + \alpha_1 dp/p_0 + \alpha_2 (dp/p_0)^2 \dots$. If α_0 approaches zero, higher order terms have to be controlled in such a way, that $\alpha \neq 0$ in the required momentum acceptance range of about $\pm 2\%$. The unstable fix point, which limits the bucket size, is located, where α as a function of the momentum deviation becomes $=0$. This point should be pushed to large momentum values.

Higher order terms can be controlled at BESSY by an appropriate sextupole setting. Instead of α , which is difficult to measure directly, we use the dipole mode of the synchrotron oscillation $f_s \propto \sqrt{\alpha}$ detected by a strip line signal. To achieve a good life time, f_s should increase if the rf-frequency deviates from the nominal value, as shown in Fig. 2, by controlling slope and curvature of the longitudinal chromaticity [10, 11]. From the measured f_s as a function of rf-frequency the nonlinear terms of α can be extracted [5], Fig.2. For small values of α ($f_s \leq 1$ kHz) our present sextupole setting can only be applied if $\alpha \leq 0$, because of the special curvature of α as a function of dp/p . For $\alpha > 0$ the frequency will hit the $f_s = 0$ axis already at small momentum and strongly limit the bucket size. From our measurements we can use as a good approximation $\alpha_0 = -3 \cdot 10^{-6}$, $\alpha_1 = 0$ and $\alpha_2 = -0.03$. With these numbers we can write down explicitly the Hamiltonian of the longitudinal phase space. From the condition for the momentum term of the fix point [12] one can show, that α_0 and α_2 should have the same sign to get the stable fix point located at $dp/p=0$, without further solutions.

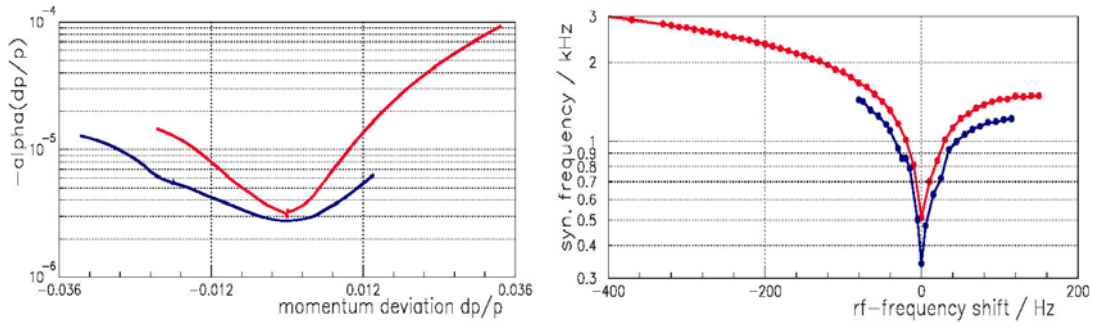


Figure 2: The right part of the figure shows two measurements of the dipole mode of the synchrotron frequency f_s as a function of the rf-frequency for an optics with $-\alpha_0 < 10^{-5}$. From this measurements α as a function of the momentum was derived, left part of the figure (vertical axis shows $-\alpha$).

For the presently constructed MLS storage ring [13], next to the BESSY II site, the option of a low alpha optics for the machine is included. The optics is based on a 4 fold DBA lattice with 2 chromatic sextupole families. An additional harmonic sextupole family will be used, to tune the slope of α with respect to the particle momentum. A family of octupoles in the centre of the achromat will control the curvature of alpha with respect to the momentum, a similar scheme is suggested for the dedicated CSR-source CIRCE [14].

The smallest value of f_s which we could achieve up to now is close to 300 Hz. When approaching this value, we see increased noise on the longitudinal beam signal, probably generated by power supplies of the rf-klystrons. If f_s approaches 300 Hz the

frequency signal on the spectrums analyzer is hardly visible. Approaching these very small α values, the beam orbit becomes increasingly sensitive to distortions. The optics up to $f_s=350$ Hz ($\alpha = -1.4 \cdot 10^{-6}$) was reproduced several times, beam accumulation at low currents directly into this optics is possible and beam lifetimes of several hours could be achieved.

The BESSY low alpha optics was (and will be) offered to users in a one-week shift during the last 2 years, tuned to a typical rms bunch length of 3 ps for THz experiments and short X-ray pulses. The operation for users requires an additional careful correction of tune and orbit distortions caused by insertion devices. A horizontal tune change influences sensitively the dispersion function, the value of α , the bunch length σ and in turn the emitted CSR power. For example, a relative current change of the Q4-family (position 3.37 m and 11.63 m in Fig.1) of 10^{-4} produces a CSR power change of 25 %. The helical insertion devices with variable polarization influence the horizontal tune and disturb the detected CSR power. For these devices a careful correction scheme is required. Due to our present experiences, the low alpha optics is stable and reliable with a good lifetime of the stored beam, suitable for user operation.

Table 1: Parameters of the low alpha and the regular user optics. The beam energy of the ring is 1.7 GeV and the circumference 240 m.

Optics Parameter	Unit	User optics	Low alpha optics
nat. emittance ε	nm-rad	6	30
nat. energy spread σ_e	%	0.08	0.08
transv. tunes, Q_x, Q_y		17.8, 6.7	14.7, 6.2
nat. chromaticities ξ_x, ξ_y		-53, -27	-35, -27
momentum comp. factor α		$7.3 \cdot 10^{-4}$	$\sim 10^{-6} - 7.3 \cdot 10^{-4}$
long. synchr. frequency f_s	kHz	7.5	0.3 - 7.5
rms bunch length σ	ps	15	1 - 15

2.6.3 Limits of Short Bunches

The bunch length in the electron storage ring is the result of an equilibrium process between damping and quantum excitation, as long as no instabilities are involved. The shortest bunches which we could achieve and analyze are about 700 fs rms long, of nearly Gaussian shape. There are two effects, which influence the longitudinal bunch length, additionally to the value of α .

Based on linear matrix theory, the longitudinal bunch extension is influenced by the natural momentum spread σ_e and by the transverse beam emittance ε . Given a 6x6 transformation matrix (a_{ij}) for a unit cell of horizontal phase advance φ_x . The longitudinal coordinate z of a particle with respect to the reference particle is given by $z = a_{51}x_0 + a_{52}x_0' + a_{55}z_0 + a_{56}z_0'$, where (x_0, x_0') and (z_0, z_0') are initial, transverse and longitudinal coordinates, $z' = dp/p$ is the momentum deviation. A coupling into the vertical plane is excluded. Recently it was shown [15, 16] that this can be written as

$$z = \sqrt{\varepsilon H} (\sin(\varphi_\beta - \varphi_H - \varphi_x) - \sin(\varphi_\beta - \varphi_H)) + (-\alpha L + H \sin(\varphi_x)) z_0' ,$$

where $(\varphi_\beta, \varepsilon)$ and (φ_H, H) have to be chosen appropriately to describe the particle coordinates (x_0, x_0') and the dispersion function (η, η') . The transverse beam width has to be described by a spread in (x_0, x_0') or a related spread in $(\varphi_\beta, \varepsilon)$, which transfers into a bunch lengthening at places where $H \neq 0$. To give a numerical example, for the BESSY II optics for $\alpha=0$ we have $\varepsilon=30$ nm rad and $H=0.009$ m at the 0 m position as shown in Fig. 1. This yields in the worst case a longitudinal rms-spread of $2\sqrt{\varepsilon H} + H\sigma_e = 34 + 7.2 = 42$ μm , 5 times less than our shortest bunch presently measured.

In case of “femtosecond slicing” of bunches by a laser, as recently installed at BESSY [17], a longitudinal density dip of about 5 μm (rms) length is produced in a bunch of $\sigma=5$ mm rms length. The sliced electrons are not considered here, it is assumed that they quickly move out of the interaction region because of their about 10 times larger momentum spread. The dip can also be considered as an ultra short bunch in a transition state, with emittance and momentum spread of the original bunch, but of much shorter length. There are several effects that will smear out the dip, also in case that ε and H are zero. First of all it is the synchrotron oscillation, which rotates the dip in the bucket. For the BESSY II user optics this rotation will lengthen the dip, described by $\tilde{x} = \sigma \sin(2\pi N / N_0)$, where N are the number of turns and $N_0=156$ are the number of turns in the BESSY ring for one full revolution in the rf-bucket. The length \tilde{x} is the projection of the rotated dip on the longitudinal axis. However, because of synchrotron radiation, the dip is very fast diffused and widened in length to about 400 μm during a 180 degree rotation, see Fig. 3, for an analytical estimate see [18]. Based on our experimental results, we can detect the dip over the first 20 revolutions in the ring by its emitted CSR radiation, before the signal vanishes, but we never have seen the signal appearing again after a 180 degree rotation, in agreement with this estimate [19].

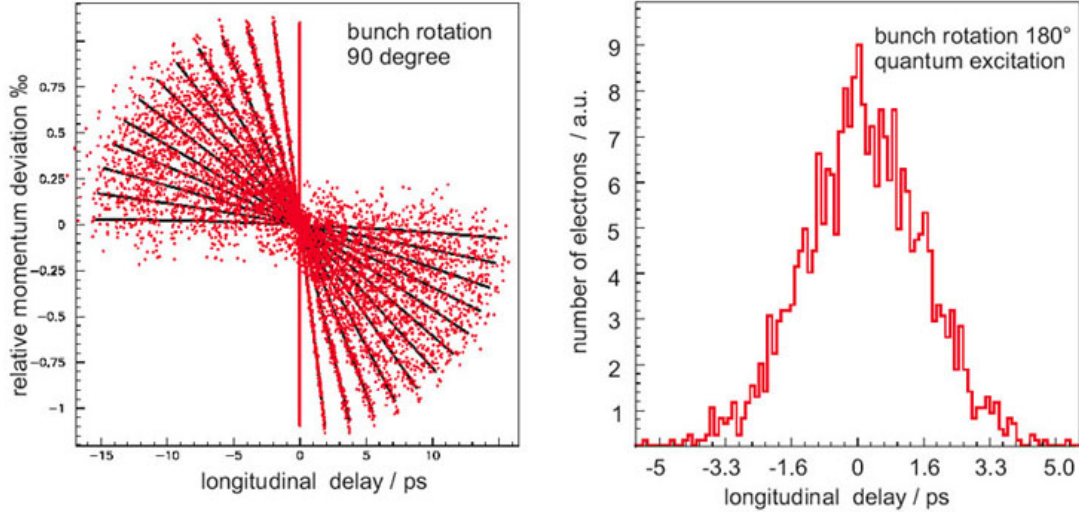


Figure 3: Rotation of a bunch-dip in the rf-bucket by 90 degrees in the longitudinal phase space (left). The plot shows the temporal development of the bunch after each 3rd circulation in the machine. The black lines include damping, the red dots an additional quantum emission. The bunch has zero emittance but a final energy spread at the starting point. After a 180 degree rotation the bunch-dip will be smeared out (right), with a projected density profile of 0.4 mm rms width. The calculation is performed with MAD [20].

2.6.4 Coherent Synchrotron Radiation

The emission of synchrotron radiation is basically a dipole radiation process, which requires that the circulating electrons produce a time dependent dipole moment. The first harmonic of the spectrum emitted by a single electron is given by the revolution frequency around the machine, the Lamor frequency c/ρ , with the speed of light, c , and the dipole bending radius, ρ . The emitted spectrum extends to much higher harmonics, up to the critical frequency $\frac{2}{3}\gamma^3 c/\rho$ and falls off rapidly above this value, where γ is the Lorenz factor.

A bunch of electrons emits coherently, at wavelength longer than the bunch. In this case the bunch can be considered as a single macro particle. The charge of this bunch, and in turn the emitted power grows enormously, with the square of the involved electrons, typically a number of order $N_e = 10^9$. To avoid the emission of huge amounts of power in the long wavelength range, the vacuum chambers are manufactured from conducting material, to shield the long wavelength radiation [21]. This shielding can be described by a chamber cut off wavelength λ_{cutoff} , which limits the detectable wavelength of coherent or incoherent synchrotron radiation to the few mm range. This chamber cut off, approximated by a parallel plate model, is given as [22]

$$\lambda_{cutoff} = 2h\sqrt{h/\rho},$$

where h is the full height of the vacuum chamber in the dipole.

In storage rings the value of λ_{cutoff} is usually much shorter than the electron bunch length. In this case the separation of the source points of the radiation, the different electrons of the bunch, could be larger than the wavelength of the emitted waves. These waves are superimposed incoherently because of their random phase relation. If the bunches are shorter than the cut off wavelength, then radiation at wavelengths longer than the bunch can be emitted. These waves of about equal phase relation superimpose now coherently. The emitted power P_n is given by [23]

$$P_n = p_n(N_e + N_e(N_e - 1)g_n),$$

where p_n is the power of the n th harmonic emitted by a single electron and g_n is a form factor. The form factor describes the degree of coherence; it is 1 for full coherence of a point-like bunch and 0 for the incoherent case of a long bunch. It is given by the modulus squared of the Fourier transform of the longitudinal charge density $n(z)$ of the bunch

$$g_n = \left| \int_{-\infty}^{\infty} n(z)e^{2\pi iz/\lambda} dz \right|^2.$$

Therefore, g_n is very sensitive to the bunch shape. Because g_n is derived from the modulus of the Fourier transform, a back transformation to the bunch shape is not directly possible, see [27]. The term p_n includes the screening effect of the vacuum

chamber. For wavelengths longer than the cut off p_n becomes 0. Gaussian bunches of rms length σ produce a Gaussian distribution of the power spectrum P_n with rms width $\sigma_{1/\lambda}$ in units of the wave numbers and $\sqrt{22\pi\sigma\sigma_{1/\lambda}}=1$.

As soon as bunches deviate from the Gaussian shape, higher harmonics in the power spectrum are enhanced. The Gaussian shape is typically assumed as an equilibrium distribution formed by the synchrotron radiation damping and quantum excitation process, for an ensemble of non-interacting electrons. In principle, nonlinear effects of the rf-acceleration field and in the magnetic guide field (nonlinear momentum compaction terms) can lead to deviations from this shape, but these effects seem to be small. As soon as the bunch is deformed by impedance effects, and, even more important, by its own CSR field [24], they can deviate from a Gaussian shape. Depending on the situation, the deformation of the bunch by its own CSR field could double the extend of the spectral range of the emitted radiation. This deformation could become so strong, that the bunch becomes unstable and the 'bursting instability' develops [3]. In this case density fluctuations smaller than the bunch will emit coherent radiation bursts at wavelength shorter than the cut off wavelength. This threshold depends on the current and machine parameters. Above the threshold value there is always bursting. With increasing current the bursts are first periodic in time and then turn to an irregular, stochastic emission [6].

Figure 4 shows measurements in time domain (persistent scope mode), where stable and bursting CSR in the BESSY ring can be clearly distinguished. The data are measured by a liquid helium cooled InSb detector, which has a bandwidth of around 1 MHz and is able to resolve the 1.25 MHz revolution time of the electrons around the BESSY ring [25]. In case of the stable CSR emission a periodic signal at the revolution frequency of the beam is seen. The stable CSR signal resembles a noisy, sawtooth-like line of periodic amplitude. This record was performed with a small contribution from bursting CSR, producing the noise. At a further reduced current this noisy modulation will vanish. The record of the bursting signal shows no longer constant amplitudes, but a spread in the amplitudes, due do the stochastic character of the signal intensity. The power signals on the oscilloscope are pointing to negative values.

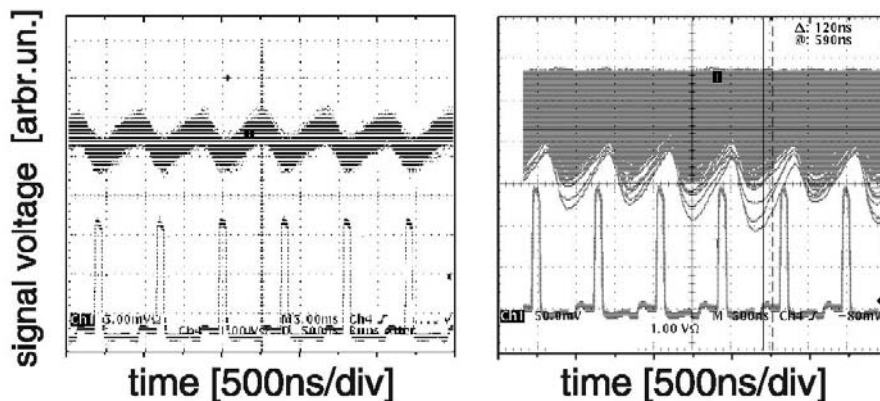


Figure 4: THz-signals of stable (left, upper part) and bursting CSR (right, upper part) together with the beam revolution trigger (lower part) in time domain. The stable CSR shows a sawtooth-like, periodic signal, of constant amplitude. The bursting CSR shows a stochastic distribution of signal amplitude. The detector is of InSb with 1 MHz bandwidth, which resolves the bunch revolution in the storage ring of 1.25 MHz.

The emitted CSR can be characterized by the frequency power spectrum, which a stable beam in a static equilibrium emits. The power spectrum can be determined by autocorrelation measurements by a Fourier transform spectrometer, as shown in Fig. 5. The interferogram is a cos-transform of the spectral intensity distribution, folded with the frequency dependent transmission efficiency. The transmission efficiency depends on the layout of the THz beam line from the source to the detector, the THz detector characteristics and the water vapour absorption in air. The symmetry of the two-sided interference scan is an indication of the quality of the equipment adjustment. We mostly use a Martin-Puplett type spectrometer [31], where a polarizing grid is used as a beam splitter, to avoid interference effects in the long wavelength range by a beam splitter foil [26].

A Fourier transform of the autocorrelation function yields the spectral intensity as a function of the wave number, see Fig. 5. This includes still a frequency dependent factor, which originates from the folding with the transmission efficiency. At BESSY we are in a special situation, that we can manipulate the bunch length and measure the autocorrelation function of the coherent (short bunches) and incoherent (long bunches) radiation with the same experimental set up, see Fig. 5.

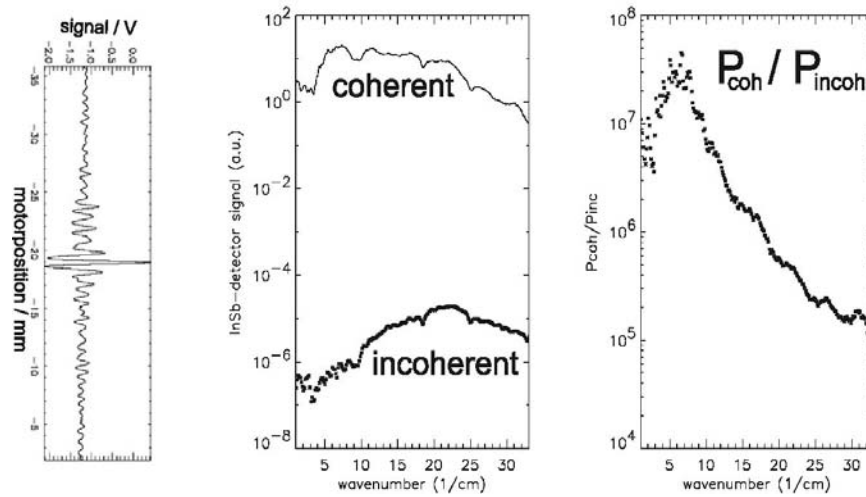


Figure 5: The left figure shows an example of an autocorrelation function of coherent emission. The figure in the middle shows the measured spectra of the coherent and incoherent case at equal bunch current, without any correction. The right figure shows the ratio of the two spectra, yielding the power spectrum times the number of particles, ranging from about 3 1/cm to 30 1/cm wave numbers ($\lambda=3.3\text{mm}$ to 0.33mm). An intensity enhancement of more than 10^7 is achieved in a single bunch filling of the regular user optics with 15 mA under bursting conditions.

The ratio of these two spectral intensities, $P_n^{\text{coh}} / P_n^{\text{incoh}}$ yields $N_e g_n$, the form factor (power spectrum) times the number of electrons. The frequency dependent transmission factor cancels out and we get the form factor of the bunch shape with high accuracy. The measurements of the autocorrelation function takes at least a few minutes in a step scan mode of the spectrometer. In case of unstable or bursting CSR emission the autocorrelation will lead to an averaged power spectrum. Because the interferogram is a cos- and not a Fourier transform it contains only part of the information. It is not directly possible, to reconstruct the bunch shape from this, especially in case of a

longitudinal bunch asymmetry. A procedure proposed by Kramers-Kronig can be applied for reconstructing the bunch shape [27]. However, at BESSY II bunches which are in an equilibrium state are of Gaussian or nearly Gaussian character. Their shape can be calculated [24] and from this a power spectrum can be derived and compared with the data by using the rms bunch length as a fit parameter, see Fig. 6. In this way we extract the bunch shape from the autocorrelation function of sub-ps bunches.

The measured form factor is declining at small wave numbers, different to the theoretical expectation where it should approach a value of 1. Figure 5 shows a maximum at around 6 1/cm. At a different beam line we found the location of the maximum at around 12 1/cm [28]. This might be related to diffraction losses at small apertures of the beam lines.

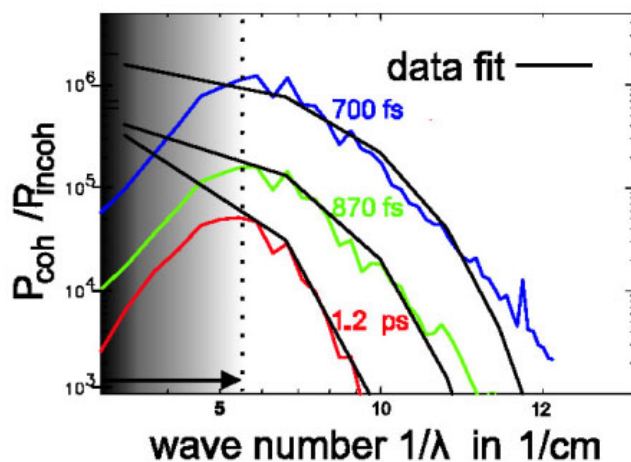


Figure 6: Power spectra of different bunches. The bunch lengths are fitted by simulations, using bunches of 700 fs at 0.3 μA , 870 fs at 0.14 μA and 1.2 ps at 0.14 μA rms length. Transmission limitations of the diagnostic system become apparent below 6 1/cm.

Examples of sub-ps pulses are shown in Fig. 6, where the power spectrum of the emitted radiation and a simulated bunch shape are compared. Best agreement was found for simulated power spectra of 700 fs, 870 fs and 1.2 ps bunch lengths. The simulation takes into account only a current dependent bunch deformation by its own CSR field [24], which changes the bunch length by less than 10 %.

Both, the stable and the bursting CSR yields a lot of detailed diagnostic information on the bunch shape and its coherent instabilities [6]. An increasing interest exists in the emitted CSR as a powerful THz-source. For spectroscopic application the stable and the bursting mode of emission can be used, where the stable CSR is less noisy and of better quality. However, already in the step mode operation of a Martin-Puplett Fourier transform spectrometer and with bursting CSR a reproducibility of the spectra in the range from 3 1/cm to 20 1/cm of 2 % and better could be achieved [29]. In the steady state case, which is about 100 times less intense, we found a more than 10 times better stability at an average power of 0.1 W to 1 W.

2.6.5 Current Dependent Bunch Length

Bunches of different lengths were generated by varying the machine parameter α and their lengths were measured [10]. Fig. 7 shows the relation between rms-bunch

length σ und bunch current I ($2\text{mA} \cong 10^{10}$ electrons). The measured data points can be empirically fitted by

$$(\sigma / \sigma_1)^4 = (f_s / f_{su})^4 + (I / I_1)^{3/2},$$

where $\sigma_1 = 13.1$ ps, $I_1 = 1.18$ mA are fit parameters. The relation between α and f_s is given by $\alpha = \alpha_u (f_s / f_{su})^2$, where $\alpha_u = 7.3 \cdot 10^{-4}$. The value f_{su} depends on the applied rf-voltage. For bunches shorter than 1.5 ps a cavity voltage of 1.5 MV ($f_{su} = 8$ kHz) was applied, and for longer bunches only 1.35 MV ($f_{su} = 7.5$ kHz) was available. The values σ_1, I_1, f_{su} and α_{su} are valid for the user optics. Bunches longer than 1.5 ps were measured with a streak camera [30], shorter bunches were analyzed with coherent THz radiation [10]. To produce these shorter bunches the optics was tuned to $\alpha < 0$. For this tuning the current dependent measurements still needs to be done.

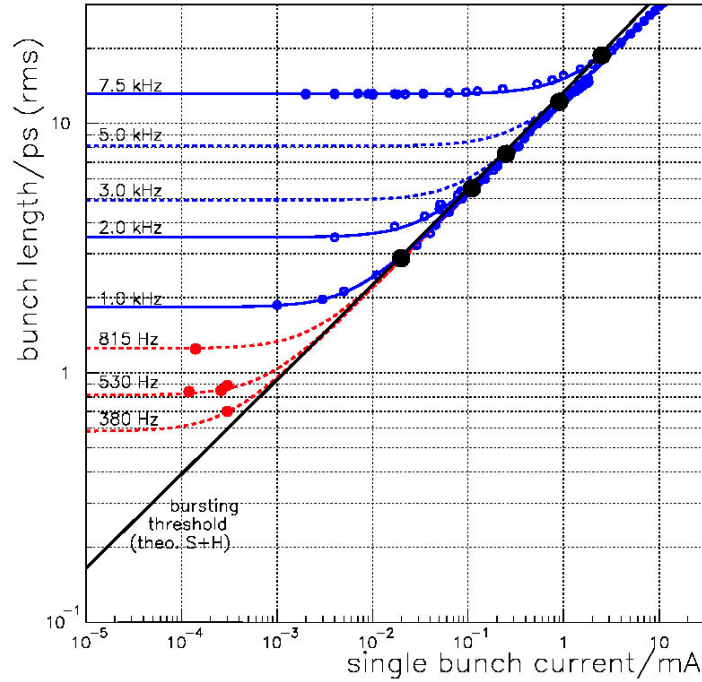


Figure 7: Measured bunch lengths as a function of the current, indicated by coloured dots. Blue: streak camera data and empirical fit to the data; black: bursting threshold of coherent THz signals; red: coherent THz radiation based data. At the fitted data lines the f_s values are indicated.

There are several examples, where the bursting threshold was measured, shown as black dots in Fig. 7. At current values above this threshold intense bursts of coherent THz radiation are observed. The bursting threshold is used as an indication here, where bunches are lengthened by the potential well distortion. The theoretical curve [3] calculated for unshielded CSR impedance agrees very well with the experimental results, if a current dependent bunch lengthening of up to 50 % is taken into account. It is extended into the sub-ps range, as a kind of bunch length estimate. This still needs an

experimental verification, especially because up to now all bursting values are measured at $\alpha > 0$. In order to calculate the threshold the product of $k\sigma = 2\pi\sigma/\lambda = 2\Lambda^{3/2}$ is required, where λ is the wavelength of the first unstable mode. The value of Λ can be calculated from our measurements and machine parameters, see next chapter. From our results we find best agreement for the threshold currents, if $k\sigma$ is chosen as 5.0 [3], [24]. If $k\sigma$ is known, the rise time τ [3] the bursting instability can be estimated. A value of $\tau f_s = 0.2$ was found, the rise time of the bursts is about 5 times faster than the inverse of the synchrotron frequency, independent on other parameters.

At our present very low alpha optics we are close to the range, where the synchrotron frequency approaches the inverse of the transverse synchrotron damping time of 8 ms (125 Hz). In this frequency range the application of the bursting model starts to become questionable.

2.6.6 Scaling of the Threshold Current

Bunches of 1 ps length and around 1 μA current could be achieved. These currents are very low, but in the BESSY ring we have a high repetition rate of 500 MHz. These very low currents deliver much more short X-ray pulses than present laser slicing methods at a comparable slice current, but at repetition rates in the kHz range. However, slices produced by the laser are still a factor 10 to 100 shorter than the storage ring based 1 ps pulses. There might be sufficient interest in ~ 1 ps long X-ray pulses, which could cover the range between normal storage ring operation and laser slicing. A way to increase the bunch current by upgrading the gradient of the rf-voltage is discussed by scaling the bursting threshold current [10]. This seems to be more reliable than scaling of the bunch length to even shorter values, where direct experimental data are still missing.

From the bursting properties we can estimate the expected length-current relation of bunches by simple scaling. The threshold currents are compared at equal bunch length, which needs to be preserved by an appropriate α tuning. This keeps the threshold condition $k\sigma = 5$ found for BESSY II fixed.

For the synchrotron frequency f_s and a bunch length σ , we use

$$\sigma = \alpha c \sigma_e / (2\pi f_s), \quad f_s^2 = \frac{e\alpha}{2\pi R m_e \gamma} \frac{dV_{rf}}{ds},$$

where e and m_e are charge and mass of the electron and σ_e is the rms energy spread of the bunch. Following [3], the beam starts to become unstable (for $\alpha > 0$) if the condition $k\sigma = 2\Lambda^{3/2}$ is satisfied. The parameter $\Lambda = (N_e r_0 \rho) / (\sqrt{2\pi} \sigma \alpha \gamma \sigma_e^2 R)$ is proportional to the number of electrons of a Gaussian bunch, r_0 is the classical electron radius and R the average storage ring radius. From the threshold condition and replacing $\alpha \gamma \sigma_e^2 R$ by $\sigma^2 dV_{rf}/ds$ we get (see also [33])

$$N \propto (\sigma / \rho)^{1/3} \sigma^2 dV_{rf} / ds,$$

a relation between number of electrons, bunch length and voltage gradient. There is a difference in the exponent of the bunch length-current relation at the bursting threshold, where the theory predicts $\sigma \propto N^{7/3}$ and our bursting data show better agreement with $\sigma \propto I^{8/3}$. This leads to longer bunches than predicted by the simple scaling.

From the scaling relation we find, that for a given machine, with fixed bending radius and rf-voltage, the threshold for a given bunch length does not depend on the machine energy. In case of a reduced energy, the desired bunch length is achieved at larger values of α and f_s , which could be an advantage.

If one considers a possible upgrade of the rf-voltage gradient, one gains in direct proportion an increase of the current threshold. Based on our present results, a 100-fold larger threshold current achieved by a 100-times increase of the voltage gradient yields $5 \cdot 10^9$ electrons resp. 0.1 mA per 1 ps bunch. Depending on the filling pattern, the repetition rate could be varied from 1.25 MHz (1 bunch and 0.1 mA average current) to 500 MHz (400 bunches and 40 mA average current). This could be performed, for example, with a passive Landau multi cell cavity running at 1.5 GHz with 45 MV integrated voltage. This might fit in one or two straight sections of the ring.

2.6.7 Summary

The BESSY low alpha optics offers the possibility to reduce the electron bunches and X-ray pulses to the ps range and to generate stable and bursting CSR in a reliable operation mode. The CSR delivers a lot and detailed information on beam dynamics [6] and it offers a powerful and stable THz-source for user applications [8].

The key to operate BESSY in such an optics mode is the flexible sextupole correction scheme for controlling the transverse and longitudinal chromaticities.

2.6.8 Acknowledgements

It is a pleasure to thank our BESSY colleagues for excellent support during this work. We acknowledge many productive discussions with M. Abo-Bakr (BESSY), J.M. Byrd (ALS), F. Sannibale (ALS), U. Schade (BESSY), G. Stupakov (SLAC), M. Venturini (ALS) and R. Warnock (SLAC).

2.6.9 References

- [1] "Micro Bunches Workshop", Upton, NY, 1995, editors E. Blume, M. Dienes, J. B. Murphy, AIP Conference Proceedings 367.
- [2] M. Abo-Bakr et al., "Steady-State Far-Infrared Coherent Synchrotron Radiation detected at BESSY II", Phys. Rev. Lett. **88**, 254801 (2002).
M. Abo-Bakr et al., "Brilliant, Coherent Far-Infrared (THz) Synchrotron Radiation", Phys. Rev. Lett. **90**, 094801 (2003).
- [3] G. Stupakov, S. Heifets, "Beam instabilities and micro bunching due to coherent synchrotron radiation", Phys. Rev. ST AB **5**, 054402, May 2002.
- [4] J.M. Byrd et al., "Observation of Broadband Self-Amplified Spontaneous Coherent Terahertz Synchrotron Radiation in a Storage Ring", Phys. Rev. Lett. **89**, 224801 (2002).
- [5] J. Feikes, G. Wüstefeld, "Experimental Studies of the Nonlinear Momentum Compaction Factor at BESSY", PAC'99, New York, p. 2376, March 1999.

- [6] P. Kuske et al., "Coherent Emission of Synchrotron Radiation and Longitudinal Instabilities", PAC'03, Portland (USA), p. 3023, May 2003.
- [7] E.J. Singley, et al., "Measuring the Josephson plasma resonance in Bi₂Sr₂CaCu₂O₈ using intense coherent THz synchrotron radiation", Phys. Rev. B **69**, 092512 (2004).
- [8] U. Schade et al., this ICFA Newsletter.
- [9] J. Feikes et al., "Compressed Electron Bunches for THz-Generation – Operating BESSY in a Low Alpha Mode", EPAC'04, Luzern (Switzerland), July 2004.
- [10] J. Feikes et al., "Sub-Pico Second Electron Bunches in the BESSY Storage Ring", Proceedings of the 2004 EPAC.
- [11] Y. Shoji et al., "Quasi-Isochronous Operation at NewSUBARU", EPAC'04, Luzern (Switzerland), July 2004.
- [12] H. Wiedemann, "Particle Accelerator Physics II", chapter 6.3 "Higher-Order Phase Focusing", Springer Verlag, 1995.
- [13] R. Klein et al., "The Metrology Light Source of the Physikalisch-Technische Bundesanstalt in Berlin-Adlershof", EPAC'04, Luzern (Switzerland), July 2004.
M. Abo-Bakr et al., "Der Metrologie-Speicherring MSR des Willi Wien Labors der Physikalisch-Technische Bundesanstalt bei BESSY", BESSY Internal Report, July, 2003.
- [14] H. Nishimura et al., "Lattice Studies for CIRCE (Coherent InfraRed CEter) at the ALS", EPAC'04, Luzern (Switzerland), July 2004.
- [15] G. H. Hoffstaetter and A. W. Chao, "Synchrotron stop bands due to a single crab cavity", Phys. Rev. ST Accel. Beam **7**, 071002 (2004).
- [16] Y. Shoji, "Bunch lengthening by a betatron motion in quasi-isochronous storage rings", Phys. Rev. ST Accel. Beam **7**, 090703 (2004).
- [17] S. Khan et al., "Layout of a Femto-Second X-ray Source at BESSY II", PAC'03, Portland (USA), p. 836, May 2003.
- [18] Y. Shoji et al., "Longitudinal radiation excitation in an electron storage ring", Phys. Rev. E **54**, R4556 (1996).
- [19] K. Holldack et al., to be published.
- [20] H. Grote, F. Ch. Iselin, "The MAD program", Version 8.22/14.
- [21] J.S. Nodvick and D.S. Saxon, "Suppression of Coherent Radiation by Electrons in a Synchrotron", Phys. Rev. **96**, 180-184 (1954).
- [22] See discussion by J.B. Murphy, in [1] "Issues and State of the Art for Short Bunches in e/e Storage Rings".
- [23] H. Wiedemann, "Particle Accelerator Physics", chapter 9.2, "Coherent Radiation", Springer Verlag, 1995.
- [24] K. Bane, S. Krinsky & J.B. Murphy in [1], "Longitudinal Potential Well Distortion Due to the Synchrotron Radiation Wakefield".
F. Sannibale et. al., "A Model Describing Stable Coherent Synchrotron Radiation in Storage Rings", Phys. Rev. Lett. **93**, 094801 (2004).
F. Sannibale et al., this ICFA Newsletter.
- [25] H.-W. Hübers, in this ICFA Newsletter.
- [26] H. Lihn et al., "Measurement of subpico second electron pulses", Phys. Rev. E **53**, 6413, (1996).
- [26] H. Lihn et al., "Measurement of subpico second electron pulses", Phys. Rev. E **53**, 6413, (1996).
- [27] R. Lai, A.J. Sievers, "On using the coherent far IR radiation produced by a charged-particle bunch to determine its shape: I Analysis", Nucl. Instr. and Meth. A **397** (1997) 221-231.
- [28] M. Abo-Bakr et al., "Powerful, Steady State, Coherent Synchrotron Radiation at BESSY II", EPAC'02, Paris (France), June 2002.
- [29] K. Holldack et al., "Coherent Synchrotron Radiation Experiments at BESSY II", PAC'03, Portland (USA), p. 3020, May 2003.
- [30] P. Kuske et al., "Bunch Length Measurements at BESSY", PAC'03, Portland (USA), p. 3020, May 2003.

- [31] D. H. Martin and E. Puplett, “Polarised interferometric spectrometry for the millimetre and submillimetre spectrum”, *Infrared Phys.* **10**, 105-109 (1969).
 P. Kung et al., “Generation and Measurement of 50-fs Electron Pulses”, *Phys. Rev. Lett.* **73**, 967-970 (1994).
- [32] P. Kuske et al., “Coherent Emission of Synchrotron Radiation and Longitudinal Instabilities”, PAC’03, Portland (USA), p. 3023, May 2003.
- [33] F. Sannibale, this ICFA Newsletter.

2.7 SOLEIL as CSR Source (Prospects and Preliminary Estimations)

O. Chubar, A. Nadji, A. Loulergue, M.-P. Level, J.-M. Filhol, P. Roy, [SOLEIL
oleg.chubar@synchrotron-soleil.fr](mailto:oleg.chubar@synchrotron-soleil.fr)

2.7.1 Introduction

The 2.75 GeV, third generation Synchrotron Radiation source SOLEIL, which is currently under construction in the vicinity of Paris, has an extended program of research with synchrotron radiation in large spectral domain extending from infrared to hard X-rays. A particular emphasis is made on the infrared region, from $\sim 1 \mu\text{m}$ to $\sim 500 \mu\text{m}$ and larger wavelengths. Starting from the phase I of operation (year 2006), the machine will have two infrared exit ports with four end stations dedicated to high-resolution spectroscopy in the THz spectral range, to far-infrared spectroscopy at intermediate resolution on condensed matter, and to microspectroscopy and imaging in the near-, mid- and far-infrared range. Therefore, a special attention is paid at SOLEIL to the investigation of possibilities for increasing the infrared spectral flux by production of the Coherent Synchrotron Radiation (CSR).

The SOLEIL magnet lattice (of “expanded Chasman-Green” type) with independently powered quadrupoles allows for the storage ring operation in a variety of different modes. Some of these modes are appropriate for the generation of the CSR in the THz spectral range. Currently, we consider three possibilities for the CSR at SOLEIL:

- Operation with low momentum compaction factor;
- Use of the CSR produced in the electron beam femtosecond slicing experiment;
- Transverse deflection of electron bunches in RF cavities.

Based on preliminary estimations, each of the three above-mentioned methods seems promising from the machine physics point of view. Some details of the lattice modes, and the expected spectral performance are presented below.

2.7.2 Operation with Low Momentum Compaction Factor

Relativistic electrons moving in external magnetic field in free space are known to emit coherently at wavelengths comparable with or larger than the electron bunch length (or the size of the electron bunch in the direction of the relativistic motion). In presence of a storage ring vacuum chamber, the coherent spontaneous emission can be extracted at wavelengths smaller than the cut-off wavelength value of the vacuum chamber, acting as a waveguide. The trend consists in providing conditions for stable electron dynamics with smallest-possible bunch length. In storage rings, this typically

requires a low value of the momentum compaction factor [1-6] (however, this does not seem to be the main issue for energy-recovery linacs [7]).

To provide a low momentum compaction factor, SOLEIL quadrupoles can be adjusted in such a way that the dispersion function $\eta(s)$ would pass from negative to positive values within bending magnets, in order to reduce the integral $\int \eta \rho^{-1} ds$, where ρ is the bending radius. The resulting lattice functions at one super-period in such mode are shown in Fig. 1. The simulations were done using the computer code BETA [8].

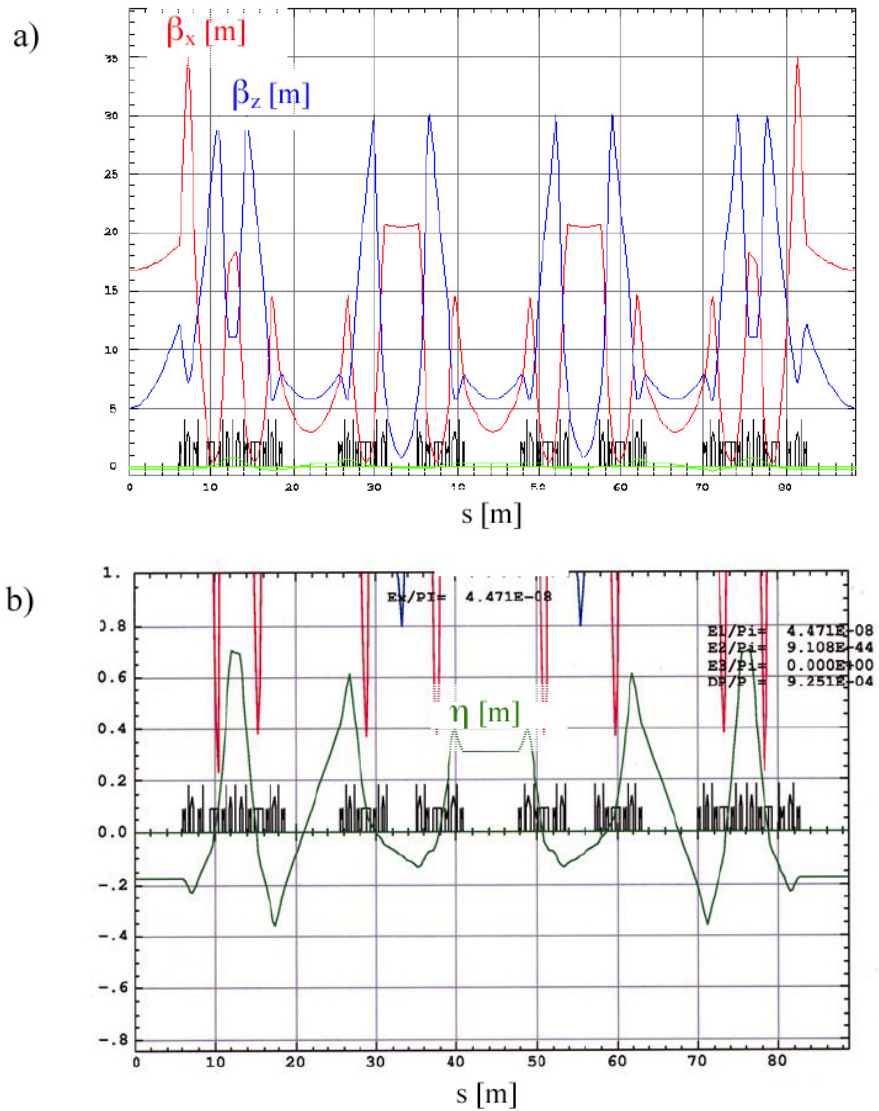


Figure 1: SOLEIL lattice functions in the mode with low first-order momentum compaction factor: (a) horizontal and vertical beta-functions and (b) horizontal dispersion function.

The value of the first-order momentum compaction factor obtained by the simulation is $\alpha_1 \approx 3 \times 10^{-6}$. This is about 150 times less than the nominal value $\alpha_{1\text{nom}} \approx 4.5 \times 10^{-4}$. The first-order momentum compaction factor can probably be further reduced; however, higher-order momentum compaction factors are much more difficult to control.

The electron bunch length at zero current will expectedly reduce from the nominal value of ~ 3.6 mm (12 ps) to ~ 0.3 mm (1 ps). A drawback of such operation is the increase of the horizontal emittance from the nominal value of 3.7 nm x rad to ~ 44 nm x rad. This is, nevertheless, harmless for far infrared spectral range.

Estimation of the higher-order momentum compaction factors, as well as calculation of the machine impedance and attainable electron beam current values and lifetime in this mode of operation are the subjects of further investigation.

Figure 2 shows the estimated total spectral flux within the angular aperture of 78 mrad x 20 mrad (SOLEIL IR port extracting the emission from central part and edges of bending magnets) in the low alpha mode, assuming Gaussian longitudinal bunch profile with RMS length of 0.3 mm, 50 electron bunches with 50 μ A current per bunch, in comparison with the spectral flux of incoherent emission in the standard SOLEIL mode at 500 mA current. In reality, the bunch profile may differ from Gaussian, so that the coherent part of the SR spectrum between ~ 0.4 mm and ~ 2 mm wavelength may appear to be non-monotonous; besides, the number of bunches can probably be larger than 50 . In any case, we expect a considerable increase of the IR flux starting from wavelengths $0.3 - 0.5$ mm (frequencies ≤ 1 THz).

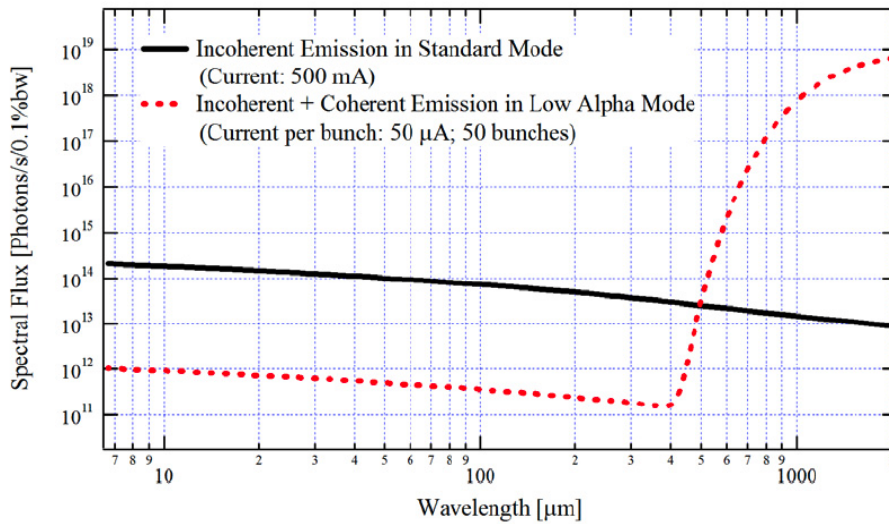


Figure 2: The estimated incoherent and coherent SR spectral flux through the SOLEIL IR extraction port..

2.7.3 CSR Produced in the Electron Beam Femtosecond Slicing Experiment

SOLEIL storage ring lattice is well suited for the generation and separation of sub-picosecond pulses of X-rays using a laser based technique [9]. It is planned to apply a spatial horizontal and a mixed angular-spatial horizontal schemes for separating the emission of the energy-modulated electrons from the core emission of the electron bunch, profiting from specific features of the SOLEIL storage ring optics [10].

The femtosecond slicing experiment can also be considered as a method for the production of the coherent SR. The THz range CSR has proved to be a powerful tool for the diagnostics of the sliced electron bunches [11, 12]. The possibility of using of the CSR produced with this method for the IR experiments in time-resolved and stationary regimes is currently under investigation.

At present time, it is probably the most accomplished solution, though the femtosecond slicing project is not yet funded at SOLEIL.

2.7.4 Transverse Deflection of the Electron Bunches in RF Cavities

One more possibility to generate the CSR can be related to the use of superconducting deflecting cavities with the excited first dipole mode, in order to produce a transverse RF “kick” to electron bunches, which would couple the longitudinal and transverse (vertical) motion of the electrons [13]. Even though this method was initially suggested for the generation of short X-rays pulses, one can think of using it also for the production of the CSR in THz spectral range [14]. To produce the CSR with this method, the electron bunches should have a sub-mm length of longitudinal projections when passing through the dipole magnet(s) used by IR beamline(s). For this, the required amplitude of the dipole mode in the RF cavity must be properly tuned. The initial investigation could be done by exciting this dipole mode, regardless of its frequency, in one of the two main superconducting accelerating cavities (the first cryomodule is planned to be installed in 2005, and the second one at the end of 2006). SOLEIL lattice can be adjusted to have large values of the vertical beta-function (up to ~ 20 m) at the locations of the RF cavities (see Fig. 3). This is favourable for the correlated longitudinal-vertical dynamics [13].

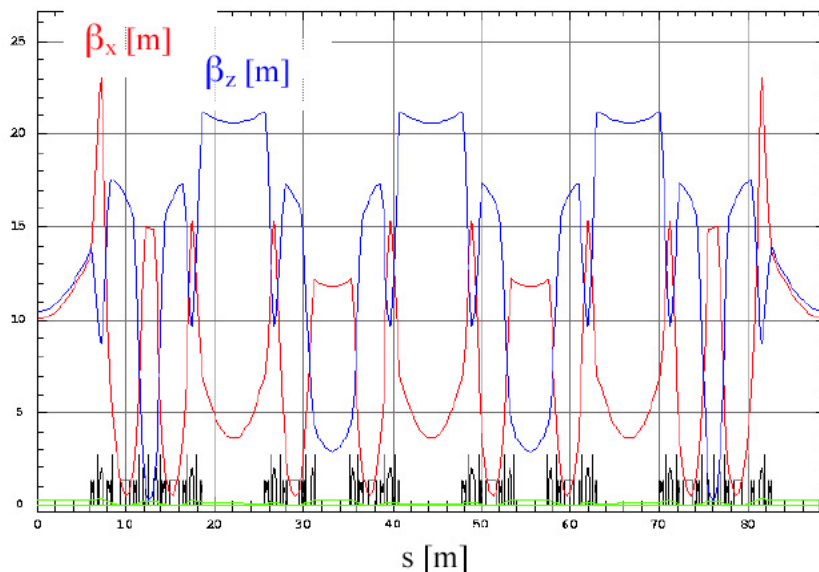


Figure 3: SOLEIL lattice providing large vertical beta-function in straight sections occupied by RF cavities.

A number of important questions still need to be addressed and worked out before concluding about the usefulness and feasibility of such mode of operation at SOLEIL, e.g.: what can be practical consequences of a considerable increase of transverse dimensions of electron bunches (taking place in this method) for the emission and extraction of the CSR (?), can the main RF cavities provide sufficiently large amplitude of the first dipole mode with a necessary stability of phase, or special “crab”-type cavities are absolutely necessary (?); can the storage ring operate in such regime without exciting synchro-betatron resonances (?).

To make a reliable prediction of the emitted spectral flux and observable spectral flux per unit surface in such or similar modes, special method for fast calculation of the CSR, taking into account electron distribution in 6D phase space, is planned to be added to the computer code SRW [15].

2.7.5 Acknowledgements

We would like to thank Prof. G.P. Williams (JLab), Dr. Y.-L. Mathis, Dr. R. Rossmanith (ANKA), Dr. A. Zholents, Dr. M. Zolotorev, Dr. J. Byrd, Dr. F. Sannibale, Dr. D. Robin (LBNL-ALS), Dr. K. Holldack (BESSY) for fruitful discussions; Dr. P. Dumas, Dr. P. Marchand and Prof. D. Raoux (SOLEIL) for precious help and support.

2.7.6 References

- [1] A. Andersson, M.S. Johnson, B. Nelander, "Coherent Synchrotron Radiation in the Far Infrared from a 1-mm Electron Bunch", *Opt. Eng.*, vol. 39, p. 3099-3105 (2000).
- [2] M. Abo-Bakr, J. Feikes, K. Holldack, D. Ponwitz, G. Wustefeld, H.-W. Hubers, "Coherent mm-Radiation Experiments at the BESSY-II Storage Ring", *Proc. of EPAC-2000*, p. 720-722.
- [3] G.L. Carr, S.L. Kramer, J.B. Murphy, R.P.S.M. Lobo, D.B. Tanner, "Observation of Coherent Synchrotron Radiation from the NSLS VUV Ring", *NIMA*, vol. 463, p. 387-392 (2001).
- [4] M. Abo-Bakr, J. Feikes, K. Holldack, G. Wustefeld, H.-W. Hubers, "Steady-State Far-Infrared Coherent Synchrotron Radiation detected at BESSY II", *Phys. Rev. Lett.*, vol. 88, 254801 (2002).
- [5] J.M. Byrd, W.P. Leemans, A. Loftsdottir, B. Marcelis, M.C. Martin, W.R. McKinney, F. Sannibale, T. Scarvie, C. Steier, "Observation of Broadband Self-Amplified Spontaneous Coherent Terahertz Synchrotron Radiation in a Storage Ring", *Phys. Rev. Lett.*, vol. 89, 224801 (2002).
- [6] J.M. Byrd et. al., "A Dedicated Storage Ring for Far-IR Coherent Synchrotron Radiation at the ALS", *Proc. of PAC-2001*, p. 2623-2625.
- [7] G.L. Carr, Michael C. Martin, Wayne R. McKinney, K. Jordan, George R. Neil and G.P. Williams, "High-Power Terahertz Radiation from Relativistic Electrons", *Nature*, vol. 420, p. 153-156 (2002).
- [8] J. Payet et. al., BETA computer code, LNS version, modified for SOLEIL.
- [9] A. Zholents and M. Zolotorev, "Femtosecond X-Ray Pulses of Synchrotron Radiation", *Phys. Rev. Lett.*, vol. 76, p. 912 (1996).
- [10] A. Nadji, O. Chubar, M. Idir, M.-P. Level, A. Loulergue, T. Moreno, L. Nadolski, F. Polack, "Femtosecond Electron Beam Slicing Project at SOLEIL", *Proc. of EPAC-2004*, p. 2329-2331.
- [11] J.M. Byrd, F. Sannibale, private commun.
- [12] K. Holldack et. al., "Terahertz Diagnostics for the Femtosecond X-Ray Source at BESSY", *Proc. of EPAC-2004*, p. 2281-2283.
- [13] A. Zholents, P. Heinmann, M. Zolotorev, J. Byrd, "Generation of Subpicosecond X-Ray Pulses Using RF Orbit Deflection", *NIMA*, vol. 425, p. 385-389 (1999).
- [14] R. Rossmanith, Y.-L. Mathis, private commun.
- [15] O. Chubar, P. Elleaume, "Accurate and Efficient Computation of Synchrotron Radiation in the Near Field Region", *Proc. of EPAC-98*, p. 1177-1179.

2.8 Observation of Intense Terahertz Bursts at UVSOR-II

Masahiro Katoh, [UVSOR](#)
mkatoh@ims.ac.jp

2.8.1 Introduction

UVSOR-II is a 750 MeV synchrotron light source. The original machine UVSOR-I had been operated for about twenty years and was recently upgraded to UVSOR-II, which has much smaller emittance and more straight sections available for undulators [1]. UVSOR-II has an infrared beam-line, which had been operated since the middle of 1980's [2] and was also recently upgraded [3]. In January 2004, we successfully detected intense bursts of terahertz radiation at the infrared beam-line, BL6B. In this report, we will present some preliminary results from our observation.

2.8.2 Experiments

2.8.2.1 Storage ring

The electron beam is injected to UVSOR-II at 600 MeV and then accelerated to 750 MeV in the normal operation for users. However, since the terahertz bursts can be observed in single bunch operation with very high bunch current, we made all the measurements at the injection energy, to accumulate the electrons as much as possible. The machine parameters during the experiments are shown in Table 1.

Table 1: Machine Parameters of UVSOR-II for the CSR experiments.

Parameters	Values
Electron Beam Energy	600 MeV
Circumference	53.2 m
Natural Emittance	17 nm-rad
Natural Energy Spread	3.4×10^{-4}
Momentum Compaction Factor	0.028
RF Frequency	90.1 MHz
RF Accelerating Voltage	55 kV
Natural Bunch Length	3.1 cm
Synchrotron Frequency	14.4 kHz
Longitudinal Damping Time	19 msec
Bending Radius	2.2 m

2.8.2.2 Infrared Beam-line and Detector

Terahertz radiation is observed at the infrared beam-line (BL6B) [3]. A noteworthy feature of this beam-line is its very large acceptance, $215(\text{H}) \times 80(\text{V}) \text{ mrad}^2$, which is realized by installing so-called “magic mirror” inside of the bending magnet chamber. A liquid He cooled InSb bolometer is used for the measurements, whose spectral

response is in the wavelength region between 0.2 – 3.0 mm and time response is about 1 micro-sec. To measure the average intensity, a mechanical chopper and a lock-in-amplifier are used.

2.8.2.3 Results

All the measurements were done in the single bunch operation at 600 MeV with the normal optics. In Figure 1, the average terahertz intensity was plotted against the beam current. For comparison, the data taken in the multi-bunch operation are also shown. In the low beam current region, the intensity is proportional to the beam current for both cases. However, for the beam current between 70 and 80 mA and above 140 mA, large deviations can be seen in the single bunch mode. In these current regions, there appear very intense bursts as shown in Figure 2. At higher beam current, the bursts appear chaotically. On the other hand, at lower beam current, they appear quasi-periodically. The burst intervals are around 10 msec for the beam current above 140 mA and about 100 msec for the beam current between 70 and 80 mA. In Figure 3, some examples of the temporal structures of the individual bursts are shown. Each burst usually contains many peaks. Those peaks appear quasi-periodically. The period is typically a few tens of micro-sec, which is roughly one half of the synchrotron period. The peak intensity of each burst is typically $10^3 - 10^4$ times more intense than the normal synchrotron radiation in same wavelength region.

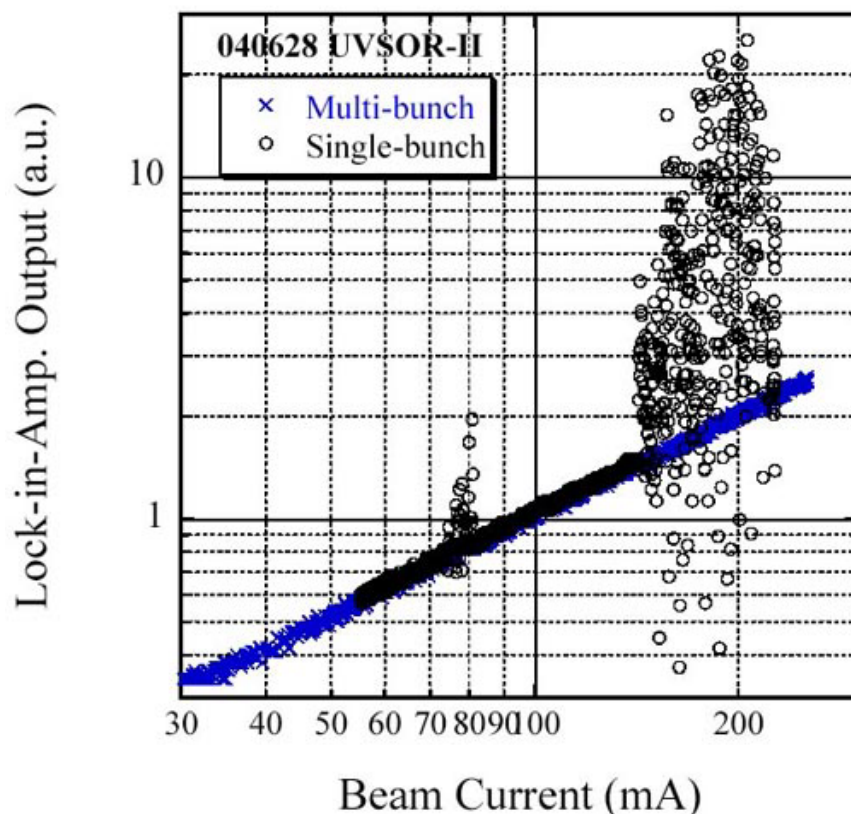


Figure 1: Intensity of the terahertz radiation observed at the infrared beam line BL6B of UVSOR-II. The blue crosses are the data taken in multi-bunch mode and the white circles in single bunch mode. The chopper frequency was 100Hz.

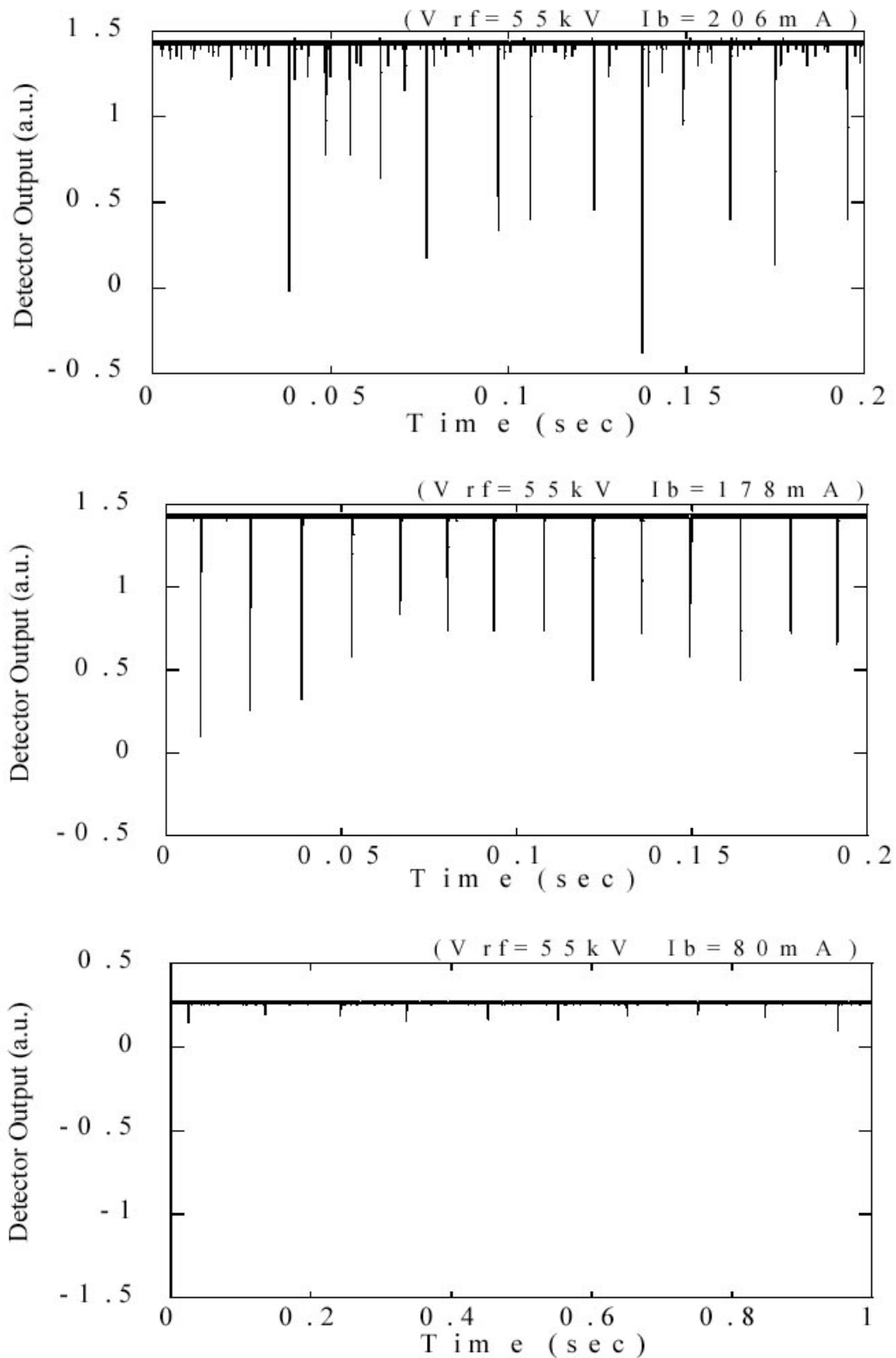


Figure 2: Terahertz bursts at three beam currents, 206mA (top), 178 mA (middle) and 80 mA (bottom). The output signal (negative) of the bolometer was recorded with a digital oscilloscope. The bursts appear chaotically at the higher beam current and quasi-periodically at the lower beam current. The horizontal scale in the lowest figure is larger than others.

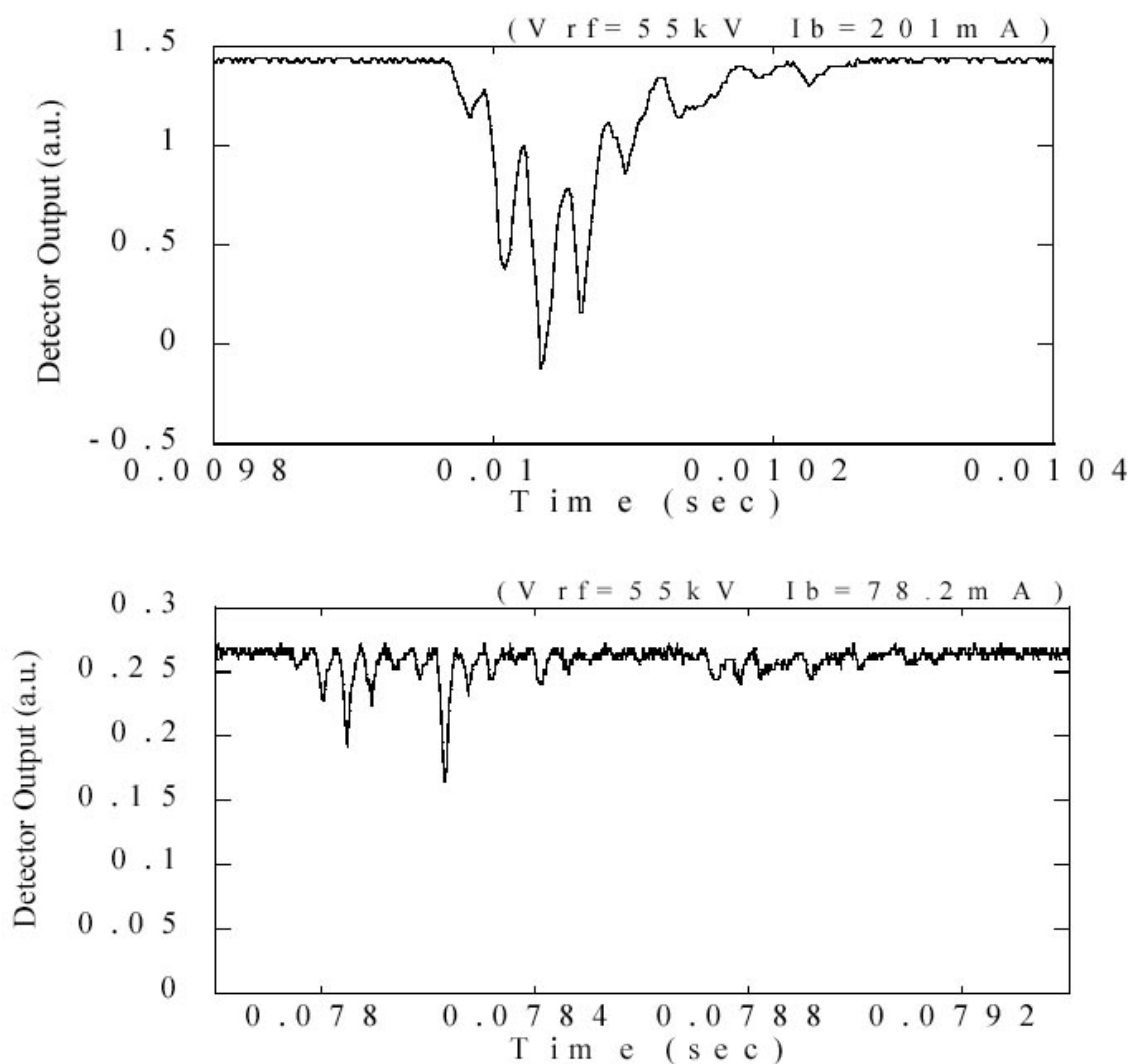


Figure 3: Some examples of the temporal profiles of the individual bursts at the beam current of 201mA (upper) and 78mA (lower). The output signal (negative) of the bolometer was recorded with a digital oscilloscope.

2.8.3 Summary

At a 750MeV electron storage ring, UVSOR-II, intense terahertz bursts were detected in single bunch operation with the normal beam optics. The bursts appear in two current regions, between 70 and 80 mA and above 140 mA. Typical duration and interval of the bursts are about a few hundred micro-sec and 10 - 100 msec, respectively. Each burst contains many peaks and shows quasi-periodicity of about a few tens of micro-sec. The peak intensities of the bursts are 10^3 - 10^4 times higher than that of normal synchrotron radiation in the same wavelength region. This extremely high intensity suggests that the bursts are produced by coherent emission, although the electron bunch length of UVSOR-II is much longer than the observed wavelength. More details of these results will be presented in future papers.

2.8.4 References

- [1] M. Katoh, K. Hayashi, T. Honda, Y. Hori, M. Hosaka, T. Kinoshita, S. Koda, Y. Takashima, and J. Yamazaki, "New Lattice for UVSOR", Nuclear Instruments and Methods in Physics Research A, **467-468**, 68-71 (2001).
- [2] T. Nanba, Y. Urashima, M. Ikezawa, M. Watanabe, E. Nakamura, K. Fukui, H. Inokuchi, "Far-infrared spectroscopy by synchrotron radiation at the UVSOR facility", Int. J. Infrared and Millimeter Waves, 7(11), 1769-1776 (1986).
- [3] S. Kimura, E. Nakamura, J. Yamazaki, M. Katoh, T. Nishi, H. Okamura, M. Matsunami, L. Chen, T. Nanba, "New Infrared and Terahertz Beam Line BL6B at UVSOR," Proceedings of 8th International Conference on Synchrotron Radiation Instrumentation, 416-419 (2004).

2.9 Observation of CSR at NewSUBARU

Yoshihiko Shoji, [LASTI](http://lasti.u-hyogo.ac.jp)
shoji@lasti.u-hyogo.ac.jp

2.9.1 Introduction

We just started observation of CSR at NewSUBARU on November 30th of 2004. We have already succeeded in the bunch compression down to less than 4ps FWHM [1]. Then we expected to observe steady-state CSR in quasi-isochronous operation mode. Here I will show some preliminary results of our measurements.

Members of our group are three accelerator physicists, A. Ando, S. Hashimoto and Y. Shoji of LASTI (Laboratory of Advanced Science and Technology for Industry, University of Hyogo) and future users of THz radiation, T. Takahashi of Kyoto University, H. Kimura, T. Hirono, K. Tamasaku and M. Yabashi of SPring-8.

2.9.2 NewSUBARU in Quasi-Isochronous Mode

The NewSUBARU storage ring [2, 3] is a 1.5 GeV synchrotron radiation ring at the SPring-8 site. LASTI is in charge of its operation, collaborating with SPring-8. A bending cell in the ring is a modified DBA with an 8° invert bend between two 34° normal bends. This facilitates the control of the linear momentum compaction factor (α_1) while keeping the cell achromatic and with only a small change of natural emittance.

We reduced α_1 , keeping the RF voltage (V_{RF}) constant, to ensure that the theoretically expected bunch length was proportional to $\sqrt{\alpha_1}$. Figure 1 shows the results for two kinds of V_{RF} settings (120kV and 300kV) at two settings of bunch current (1.8 μ A/bunch and 0.24 μ A/bunch). The bunch length became longer than that expected from the $\sqrt{\alpha_1}$ law at $\alpha_1 < 1 \times 10^{-5}$. At such a low alpha, the reduction of α_1 did not shorten the bunch but the raise of V_{RF} did. We observed no current dependence of bunch length with such a weak beam.

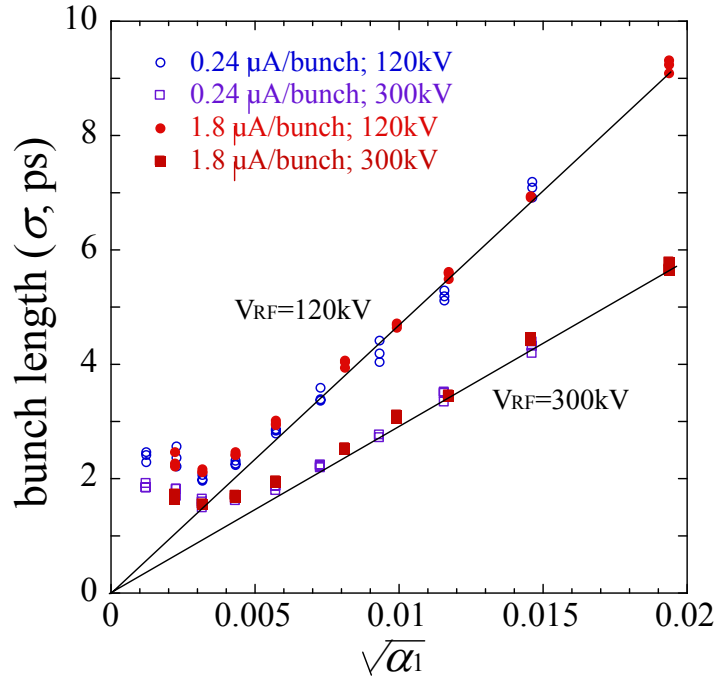


Figure 1: Bunch length vs. $\sqrt{\alpha_1}$. The symbols are measured length and the lines are theoretical calculation. The RF acceleration voltage was kept constant at 120kV or 300kV while changing α_1 . The open symbols and the shaded symbols are the results with stored beam current of 1.8 and 0.24 $\mu\text{A}/\text{bunch}$, respectively. The resolution of the camera was not corrected.

2.9.3 Measurement of Radiation Power

Because NewSUBARU has no FIR beam line at the present, we set a Si bolometer at a SR light extraction port for beam diagnostics. A low-pass filter of 35cm^{-1} was set inside of the bolometer. We have measured beam charge dependence of radiation power in three machine conditions.

- (1) Multi-bunch normal alpha (probably normal incoherent radiation).
- (2) Single-bunch normal alpha (probably burst mode CSR).
- (3) Multi-bunch low alpha (probably steady state CSR).

At normal alpha, the bunch length depends on the stored beam current [4] and was about 40ps FWHM at the zero current limit ($V_{RF} = 122\text{kV}$). The CSR measurement at low alpha took place at $\alpha_1 \approx 5 \times 10^{-6}$ and $V_{RF} = 356\text{kV}$, where the expected bunch length was about 4ps FWHM. Figure 2 shows the radiation power in the above three cases. In case (2) the radiation power had a threshold at 3mA/bunch. This threshold current was lower for shorter bunch. In case (3) the radiation power was proportional to the square of the beam current, which we had expected.

Our next step is to measure the energy spectrum of CSR and also a time structure of CSR.

At normal alpha, the bunch length depends on the stored beam current [4] and was about 40ps FWHM at the zero current limit ($V_{RF} = 122\text{kV}$). The CSR measurement at low alpha took place at $\alpha_1 \approx 5 \times 10^{-6}$ and $V_{RF} = 356\text{kV}$, where the expected bunch length was about 4ps FWHM. Figure 2 shows the radiation power in the above three cases. In case (2) the radiation power had a threshold at 3mA/bunch. This threshold current was lower

for shorter bunch. In case (3) the radiation power was proportional to the square of the beam current, which we had expected.

Our next step is to measure the energy spectrum of CSR and also a time structure of CSR.

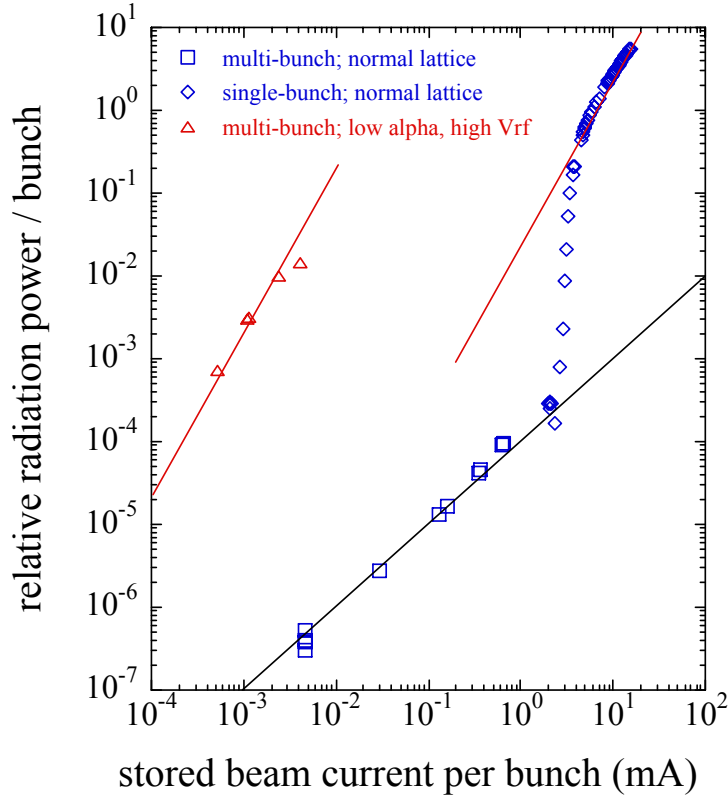


Figure 2: Radiation power vs. stored beam current per bunch in three cases; (1) and (2) normal alpha and (3) low alpha. The red lines and black line are guides which indicate the expected dependences when the power is proportional to the square of the current (CSR) or simply to the current (incoherent SR).

At normal alpha, the bunch length depends on the stored beam current [4] and was about 40ps FWHM at the zero current limit ($V_{RF} = 122\text{kV}$). The CSR measurement at low alpha took place at $\alpha_1 \approx 5 \times 10^6$ and $V_{RF} = 356\text{kV}$, where the expected bunch length was about 4ps FWHM. Figure 2 shows the radiation power in the above three cases. In case (2) the radiation power had a threshold at 3mA/bunch. This threshold current was lower for shorter bunch. In case (3) the radiation power was proportional to the square of the beam current, which we had expected.

Our next step is to measure the energy spectrum of CSR and also a time structure of CSR.

2.9.4 Acknowledgement

The author thanks members of accelerator group of BESSY-II, especially Dr. G. Wüstefeld for his encouragement and giving suggestions on our measurements. The author also thanks Prof. T. Mochizuki, a director of LASTI, for his support on this work.

2.9.5 References

- [1] Y. Shoji, S. Hisao, and T. Matsubara, "Ouasi-Isochronous Operation at NewSUBARU", proceedings of the 2004 European Particle Accelerator Conference, Lutzern, (2004).
- [2] A. Ando, *et al.*, J. Synchrotron Rad. 5, 342-344 (1998).
- [3] Y. Shoji, *et al.*, "NewSUBARU Storage Ring: Operational Progress in These Three Years", proceedings of the 3rd Asian Particle Accelerator Conference, Gyeongju, (2004)
- [4] A. Ando, S. Hashimoto and Y Shoji *et al.*, "Negative Alpha-p Operation at NewSUBARU", proceedings of 8th International Conference on Synchrotron Radiation Instrumentation, San Francisco (2003), AIP CP705, pp.13-16(2004).

2.10 Terahertz Coherent Synchrotron Radiation at DAΦNE

C. Biscari, M. Castellano, A. Gallo, A. Ghigo, A. Marcelli, F. Marcellini, G. Mazzitelli, C. Milardi, M.A. Preger, P. Raimondi, M. Serio, M. Zobov, [INFN-LNF](#)
 J.M. Byrd, F. Sannibale, [LBNL](#); P. Morini, D. Sali, [Bruker Optics, Milano](#)
caterina.biscari@lnf.infn.it

2.10.1 Introduction

DAΦNE is a double ring $e^+ e^-$ collider working at the Φ -resonance [1], at energy of 510 MeV per beam. The peak luminosity reached at the end of 2004 is $1.3 \times 10^{32} \text{ cm}^{-2} \text{ sec}^{-1}$. The electron ring, equipped with two synchrotron radiation lines extracting the light from a wiggler and for a dipole, is also used as a synchrotron radiation source [2]. It has stored the world highest e^- current (2.4 A). Usually the synchrotron light source (SLS) lines work parasitically during the luminosity runs with peak currents of the order of 1.7 A. Some dedicated SLS runs at currents exceeding 2 A have been recently done.

The future of the DAΦNE complex after the completion of the original physics program, which is foreseen in three years from now, is now argument of debate. Among the proposed projects is the super- Φ -factory design [3], based on the regime of strong rf focusing (SRFF) [4], in which a strong rf voltage and a high momentum compaction ring lattice produce a bunch length modulation along the ring which should allow reaching bunch lengths in the millimeter range at the Interaction Point (IP). The limits imposed by the microwave instability in principle can be controlled by placing the high impedance objects in the ring zones corresponding to the longer bunch. An experiment on DAΦNE has been proposed to test the SRFF regime, for which the installation of a new rf system at 1.3 GHz is needed [5].

The research program on SLS will be prosecuted in any case, profiting of the particular high flux of the DAΦNE beam. The possibility of producing CSR is also foreseen.

An important issue both for the luminosity and the CSR production is the evaluation and understanding of the effect of the machine impedance on the bunch length and energy spread for the very short bunch regimes. One effect is the microbunching instability (MBI) driven by the radiation impedance, which perturbs the longitudinal dynamics when the current per bunch is above the MBI threshold. For most storage rings and just above the MBI threshold, the perturbation is weak and shows measurable effects only as bursts of CSR in the far infrared (FIR). For currents much higher than

the MBI threshold the effects could be relevant inducing average bunch lengthening and strong transient modulation of the longitudinal distribution.

In this paper a preliminary evaluation of the MBI effects on DAΦNE is presented. The threshold for the MBI is calculated and some considerations are done. A more careful and detailed analysis of the instability effects should include simulations of the longitudinal dynamics as the ones presented in reference [6]. Experimental characterization of the MBI in DAΦNE remains the most direct way for approaching the issue. To this end we suggest some experiments.

If the current per bunch is kept below the MBI threshold, DAΦNE could become an interesting source of stable CSR in the terahertz frequency range. In fact, generating CSR requires relatively short bunches and according to the criteria of references [7, 8], several beneficial features are simultaneously present in the Frascati collider: the relatively low energy contributes to obtaining short bunches; the small bending radius and the large dipole gaps reduce the shielding of the vacuum chamber that tends to suppress the CSR emission; the aluminum vacuum chamber minimizes the contribution of the resistive wall impedance that induces bunch lengthening; several families of sextupole and octupole magnets allow for a precise control of the linear and non-linear terms of the momentum compaction, which is a fundamental requirement when tuning the machine to vanishing α_C and short bunches; last but not least, DAΦNE has SINBAD [9], a beam line optimized for the far-infrared (FIR) in the electron ring. The only non-ideal feature is represented by the existing RF system that allows for relatively small voltage in the cavities. However, with the proposed strong focusing RF scheme and its 1.3 GHz superconducting cavity operated at several megavolts, DAΦNE could become an outstanding source of CSR.

In the following analysis the contribution of the wigglers in the arcs to the CSR wakefield is not considered. While the wiggler effect is small for most existing storage rings, it could not be the case for DAΦNE, where the SR power radiated from the wigglers is comparable with that radiated from the dipole magnets. This situation makes DAΦNE an interesting machine for studying the wiggler wakefield effects experimentally. If the effect of the wigglers is significant, the results of the optimisation of DAΦNE as a CSR source can still be used for a lattice with the electromagnetic wigglers OFF. Two lattices, with wigglers ON and OFF respectively, are examined in paragraph 2.

Another interesting point that could be studied in DAΦNE is the effect of the beam-beam on the MBI. In fact in DAΦNE, the strong beam-beam regime could have significant effects on the MBI dynamics.

2.10.2 The microbunching instability in DAΦNE

According to references [10, 11] the threshold for the MBI is given by:

$$I_b > \frac{\pi^{1/6}}{\sqrt{2}} \frac{ec}{r_0} \frac{\gamma}{\rho^{1/3}} \alpha_C \delta_0^2 \sigma_z \frac{1}{\lambda^{2/3}} \quad (1)$$

where I_b is the average current per bunch, e the electron charge, c the speed of light, r_0 the electron classical radius, γ the beam energy in rest mass units, ρ the dipole bending

radius, α_C the momentum compaction, δ_0 the relative energy spread, σ_z the rms bunch length and λ the SR wavelength.

Expression (1) has been calculated for $\sigma_z \gg \lambda/2\pi$ and for a gaussian longitudinal distribution. The largest values that λ can assume is limited by the vacuum chamber cutoff.

The MBI is associated with the appearance of temporary structures in the longitudinal distribution with characteristic length smaller than the bunch length. These microbunches radiate CSR with a spectrum limited roughly to wavelengths as short as the characteristic length of the microbunch. For this reason, the SR wavelength λ appearing in Eqn. 1, can be also interpreted as the characteristic length of the microbunch itself. Shorter structures can be generated only at higher currents per bunch.

The experimental results in references [12,13] have clearly shown that Eqn. 1 can be used for careful predicting the MBI absolute threshold (first appearance of the instability) when the natural bunch length is used as the value for λ .

In DAΦNE the microwave instability threshold appears at very low currents (~below 1 mA/bunch), while the MBI threshold is higher, as shown in Fig. 1, where calculations have been done assuming natural bunch length and energy spread.

The microwave instability lengthens the bunches and increases energy spread and therefore also the MBI threshold.

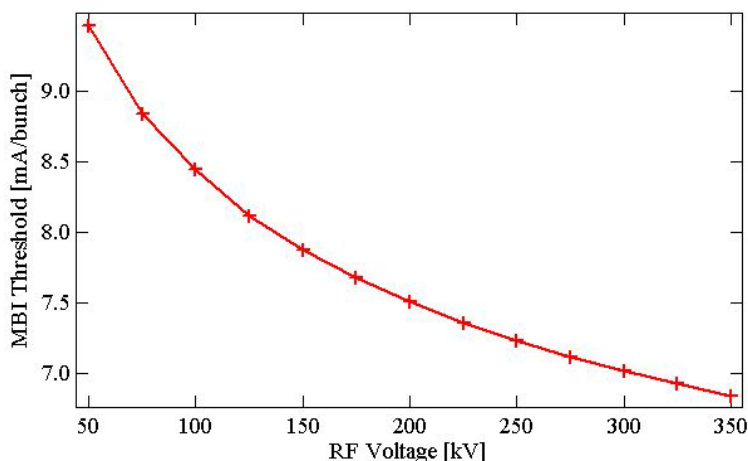


Figure 1: Single bunch average current threshold for the MBI calculated for DAΦNE with $E = 510$ MeV, $\rho = 1.4$ m, $\alpha_C = 0.02$.

At very high currents per bunch both instabilities could appear, and this could be experimentally verified at the SIMBAD FIR beam line. In fact, the CSR bursts associated with the appearance of the MBI, can be easily detected by a bolometer with sensitivity in the THz frequency range.

In the proposed strong focusing RF scheme for DAΦNE, short bunches are foreseen. According to Eqn.1, shorter bunches lead to lower MBI thresholds, but because of the very peculiar characteristics of this mode of operation, Eqn. 1 cannot be directly used and a new expression accounting for the new situation should be instead derived. Nevertheless, the MBI effects should be carefully investigated in order to evaluate the presence of undesired effects, such as bunch lengthening for example, that could limit the performance of this special mode of operation.

2.10.3 DAΦNE as an ultra-stable source of CSR

Recently it has been experimentally demonstrated at the BESSY II synchrotron light source that electron storage rings can be operated in a special mode where the CSR emission in the terahertz frequency is extremely stable and powerful [12,13]. Afterward works [7, 8] presented a physical model that explains the results of BESSY II and that allows to optimize new and existing storage rings for the CSR performance [14]. In this special mode, the momentum compaction is tuned to significantly lower values than in normal operation. As a consequence, the bunch shortens and the SR becomes the dominant wake. In such a situation, the SR wake induces a stable distortion of the bunch longitudinal distribution from Gaussian to a sawtooth-like shape with a sharp leading edge. This distortion significantly extends the CSR emission towards shorter wavelengths. For a stable emission, the current per bunch must be maintained below the MBI instability threshold that decreases for decreasing momentum compaction. We have applied such a model to DAΦNE for the two cases with the existing RF system and with the 1.3 GHz superconductive system, foreseen in the proposed strong RF focusing scheme.

2.10.3.1 DAΦNE as a CSR source with the existing 368 MHz RF system

Table 1 shows the relevant parameters of DAΦNE, while Table 2 presents the principal characteristics for three possible CSR modes of operation. The minimum momentum compaction of SET 1 is ~ 300 times smaller than the normal operation one and the (very small) currents per bunch for all the three modes are ~ 0.5 times the threshold for the MBI.

Table 1: DAΦNE relevant parameters

Energy [MeV]	510	Ring Length [m]	97.7
Bend Radius [m]	1.4	Harm. Number	120
RF freq. [MHz]	368.26	RF Voltage [kV]	250
Natural Relative Energy Spread (rms)	4.0×10^{-4}	Normal Momentum Compaction	0.02
Vacuum Chamber Height [mm]	50	Vacuum Chamber Material	Al

Table 2: Three possible sets for DAΦNE in the ultra-stable CSR mode. The CSR power is integrated between 1 and 30 cm^{-1} over an horizontal acceptance of 40 mrad. The sets correspond to the three curves shown in Figures 3, 4 and 5.

	Nat. bunch rms length [mm]	Momentum compaction	Total Current [mA]	Current per bunch [μA]	Total CSR Power [mW]
SET 1	0.5	7.5×10^{-5}	0.52	4.3	2.27
SET 2	1.0	3.0×10^{-4}	2.92	24.3	15.6
SET 3	2.0	1.2×10^{-3}	19.2	160	31.9

Figure 2 shows the equilibrium distributions for the three sets of Table 2. All the calculations include also the shielding effects of the vacuum chamber and the resistive wall impedance contribution. The effect of the geometric impedance of the vacuum

chamber is negligible in this short bunch regime. The sawtooth like distortion due to the SR wakefield is clearly visible. The curve for the 2 mm length case, shows a hump-like shape on the trailing edge. This is an indication that for such a bunch length (and longer ones), the shielding effect of the vacuum chamber starts to be significant.

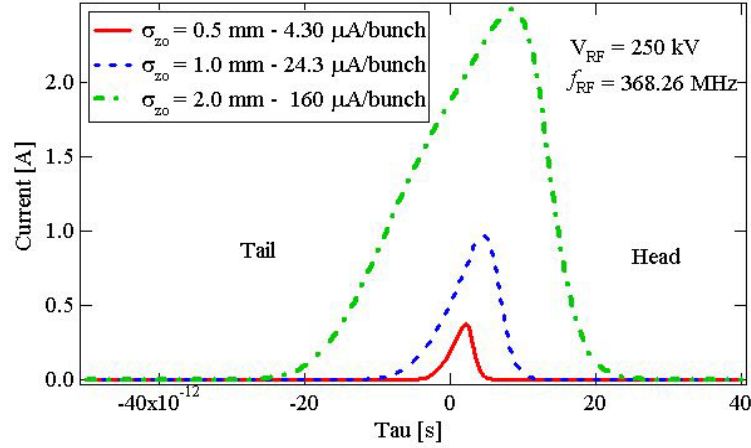


Figure 2: Calculated longitudinal distribution of the bunch for three different modes of DAΦNE as ultra-stable source of CSR.

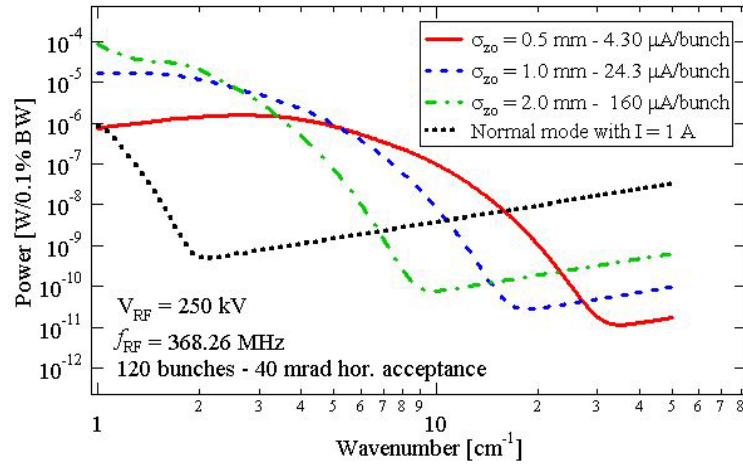


Figure 3: Calculated SR Spectra for three different sets of DAΦNE as ultra-stable source of CSR.

Figure 3 shows the SR power spectra for the three sets. The lower limit of the spectra has been set to 1 cm^{-1} that roughly corresponds to the DAΦNE vacuum chamber cutoff. Also shown as a dotted line, is the spectrum for DAΦNE in the normal mode of operation with 1 A of stored current. If we normalize the other spectra with respect to this last one, we obtain the curves in Figure 5 where the gain in power, for the three CSR sets with respect to the normal mode with 1 A, is shown. As Figure 4 shows, several order of magnitudes increase in power are obtained in the bandwidth from 1 to $\sim 15 \text{ cm}^{-1}$. Shorter bunch lengths extend the bandwidth but decrease the peak power. The small difference in the peak gain between the 1 and 2 mm cases, is due to the stronger shielding effect that the vacuum chamber has in the longer bunch case.

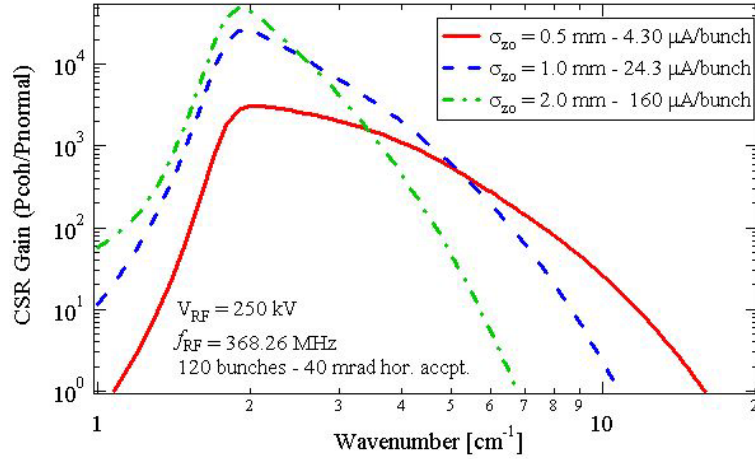


Figure 4. Calculated CSR gain for the three different sets of DAΦNE as ultra-stable source of CSR. The curves have been obtained dividing the power spectra by the spectrum of DAΦNE in the normal operation mode with 1 A stored.

2.10.3.2 DAΦNE as a CSR source with the 1.3 GHz SC RF system

In the proposed strong RF focusing scheme [5], a 1.3 GHz superconductive RF system is considered. Such a system will be capable of a RF voltage of up to ~ 10 MV. In what follows, we have repeated the analysis of the previous paragraph for the case with this more powerful RF system and assuming an RF voltage of 1 MV. The presented configuration has not been optimized with respect to the RF voltage and it is shown only as example of the better performances that can be obtained with such a RF system. Again the currents per bunch have been kept at ~ 0.5 the MBI threshold. The number of bunches used is 60, the maximum compatible with the present DAΦNE injection system. Table 3 and 4 show the parameters for this new mode of operation, while Figures 6, 7 and 8 the obtained results.

Table 3: New parameters for DAΦNE with the superconductive RF system.

RF freq. [GHz]	1.3
Harm. Number	424
RF Voltage [MV]	1.0

Table 4: Three possible sets for DAΦNE in the ultra-stable CSR mode with the superconductive RF system. The total current is distributed among 60 bunches. The CSR power is integrated between 1 and 60 cm^{-1} over a horizontal acceptance of 40 mrad. The sets correspond to the three curves shown in Figures 5, 6 and 7.

	Nat. bunch rms length [mm]	Momentum compaction	Total Current [mA]	Current per bunch [μA]	Total CSR Power [mW]
SET 4	0.25	2.5×10^{-4}	0.68	11.3	25
SET 5	1.0	1.0×10^{-3}	3.40	56.7	220
SET 6	2.0	4.0×10^{-3}	18.48	308	1506

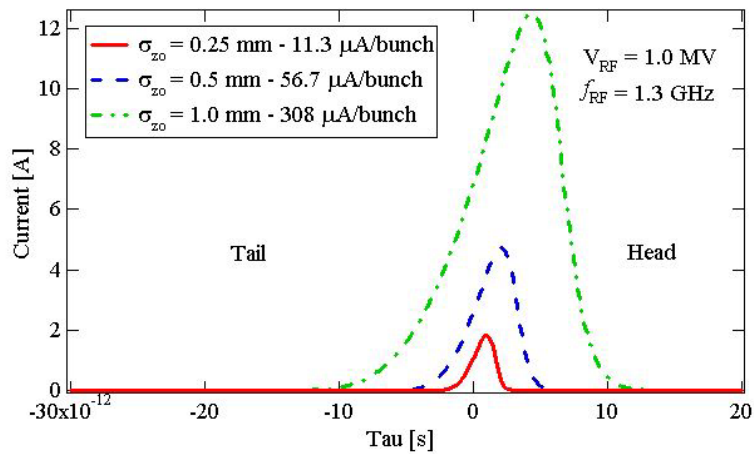


Figure 5: Calculated longitudinal distribution of the bunch for the three different modes of DAΦNE with the superconductive RF system.

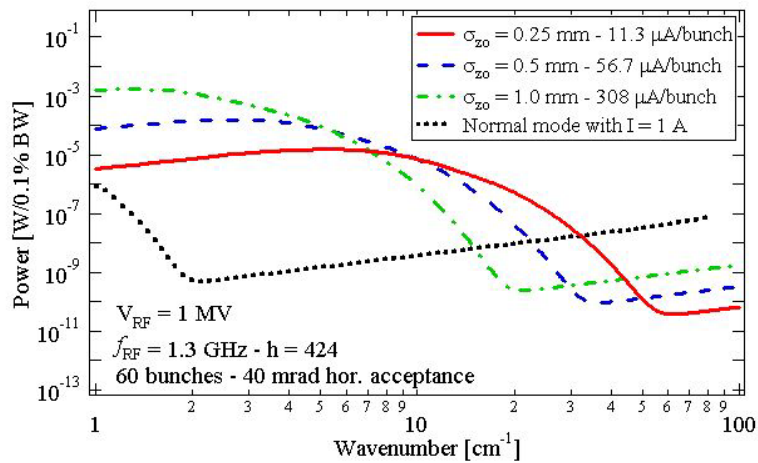


Figure 6: Calculated SR Spectra for the three different sets of DAΦNE with the superconductive RF system.

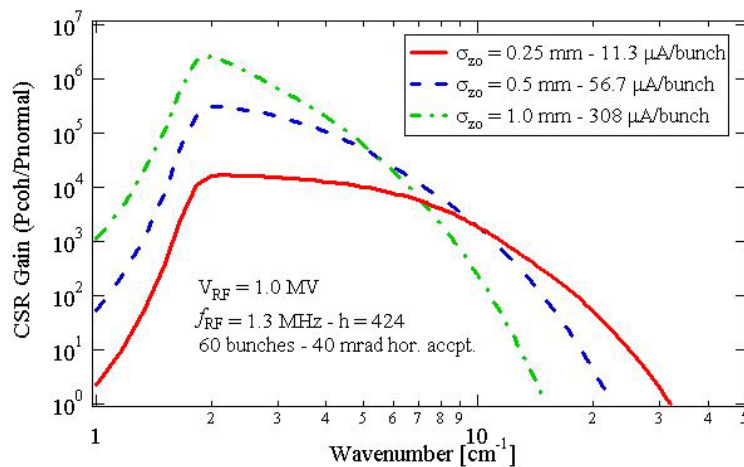


Figure 7: Calculated CSR gain for the three different sets of DAΦNE with the superconductive RF system. The curves have been obtained dividing the power spectra by the spectrum of DAΦNE in the normal operation mode with 1 A stored.

Figure 7 shows the impressive performances of DAΦNE with the superconductive RF system. The power gain greatly increased in both bandwidth and absolute value.

2.10.3.3 Two low alpha lattices for DAΦNE as a CSR Source

DAΦNE lattice can be flexibly tuned in the momentum compaction factor by modifying the behaviour of the dispersion in the dipoles facing the short and the long sections. By keeping zero dispersion and derivative dispersion at both Interaction Points, the dispersion behaviour in the dipoles near to the Interaction Regions is in fact almost fixed. The range of tunability is wide: measurements with negative momentum compaction of the order of few 10^{-2} have been already done [15]. Lattices with high momentum compaction (near 10^{-1}) have been also designed in view of the strong rf focusing experiment [5]. The lattice can also be tuned to the isochronicity condition straightforwardly. In this situation the maximum dispersion along the ring is of the order of 2 m.

A quasi-isochronous lattice has been defined for two cases: one with the wigglers ON in the arcs on and the other with the wigglers OFF. Figures 8 and 9 refer to the first case and show respectively the betatron functions and the dispersion along the ring, while Figures 10 and 11 refer to the wigglers OFF solution. Table 5 summarizes the main parameters for the two configurations.

The main differences between the two lattices are essentially the damping times, which differ by more than a factor 2, and of course the energy lost per turn. The emittance is almost the same and this has been obtained by decreasing the synchrotron radiation integral I_5 in the wigglers-OFF solution by about a factor of 2, for counteracting the doubling of the synchrotron radiation integral I_2 . The betatron vertical tune is one integer lower in the case of wigglers OFF and in both cases the tunes can be varied in the usual range of ± 0.2 with the short section working point knob. The revolution frequency with wigglers OFF is 1 kHz higher, since the wiggling trajectory is longer by 7 mm per wiggler.

When tuning the lattice into small values of the momentum compaction, particular attention must be put on the energy dependent high order terms of the momentum compaction. For example, special care must be used in minimizing the second order term that directly affects the momentum acceptance of the machine. In DAΦNE the presence of several families of sextupole and octupole magnets should ensure a direct control of the energy dependent terms of the momentum compaction up to the third order.

Table 5: Relevant parameters of the lattices for DAΦNE as a CSR source.

	Wigglers ON	Wigglers OFF
C (m)	97.68	97.66
α_c	$5 \cdot 10^{-4}$	$5 \cdot 10^{-4}$
U₀ (keV)	9.6	4.3
τ_x (msec)	37	85
ϵ_x (mm mrad)	0.26	.33
Q_x	5.16	5.08
Q_y	5.22	4.22

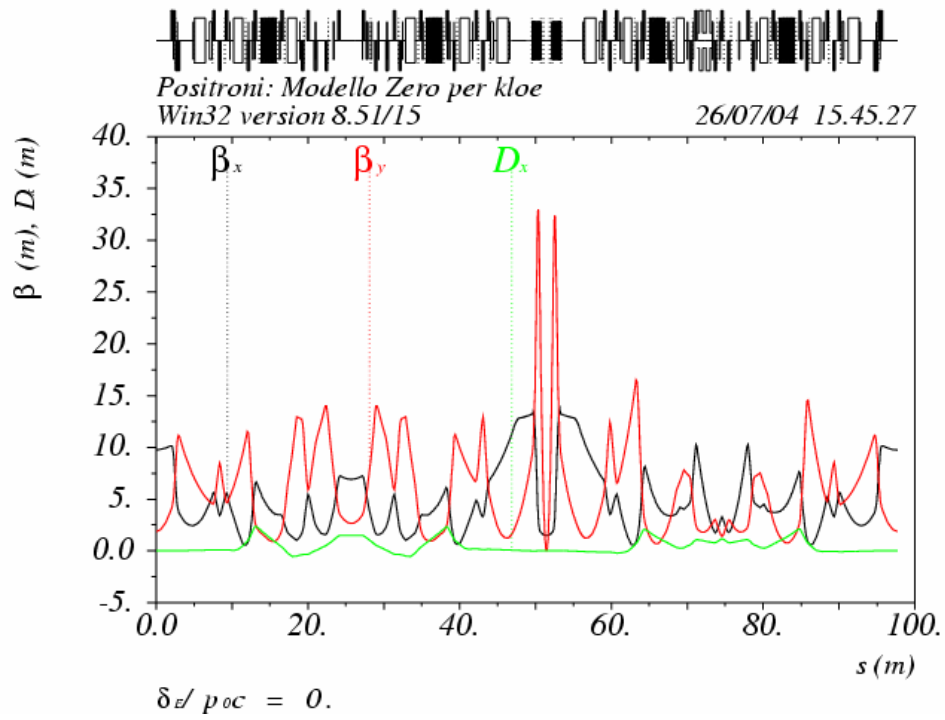


Figure 8: Betatron functions along the ring with wigglers ON.

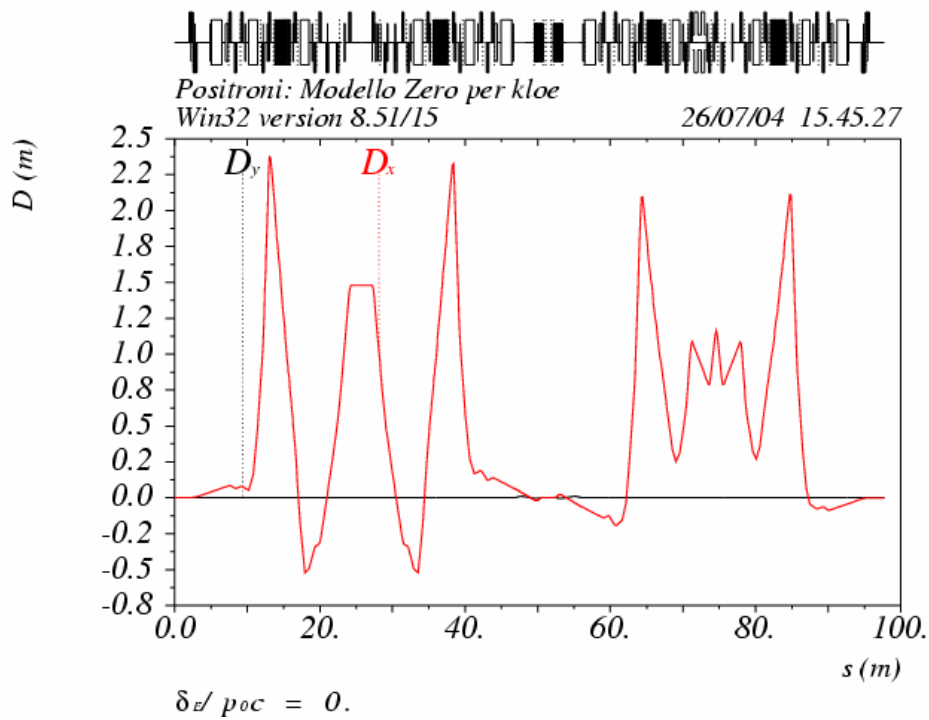


Figure 9: Dispersion function along the ring with wigglers ON.

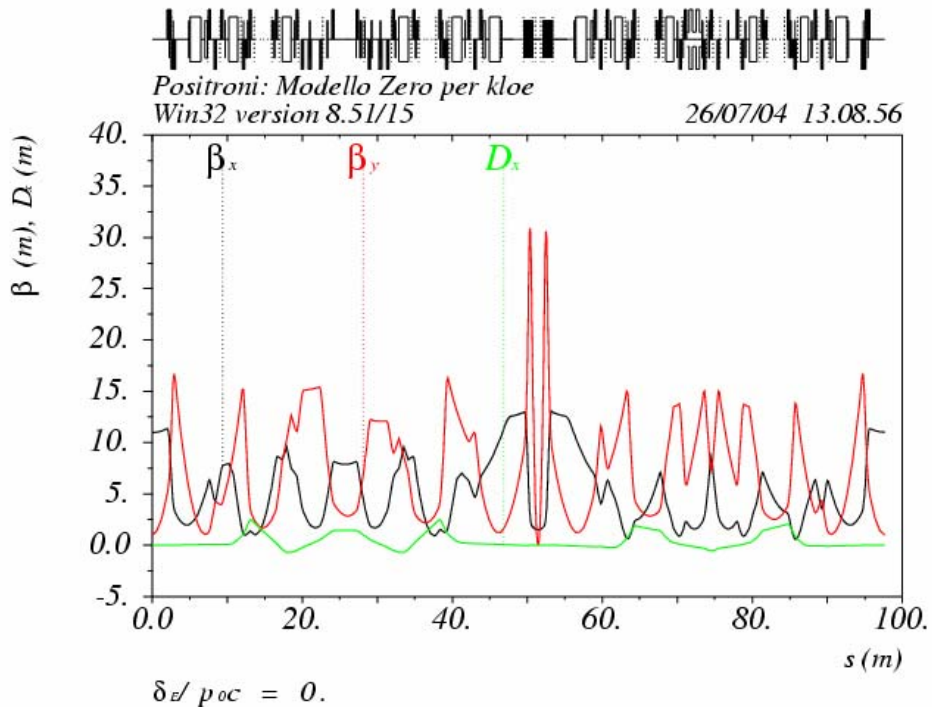


Figure 10: Betatron functions along the ring with wigglers OFF.

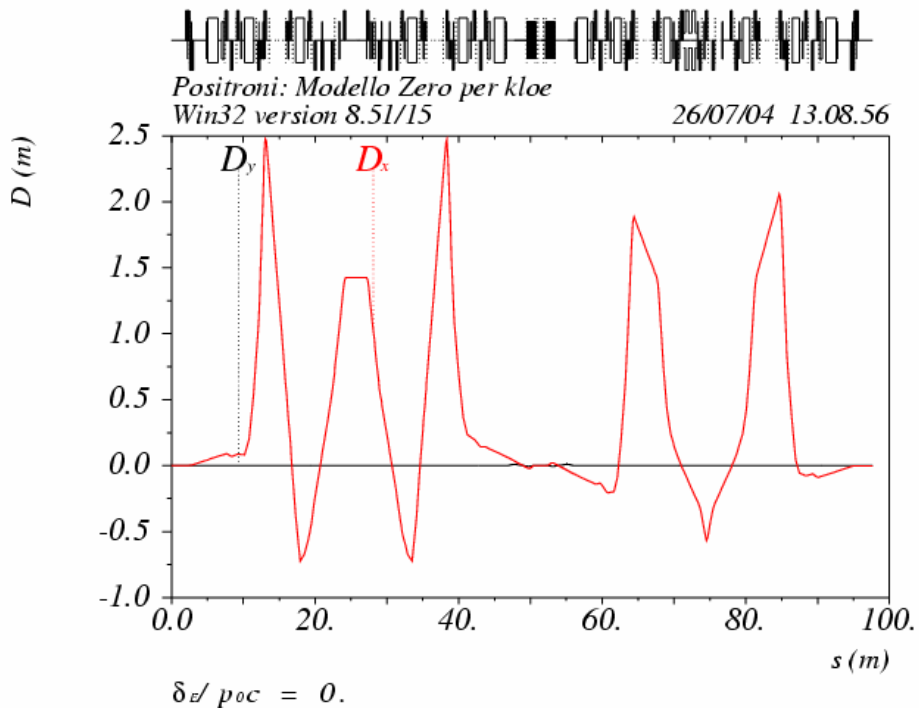


Figure 11: Dispersion function along the ring with wigglers OFF.

2.10.4 Conclusions

The CSR issues associated with DAΦNE have been analysed. The threshold for the MBI has been calculated. The results showed that MBI is not a concern in the present high current collision operation while it could appear at very high current per bunch. Analogously, the MBI could be important in the proposed strong RF focusing scheme, where shorter bunches are foreseen. Experimental characterization of the MBI in DAΦNE, well above the single bunch threshold, will help to better define the question.

Additionally, a detailed analysis of DAΦNE optimized as a powerful source of ultra-stable CSR in the terahertz frequency region has been performed. Two cases, one with the present RF system, the other with the superconductive 1.3 GHz one foreseen in the strong RF focusing scheme, were investigated. The results are very interesting and show the high potentiality of DAΦNE as a CSR source.

2.10.5 References

- [1] G. Vignola, The DAΦNE Project Team, "[DAΦNE: the Frascati Phi-Factory](#)", 1991 Particle Accelerator Conference, San Francisco, May 1991, p. 68.
- [2] A. Nucara, P. Calvani, A. Marcelli and M. Sanchez del Rio, 'The Φ-factory DAΦNE as a source of infrared radiation: An estimate of source size and brilliance', *Rev. Sci. Instr.* **66**, 1934 (1995).
- [3] C. Biscari *et al.*, [Feasibility Study for a Very High Luminosity Phi-factory](#), EPAC04, Lucerne, Switzerland, July 2004.
- [4] A. Gallo, P. Raimondi and M. Zobov, DAΦNE Technical Note G-60, August 18, 2003.
- [5] A. Gallo, *et al.*, "Strong RF focusing experiment at DAΦNE", EPAC04, Lucerne, Switzerland, July 2004.
- [6] M. Venturini and R. Warnock, *Phys. Rev. Letters* **89**, 224802 (2002).
- [7] F. Sannibale *et al.*, *Proc. 2003 IEEE Part. Accel. Conf.*, Portland, OR, 2003, p. 863.
- [8] F. Sannibale *et al.*, this Newsletter and *Phys. Rev. Letters* **93**, 094801 (2004).
- [9] A. Marcelli, *et al.*, *Journal of Synchr. Radiation* **5**, 575 (1998).
- [10] S. Heifets. And G. Stupakov., *Phys. Rev. ST Accel. Beams* **5**, 054402 (2002).
- [11] J. M. Byrd, *et al.* *Phys. Rev. Letters* **89**, 22, 224801 (2002).
- [12] M. Abo-Bakr *et al.*, *Phys. Rev. Letters* **88**, 254801 (2002).
- [13] M. Abo-Bakr *et al.*, *Phys. Rev. Letters* **90**, 094801 (2003).
- [14] J. M. Byrd, *et al.*, "CIRCE the Coherent InfraRed CEnter at the ALS", EPAC04, Lucerne, Switzerland, July 2004.
- [15] M. Biagini, *et al.*, DAΦNE Technical Note BM-15, July 12, 2004.

2.11 Far-Infrared Detectors for Coherent Synchrotron Radiation

H.-W. Hübers, A. Semenov, [DLR](#)
 K. Holldack, U. Schade, G. Wüstefeld, [BESSY](#)
heinz-wilhelm.huebers@dlr.de

2.11.1 Introduction

Coherent synchrotron radiation (CSR) is a novel source of high intensity radiation at THz frequencies. Although CSR was predicted to occur in high energy storage rings

more than 50 years ago [1], it was only recently that steady state CSR has been observed for the first time [2,3]. At BESSY steady state CSR can be generated when the optics of the storage ring is tuned into a dedicated ‘low α ’ mode, where α is the momentum compaction factor. The emission falls into the far-infrared (also called terahertz) portion of the electromagnetic spectrum and covers the band from $\sim 1 \text{ cm}^{-1}$ to 50 cm^{-1} . The minimum separation between two pulses at BESSY is 2 ns and the maximum separation is determined by the revolution frequency (1.25 MHz or 0.8 μs). Another mechanism to generate CSR is slicing of an electron bunch by interaction with the electric field from a femtosecond laser pulse. This yields a spectrum from $\sim 10 \text{ cm}^{-1}$ to 150 cm^{-1} with a pulse length of $\sim 100 \text{ fs}$. The repetition rate is typically $\sim 1 \text{ kHz}$. It is determined by the laser. There are two major applications for CSR. First of all the broadband emission in conjunction with very stable, high average, and high peak power makes CSR an ideal source for FIR Fourier transform spectroscopy (FTS). First applications in FIR imaging as well as superconductor and semiconductor spectroscopy have been demonstrated [4]. The second application is based on the fact that its spectrum depends on the shape of the electron bunch from which the FIR radiation is emitted. The bunch shape can be retrieved from the CSR spectrum by means of FTS [5].

In order to detect and characterize CSR as well as to get the best possible result when using CSR for an user experiment at a beamline the choice of the detector is of prime importance. Four parameters are most important for the assessment of a detector:

- the wavelength range over which it responds,
- the minimum detectable power, usually referred to as the noise equivalent power (NEP),
- the responsivity, measured as a change of voltage or current produced by a change of incident power,
- the response time of the detector.

In the following section the detection mechanism and the detector parameters of several detectors which are currently in use at BESSY will be presented. There exists a large amount of literature about these detectors (see for example [6]). It is beyond the scope of this contribution to give an extensive review on detectors as well as on the literature. Instead the reader will be referred to some review articles where more details and references are given. In the third section some results obtained with these detectors will be highlighted.

2.11.2 Detectors

FIR detectors can be divided into two categories, thermal and photoconductive detectors. In thermal detectors the radiation is absorbed by the detecting element itself or by a dedicated absorbing material (Fig. 1). The absorption of radiation leads to an increase of temperature of either the detector or the absorber. The temperature change results in some change of the electrical properties of the detector or a thermistor, which is coupled to the absorber. This can be read out by an appropriate electrical circuit. The spectral response of thermal detectors depends on its absorbing characteristic that can be made quite uniform throughout the FIR spectral region. However thermal detectors are rather slow because a high sensitivity requires a relatively weak thermal coupling with the heat sink.

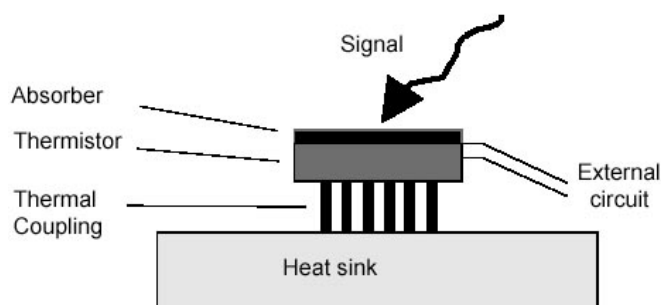


Figure 1: Schematic of a bolometric detector.

The response mechanism of photoconductive detectors is based on the generation of free electrons or holes in a semiconductor that in turn changes the conductivity of the material (Fig. 2). This mechanism depends on the wavelength because photons of certain energy are required but on the other hand photoconductive detectors are usually faster than bolometers. Hot electron semiconductor bolometric detectors are somewhat in between. The incident radiation is absorbed by the charge carriers in the detector which leads to a redistribution of the carriers due to radiative heating. This changes the resistance of the detector (Fig. 2). As for photoconductive detectors the response can be made quite fast.

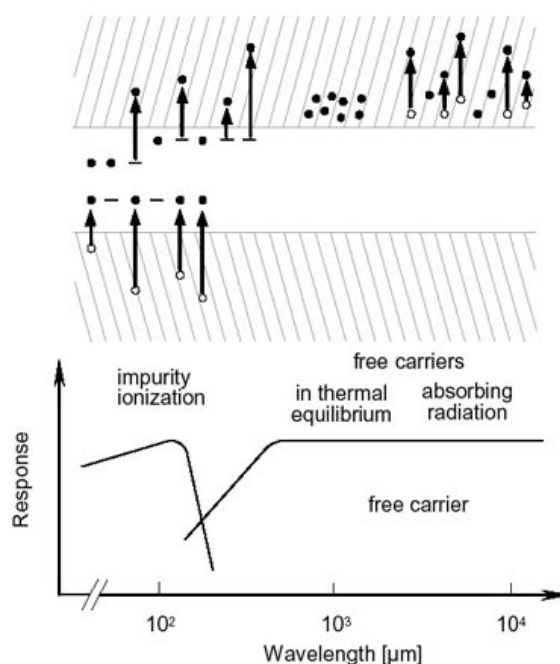


Figure 2: Detection mechanisms of a photoconductive detector (impurity ionization) and an InSb hot electron bolometer (free carrier absorption) (after [6]).

2.11.2.1 Silicon bolometer

A silicon bolometer [7] consists of a doped silicon element, which is connected to a cooled heat sink. When chopped radiation falls onto the element an AC output signal is produced with its amplitude proportional to the change of resistance of the silicon element. The responsivity and the response time depend on the heat capacity and the conduction to the heat sink. A low conduction gives an improved sensitivity but at the expense of a larger response time. Coupling of the radiation to the detector can be

achieved either by direct focussing or by a light-collecting cone (so called Winston cone [8]), which concentrates the radiation on the detector. Appropriate filtering is required in order to reduce background radiation. The typical response time is about 1 ms. The spectral coverage is very broad from $\sim 2 \mu\text{m}$ to $\sim 3 \text{ mm}$ with a NEP of about $1 \times 10^{-13} \text{ W/Hz}^{1/2}$ at a temperature of 4.2 K. This can be even improved by lowering the operating temperature because the noise grows with the square of the detector temperature.

2.11.2.2 *InSb hot electron bolometer*

The detection process is due to the absorption of radiation by electrons in the conduction band [9]. This detector has to be cooled with liquid helium. In thermal equilibrium the electrons are at the bottom of the conduction band. When FIR radiation falls onto the detector the electrons absorb the radiation and their mean temperature, T_{el} , rises above that of the host lattice. Since the electron mobility is proportional to $T_{\text{el}}^{2/3}$ the resistance of the detector increases. The low thermal mass of the electrons and their short relaxation time makes the InSb detector fast (rise time $\sim 200 \text{ ns}$) and sensitive (NEP $< 10^{-12} \text{ W/Hz}^{1/2}$). The detectors spectral response ranges from about $200 \mu\text{m}$ to 5 mm . It is determined by the absorption cross-section of the electrons. The signal is coupled to the detector by a Winston cone. To increase the response the detector is placed in a cavity whose entrance is connected to the output opening of the cone. Due to multiple reflections inside the cavity the absorptivity of the detector is increased.

2.11.2.3 *Superconducting hot electron bolometer*

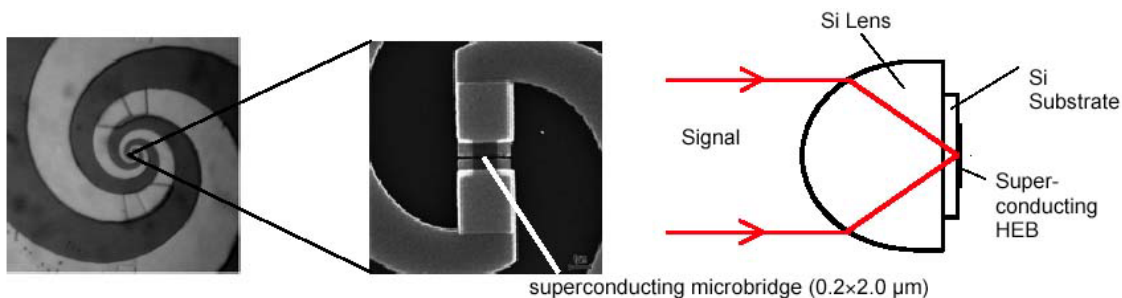


Figure 3: Superconducting NbN HEB: SEM picture of the planar logarithmic-spiral antenna with the superconducting microbridge in the center (left) and complete detector including the lens for coupling of the signal.

In order to realize a bolometric detector with a response time of several ten ps superconducting microbridges made from a thin NbN film turned out to be very useful. This is a relatively new detector [10,11]. The device is operated just below the superconducting transition temperature of the microbridge ($\sim 8 \text{ K}$). The incoming radiation breaks the cooper pairs in the microbridge. The energy released in the electron subsystem is transferred to the phonon subsystem in the bridge. Subsequently the phonons move out of the bridge into the silicon substrate. The typical length of the bridge is $0.2\text{-}0.4 \mu\text{m}$, the width is $2\text{-}4 \mu\text{m}$, and the thickness of the superconducting film is 3.5 nm . NbN has shown to be the best material for phonon cooled hot electron bolometers (HEB) since the time constants involved in the detection process are very small and thin films of good quality can be produced. The process that dominates the speed of the device is the escape of phonons out of the bridge while the electron-phonon

interaction time is comparatively small. The time constant for a NbN hot electron bolometer with a 3.5 nm thick film is ~ 50 ps. In order to couple the FIR radiation to the detector the microbridge is embedded into a planar antenna (Fig. 3). Different designs are possible: Logarithmic-spiral or logarithmic-periodic antennas can be designed to yield an almost frequency independent response throughout the FIR spectral range. Narrow band antennas such as double dipole or double-slot antennas are preferable if the detector should operate at a particular frequency. The detector chip is glued to an extended hemispheric lens. Both the lens and the planar antenna determine the optical coupling of the signal (Fig. 3).

2.11.2.4 Photoconductive detectors

Doping of a semiconductor with an element of the next higher group will produce donor levels while doping with an element from the next lower group will produce acceptor levels. If these levels are close to the conduction band or to the valence band, respectively, the energy of FIR photons is sufficient to free an electron or a hole. These detectors are called extrinsic in contrast to intrinsic detectors where the detection process is due to a direct excitation of electrons from the valence band to the conduction band. When doped with shallow level impurities fast and sensitive detectors are provided. Germanium doped with gallium (Ge:Ga) is widely used as detector material for FIR wavelengths. The detection mechanism is based on a transition from the Ga ground state to the valence band. The long-wavelength cut-off of such a detector is determined by the energy of the ground state, for Ge:Ga ~ 120 μm . This cut-off can be extended to longer wavelengths (~ 240 μm) by applying a compressive force to the crystal. Recently it has been shown that this detector has a significant response at long wavelengths > 500 μm [4]. This is caused by transitions from excited Ga states into the valence band. The NEP depends on the wavelength and can be as low as 10^{-12} - 10^{-13} $\text{W/Hz}^{1/2}$ at 4.2 K. Similar to the InSb detector the signal coupling can be optimized by a Winston cone and an integrating cavity.

2.11.3 Results obtained at BESSY

The CSR spectrum obtained at BESSY ranges from about 1 cm^{-1} to 50 cm^{-1} . This frequency range is covered by the silicon bolometer, the InSb HEB and the superconducting NbN HEB as well. A composite plot of two CSR spectra measured with the NbN and InSb HEBs and a polarizing Fourier transform spectrometer (FTS) or Martin-Puplett spectrometer, as it is called alternatively, is shown in Fig. 4. A sensitive lock-in detection scheme with reference to the revolution frequency of BESSY has been employed. An additional advantage of this detection scheme is that FIR background radiation is not detected, since it is not modulated. The spectrum measured with the InSb detector extends from 4 cm^{-1} to about 35 cm^{-1} with a steep roll-off starting at about 15 cm^{-1} . The lower cut-off is determined by the cut-off of the beamline while the large wavenumber roll-off is due to the decreasing detector responsivity. The NbN HEB detects from about 8 cm^{-1} , which is the low frequency cut-off of the logarithmic-spiral antenna. The spectrum extends beyond 35 cm^{-1} . Compared to the InSb detector the roll-off of the HEB-detector is less steep and is determined by the roll off of the CSR. However, the signal-to-noise ration is somewhat worse due to the lower responsivity of the NbN HEB. The structure in both spectra is due to absorption of radiation by the atmosphere, mainly water. The spectra measured with a silicon bolometer extend to

about the same wavenumber as measured with an NbN HEB but with better signal-to-noise ratio [5].

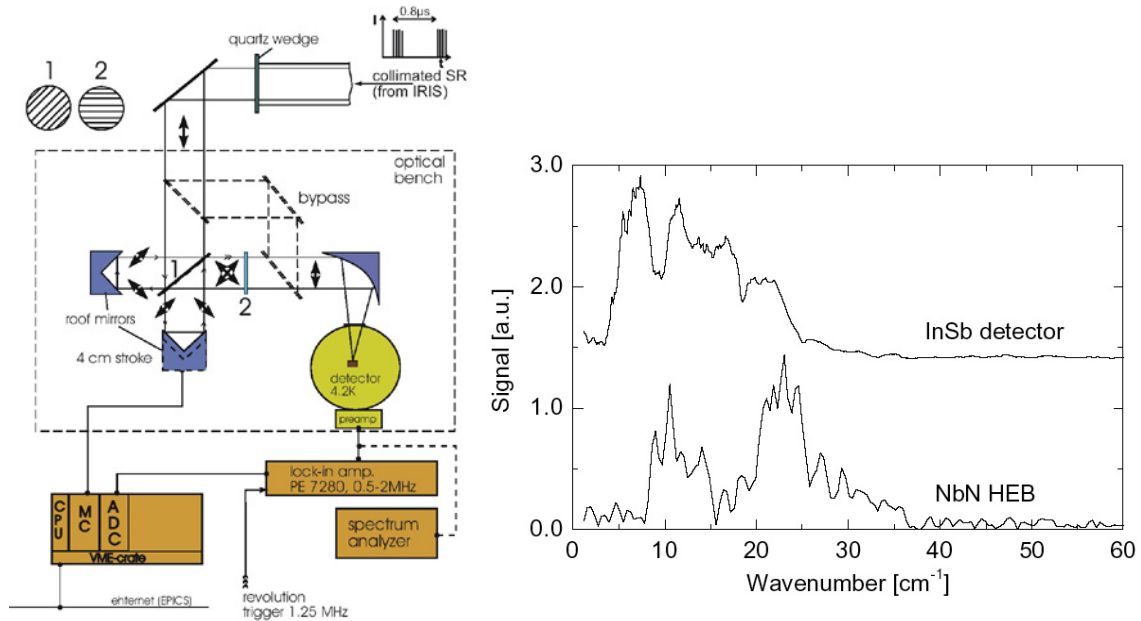


Figure 4: Experimental set-up and CSR spectra measured with different detectors for the same experimental conditions ($I_{\text{Beam}} \approx 40$ mA, $\alpha = 4 \times 10^{-5}$, Martin-Puplett FTS).

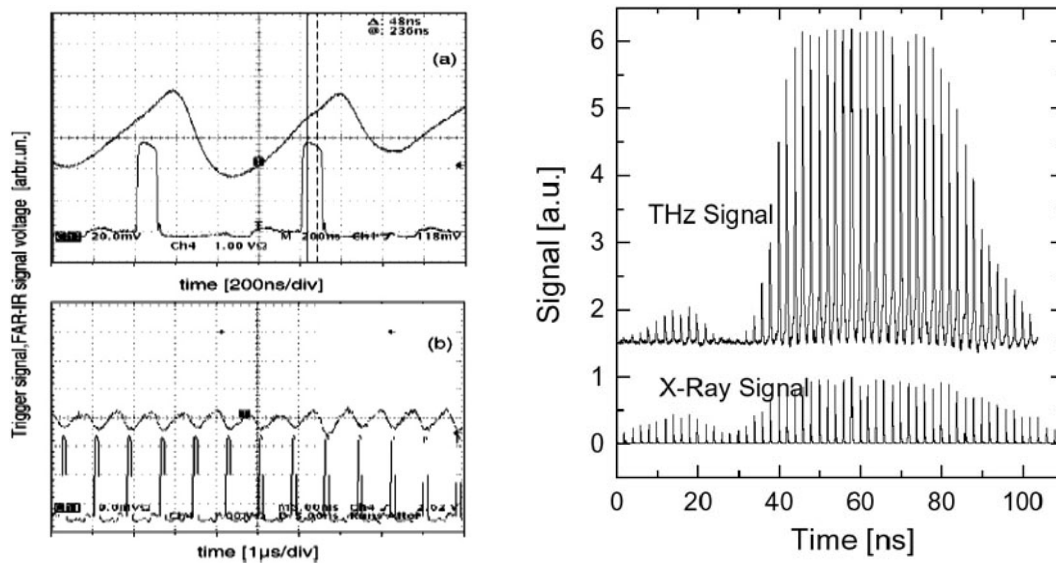


Figure 5: Fill pattern measured with an InSb detector (left, upper trace: InSb signal, lower trace: trigger signal, from [2]) and a superconducting NbN HEB (right, lower trace: x-ray signal measured with APD). Note the different time scales: only the NbN HEB allows to resolve single bunches.

The revolution frequency of the BESSY storage ring is 1.25 MHz and the separation of two subsequent bunches is 2 ns with a bunch length in the order of one to several ps. These times are much shorter than the response time of the silicon bolometer, which can therefore measure only an average value. The InSb detector is fast enough to resolve the revolution of an electron bunch (Fig. 5).

With the superconducting HEB it is possible to separate two subsequent electron bunches. Fig. 5 shows a fill pattern measured with an avalanche photodiode (APD) sensitive at x-ray energies and the same fill pattern measured with the NbN HEB at FIR wavelengths. There is a distinct difference between both patterns. While the first group of bunches has approximately the same shape when measured in the two different spectral regions the second group shows a dramatic power increase at FIR frequencies compared to the x-ray signals. The latter ones are proportional to the number of electrons in the bunch while the FIR signals are proportional to the square number. The emission of a single bunch is displayed in Fig. 6. The pulse is about 1 ns long, much more than expected from the momentum compaction factor of 5.7×10^{-5} which corresponds to a rms pulse length of 1.5 mm or 5 ps. This lengthening can be attributed to multiple reflections at the metal walls of the beamline. The rise time of the signal is 50 ps. It is determined by the NbN HEB and the electronic circuitry.

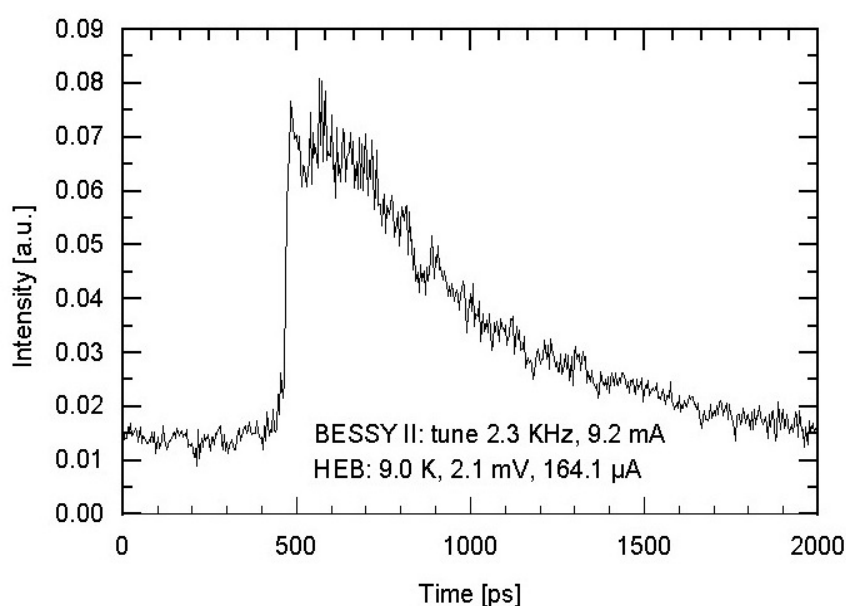


Figure 6: Emission of a single electron bunch measured by a NbN HEB. The length is due to multiple reflections in the beamline.

2.11.4 Conclusion

Several detectors exist which are very well suited for the detection of CSR. Currently no single detector exists which fulfills all requirements set by the characteristics of CSR. Depending on the particular task the optimal one should be chosen. For experiments which require the resolution of single electron bunches a superconducting NbN HEB is the detector of choice. In case a flat spectral response has the highest priority a silicon bolometer as well as a NbN HEB are possible detectors. However, the silicon bolometer provides a higher sensitivity. If the focus is on wavelengths below 25 cm^{-1} the InSb detector is the best choice. The Ge:Ga photoconductive detector might become of importance if one wants to detect CSR from femtoslicing experiments, because it has a sensitivity comparable to a silicon bolometer, a short response time as the InSb detector and the spectral sensitivity corresponds to the emission spectrum of femtoslicing CSR.

2.11.5 References

- [1] J.B. Murphy, this newsletter and references therein.
- [2] M. Abo-Bakr, J. Feikes, K. Holldack, G. Wüstefeld, H.-W. Hübers, “Steady-State Far-Infrared Coherent Synchrotron Radiation Detected at BESSY II”, *Phys. Rev. Lett.* **88**, 254801 (2002).
- [3] M. Abo-Bakr, J. Feikes, K. Holldack, P. Kuske, W.B. Peatman, U. Schade, G. Wüstefeld, H.-W. Hübers, “Brilliant, Coherent Far Infrared (THz) Synchrotron Radiation”, *Phys. Rev. Lett.* **90**, 094801-1 (2003).
- [4] D.N. Basov, J. Feikes, D. Fried, K. Holldack, H.W. Hübers, P. Kuske, M.C. Martin, S.G. Pavlov, U. Schade, E.J. Singley, G. Wüstefeld, “Initial scientific uses of coherent synchrotron radiation in storage rings”, this newsletter and references therein.
- [5] F. Sannibale, J.M. Byrd, A. Loftsdottir, M. Venturini, M. Abo-Bakr, J. Feikes, K. Holldack, P. Kuske, G. Wüstefeld, H.-W. Hübers, R. Warnock, “A Model for Producing Stable, Broadband Terahertz Coherent Synchrotron Radiation in Storage Rings”, *Phys. Rev. Lett.* **93**, 094801 (2004).
- [6] M.F. Kimmitt, “Far-Infrared Techniques”, Pion Ltd., London (1970).
- [7] P.L. Richards, “Bolometers for Infrared and Millimeter Waves”, *J. Appl. Phys.* **76**, 1 (1994).
- [8] D.A. Harper, R.H. Hildebrand, R. Stiening, R. Winston, “Heat Trap: An Optimized Far Infrared Field Optics System”, *Appl. Optics* **15**, 53 (1976).
- [9] E. H. Putley, “InSb submillimeter photoconductive detectors”, in “Semiconductors and Semimetals” **13** (R.K. Willardson and A.C. Beer, eds.), Academic Press, New York, 143, (1977).
- [10] H.-W. Hübers, J. Schubert, A. Semenov, G. Gol’tsman, B. Voronov, G. Gershenson, A. Krabbe, H.P. Röser, “NbN Hot Electron Bolometer as THz Mixer for SOFIA”, *Proc. of the SPIE Conf. on Airborne Astronomy Systems*, SPIE **4014**, 195, Munich (2000).
- [11] A.D. Semenov, H.-W. Hübers, J. Schubert, G.N. Gol’tsman, A.I. Elantiev, B.M. Voronov, E. M. Gershenson, “Design and Performance of the Lattice-Cooled Hot-Electron Terahertz Mixer”, *J. Appl. Phys.* **88**, 6758 (2000).

3 International Linear Collider (ILC)

3.1 Report on the ILC Workshop KEK (Japan) November 2004

S. Guiducci, [INFN-LNF](#)
Susanna.Guiducci@lnf.infn.it

3.1.1 Introduction

The First International Linear Collider (ILC) Workshop was held at KEK (Japan) on 13÷15 November 2004 under the auspices of ICFA and the International Linear Collider Steering Committee (ILCSC). The goal of the Workshop was to facilitate the worldwide formation of an international design team and to initiate the work for the ILC, after the choice of the “cold” Super Conducting (SC) RF technology, made in August 2004 by the International Technology Recommendation Panel (ITRP).

The workshop charge was the following:

- To review the technical issues with SC-LC, develop lists of design elements and decide whether they are:
 1. non-controversial in concept and may only need some optimisation; or
 2. should be considered open to reevaluation, in the conceptual design phase.
- To present the topics the different groups are interested in, and can contribute to the overall design.

At the opening plenary the ITRP recommendations and the status of GDI (Global Design Initiative) formation have been described.

Then a representative of each region: America, Asia, and Europe, has described the activity and plans for the LC.

The work has been divided in 5 Working Groups dedicated to the following items:

- WG1. Overall Design
- WG2. Main linacs
- WG3. Injector
- WG4. Beam Delivery
- WG5. High gradient cavities.

In the closing plenary, after the summary of the working groups, a discussion has been held on the GDI organization.

3.1.2 Opening Plenary

In the introductory talk the recommendations of the ITRP have been reported [1]. The ITRP Report has stated that: “During the past decade, dedicated and successful work by several research groups has demonstrated that a linear collider can be built and reliably operated.” The “wise men” of the ITRP have stressed that they have recommended a technology, not a design: “We expect the final design to be developed by a team drawn from the combined warm and cold linear collider communities, taking full advantage of the experience and expertise of both.” This workshop was the first occasion for the two different communities to meet and start to work together for an unique international project.

A road map has been established toward a Global Design Initiative to produce a Conceptual Design Report (CDR) and a Technical Design Report (TDR) within three years.

A search committee to recruit the GDI Central Team Director has been appointed.

Another committee is evaluating the site offerings for Central Team Host, nine offerings have been received: KEK, LBNL, SLAC, TRIUMF, FNAL, BNL, CORNELL, RAL (2), DESY.

A Memorandum of Understanding will be ratified between the big labs to carry on the work of the ILC design. It is hope to have Director and Central team location chosen at the next ICFA meeting in February.

Representatives of each of the three regions have described the ongoing activity and future plans for the ILC.

In America [2] the major labs have expressed their interest in the ILC R&D activity for the Injector, Main Linacs and Beam Delivery systems. In particular Fermilab is planning to build a test facility for SC cavity modules (SMTF). Two groups of Universities have R&D activity already financed going on different arguments. A preparatory Workshop was held at SLAC in October 2004:

<http://www-project.slac.stanford.edu/ilc/meetings/workshops/US-ILCWorkshop/workshop.html>

In Asia [3] has been organized a working group structure similar to that of this workshop in order to carry on the work. In a meeting at Kolkata (India) ACFA has proposed KEK as host of the ILC Regional and Central Team of GDI and has urged the Japanese Government to fully support the efforts to host the ILC at KEK. KEK is building a test facility for SC cavities with the ambitious goal to build and test high gradient cavities and is planning a final focus test facility at ATF.

Europe [4] has carried out the research on SC cavities within the TESLA collaboration and proved the feasibility of a SC Linac at TTF, the TESLA Test facility.

EU has financed different ILC related activities within CARE (the project to Coordinate the Accelerator Research for Particle Physics in Europe): ELAN, Electron Linear Accelerator Network, and SRF, Joint Research Activity on Superconducting RF. EUROTEV is a design study on global TeV linear collider financed by the EU, it has been proposed before the technology choice and it is dedicated to the items independent on the technology.

3.1.3 WG1 - Overall Design

Many joint sessions with other groups have been held to discuss the general parameters and the global design. The following issues have been discussed [5]:

- Choice of the initial and final stage energies and accelerating gradient.
- Review of the machine parameters and their inter-relationship.
- Conventional facilities for the main linacs and damping rings: tunnel layout.
- Beam dynamics issues, tolerances, and instrumentation.

After a description of the main physics requirements the discussion has been centered on the parameters choice. The competition between the “warm” and “cold” projects has pushed toward a higher luminosity with a critical parameter set; now these parameters need a critical revision with the contribution of both communities.

A parameter task force has been set up in order to try different sets covering potential operation scenarios and to evaluate the risks in achieving the design luminosity:

- Nominal TESLA parameters with larger vertical emittance and less beamstrahlung at $L = 2 \cdot 10^{34} \text{ cm}^{-2}\text{s}^{-1}$.
- Lower bunch charge.
- Larger vertical emittance.
- Lower beam power.
- Different repetition frequency.

The European XFEL project in preparation at DESY, based on a 20 GeV SC linac, has been presented in a joint session with WG2. The beam operation experience at the DESY TESLA Test Facility (TTF) has been also reported. The strong synergy of this project with ILC has been described.

Other sessions were dedicated to the discussion of:

- High gradient issues.
- Common database and simulation tools.
- Single vs. two tunnels configuration and commissioning strategies.

Four working groups have been created with the following objectives:

1. Define Parameter ranges in the next two months.
2. Study construction schedule, commissioning and availability, positron source, tunnel configurations.
3. Simulate Low Emittance Transport, including failure modes.
4. Define requirements and perform R&D on Instrumentation.

3.1.4 WG2 - Main Linacs

The following items have been addressed [6]:

- Synergy with European XFEL (Joint WG1, WG2).
- Beam related topics (Joint WG1, WG2).
- Power sources and Low level RF.
- High Gradient impact (Joint WG1, WG2, WG5).
- Cryomodule, Couplers and Test Facilities (joint WG2, WG5).

The joint session on high gradient (WG1, WG2, WG5) has reached the following conclusions:

There is a flat cost optimum at 35-40 MV/m, therefore there is no significant cost reduction for higher gradient although site choice may impact this. The module at 35 MV/m still needs demonstration. Other optimizations yield small improvements. Regarding the RF frequency it is not clear if an improvement is possible and there is no reason to change.

The conclusion is that the maturity of the cold technology has been demonstrated. It is important to progress with the industrialization and the ILC will profit of the work done for the European XFEL.

Many laboratories have announced their participation to ILC R&D and two of them have plans for large test facilities on superconducting RF: SMTF at FNAL (US) and STF at KEK (Japan).

3.1.5 WG3 – Injector

The WG3 sessions have been dedicated to the following items:

- Polarized electron sources.
- Positron source system.
- Damping ring.
- Bunch compressor.

An overview of the different possible solutions for the positron source, the conventional and the gamma based scheme, has been given. The crucial problems both for the conventional and the undulator-based schemes are the heat and radiation damage on the target and the focusing device (adiabatic matching lens).

The conventional production system (high intensity e^- beam at ~ 6 GeV energy hitting on a target) would be highly desirable but at present a design with the required intensity and repetition rate is not available.

The undulator source should provide the required intensity and repetition rate but needs a more complex scheme and requires that the high energy, high quality e^- beam be ready before starting the positron production.

For the damping ring the following items have been discussed:

- General layout.
- Fast Kickers.
- Instabilities and collective effects.
- Experience with wigglers.

Several possible approaches to the DR design are being considered, circumferences range from 3 km to 17 km. The long linac bunch train (2820 bunches in ~ 1 ms i.e. 300 Km) has to be compressed down to the damping ring length $17 \div 3$ Km with a corresponding bunch distance of $20 \div 3.5$ ns. The kickers rise/fall time has to be smaller than the bunch distance. Therefore more R&D on fast kickers is needed and many laboratories are studying possible solutions. New ideas have been proposed and are under study: use of two crab cavities and a kicker, multifrequency RF deflectors with a CTF3-like injection extraction scheme (see Fig. 1), Fourier series kickers.

The design vertical emittance (2 pm) is smaller than the minimum emittance ever achieved in a storage ring (KEK-ATF 4.5 pm).

Instabilities and collective effects are important due to the high bunch density. We have to learn from experience & limitations at past or existing rings with similar features. More detailed simulations studies & experiments are needed for many of the expected collective phenomena as e-cloud and fast ion instability.

Space charge incoherent tune shift is one of the critical items, since it causes a vertical emittance growth. It was the motivation to increase the DR energy up to 5 GeV in the TESLA design. The good news of the workshop is that the emittance growth is mitigated by the strong radiation damping [8].

The most controversial items are the DR layout (17, 6, 3 Km) and its installation in the linac tunnel (a separate tunnel would be preferable for commissioning and availability). The design choice will be based on: achievable performance from kickers, beam dynamics, operational flexibility and costs. A “To do list” has been prepared with the work to be done in the next 8 months in order to provide the basis for this decision.

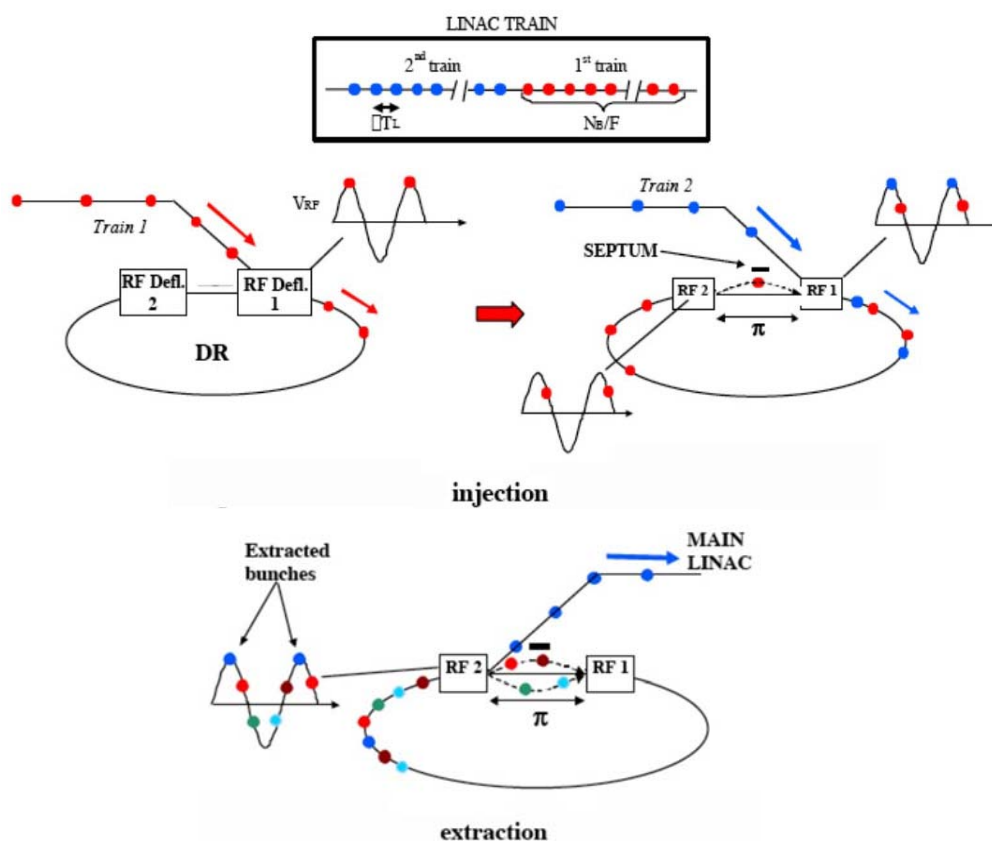


Figure 1: CTF3-like Injection/extraction scheme.

3.1.6 WG4 - Beam Delivery

The following items have been discussed [9]:

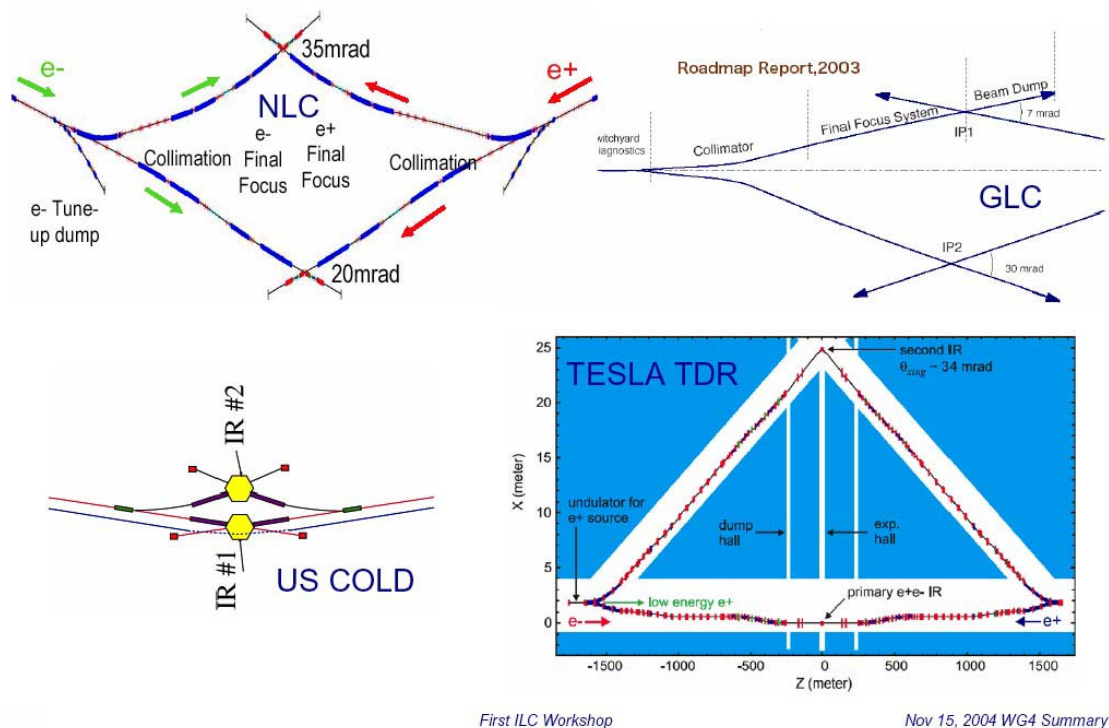
- Collimators & machine protection,
- Final focus, machine detector interface,
- Beam dumps.

For the high energy Beam Delivery (BD) system the proposals from the different design groups (TESLA, NLC, JLC), shown in Fig.2, will be rethought and integrated into a new beam line. In particular it has to be chosen the crossing angle and the layout for two Interaction Regions (IR) in order to get the maximum luminosity for the e^+e^- option and to allow the feasibility of the $\gamma\gamma$ option. A tentative configuration has been agreed on and will be studied in the next months.

Other points under discussion are the choice of the final focus quadrupole doublet (SC or Permanent Magnet) and the position of the positron source undulator (at full energy or at lower energy).

The optimization of IP collision requires a fast feedback to restore vertical position within the first 100 bunches. More work is needed to ensure that the jitter coming from the linac is manageable for tuning of the machine and to verify the stability specifications of all the components.

Many beam tests crucial for risk mitigation on the CDR and TDR time scale are ongoing or have been proposed, in particular at ATF (KEK) and .ESA (End Station A) at SLAC.



First ILC Workshop

Nov 15, 2004 WG4 Summary

Figure 2: Overall BDIR Layout.

Workshops are planned in order to arrive to the Snowmass meeting (August 2005) with a major progress toward detailed design: Workshop on Machine-Detector Interface (January 6-8, SLAC), and Beam Delivery Interaction Region (BDIR) Workshop (June 20-23, Royal Holloway, UK).

Wg4 made significant progress on the working hypotheses for the BDIR configuration. The urgent work needed in the next 8 months and in many cases the people that will do the work, have been identified.

3.1.7 WG5 - High Gradient Cavities

The objective was to discuss the baseline performance of the accelerating cavities and going beyond it [10].

Many issues have been discussed in WG5: basic R&D on surface and materials, fabrication, processing, cost reduction, industrialization, cavity shape, superstructures, gradient, couplers, tuners, cryo-modules, and test facilities.

Electro polished cavities with gradients up to 35 MV/m have been produced and will be tested in the VUV-FEL linac at DESY. A picture of the electro polishing setup at DESY is shown in Fig. 3.

The baseline parameters of the TESLA cavities at 25 MV/m have been accepted. A gradient of 35 MV/m is expected to be achieved with electro polished cavities in time for the TDR. New cavity shapes are being developed for the TDR with the ambitious goal to reach 45 MV/m. It has been stated that industrialization is of critical importance for X-FEL and ILC. Many issues have been addressed by the TESLA collaboration. New activities, financed by XFEL and EC projects (CARE-SRF, EUROFEL), will be of substantial benefit for ILC.



Figure 3: Electro polishing setup at DESY.

3.1.8 Discussion on GDI Organization

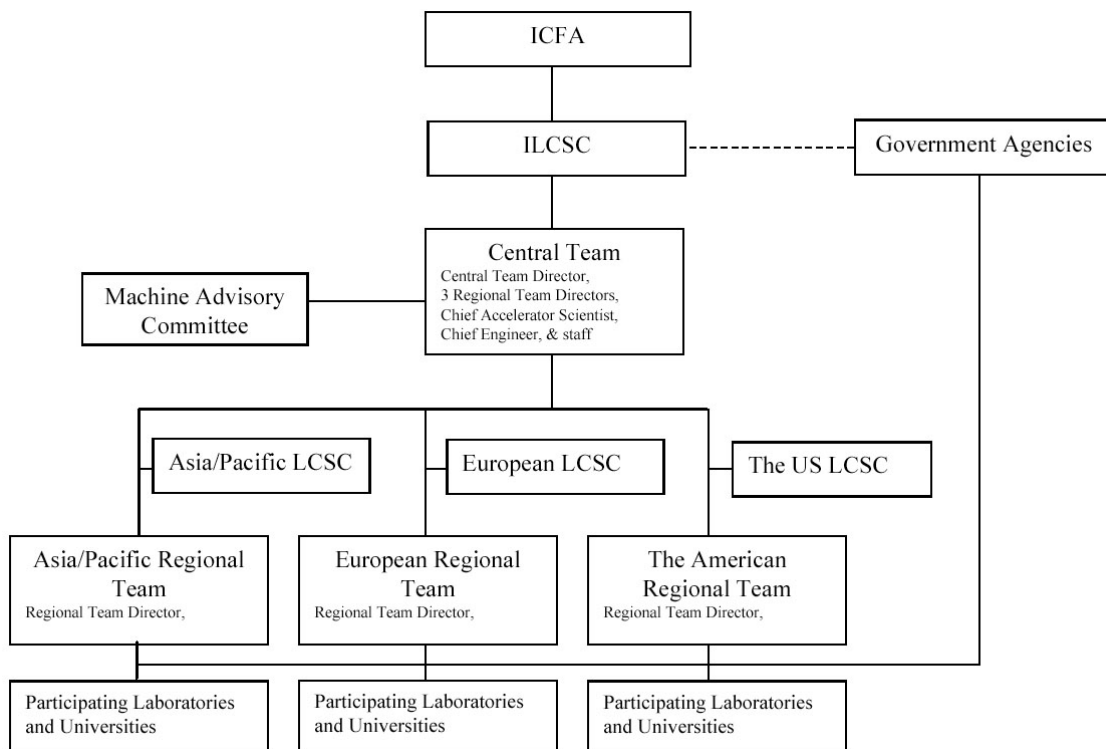


Figure 4: Chart of GDI organization in its early phase.

The ILCSC will initiate the Global Design Initiative; its first mission is to quickly produce a globally agreed upon Conceptual Design Report of the machine and to develop the roadmap for future activities[11]. This Initiative will be established using Memorandum of Understanding among participating institutions and will be supported by their funds.

In the latter phase the organization is expected to metamorphose, as governments will begin to provide additional funding and formal international arrangement. The mission in this phase will be to deliver a Technical Design Report including detailed schedule and cost estimates.

The proposed chart of GDI organization in its early phase is shown in Fig. 4.

A timeline for the ILC with the objective of obtaining the first collisions around 2015 has been proposed: Organize the GDI and complete the CDR in 2005, complete the TDR with cost and schedule plan in 2007 and begin the process for site proposals, be ready for site selection and approval by the governments in 2008.

3.1.9 Conclusion

The workshop was very successful, a lot of preparatory work has been done and all the big labs and many universities have demonstrated their interest in participating to the ILC project. After the technology choice both the warm and cold communities have joined their efforts toward a common design and planned the R&D activity required in the next months.

The information on the Workshop and the transparencies of all the talks can be found at: <http://lcdev.kek.jp/ILCWS/>.

The Working Group structure of the Workshop has been maintained to prepare the Second ILC Workshop (Snowmass ,USA, 14-27 August 2005), with the goal to lead to a Baseline Design Document for the ILC.

3.1.10 References

- [1] M. Tigner, "ITRP Recommendation and status of GDI", <http://lcdev.kek.jp/ILCWS/skd.php>
- [2] G. Dugan, "North America", <http://lcdev.kek.jp/ILCWS/skd.php>
- [3] K. Yokoya, "Asia", <http://lcdev.kek.jp/ILCWS/skd.php>
- [4] B. Foster, "Europe", <http://lcdev.kek.jp/ILCWS/skd.php>
- [5] K. Kubo, D. Schulte, T. Raubenheimer, "WG1 Summary", <http://lcdev.kek.jp/ILCWS/skd.php>
- [6] H. Hayano, T. Garvey, C. Adolphsen, "WG2 Summary", <http://lcdev.kek.jp/ILCWS/skd.php>
- [7] M. Kuriki, S. Guiducci, G. Dugan, "WG3 Summary", <http://lcdev.kek.jp/ILCWS/skd.php>
- [8] K. Oide, "A quick look at the Dogbone damping ring", Contribution, <http://lcdev.kek.jp/ILCWS/WG3.php>
- [9] T. Sanuki, G. Blair, A. Seryi, "WG4 Summary", <http://lcdev.kek.jp/ILCWS/skd.php>
- [10] K. Saito, D. Proch, H. Edwards, "WG5 Summary", <http://lcdev.kek.jp/ILCWS/skd.php>
- [11] S. Ozaki, "Towns meeting on GDI Organization", <http://lcdev.kek.jp/ILCWS/skd.php>

4 Activity Reports

4.1 Beam Physics at the University of Maryland Electron Ring (UMER)

S. Bernal, T. Godlove, I. Haber, J. Harris, R.A. Kishek, B. Quinn, M. Reiser, M. Walter and P.G. O'Shea, [IREAP](#)
mail to: sabern@umd.edu

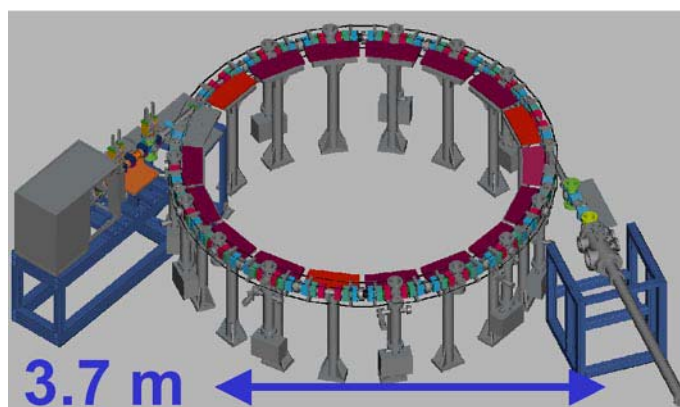
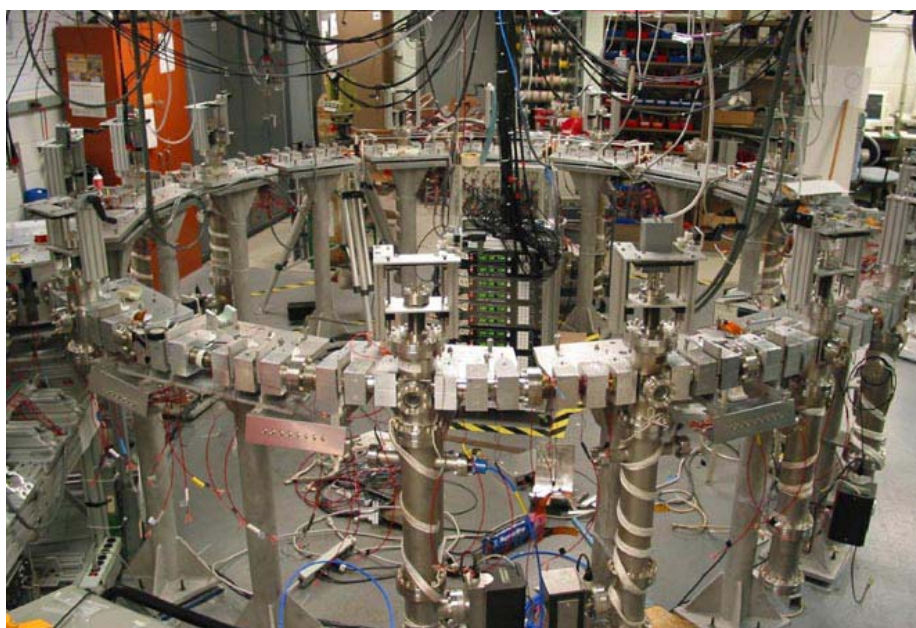


Figure 1: University of Maryland Electron Ring photograph (top) and final future layout (bottom) with extraction section on the right-hand side.

The University of Maryland Electron Ring (UMER) is approaching completion. At the time of writing (Nov. 2004), the ring has been closed (see Figure 1) and tests of pulsed injection are underway. In this article, we review the motivation for UMER and the main results of DC injection experiments over the last three years. We also present a summary of our near and long-term plans for beam physics experiments and upgrades.

Space charge is an important factor for the operation of low-energy sources and matching section/injectors of most accelerators, but becomes less important as the beams are accelerated to relativistic energies. By contrast, UMER is designed to operate as a storage ring of highly space charge dominated beams [1,2]. Nominally, the ring can transport 10 keV, 100 mA electron beams at tune depressions around 0.14 (see Table below); this is a regime of unprecedented intensity, especially for a circular machine. The ring can also operate in the regime of emittance-dominated transport (e.g., 10 keV, 0.6 mA and 0.8 tune depression), which is standard in both linear and circular accelerators. The new regime has potential applications for many areas: from improved FELs, to modeling of ion-beam transport for high-energy density experiments, spallation neutron sources, muon accelerators, galactic dynamics simulations, etc. Other facilities exist for experiments involving or related to space charge dominated beam transport [3,4]. UMER complements such endeavors and also provides a cost-effective alternative for investigating beam physics issues without the complications associated with, for example, ion-beam technology and radiation.

4.1.1 UMER Layout and Beam Parameters

The UMER layout is shown in Fig. 1. The main lattice and beam parameters are summarized in the Table below.

Circumference	11.52 m
Full lattice period	0.32 m
No. of quads / Peak gradient ¹	72 / 7.8 G/cm
No. of dipoles / Nominal field ²	36 / 15 G
Energy	< 10 keV
Current	< 100 mA
Generalized Perveance	< 1.5×10^{-3}
Emittance (norm. rms)	> 2.5 μm
Tune Depression	> 0.12
Pulse Length	50-100 ns
Lap Time	197 ns

¹For nominal $\sigma_0=76^\circ$, zero-current phase advance per period.

²For 10° bend, assuming earth's field compensation.

The UMER lattice consists of 18, 20-degree sections with two FODO units and two main bending dipoles per section. All the magnets in the ring lattice are based on air-core printed circuits [5], with relatively low peak gradients or fields (see Table above) appropriate for the low-energy electrons. Under these conditions, the earth's magnetic field is an important factor to consider. In fact, beam injection is oriented in such a way that the earth's field assists in bending the beam around the ring, but earth's field compensation is necessary over the straight matching section.

Fourteen sections contain diagnostics: a capacitive beam-position monitor (BPM) and a phosphor screen (PS). The schematic of a diagnostics chamber is shown in Fig. 2. The phosphor screen and video system allow us to resolve the beam centroid position to better than 0.1 mm near the center of each ring chamber. This visual diagnostic is also a key component for beam dynamics studies for < 1 turn. The BPMs, on the other hand, provide similar spatial resolution as the PS-video, for all but the lowest current beams, and fast response (~ 1 ns rise time).

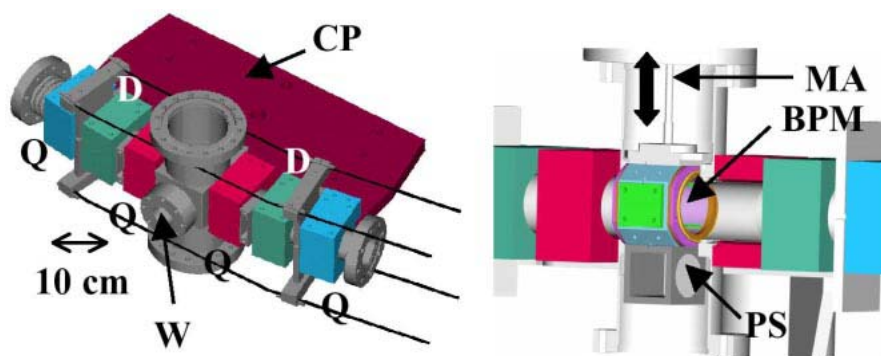


Figure 2: UMER 20° ring section (solid schematic on the left, and cut-out on the right). Q: Quadrupole, D: bending dipole, CP: cluster plate, W: viewing window, MA: mechanical actuator, BPM: beam-position monitor, PS: phosphor screen.

In addition, three sections will house induction modules for longitudinal focusing and acceleration. A movable phosphor screen, pepperpot and slit-wire emittance meters, energy analyser and other diagnostics are available in a large diagnostics tank (DT). The DT has been used at different stages of the project, and will ultimately be installed at the end of an extraction section currently under development. The injection section [6] employs 2 large Panofsky quadrupoles, one of which is a combined function element for focusing and deflection of the beam into the ring lattice on injection and also on the beam's return. An injection magnetic dipole switches polarity in less than the lap time to allow multi-turn operation.

We are also using a drive laser to get photoemission from the dispenser cathode, so that we can create exotic longitudinal and transverse beam shapes to explore the generation and evolution of transverse and longitudinal space charge waves.

Construction of the ring and research has progressed simultaneously. In fact, upgrades of several components, e.g., the lattice magnets, diagnostics and computer control, have been implemented with minimum disruption and cost. We have addressed a number of issues in beam physics and generation and focusing of low-energy electron beams: electron source, focusing and bending magnets, beam matching and control, emittance measurements, quadrupole rotational errors, halo formation, longitudinal dynamics, etc. We describe some of these in more detail below. In addition, the experiments serve to benchmark computer simulation programs like the particle-in-cell (PIC) code WARP [7], which already has been a key tool for the understanding of observed phenomena. Our immediate goals are to demonstrate pulsed injection for multi-turn operation. Up to ten turns of low-current operation is expected within one year and a minimum of 3 turns of the full beam current within an additional year. A future upgrade will entail acceleration to 50 –80 keV and transport over 10 turns or more.

4.1.2 Beam Transport Optimization

Experiments in UMER over <1 turn have employed beam currents from 0.6 mA to 107 mA [8], all at 10 keV and with a nominal zero-current phase advance per period of $\sigma_0=76^\circ$. Work for beam optimization, however, has concentrated on two beams, 7.2 mA and 24 mA, both in the regime of strongly space charge dominated transport. By contrast, the beams in the vicinity of 100 mA (“extreme” space charge) have relatively

large cross sections and make transport optimization more difficult because of image forces. These forces tend to offset an already off-axis beam and can also cause distortions of the beam cross-section. Thus, additional effort for alignment and matching is required in those cases. Figure 3 shows the beam envelopes in one FODO cell of the ring for three beam currents. The beam currents and the edge, unnormalized emittances (in μm) are indicated.

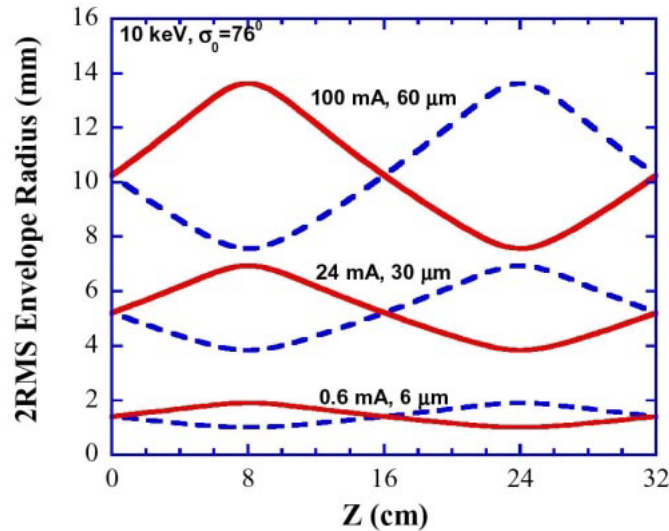


Figure 3: Calculated matched rms envelopes in one FODO period of UMER for $\sigma_0=76^\circ$ (zero-current phase advance per period). For comparison, the vacuum pipe radius is 25.4 mm.

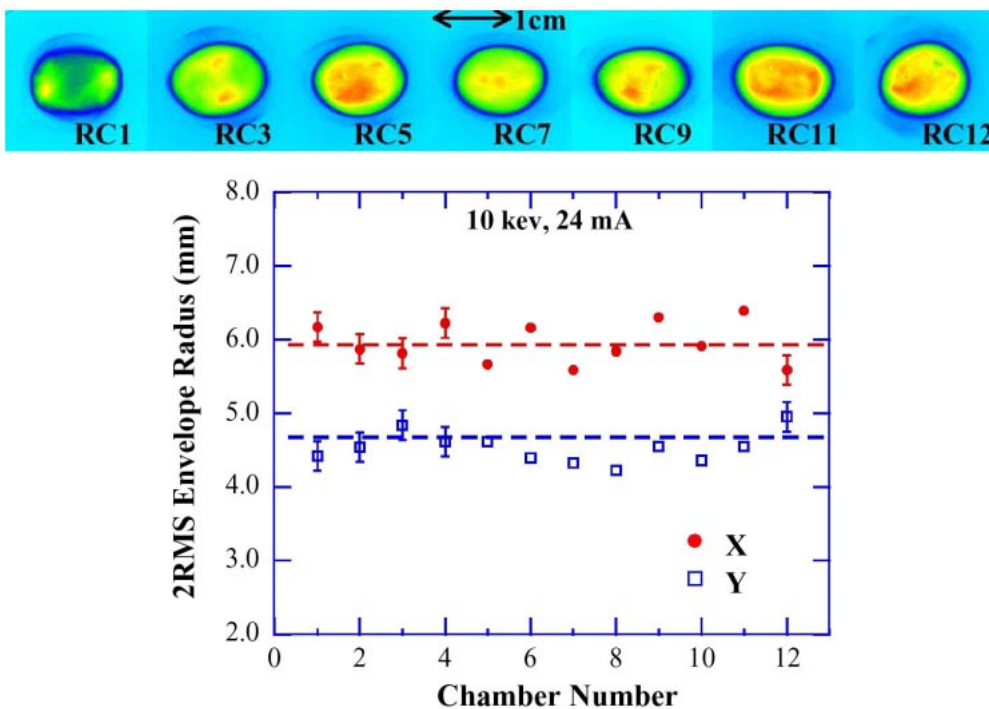


Figure 4: False color rendering of beam pictures at 7 of 12 ring chambers (top), and measured 2rms beam dimensions (X: horizontal, Y: vertical) vs. calculated values represented by dashed lines (bottom). The distance between chambers is 64 cm.

Orbit corrections are established for <1 turn through a combination of beam steering, real-time image processing/analysis and quadrupole and dipole scans [9]. Furthermore, a specially designed quadrupole skew corrector near injection is employed to reduce the beam cross-section tilts induced by mechanical errors and other factors before injection [9]. Initial envelope matching calculations are based on a linear lattice model and the K-V envelope equations [10]. Refined calculations are possible with the PIC code WARP [7], but model errors and uncertainties in the beam initial conditions make necessary to empirically optimize matching [9]. Results of calculations and experiments for a 24 mA, 10 keV beam are shown in Fig. 4. These results correspond to DC injection, i.e., DC operation of all magnets in the ring, including those in the bending section upstream of the periodic lattice.

Beam optimization over <1 turn is underway with the new pulsed injector. Beam steering, skew corrections and empirical matching are being implemented with the new injection geometry. Plans for optimization in the new regime of >1 turn is also under study.

4.1.3 Beam Dynamics

The objects of study of space charge dominated transport are the beam phase-space distribution and its evolution from the source through the injector and over a number of periods of the strong focusing lattice. The phosphor screen diagnostic permits time-integrated observations of the spatial part of the phase-space distribution, while the velocity part (time-integrated also) can be obtained in a coarse way with pepperpot and pinhole masks. Direct measurements of time-integrated transverse phase space are also possible through tomographic techniques, which, however, are best applied self-consistently to emittance-dominated beams [11]. When the information from experiments is complemented with PIC simulations, a picture emerges for a model of the initial particle distribution. Such studies have proven useful for detailed understanding of the beam dynamics over the length, approximately 1-m, of the matching/injection section in UMER [12,13]. The extension of these simulations to longer transport distances provides at least a plausible prediction of beam stability.

The general picture of space charge dominated beam transport consists of a coasting non-neutral collisionless plasma confined transversely by an approximately harmonic potential. Thus, any initial perturbation or modulation of the particle distribution persists for at least one plasma wavelength, of the order of 1-m for the nominal UMER beam parameters. This “beam memory” is observed in UMER, where beam modulation by grids in the electron gun is visible at least over the length of the matching section. Other beam perturbations near the source (e.g., apertures) and/or mismatch may lead to additional phenomena like transverse space charge waves, now under investigation.

Halo formation, as seen in the beam pictures of Fig. 4 is also of major interest because of practical as well as fundamental reasons [14]. Although mismatch oscillations, suggested by the plot at the bottom of Fig. 4, are likely connected to the appearance of halos, other factors like quadrupole rotational errors, the electron source and others are being considered [15]. The results of pepperpot emittance measurements for the 24 mA (10 keV and $\sigma_0=76^0$) are the following:

- 4rms, unnormalized emittance near source: $\varepsilon_{x,y} = 30 \pm 5 \text{ } \mu\text{m}$.
- Horizontal emittance $\varepsilon_x = 30 \pm 5 \text{ } \mu\text{m}$; vertical emittance $\varepsilon_y = 36 \pm 5 \text{ } \mu\text{m}$ after μturn .

- Horizontal emittance $\varepsilon_x = 42 \pm 5 \mu\text{m}$; vertical emittance $\varepsilon_y = 28 \pm 5 \mu\text{m}$ after 1/4 turn.
- Horizontal emittance $\varepsilon_x = 33 \pm 5 \mu\text{m}$; vertical emittance $\varepsilon_y = 51 \pm 5 \mu\text{m}$ after 1/2 turn.

The tune depression for this experiment is 0.3, i.e., highly space charge dominated transport. The measurements reveal no serious beam degradation, but coupling of the transverse dynamics is evident.

4.1.4 Future Work

Some of the areas for near term development in UMER are:

- Optimized beam transport of an emittance dominated beam (“zero-current”) over <1 turn with pulsed injection.
- Steering algorithms for multi-turn operation and tests with zero-current.
- Multi-turn operation with 7.2, 24 mA beams.
- Detailed halo studies.
- Transport with highly asymmetric focusing, i.e., $\sigma_{0x} \neq \sigma_{0y}$, beyond the correction for focusing from the bending dipoles.

Long-term studies and upgrades will include:

- Multi-turn operation with beams near the space charge limit (100 mA beams).
- Evolution of density perturbations and transverse space-charge waves.
- Longitudinal dynamics: energy spread, longitudinal space charge waves.
- Longitudinal dynamics: bunch capture/shaping.
- Acceleration and resonance traversal.

4.1.5 Acknowledgements

We acknowledge the contributions from former members of the UMER team: H. Li, Y. Zou, C. Yui and Y.Huo. The University of Maryland electron ring project is supported by the U.S. Department of Energy.

4.1.6 References

- [1] P.G. O’Shea, M. Reiser, R.A. Kishek *et al.*, Nucl. Instrum. Methods Phys. Res. A **464**, 646 (2001).
- [2] P.G. O’Shea, R.A. Kishek, M. Reiser *et al.*, Laser Part. Beams **20**, 599 (2002).
- [3] P.A. Seidl, D. Baca, F. M. Bieniosek *et al.*, “The high current transport experiment for heavy ion inertial fusion,” PAC 03.
- [4] E.P. Gilson, R.C. Davidson, P.C. Efthimion, R. Majeski, and H. Qin, “Recent results from the Paul trap simulator experiment,” PAC03.
- [5] W.W. Zhang, S. Bernal, H. Li *et al.*, Phys. Rev. ST Accel. Beams **3**, 122401 (2000).
- [6] M. Walter *et al.*, Proc. of the 2004 Symposium on Heavy-Ion Fusion (submitted to Nucl. Instrum. Methods Phys. Res. A).
- [7] A. Friedman, D.P. Grote, and I. Haber, Phys. Fluids B **4**, 2203 (1992).
- [8] S. Bernal, H. Li, T. Godlove *et al.*, Phys. Plasmas **11**, 2907 (2004).
- [9] H. Li *et al.*, Proc. of the 2004 Symposium on Heavy-Ion Fusion (submitted to Nucl. Instrum. Methods Phys. Res. A).
- [10] M. Reiser, *Theory and Design of Charged-Particle Beams*, (Wiley, New York, 1994).

- [11] H. Li, Ph.D. Dissertation, Department of Electrical Engineering, University of Maryland (2004).
- [12] I. Haber *et al.*, Proc. of the 2004 Symposium on Heavy-Ion Fusion (submitted to Nucl. Instrum. Methods Phys. Res. A).
- [13] R.A. Kishek *et al.*, Phys. Plasmas **10**, 2016 (2003).
- [14] *Proceedings of the 29th ICFA Advanced Beam Dynamics Workshop on Beam Halo Dynamics, Diagnostics, and Collimation*, Montauk, NY, May 2003, edited by J. Wei, W. Fischer, and P. Manning (AIP, New York, 2003).
- [15] R.A. Kishek *et al.*, Ref. [13] p.89.

4.2 SESAME

M. Attal, S. Varnasseri, [SESAME](#)

m.attal@unesco.org.jo, s.varnasseri@unesco.org.jo

4.2.1 Introduction

SESAME is a third generation light source, developed under the auspices of UNESCO. It will provide synchrotron radiation for the users community of the Middle East region and will be located in Allan, Jordan. SESAME has gone through an evolution process ranging from the reinstallation, in the Middle East, of Bessy I to the final version based on a 2.5 GeV storage ring. (See also the official web site: www.sesame.org.jo).

The storage ring is composed of 8 super periods with 2 straight sections of different length, 4.4 m and 2.0 m for each. The machine main parameters are listed in Table 1.

Table 1: SESAME Main parameters.

Energy (GeV)	2.5
C (m)	129
B_0 (T)	1.455
Gradient (T/m)	-2.794
Q_x, Q_z	7.23, 5.19
ε (nm.rad)	26
ξ_x, ξ_z	-14.64, -14.81
U_0 (keV/turn)	589.7
τ_s, τ_x, τ_z (ms)	2.71, 2.21, 3.65
Quadrupoles	64 (2 families)
Sextupoles	64 (2 families)
RF freq. (MHz)	499.654
Design current (mA)	400

4.2.2 Transverse Beam Dynamics

Due to the symmetric optics and the accurately chosen working point, two families of sextupoles were enough to have high transverse beam stability (see Fig. 1). Correcting the chromaticity to +2 in both planes didn't reduce the dynamic aperture drastically.

The tune shift with energy deviation ($\pm 6\%$) (see Fig. 2) together with the shown ideal off-momentum and on-momentum dynamic apertures indicate an acceptable particle stability and enough momentum aperture leading to a good beam lifetime, however the momentum aperture will be limited by the RF acceptance ($\pm 1.4\%$).

The impact of high order multipoles on the beam stability is in progress and we do expect high tolerance.

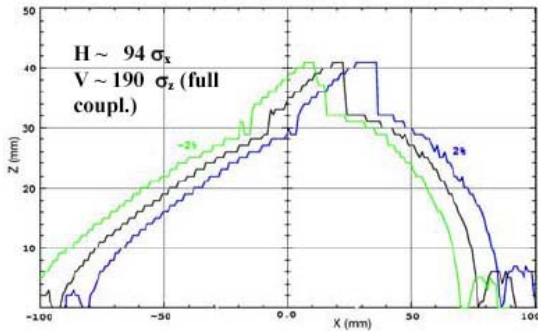


Figure 1

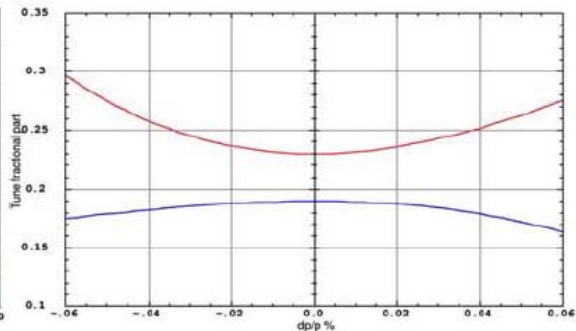


Figure 2

4.2.3 Longitudinal Beam Dynamics and Instabilities

The instabilities caused by the vacuum chamber components and the RF cavities put a limitation on the circulating beam current and deteriorate the beam quality, which made it a crucial point need to be investigated. Evaluating the longitudinal instability took the priority in our investigation while the study of the transverse part has to be completed.

In general there are two types of instabilities: Single bunch instability (SBI) and multi bunch instability (MBI). SBI is strongly influenced by short-range wake fields arising from small structures in the vacuum chamber such as bellows, discontinuities, vacuum ports, BPMs, etc. MBI are strongly influenced by long-range wake fields. The most important mechanism that gives rise to such wake fields is the excitation of HOMs in resonant structures, mainly the RF cavities.

4.2.4 The Vacuum Chamber Impedance

As a key point to know the longitudinal instability limits is to estimate the longitudinal impedance of the chamber and its components. A preliminary estimation has been done using known analytical formulas and the code GdFidl.

The vacuum chamber was approximated to an ellipse in order to calculate the resistive wall impedance using the formulas. The surface roughness of the vacuum chamber has not been taken into account.

The slot and the antechamber were expected to have negligible impedance effect. A taper structure is a frequently used structure to transfer the normal chamber section to insertion device. This structure is composed of step-in taper followed by straight section with smaller vertical aperture followed by a step-out taper to go back to the normal vertical aperture again.

The geometric impedance of this structure has been calculated using GdFidl while the resistive wall one has been estimated using the formulas approximating the taper step as consecutive small steps of different constant gaps.

The BPM impedance was estimated to be small, but due to the large number of BPMs their total impedance had to be taken into account.

Another components like bellows, valves and flanges are expected to be RF shielded and hence their impedance effect was neglected.

Table 2 displays the estimated longitudinal impedance of the chamber components at 2.5GeV, for 11mm bunch length.

Table 2

$ Z_l / n $ (Ohm)	Bare machine C=129m	1 in-vac.Und L=1 m	1 ID L=3m	Machine with 1 in- vac Und. & 10 IDs
RW	0.103	0.012	0.0077	0.192
32 BPMs				0.0015
Total				0.1935

The threshold bunch current for microwave instability was calculated to be 174.85mA and it is not a problem.

4.2.5 Longitudinal Coupled Bunch Instability

In general the interaction of the beam with the wakefields leads to both an amplitude growth and a frequency shift of the longitudinal beam oscillations.

We have carried out the calculation for growth time and threshold current of SESAME from the point of view of cavity HOMs (we assume to use **Elettra type Cavities**), assuming the worst case scenario, that means 100% coupling.

Growth rate for each single HOM with the nominal current of 400 mA and a fixed synchrotron frequency of 38.35 kHz for different energies from injection energy of 800 MeV to 2.5 GeV has been given in Fig. 3.

As the Fig. 3 shows, the natural damping time (continues curve) of SESAME is far greater than the growth time of HOM instability. The worst-case instability is predicted for the frequencies of 947.16 MHz and 2122.36 MHz. Instability for the best case is expected to be for 1874.88 MHz.

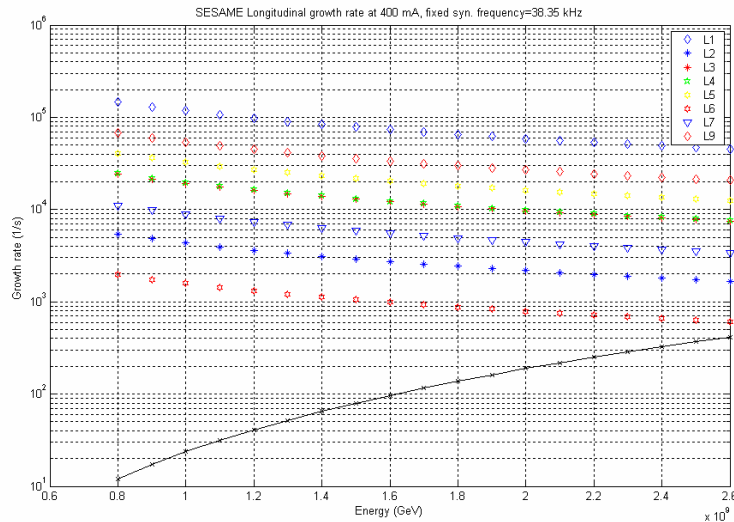


Figure 3: Growth rate (1/s) versus energy for the cavity HOMs

Also the threshold current for the longitudinal coupled bunch instability for a range of energy from injection energy of 800 MeV to 2.5 GeV has been given in Fig. 4.

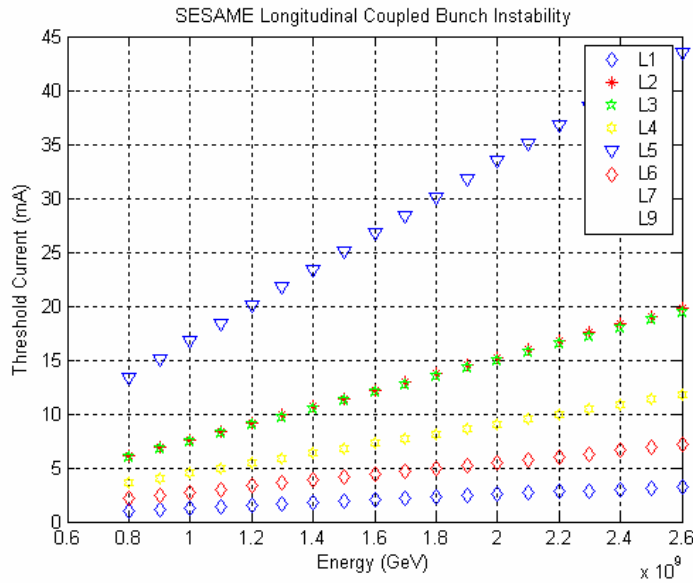


Figure 4: Threshold current due to HOMs versus energy

Figure 4 shows the threshold current for different HOMs and ramping energy from 800 MeV to 2.5 GeV. The best case for instability is for the frequencies of 1947.06 MHz and 2122.36 MHz. The minimum threshold current is for 947.16 MHz with a current of 1.5 mA in the injection and 3.5 mA for 2.5 GeV.

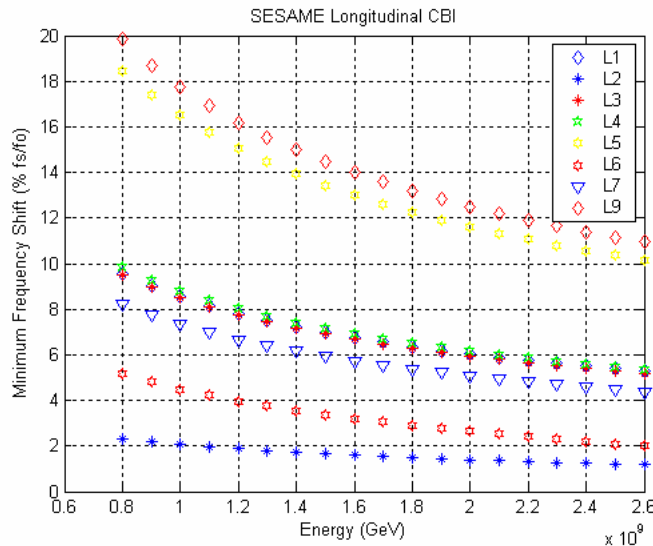


Figure 5: Minimum related frequency shift versus energy

In case of using the frequency shift, the minimum frequency shift which is needed to stabilize the coupled bunch instability created by the HOM is given in Fig. 5 for each single HOM. Again in the frequency of 2122 MHz we need the maximum frequency shift, to stabilize the LCBI.

5 Recent Doctoral Theses

Author: Arvind Kumar (Arvind.Kumar@cern.ch)
 Institution: [CAT](#) - Centre for Advanced Technology, Indore, India
 Title: Novel RF Structures For High-Brightness Photoinjectors and Linear Accelerators
 Thesis defence date: August 2004
 Supervisor: Srinivas Krishnagopal (skrishna@cat.ernet.in)

Abstract

This dissertation elucidates the design, simulation, construction, characterization and high-power tests of a Plane-Wave Transformer (PWT) linac. This is an S-band, 4-cell structure designed to resonate at 2856 MHz in the π mode. The only operating PWT linac in the world is at UCLA. The PWT linac overcomes many of the short-comings of conventional linacs and provides high acceleration field, high electrical efficiency, relaxed fabrication tolerances, broad bandwidth, large inter-cell coupling and favourable electrical properties like quality factor, and shunt impedance. We discuss the principal properties of the PWT linac and explain in detail the electrical design, beam dynamics, wake-field analysis, fabrication, cold-tests and commissioning at high power of the PWT linac*.

The design, simulations, construction and characterization of a photocathode rf gun is also presented. The rf photoinjector discussed here is the BNL/SLAC/UCLA 1.625 cells photocathode rf gun with an emittance compensation solenoid magnet. It is an S-band structure, designed to resonate at 2856 MHz in the π mode. Our simulations show that the photocathode rf gun can generate 1 nC, 10 ps electron beam pulses with a transverse emittance $< 2\pi$ mm-mrad. We present the rf and beam dynamics design, wake field analysis, fabrication and cold tests of the photocathode rf gun. We have also studied a split rf photoinjector which consists of a photocathode rf gun followed by a booster (PWT) linac.

An alternative to the split rf photoinjector is an integrated PWT photoinjector, which combines the properties of photocathode rf gun and PWT linac. We have studied this structure through simulations and predicted that an emittance of $< 2\pi$ mm-mrad can be achieved in a 4-cell integrated PWT photoinjector for a 1 nC, 10 ps electron beam pulse accelerated at 105 MV/m field gradient. We present the electromagnetic design, wake field study and beam dynamics of this structure and compare its performance with the split rf photoinjector. This structure is favourable in terms of ease of construction and operation. This structure provides a high quality electron beam with high energy at lower field gradient in comparison to the split photoinjector.

*Subsequent to the submission of this thesis, beam was accelerated to 3.5 MeV in this 4-cell structure.

6 Forthcoming Beam Dynamics Events

6.1 32nd Advanced ICFA Beam Dynamics Workshop on Energy Recovering Linacs, “ERL2005”

March 19-23, 2005
Jefferson Laboratory

The 32nd ICFA Advanced Beam Dynamics Workshop on Energy Recovering Linacs “ERL2005” will be held at Jefferson Laboratory, Virginia, USA, March 19-23, 2005.

This workshop is sponsored by the ICFA Panel on Beam Dynamics, Jefferson Laboratory, Brookhaven National Laboratory, Cornell University and Daresbury Laboratory. It will address issues related to the generation of high brightness and simultaneously high average current electron beam, and its stability and quality preservation during acceleration and energy recovery. Specifically, the workshop will focus on:

- Design and development of high-average current, low emittance polarized and unpolarized photoinjectors
- Optimized lattice design and longitudinal gymnastics
- Beam stability and multibunch, multipass instabilities
- Beam halo formation and control of beam loss
- Superconducting rf optimization for cw, high-current applications
- Higher order mode damping and efficient extraction of higher order mode power
- RF control and stability under the maximum practical Q_L
- Synchronization issues
- High current diagnostic and instrumentation techniques.

The program consists of an opening and a closing plenary session and four parallel Working Group sessions with the following topics and conveners:

1. Electron guns and injector designs - Ivan Bazarov, Ilan Ben-Zvi
2. Optics and Beam transport - Georg Hoffstaetter, Vladimir Litvinenko, Hywel Owen
3. Superconducting RF and RF control - Jens Knobloch, Matthias Liepe, Mike Dykes
4. Synchronization and Diagnostics/Instrumentation – Bill Graves, Graeme Hirst, Holger Schlarb.

The deadline for advanced registration is February 15, 2005. We are now encouraging the submission of contributed papers for the Working Group sessions. Proceedings will be published for both invited and contributed papers. For further information and registration, please visit:

<http://www.jlab.org/intralab/calendar/archive04/erl/index.html>

Swapn Chattopadhyay (swapan@jlab.org) and Lia Merminga (merringa@jlab.org)

International Advisory Committee

I. Ben-Zvi, BNL
 J. Bisognano, SRC
 C. Bocchetta, Sincrotrone Trieste
 S. Chattopadhyay (Chair), JLAB
 M. E. Couprie, Univ. Paris-Sud
 D. Dowell, SLAC
 K.-J. Kim, ANL
 G. Kulipanov, BINP
 E. Minehara, JAERI
 D. Moncton, MIT
 M. Poole, CLRC Daresbury Lab
 T. Smith, Stanford University
 M. Tigner, Cornell University
 K. Yokoya, KEK
 Members of the ICFA Beam Dynamics Panel

International Program Committee

M. Borland, ANL
 J. Corlett, LBNL
 D. Douglas, JLAB
 M. Dykes, Daresbury Lab
 W. Graves, MIT
 R. Hajima, JAERI
 G. Hoffstaetter, Cornell University
 J. Knobloch, BESSY
 G. Krafft, JLAB
 V. Litvinenko, BNL
 L. Merminga (Chair), JLAB
 A. Mosnier, CEA
 G. Neil, JLAB
 H. Padamsee, Cornell University
 L. Palumbo, INFN/Univ. Roma
 S. Schreiber, DESY
 J. Sekutowicz, DESY
 S. Simrock, DESY
 C. Sinclair, Cornell University
 S. Smith, Daresbury Lab
 T. Suwada, KEK
 Z. Zhao, Shanghai Institute of Applied Physics

Local Organizing Committee

I. Ben-Zvi, BNL
 S. Chattopadhyay, JLAB
 G. Krafft, JLAB
 L. Merminga, JLAB
 M. Poole, CLRC Daresbury Lab
 C. Sinclair, Cornell University

7 Announcements of the Beam Dynamics Panel

7.1 ICFA Beam Dynamics Newsletter

7.1.1 Aim of the Newsletter

The ICFA Beam Dynamics Newsletter is intended as a channel for describing unsolved problems and highlighting important ongoing works, and not as a substitute for journal articles and conference proceedings that usually describe completed work. It is published by the ICFA Beam Dynamics Panel, one of whose missions is to encourage international collaboration in beam dynamics.

Normally it is published every April, August and December. The deadlines are 15 March, 15 July and 15 November, respectively.

7.1.2 Categories of Articles

The categories of articles in the newsletter are the following:

1. Announcements from the panel.
2. Reports of Beam Dynamics Activity of a group.
3. Reports on workshops, meetings and other events related to Beam Dynamics.
4. Announcements of future Beam Dynamics-related international workshops and meetings.
5. Those who want to use newsletter to announce their workshops are welcome to do so. Articles should typically fit within half a page and include descriptions of the subject, date, place, Web site and other contact information
6. Review of Beam Dynamics Problems: this is a place to bring attention to unsolved problems and should not be used to report completed work. Clear and short highlights on the problem are encouraged.
7. Letters to the editor: a forum open to everyone. Anybody can express his/her opinion on the beam dynamics and related activities, by sending it to one of the editors. The editors reserve the right to reject contributions they judge to be inappropriate, although they have rarely had cause to do so.
8. Editorial.

The editors may request an article following a recommendation by panel members. However anyone who wishes to submit an article is strongly encouraged to contact any Beam Dynamics Panel member before starting to write.

7.1.3 How to Prepare a Manuscript

Before starting to write, authors should download the template in Microsoft Word format from the Beam Dynamics Panel web site:

<http://www-bd.fnal.gov/icfabd/news.html>

It will be much easier to guarantee acceptance of the article if the template is used and the instructions included in it are respected. The template and instructions are expected to evolve with time so please make sure always to use the latest versions.

The final Microsoft Word file should be sent to one of the editors, preferably the issue editor, by email.

The editors regret that LaTeX files can no longer be accepted: a majority of contributors now prefer Word and we simply do not have the resources to make the conversions that would be needed. Contributions received in LaTeX will now be returned to the authors for re-formatting.

In cases where an article is composed entirely of straightforward prose (no equations, figures, tables, special symbols, etc.) contributions received in the form of plain text files may be accepted at the discretion of the issue editor

Each article should include the title, authors' names, affiliations and e-mail addresses.

7.1.4 Distribution

A complete archive of issues of this newsletter from 1995 to the latest issue is available at

<http://icfa-usa.jlab.org/archive/newsletter.shtml>

This is now intended as the primary method of distribution of the newsletter.

Readers are encouraged to sign-up for to electronic mailing list to ensure that they will hear immediately when a new issue is published.

The Panel's Web site provides access to the Newsletters, information about Future and Past Workshops, and other information useful to accelerator physicists. There are links to pages of information of local interest for each of the three ICFA areas.

Printed copies of the ICFA Beam Dynamics Newsletters are also distributed (generally some time after the Web edition appears) through the following distributors:

Weiren Chou	chou@fnal.gov	North and South Americas
Rainer Wanzenberg	rainer.wanzenberg@desy.de	Europe* and Africa
Susumu Kamada	Susumu.Kamada@kek.jp	Asia** and Pacific

* Including former Soviet Union.

** For Mainland China, Jiu-Qing Wang (wangjq@mail.ihep.ac.cn) takes care of the distribution with Ms. Su Ping, Secretariat of PASC, P.O. Box 918, Beijing 100039, China.

To keep costs down (remember that the Panel has no budget of its own) readers are encouraged to use the Web as much as possible. In particular, if you receive a paper copy that you no longer require, please inform the appropriate distributor.

7.1.5 Regular Correspondents

The Beam Dynamics Newsletter particularly encourages contributions from smaller institutions and countries where the accelerator physics community is small. Since it is impossible for the editors and panel members to survey all beam dynamics activity world-wide, we have some *Regular Correspondents*. They are expected to find interesting activities and appropriate persons to report them and/or report them by themselves. We hope that we will have a “compact and complete” list covering all over the world eventually. The present *Regular Correspondents* are as follows

Liu Lin	liu@ns.inls.br	LNLS Brazil
S. Krishnagopal	skrishna@cat.ernet.in	CAT India
Ian C. Hsu	ichsu@ins.nthu.edu.tw	SRRC Taiwan

We are calling for more volunteers as *Regular Correspondents*.

7.2 ICFA Beam Dynamics Panel Members

Caterina Biscari	caterina.biscari@lnf.infn.it	LNF-INFN, Via E. Fermi 40, 00044 Frascati (RM), Italy
Swapan Chattopadhyay	swapan@jlab.org	Jefferson Lab, 12000 Jefferson Avenue, Newport News, VA 23606, USA
Pisin Chen	chen@slac.stanford.edu	SLAC, P.O. Box 4349, MS26, Stanford, CA 94309, USA
Weiren Chou (Chair)	chou@fnal.gov	FERMILAB, MS 220, P.O.Box 500, Batavia, IL60510, USA
Yoshihiro Funakoshi	yoshihiro.funakoshi@kek.jp	KEK, Oho, Tsukuba, IBARAKI 305-0801, Japan.
Miguel Furman	mafurman@lbl.gov	Center for Beam Physics, Lawrence Berkeley National Laboratory, Bldg 71, R0259, 1 Cyclotron Road, Berkeley, CA 94720-8211, USA
Jie Gao	gao@lal.in2p3.fr	Laboratoire de L'Accélérateur Linéaire, B.P. 34, 91898 Orsay cedex, France
Ingo Hofmann	i.hofmann@gsi.de	High Current Beam Physics, GSI Darmstadt, Planckstr. 1, 64291 Darmstadt, Germany
Sergei Ivanov	ivanov_s@mx.ihep.su	Inst. for High Energy Physics, Protvino, Moscow Region, 142281 Russia
Kwang-Je Kim	kwangje@aps.anl.gov	Argonne Nat. Lab., Advanced Photon Source, Accelerator Systems Division, 9700 S. Cass Avenue, Bldg 401/C4265, Argonne, IL 60439
In Soo Ko	isok@postech.ac.kr	Pohang Accelerator Laboratory, San 31, Hyoja-Dong, Pohang 790-784, South Korea
Alessandra Lombardi	Alessandra.Lombardi@cern.ch	CERN, CH-1211 Geneva 23, Switzerland
Yoshiharu Mori	Yoshiharu.mori@kek.jp	KEK, 1-1 Oho, Tsukuba-shi, Ibaraki-ken, 305-0801, Japan
David Rice	dhrl@cornell.edu	Cornell University, 271 Wilson Lab, Ithaca, NY 14853-8001, USA
Yuri Shatunov	Yu.M.Shatunov@inp.nsk.su	Acad. Lavrentiev prospect 11, 630090 Novosibirsk, Russia
Junji Urakawa	junji.urakawa@kek.jp	KEK, 1-1 Oho, Tsukuba-shi, Bldg. 911, Upton, NY 11973-5000, USA
Jiu-Qing Wang	wangjq@mail.ihep.ac.cn	Institute for High Energy Physics, P.O. Box 918, 9-1, Beijing 100039, China
Rainer Wanzenberg	Rainer.wanzenberg@desy.de	DESY, Notkestrasse 85, 22603 Hamburg, Germany
Jie Wei	wei1@bnl.gov	BNL, Bldg 911, Upton, NY 11973-5000, USA

The views expressed in this newsletter do not necessarily coincide with those of the editors. The individual authors are responsible for their text..